An integrative and translational assessment of altered atrial electrophysiology, calcium handling and contractility in patients with atrial fibrillation

Doctoral Thesis

In partial fulfilment of the requirements for the degree

“Doctor of Philosophy (PhD)”

in the Molecular Medicine Study Program

at the Georg-August University Göttingen

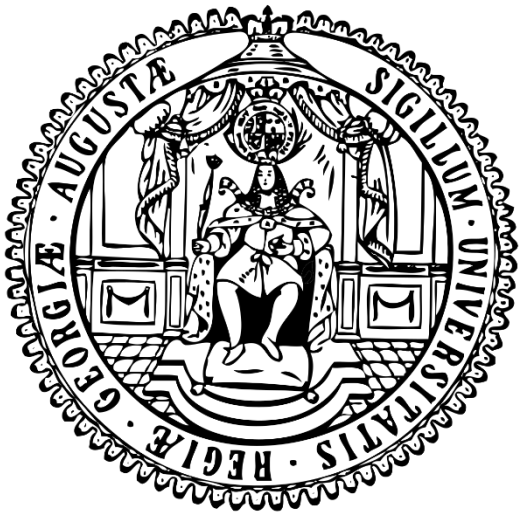

Submitted by

Funsho Emmanuel Fakuade

Born in

Yola, Nigeria

Göttingen, 2020

Members of thesis committee

Prof. Dr. med. Niels Voigt (Reviewer)

Institute of Pharmacology and Toxicology

University Medical Centre Göttingen

Robert-Koch-Strasse-40, Göttingen, Germany

Prof. Dr. Manuel Mayr (co-supervisor)

The James Black Centre, King´s College London

125 Coldharbour Lane, London SE5 9NU, United Kingdom

Prof. Dr. mult. Thomas Meyer (Reviewer)

Department of Psychosomatic Medicine and Psychotherapy

University Medical Centre Göttingen

Waldweg 33, Göttingen, Germany

Prof. Dr. rer. nat. Blanche Schwappach

Dean, Faculty of Medicine,

University Medical Centre Hamburg-Eppendorf

Martinistrasse 52, Hamburg, Germany

Extended members of the examination board

PD Dr. rer. nat. Sven Thoms

Department of Child and Adolescent Health

University Medical Center Göttingen

Robert-Koch-Strasse-40, Göttingen, Germany

Prof. Dr. med. Ralf Dressel

Institute for Cellular and Molecular Immunology

University Medical Center Göttingen

Humboldtalle 34, Göttingen, Germany

Prof. Dr. med. Paulus Kirchhof

Director, Department of Cardiology,

University Medical Centre Hamburg-Eppendorf

Martinistrasse 52, Hamburg, Germany

Date of Disputation: _____

Affidavit

I hereby declare that the work presented in this thesis titled "*An integrative and translational assessment of altered atrial electrophysiology, calcium handling and contractility in patients with atrial fibrillation*" has been written independently with no other source and aids than quoted.

_____

Funsho Emmanuel Fakuade

Göttingen, 2020

Acknowledgements

Firstly I would like to express my utmost gratitude to my supervisor Prof. Niels Voigt for his tireless support and continuous encouragement throughout my PhD. His immeasurable patience, dedication, intellectual discipline and scientific direction have been impactful during the course of my research. I would like to also give special thanks to my co-supervisor Prof. Manuel Mayr, for providing thought-provoking ideas and a stimulating environment at Kings College London that developed my project in a new direction. I also appreciate the entire members of the Mayr Lab, particularly Dr. Javier Barallobre-Barreiro, Dr. Fava Marika and Lukas Schmidt for their immense support on providing practical guidance and continuous support on the analysis of the complex proteomics data even after I departed Kings.

I also express sincere thanks to my thesis committee members Prof. Blanche Schwappach and Prof Thomas Meyer for their insightful comments and generous support which facilitated the advancement of my thesis. Furthermore, I highly appreciate Prof. Ralf Dressel and PD Dr Sven Thoms for kindly agreeing to serve on my examination board.

I would like to give a special thanks to Prof. Blanche Schwappach and Dr Julia Menzel for their assistance and provision of both expert advice on biochemistry related issues throughout my PhD. I also appreciate Dr Khaled Alhussini and Dr Constanze Bening for helping with myofibre force measurements. I am particularly grateful to Dr Fereshteth Haghighi for assisting with the gene analysis experiments.

I am indebted to the entire cardiac surgery team of the University Medical Centre Gottingen, headed by Prof. Ingo Kutschka, for their invaluable collaboration in providing tissue samples, which is the foundational core of all experiments conducted in this thesis.

Special thanks to the IRTG1816 program funded by the (Deutsche Forschungmeinschaft, DFG) for providing the very structured platform that facilitated the conductance of my research. I also appreciate the phenomenal administrative support provided Dr Christina Würtz and Fulya Ören for the entire duration of my PhD.

I would also like to acknowledge both past and present members of the Voigt lab and the institute of pharmacology and toxicology for their support and encouragement throughout my PhD. I thank the very hard working Vanessa Steckmeister, who I supervised, for her immense contribution to this thesis. I also appreciate the constant

motivation and impactful support from Fleur, Judith, Julius, Lena, Luisa, Ricky, Tony and Will during both good and challenging times of this thesis. Furthermore, I highly appreciate Stefani Kestel for her outstanding technical assistance and conduction of most of the western blot experiments in this thesis. I am as well grateful to Ines Muller for ensuring quality isolation of cells for electrophysiological studies throughout my PhD.

Finally, words cannot describe the debt of gratitude I owe to my family especially my parents, for their prayers, endless love, encouragement and support which has guided me throughout my life till this point. I will forever remain grateful and steadfast in the principles you have instilled in me.

And for those unmentioned who have supported me during this journey of mine, I am deeply grateful for your kindness over the years.

List of publications

Ohieku, J.D. & **Fakuade**, **F**.**E**. (2013). Otitis Media: A Clinical Assessment of Etiological Pathogens Susceptibility Status and Available Therapeutic Options Among 19 Antibacterial Agents in Maiduguri City, Nigeria. *World Journal of Pharmacy and Pharmaceutical Sciences*. 2 (4), 1548-1564.

Brandenburg S., Pawlowitz J., **Fakuade**, **F**.**E**., Kownatzki-Danger, D., Kohl, T., Mitronova, G.Y., Scardigli, M., Neef, J., Schmidt, C., Wiedmann, F., Pavone F.S., Sacconi, L., Kutschka, I., Sossalla, S., Mosier, T., Voigt, N. & Lehnart, S. (2018). Axial Tubule Junctions Activate Atrial Ca^{2+} Release Across Species. *Frontiers in Physiology 9*. 1227.

Hofhuis, J., Bersch, K., Wagner, S., Molina, C., **Fakuade, F. E**., Iyer, L. M., Streckfuss-Bömeke, K., Toischer, K., Zelarayán, L. C., Voigt, N., Nikolaev, V. O., Maier, L. S., Klinge, L. & Thoms, S. (2020). Dysferlin links excitation-contraction coupling to structure and maintenance of the cardiac transverse-axial tubule system. *EP Europace*, *22*(7), 1119–1131.

***Fakuade**, **F**. **E**., Steckmeister, V., Seibertz, F., Gronwald, J., Kestel, S., Menzel, J., Pronto, J. R. D., Taha, K., Haghighi, F., Kensah, G., Pearman, C. M., Wiedmann, F., Teske, A. J., Schmidt, C., Dibb, K. M., El-Essawi, A., Danner, B. C., Baraki, H., Schwappach, B., Kutschka I., Mason, F.E. & Voigt, N. (2020). Altered Atrial Cytosolic Calcium Handling Contributes to the Development of Postoperative Atrial Fibrillation. *Cardiovascular Research.* In press. doi: 10.1093/cvr/cvaa162

*Data published in the article is presented in chapter 4 of this thesis.

Statement of conjoint work

Chapter 3: Dr Khaled Alhussini and Dr Constanze Bening kindly provided the force measurements of skinned human atrial myofibres.

Chapter 4: Judith Gronwald analysed echocardiography recordings using speckle-tracking. Vanessa Steckmeister, an MD student I supervised, performed and analysed the current-clamp experiments. Dr Fereshteth Haghighi helped with the gene expression analysis.

Table of contents

List of figures

List of tables

Abbreviations

$[Ca^{2+}]_i$	Intracellular calcium
AF	Atrial fibrillation
Ag	Silver
Ag/Cl	Silver chloride
AP	Action potential
ATP	Adenosine triphosphate
B_{max}	Maximum buffer capacity
BSA	Bovine serum albumin
cAF	Chronic atrial fibrillation
CaMKII	Calcium/calmodulin-dependent protein kinase II
CaT	Calcium transient
cCaT	Caffeine-induced calcium transient
cDNA	Complimentary deoxyribonucleic acid
CRP	Complement reactive protein
cTnC	Cardiac troponin C
cTnT	Cardiac troponin T
CX40	Connexin 40
CX43	Connexin 43
Da	Dalton
DAD	Delayed afterdepolarisations
$_{dd}H_2O$	Double distilled water
DEPC	Diethyl pyrocarbonate
DNA	Deoxyribonucleic acid
DTT	Dithiothreitol
EAD	Early afterdepolarisation
ECM	Extracellular matrix
$I_{Ca,L}$	The L-type calcium current
$I_{K,ACh}$	Acetylcholine-dependent inward rectifier current
I_{K1}	Inward rectifier potassium current
I_{Kr}	Rapid delayed rectifier potassium current
I_{Ks}	Slow delayed rectifier potassium current
I_{Kur}	Ultra-rapid potassium current
I_{Na}	Sodium current

I_{NaL}	Late sodium currents
I_{NCX}	Sodium calcium exchanger current
I_{to}	Transient outward potassium current
mRNA	Messenger ribonucleic acid
MS	Mass spectrometer
mV	Millivolts
NCX1	Sodium calcium exchanger
pAF	Paroxysmal fibrillation
PBS	Phosphate buffered saline
pCa	-log of free Ca^{2+}
PCR	Polymerase chain reaction
PKA	Protein kinase A
PMCA	Plasma membrane calcium ATPase
PMT	Photomultiplier
PNGase F	Peptide -n-glycosidase F
poAF	Postoperative atrial fibrillation
PP2a	Protein phosphatase 2a
RMP	Resting membrane potential
RNA	Ribonucleic acid
RYR2	Cardiac ryanodine receptor
SDS-PAGE	Sodium dodecyl sulphate-polyacrylamide gel electrophoresis
SERCA	Sarcoplasmic reticulum calcium-ATPase
SLN	Sarcolipin
SUMO	Small ubiquitin-like modifiers
TCA	Trichloroacetic acid
TFA	Trifluoroacetic acid

Abstract

Atrial fibrillation (AF) is the most prevalent sustained arrhythmia reported in clinical practice, and it is associated with deleterious outcomes such as stroke, that increase patient morbidity and mortality. Previous studies have reported atrial remodelling, including structural and electrophysiological remodelling as well as alterations in Ca^{2+} handling, as contributors to the initiation and perpetuation of AF. However, the contributory role of these remodelling to the pathophysiology of different forms of AF and their corresponding complications is incompletely understood. Hence, the aims of this study are to (i) assess the role of altered intracellular Ca^{2+} handling in the atrial contractile dysfunction seen in patients with long-term persistent ('chronic') AF (cAF); (ii) investigate the role of abnormal intracellular Ca^{2+} handling in the arrhythmogenesis of postoperative AF (poAF) and its associated contractile dysfunction; (III) study the alteration in extracellular matrix (ECM) protein secretion and their possible role in poAF and cAF associated contractile dysfunction. In pursuance of these aims, right atrial appendages excised from cardiac surgery patients were obtained.

In the first part of this thesis, the role of abnormal Ca^{2+} handling in the atrial contractile dysfunction associated with cAF was studied. Right atrial myocytes of cAF patients examined by simultaneous measurement of their membrane currents (voltage-clamp), intracellular Ca^{2+} ($[Ca^{2+}]_i$) and cell fractional shortening, exhibited an impaired contractile response to Ca^{2+}. Expression of cTnC was reduced in cAF patients, which could account for the abnormal contractile response of atrial myocytes from cAF patients. Also, Ca^{2+} buffering was impaired in cAF myocytes as a consequence of lower Ca^{2+} buffers which is supported by the reduced cTnC expression observed in cAF patients. Conclusively, the findings in this part of this study suggest that reduced cTnC not only contributes to the atrial contractile dysfunction, but also the impaired buffering seen in cAF patients.

In the next chapter, we evaluated the participation of altered intracellular handling of Ca^{2+} in the development of poAF and its related contractile dysfunction. Analysis of preoperative echocardiography recordings by speckle-tracking revealed diminished left atrial contraction in poAF patients. $[Ca^{2+}]_i$ measurements indicated reduced systolic Ca^{2+} transient (CaT) amplitude and sarcoplasmic reticulum (SR) Ca^{2+} load in myocytes from poAF patients, with a delay in the sequestration the SR due to reduced SERCA2a activity identified as the underlying cause. In consonance, protein expression of SERCA2a was reduced in poAF patients, but the phosphorylation and expression of its

regulatory protein phospholamban were unchanged. Atrial myocytes from poAF patients exhibited increased vulnerability to CaT and AP alternans, which is attributed to the reduced SERCA activity, based on computational modelling. In summary, our findings suggest that SERCA mediated impairment in SR Ca^{2+} uptake contributes majorly to the proarrhythmic mechanisms responsible for the development of poAF as well as the associated impaired preoperative atrial contractile function.

Finally, we assessed the alterations in the secretions of ECM proteins in poAF and cAF patients using liquid chromatography-tandem mass spectrometry (LC-MS/MS). Proteomic analysis of the secretome of atrial appendages from poAF and cAF patients showed minimal changes in ECM protein secretion in the poAF group, with approximately 6% of identified ECM proteins differentially regulated. In comparison, 40% of ECM proteins were differentially regulated in cAF, demonstrating marked alteration in ECM protein secretion. ECM proteins such as collagen I, microfibrillar associated protein, connective tissue growth factor and several other members of the different ECM were identified to contribute to remodelling in atrial ECM protein secretion, with the pro-fibrotic transforming growth factor β1 (TGFβ1), identified by further analysis as a contributor to the modification in ECM protein secretion seen in both poAF and cAF.

Altogether this thesis provides novel mechanistic insight on the role of altered Ca^{2+} handling in the development of cAF and poAF and their associated contractile dysfunction as well as the characteristic remodelling of ECM protein secretion in both forms of AF.

1 General introduction

1.1 Atrial fibrillation

Atrial fibrillation (AF) is a common heart condition that alters the electrical conduction system of the heart leading to rapid and irregular rhythms in the atria. It has emerged as a growing epidemic and a serious public health problem on a global scale, exhibiting a continuous rise in prevalence and incidence (Lip et al., 2012, 2016). An estimate of 34 million people in the global population are currently living with AF, with a round number of 5 million cases reported yearly (Chugh et al., 2014). Besides being prevalent, AF is associated with detrimental consequences, including an increased risk of stroke and worsened heart failure, which contributes to morbidity and mortality (Mou et al., 2018; T. J. Wang et al., 2003). The atrial contractile dysfunction seen in AF patients is suggested to enable stasis of blood flow, which encourages the formation of intraatrial thrombi, leading to thromboembolic stroke (Darlington & McCauley, 2020). Although occasionally observed in the young, AF is more predominant in the elderly, usually coexisting with other comorbidities, including hypertension, heart failure and obesity (M. K. Chung et al., 2020; Mou et al., 2018). Thus, with the advancing age of the global population, AF poses a serious economic challenge.

AF patients, due to the deleterious complications associated with AF, experience more malady and tend to have increased hospital admissions. An estimated lump sum of $26 billion in healthcare cost is accrued annually from AF management in the US (Kim et al., 2011). Also, a reported €660 million healthcare cost annually is reported to be associated with AF in Germany (McBride et al., 2009). Although such large investments have been allocated to the management of AF, current treatment strategies are still inadequate (Nattel et al., 2020). A possible reason for these less efficacious treatment strategies is due to poor understanding of the underlying mechanisms of AF. Therefore, these outcomes highlight the dire need for the development of novel therapeutic strategies in the management of AF.

The structural integrity, electrical properties and Ca^{2+} handling of the heart are cardinal factors responsible for its efficient functioning. These factors are severely altered in the atria of AF patients (Heijman et al., 2014), contributing to the phenotype of this cardiac condition. Therefore, this thesis is aimed at providing more insights on the impairment in

structure, electrical properties and Ca^{2+} homeostasis in the atria, which contributes to the pathophysiology of AF.

1.2 Clinical presentation of AF

AF is the most common arrhythmia seen in clinical practice, characterised by swift and erratic atrial activity, which results in inefficient atrial contractions. This phenomenon manifests as the absence of prominent P waves, irregular R-R intervals and exhibition of oscillating waves in the electrocardiogram (ECG) (January et al., 2014). Being a progressive disease, AF is clinically classified into three groups, namely paroxysmal, persistent and permanent AF, based on its duration and response to treatment (Heijman et al., 2014). Paroxysmal AF (pAF) refers to AF episodes that terminate either spontaneously or by electrical cardioversion within seven days. However, some pAF patients progress to persistent/permanent forms, while others never advance to persistent AF. Persistent AF, on the other hand, is characterised by AF episodes that persist beyond seven days but can be restored to normal cardiac rhythm either by pharmacological approaches or electrical cardioversion. As the name implies, permanent AF describes AF that is irreversible regardless of the treatment approach applied (Heijman et al., 2014; Kirchhof et al., 2016). Cases of AF that persist beyond seven days, i.e. persistent and permanent, can be generally classified as chronic atrial fibrillation (cAF) (Lane et al., 2015). AF could also be classified based on secondary causes, such as cardiac and non-cardiac surgery. The postoperative AF (poAF) that occurs after surgery, typically cardiac surgery is an important form of AF as it also prolongs hospital stay and increases the risk to thromboembolic events (Dobrev et al., 2019).

1.3 Normal cardiac electrophysiology

In order to appreciate the pathophysiology of AF, we must first understand the electro-mechanical properties of a normally functioning heart. The organised contraction of the heart is a product of coordinated generation and transmission of electrical impulses across the chambers of the heart. This rhythm of the heart is initiated and regulated by a group of specialised pacemaker cells resided in the sinoatrial node, which generate spontaneous electrical impulses. This inherent property to spontaneously generate electrical impulses is called automaticity (Antzelevitch & Burashnikov, 2011).

In the normal rhythm of the heart (sinus rhythm), the electrical impulse generated in the sinoatrial node, transverses throughout the atria, stimulating atrial contraction, which

pumps blood into the ventricles. The electrical signal subsequently travels through the atrioventricular node to the bundle of His. The atrioventricular node, situated between the conduction systems of the atria and the ventricle, ensures retardation of electrical impulses travelling from the atria, to enable efficient and complete contraction of the atria, and subsequent transfer of blood from the atria into the ventricle. From the bundle of His, the electrical impulse travels through the specialised conduction system of Purkinje fibres exciting the ventricles, consequently resulting in organised ventricular contraction. In AF, this closely regulated sequence of electrical activation, conduction and contraction is disrupted, resulting in rapid and irregular atrial activity and subsequent abnormal atrial contraction (Lip et al., 2016).

1.3.1 The cardiac action potential (AP)

Excitation of cardiac myocytes by travelling electrical signals triggers a typical electrical response of their membranes characterised by the generation of a time-dependent waveform called action potential (AP). These APs are a product of organised, sequential fluxes of ions through appropriate ion channels within the sarcolemma, which are crucial for the coordinated contraction of the myocardium (Bartos et al., 2015). The morphology of the APs differs in different regions of the heart, and this is mainly due to the distinct expression of ion channels, as well as transporters and components of other signalling pathways in these regions (Schotten et al., 2011).

The tightly-regulated systematic flux of ions across the membranes of cardiomyocytes, due to the coordinated activation and inactivation of ion channels, prompt the exhibition of 5 distinct phases in the AP, i.e. phase 0-4 (**Figure 1**). In a typical human atrial myocyte, APs begin at phase 0, when APs transduced via gap junctions from adjacent myocytes, depolarise the membrane of the atrial myocyte from a resting membrane potential (RMP) stabilised between -65 and -80 mV to a threshold potential of voltage-gated Na^+ channels. This change in membrane potential causes a change in conformation of the Na^+ channel from closed to open, resulting in a fast influx of Na^+ into the myocyte, generating a sizeable inward current (I_{Na}). This I_{Na} further depolarises the myocyte to a potential of approximately +40 mV, reflected by a fast upstroke in the waveform. The Na^+ channel, being a time-dependent channel, quickly inactivates after a few milliseconds kickstarting the next phase (phase 1) of the AP. The inactivation of Na^+ channels is succeeded by an immediate repolarisation of the membrane, by the activation of the transient outward K^+ current (I_{to}) and the atrial-specific ultra-rapid current (I_{Kur}). This swift process, termed the early repolarisation phase, causes a downward deflection of the waveform of the AP, reverting

the membrane potential to approximately 0 mV. The AP continues to phase 2, the “plateau” of the AP, which is maintained by a balance between the depolarising inward Ca^{2+} current ($I_{Ca,L}$) via the L-type Ca^{2+} channels, and repolarising outward K^+ currents through, rapid (I_{Kr}) and slow (I_{Ks}) delayed rectifier K^+ channels (Wettwer et al., 2004). These balanced fluxes of ions ensure the membrane potential is maintained just below 0 mV throughout phase 2. In phase 3, the L-type Ca^{2+} channel progressively inactivates, causing the outward repolarising K^+ currents to outbalance the depolarising $I_{Ca,L}$, which leads to a reduction in membrane potential that further activates the inward rectifier K^+ current (I_{K1}). The contribution of the I_{K1} further repolarises the membrane potential to resting levels (phase 4) which is approximately -75 mV. The atrial specific acetylcholine-dependent inward rectifier current ($I_{K,ACh}$), which is activated by muscarinic receptors reacting to vagal stimulation, also contributes to the repolarisation to resting levels RMP is maintained mainly by I_{K1} with contribution from $I_{K,ACh}$ (Bartos et al., 2015; Grant, 2009).

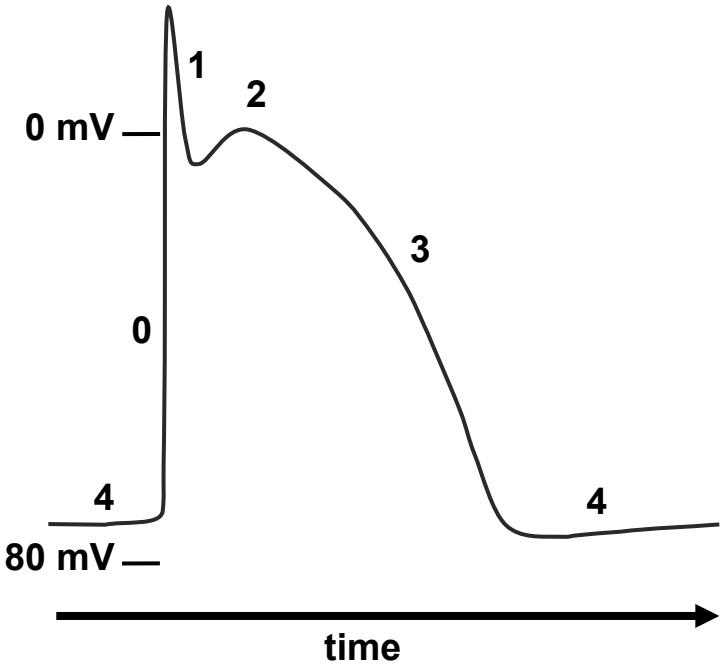

Figure 1. Cardiac action potential. A representative atrial action potential depicting the depolarization (0), early repolarisation (1), plateau (2), repolarization (3) and resting (4) phases. mV = millivolts

1.3.2 Excitation-contraction coupling

Excitation-contraction coupling describes the physiological process in the heart where the electrical excitation of the surface membrane of a cardiomyocyte translates into a mechanical response. The influx of extracellular Ca^{2+} into the myocyte via the voltage-gated L-type Ca^{2+} channel during the plateau phase of APs produces a small increase in

cytosolic Ca^{2+} (**Figure 2**). This increase in cytosolic Ca^{2+} levels signals the opening of the cardiac ryanodine receptors (RYR2), which is located within the membrane of the sarcoplasmic reticulum (SR), triggering a larger release of Ca^{2+} from the SR by a mechanism called Ca^{2+}-induced Ca^{2+} release (Fabiato, 1983). The corresponding increase in cytosolic Ca^{2+} facilitates the binding of Ca^{2+} to troponin C (cTnC), which promotes the formation of actin-myosin cross-bridges, subsequently initiating the mechanical contraction of the myocyte. For relaxation to occur, cytosolic Ca^{+} levels need to be restored to diastolic ranges. This is achieved by either Ca^{2+} extrusion to the extracellular space via the bidirectional Na^{+}-Ca^{2+} exchanger (NCX), which exchanges one Ca^{2+} ion for three Na^{+} ions across the membrane or reuptake of Ca^{2+} into the SR by SR Ca^{2+}-ATPase (SERCA2a) and sarcolipin (SLN), as well as the transfer Ca^{2+} into the mitochondria by mitochondrial Ca^{2+} uniporter (Bers, 2002; Eisner et al., 2017).

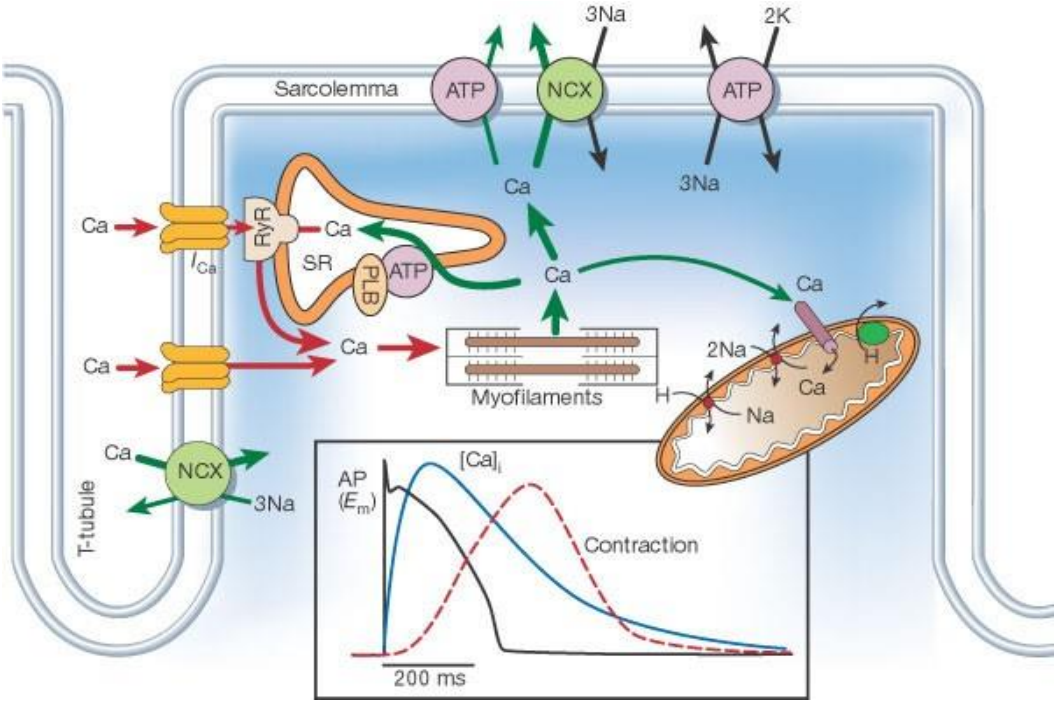

Figure 2. Excitation-contraction coupling (ECC) in a cardiac myocyte. See text for description. Replotted from Bers, 2002 (with permission).

It should be pointed out that the $I_{Ca,L}$-mediated increase in cytosolic Ca^{2+} level during excitation-contraction coupling is highly buffered. Only 1% of the cytoplasmic Ca^{2+} is free, with the remaining 99% bound to intracellular buffers, i.e. for every free Ca^{2+} ion, 100-200 are bound to cytosolic Ca^{2+} buffers (Berlin et al., 1994; Smith & Eisner, 2019; Trafford et al., 1999). This Ca^{2+} buffering controls the persistence of Ca^{2+} in the cytosol, which is an essential signalling molecule. The myofilament proteins, mainly cTnC, is the major buffer of Ca^{2+} in cardiac myocytes, accounting for approximately 50% of total buffers (Smith &

Eisner, 2019). Therefore, changes in buffer properties would majorly influence Ca^{2+} signalling as well as cardiac myocyte contraction.

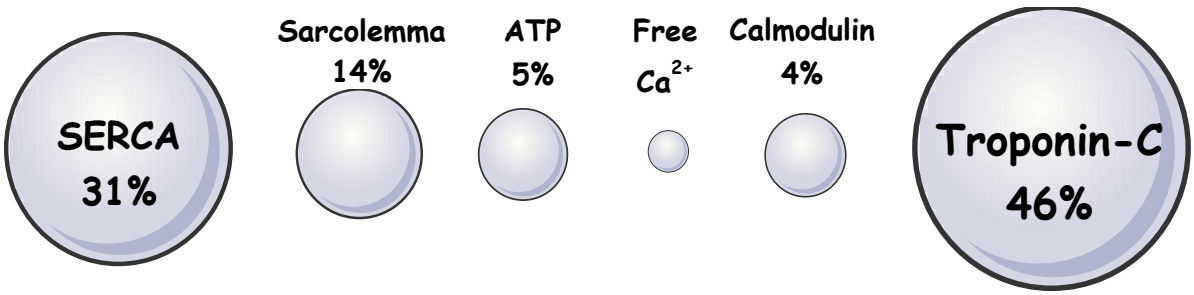

Figure 3. Illustration depicting the contribution of major cellular buffers to Ca^{2+} buffering in cardiac myocytes. Percentages represent estimates of Ca^{2+} buffering of named buffers as reviewed by Smith & Eisner, 2019.

1.4 Basic mechanisms of AF

AF on an organ level occurs when the systematic excitation of the atrial myocardium is disrupted. Conceptually, two principal mechanisms initiate and maintain AF. Foremost, is the existence of one or more fast-firing ectopic foci (triggers) within the atria, which prompts erratic conduction to other parts of the atria leading to irregular fibrillatory activity. On the other hand, a single re-entry circuit may cause rapid localised firing in the atria, prompting fibrillatory conduction throughout the atria causing AF. Also, AF may be caused by many functional re-entry circuits with chaotic and inconsistent activation patterns (Lip et al., 2016).

1.4.1 Atrial ectopic activity

Ectopic firing in the simplest of terms refers to electrical impulses generated by a group of cells located outside the sinoatrial node (Wakili et al., 2011). For decades, multiple reentrant mechanisms were believed to cause all cases of AF. However, recent studies kickstarted by the formative findings of Haïssaguerre et al. reinforced the idea that triggered activity, typically from the pulmonary veins, was implicated in the initiation of AF (Haïssaguerre et al., 1998). Using intracardiac mapping, Haïssaguerre et al. showed that the ectopic beats located in the pulmonary veins initiated frequent episodes of AF in most patients. Notably, 90% of all pAF bouts in this study were terminated by ablation (Haïssaguerre et al., 1998). Additional non-pulmonary vein sources triggering AF have been identified, including the appendages, the vena cava and the intra-atrial septum (Elayi et al., 2013; Enriquez et al., 2017).

Triggered activities are usually a product of afterdepolarisations, which are oscillations in membrane potentials preceding APs, that can provoke premature APs if a sufficient depolarising voltage threshold is achieved (Schotten et al., 2011). Two types of afterdepolarisations may produce triggered activities. Afterdepolarisation occurrences that disrupt the end of the AP plateau phase (phase 2) or begin of the repolarisation phase (phase 3) are called early afterdepolarisations (EAD) (Schotten et al., 2011). Events synchronous with prolongation of AP duration (APD), such as anomalies in I_{Na} inactivation, the persistence of late Na^+ currents (I_{NaL}) and decreased efflux from K^+ channels, which favours the inward direction of the delicate balance of active channels during phase 2 or 3 of APs, generally support the occurrence of EADs. Also, prolongation of the APD permits the recovery of the L-type Ca^{2+} channel after inactivation, with the consequential depolarising $I_{Ca,L}$ triggering an EAD (January et al., 1988; Weiss et al., 2010; Zeng & Rudy, 1995).

On the other hand, afterdepolarisations that occur after full or near-complete repolarisation (phase 4) are called delayed afterdepolarisations (DAD). DADs are favoured by conditions that elevate cytosolic Ca^{2+} levels, mainly due to abnormal Ca^{2+} release from the SR, which causes an electrogenic influx of 3 Na^+ for every Ca^{2+} ion, which could invoke another AP (Nattel et al., 2020).

1.4.2 Re-entry

Re-entry describes a disorder in impulse propagation, where an excitation wave fails to extinguish completely after routine activation, moving on to re-excite other regions that have exited the refractory phase. This phenomenon was first described as far back as 1906, by a series of seminal experiments conducted by Alfred Mayer, using the jellyfish, *Cassiopea xamachana* (Mayer, 1906). With ring-like muscle preparations from the jellyfish, Mayer showed that electrical stimulation of these ring structures could induce impulses that transverses the circumference of the rings indefinitely, without needing further stimulation. This concept was soon after applied clinically in cardiac tissue by George Mines, with an alias called “circus movement re-entry”, which he suggested was responsible for some cases of paroxysmal tachycardia at that time (Mines, 1914). The works of these early studies provided the fundamental basis for the circular model, which remains in use today. For re-entry to occur, the conduction of the propagating wave needs to be slow, to enable expiration of the refractory phase of the blocked pathway ahead in the circuit, allowing its re-excitation by the travelling wave (**Figure 4A**). In other words, there should be an “excitable” gap between the wavefront and the wavetail for re-entry to

occur. Therefore, successful re-entry is dependent on the conduction velocity (CV) of the propagating wave and the refractory period of the tissue. The length of the stimulating wave, which is a product of its CV and the refractory period, needs to be smaller than the circuit path for re-entry to occur (Tse, 2016).

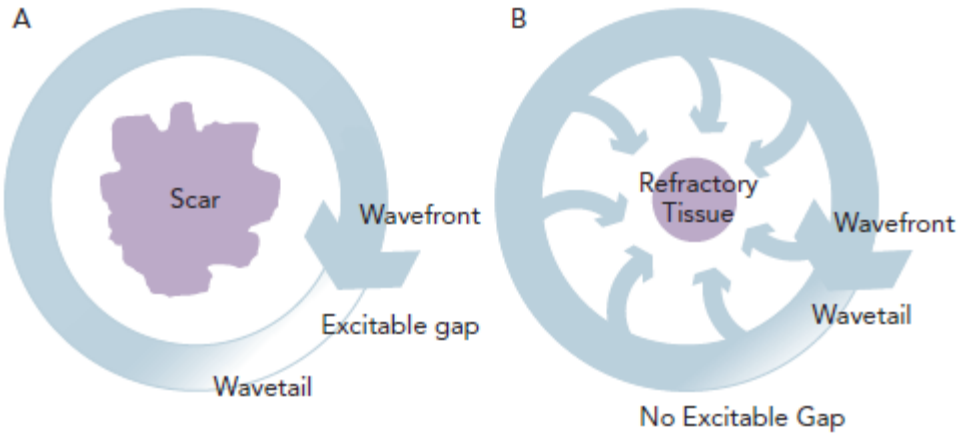

Figure 4. Schematic illustrating re-entry mechanisms. A, A re-entry circuit, with the wave (blue arrow) travelling around an anatomical obstacle. The arrowhead represents the travelling wavefront, while the shaded end depicts the wavetail separated by an excitable gap. **B,** A functional re-entry (leading circle re-entry) circuit with the wavefront repeatedly invading the space of the wavetail, due to the constant centripetal activation which sustains the re-entry in the absence of an anatomic barrier. Replotted from Waks & Josephson, 2014 (with permission)

Also, it is pertinent that the excitation wave travels in one direction for re-entry to occur; hence the need for a unidirectional conduction block. The unidirectional block could be anatomical obstacles as demonstrated by Mines and Meyer, or functional obstacles (Lip et al., 2016). The elegant study by Allessie et al. first demonstrated the occurrence of the re-entry without an anatomical obstacle, termed functional re-entry, by inducing tachycardia through the premature application of electrical impulses in the left atria of rabbits (Allessie et al., 1973). In functional re-entry (**Figure 4A**), the circus movement of the propagating wave in the circuit leads to incessant centripetal activation of the circuit centre, putting it in a continuous refractory state. The resultant refractory region creates a unidirectional conduction block similar to an anatomical obstacle, which can sustain re-entry (Waks & Josephson, 2014). Although both models of re-entry are different, they both require a trigger for initiation. Ectopic discharges generated by EADs and DADs are believed to serve as these triggers.

1.5 Atrial remodelling associated with AF

1.5.1 Electrical remodelling in AF

Remodelling of the electrical properties in the atria is one of the most characterised mechanisms responsible for the initiation and maintenance of AF. This remodelling constitutes molecular alterations of ion channels that result in APD shortening. The formative study by Wijffels et al. elegantly provided early insight into the electrophysiological modifications in the atria during AF using a goat model (Wijffels et al., 1995). They demonstrated that bursts of electrical stimulation of the atria generated short-lived paroxysms of AF. Maintenance of these short-lived AF episodes by persistent and repetitive induction prolonged duration of these AF paroxysms. Subsequent application of this AF maintenance strategy for more extended periods of 2-3 weeks, resulted in the sustenance of AF in many of the experimental animals. This gradual progression from paroxysms of AF to persistent AF was synchronous with the abbreviation of the AP, with the APD reduced by approximately 45% (Wijffels et al., 1995). This key finding is also observed in many other animal models (reviewed in Clauss et al., 2019) and has provided valuable insights into the progressive characteristic of AF, coining the concept termed “AF begets AF”.

Consistent with the findings in animal studies, cAF patients also exhibit a reduction in APD when compared with normal sinus rhythm patients (Franz et al., 1997; Voigt et al., 2012; Wettwer et al., 2004). However, this classical electrical remodelling is absent in pAF (Schmidt et al., 2015; Voigt et al., 2010, 2014). The change in APD observed in cAF, has been attributed alterations in the delicate balance between inward depolarising currents (mainly $I_{Ca,L}$) and outward repolarising currents (K^+ channels). The current density of $I_{Ca,L}$ is markedly reduced in right atrial myocytes from cAF patients (Van Wagoner et al., 1999; Voigt et al., 2012). Also, mRNA expression levels and protein levels are reduced in cAF patients (Brundel, Van Gelder, Henning, Tieleman, et al., 2001). This reduction in $I_{Ca,L}$ shortens the plateau phase of the AP, consequently shortening APD, which is favourable for the development of re-entry. A decreased phosphorylation of the L-type Ca^{2+} channel due to increased activity of the phosphatase, protein phosphatase 2a (PP2a) has been reported to contribute to the reduced $I_{Ca,L}$ (Christ et al., 2004). Additionally, alterations in the function of the scaffolding adaptor protein ankyrin B (Cunha et al., 2011) and the protease calpain (Brundel et al., 2002) have also been reported to contribute to the reduction in $I_{Ca,L}$. Recently, the microRNAs, miR-328 and miR-21, have been shown to target genes expressing the L-type Ca^{2+} channel, thereby reducing $I_{Ca,L}$ (Barana et al.,

2014; Lu et al., 2010). Molecular studies have reported no change in neither $I_{Ca,L}$ current density and the expression of its pore-forming α_{1C} subunit (Brundel et al., 1999; Voigt et al., 2014).

The activity and expression of many repolarising K^+ channels are also altered in AF. An increased I_{K1} (Dobrev et al., 2002; Voigt et al., 2010), accompanied by both elevated transcript and the protein expression levels of its subunit Kir2.1, has been reported in cAF patients (Gaborit et al., 2005; Voigt et al., 2010). This documented increase in I_{K1} is believed to contribute to the abbreviation of APD associated with cAF (Zhang et al., 2005). Also, both protein and mRNA levels of the subunits of $I_{K,ACh}$ are reduced (Kir 3.1 and 3.4) in cAF patients, likewise the response of the channels to acetylcholine (Brundel, Van Gelder, Henning, Tuinenburg, et al., 2001; Voigt et al., 2010). However, $I_{K,ACh}$ is constitutively active in cAF, i.e. $I_{K,ACh}$ remains active even in the absence of active modulation by the G-protein coupled-muscarinic receptors (Dobrev et al., 2001; Makary et al., 2011; Voigt et al., 2010). This enhanced activity of $I_{K,ACh}$, which is reported to be due to abnormal protein kinase C phosphorylation (Voigt et al., 2007), contributes to the shortening of APD, which encourages re-entry (Kneller et al., 2002). Furthermore, a significantly diminished I_{to} density is a consistent finding in cAF, accompanied by downregulation of mRNA levels of its α-subunit Kv 4.3 (Bosch et al., 1999; Grammer et al., 2000). A similar observation has been documented for the atrial specific I_{Kur} where a reduction in the current density was observed in cAF patients compared to patients with normal sinus rhythm (Wettwer et al., 2004).

1.5.2 Structural remodelling in AF

Structural remodelling in the atria is one of the most recognised changes in AF and is defined by fibrosis, hypertrophy of cardiac myocytes and disruption in the distribution of connexins (Schotten et al., 2011). Fibrosis, which describes the excessive accumulation of extracellular matrix (ECM) proteins, is the predominant structural change that forms a substrate for the development of AF. Experimental findings in different AF animal models have demonstrated an increase in atrial fibrosis (reviewed in Schüttler et al., 2020). A rapid pacing goat AF model demonstrated an increase in the ECM volume per myocyte after four months of pacing (Ausma et al., 2003). Furthermore, both a rapid pacing equine AF model and canine AF model mediated by induction of congestive heart failure also showed increased collagen deposition in the atria (Everett IV et al., 2006; Hesselkilde et al., 2019). Importantly, increased collagen accumulation has also been observed by many immunohistochemical studies in biopsies from cAF patients (reviewed in Dzeshka et al.,

2015), as well as patients with identified risk factors of AF, namely valvular diseases (Anné et al., 2005), dilated cardiomyopathy (Ohtani et al., 1995) and increasing age (Gramley et al., 2009). Additionally, the degree of collagen accumulation has been reported to correlate with the development of poAF and the recurrence of AF after open-heart surgery (Goette et al., 2002).

The structural changes described above are well known to cause conduction disturbances in atrial tissue. In a canine AF model induced by mitral regurgitation, optical mapping revealed in areas with patches of interstitial fibrosis slower electrical conduction and increased directional dependency, which favour a unidirectional conduction block and subsequent inducibility of AF (Verheule, Wilson, et al., 2004). Similarly, in a recent study, left atrial appendages of cAF patients with thick interstitial collagen strands which caused a separation in myocardial fibres, exhibited slower conduction of electrical impulse and increased conduction block, which are substrates for re-entry development (Krul et al., 2015).

Alteration in distribution and expression of gap junction proteins (connexins) is also a structural alteration that is associated with AF (Kato et al., 2012). The connexins (mainly connexin 40 [Cx40] and 43 [Cx43] in the atria) situated in the intercalated disk are clusters of transmembrane channels connecting the cytoplasm of adjacent cardiomyocytes and enabling anisotropic signal conduction in cardiac tissue (Severs et al., 2008). Therefore, irregularities in the localisation, expression and activity of these channels could impair the propagation of electrical impulses, which could initiate and stabilise AF. Remodelling induced by AF in a goat model presented significant heterogeneity in the distribution of Cx40, reflected by redistribution of the Cx40 from the intercalated disks to the lateral margins of the myocytes (Van Der Velden et al., 1998, 2000). Also, atrial biopsies from cAF patients have shown reduced protein expression of both Cx40 and Cx43, as well as heterogeneous localisation of both connexins (Kostin et al., 2002). Interestingly, the disorganisation of connexins has been shown to correlate with increased collagen deposition (Rucker-Martin et al., 2006). Therefore, the impairment of myocyte coupling through fibrotic change within the atrium and added disorganisation of connexins can plausibly influence atrial conduction properties which could support re-entry.

Taken together, it is evident that the accumulation of ECM proteins plays an important role in the development of AF. However, most studies on ECM accumulation in AF are based on collagens. Understandably, collagens are the predominant markers of the ECM; nonetheless, other ECM proteins, such as the proteoglycans, fibronectin and fibrillin, which

have been implicated in other cardiac pathologies, may play a significant role in defining the composition of the ECM in AF. We further study these proteins in chapter 5 with particular focus on remodelling in the secretion of these ECM proteins in AF.

1.5.3 Remodelling of Ca^{2+} handling in AF

Studies in recent years have indicated abnormalities in the intracellular handling of Ca^{2+} in AF. These studies have connected the alteration in Ca^{2+} handling to afterdepolarisations (mainly DADs) which facilitate the emergence of ectopic foci and subsequent initiation of AF (Nattel & Harada, 2014). In normal cardiac myocytes, a robust Ca^{2+} release from the SR via the RyR2 is triggered mainly by $I_{Ca,L}$, during excitation-contraction coupling. However, altered Ca^{2+} handling could promote the unwarranted release of Ca^{2+} from the SR which can activate NCX1 leading to an inward electrogenic depolarising current which could lead to DADs (Voigt et al., 2012). This spontaneous SR Ca^{2+} release has been suggested to arise from either increased sensitivity of the RYR2 or elevated SR Ca^{2+} content levels (Nattel et al., 2020). An increase in RYR2 sensitivity has been demonstrated in a canine model of AF, with the abnormal activity attributed to hyperphosphorylation of RYR2 at the protein kinase A (PKA) site (Vest et al., 2005). This increased RYR2 sensitivity has also been observed in mice, increasing their susceptibility to AF (Chelu et al., 2009).

In concordance with animal studies, Hove-Madsen et al. revealed an increased occurrence of diastolic Ca^{2+} leaks in right atrial myocytes from patients with cAF (Hove-Madsen et al., 2004). Similar findings have been reported in both atrial myocytes from pAF and cAF patients regardless of their differences in molecular mechanisms (Neef et al., 2010; Voigt et al., 2012, 2014). In cAF patients, the SR Ca^{2+} content levels were comparable with normal sinus rhythm patients which excludes SR Ca^{2+} overload as a predisposing factor, but instead supports the altered activity of RYR2 (Neef et al., 2010; Voigt et al., 2012). Hyperphosphorylation by PKA has been suggested to be responsible for the excessive SR Ca^{2+} release events seen in cAF patients, causing an enhanced open probability of RYR2 (Vest et al., 2005). In a separate study, RYR2 hyperphosphorylation in cAF was observed in the Ca^{2+}/calmodulin-dependent protein kinase II (CaMKII) sites, accompanied by increased protein expression of CaMKII (Neef et al., 2010; Voigt et al., 2012). This phosphorylation by CAMKII, which occurs at the Ser2814 site of RYR2, is the principal factor responsible for the spontaneous Ca^{2+} release-mediated DADs seen in cAF (Voigt et al., 2012). On the other hand, CaMKII activity is unaltered in pAF patients compared to normal sinus rhythm patients, implying the aberrant Ca^{2+} release events in pAF are not a consequence of phosphorylation-mediated RYR2 dysregulation. An increased SR Ca^{2+}

content due to enhanced SERCA2a activity, which enhances the open probability of RYR2, and increased RYR2 protein expression are suggested to account for the RYR2 dysregulation seen in pAF (Voigt et al., 2014). Overall, alterations in Ca^{2+} handling indeed participate significantly in the initiation and maintenance of AF. However, although Ca^{2+} handling abnormalities in cAF and pAF are extensively documented, the role of Ca^{2+} in poAF is mostly unexplored.

Also, although the arrhythmogenic contribution of abnormal Ca^{2+} handling has been studied in detail, its role in the contractile dysfunction associated with AF, which is an independent risk factor for stroke, is still elusive. Some studies in animal models of AF have identified downregulation of $I_{Ca,L}$ as a contributing factor to the atrial contractile dysfunction associated with AF (Greiser et al., 2014; Lenaerts et al., 2009; Sun et al., 1998; Yue et al., 1997), however, atrial hypocontractility in cAF patients persists even after the restoration of electrical properties following cardioversion (electrical or pharmacological restoration of arrhythmia to normal sinus rhythm) (Schotten et al., 2011). Hence, the reduced $I_{Ca,L}$ alone does not account for the depressed contractile function of the atria in cAF patients. Assessment of the role of Ca^{2+} in the contractile dysfunction seen in cAF would provide valuable information which could be utilised in the development of therapeutics in the management of AF-induced complications. As poAF is an integral part of this thesis, we briefly introduce this atrial arrhythmia in the next section.

1.6 Postoperative atrial fibrillation (poAF)

PoAF, defined as new atrial arrhythmic episodes occurring immediately after surgery in patients with no prior history of AF, is the most important AF secondary to identifiable acute conditions (Dobrev et al., 2019). This postoperative arrhythmia is a frequent complication of patients undergoing cardiac surgery, with 10-60% of these patients developing poAF mainly between 2-4 days post-surgery (Dobrev et al., 2019; Lapar et al., 2014; Maesen et al., 2012). This complication also occurs within the postoperative period of patients undergoing non-cardiac surgeries, in other organs including the lungs and abdomen (Garner et al., 2017; Riber et al., 2014); however, incidences in these patients are lower (0.3-29%) (Bhave et al., 2012; Maesen et al., 2012). Advancing age is the most decisive risk factor of poAF, with elderly patients above 75 years presenting with impaired left atrial contractile function, which is a predictor of poAF (Melby et al., 2015; Verdejo et al., 2016). Although the episodes of poAF are usually transient and characterised by spontaneous termination with or without therapy, they are associated with an increased incidence of

postoperative complications, including stroke, acute kidney disease, lengthy hospitalisations and mortality (Dobrev et al., 2019). The prolonged hospital stay results in a consequent substantial increase in hospital costs of approximately $14,000 per patient, incurred from additional investigations and treatments on added days (Almassi et al., 2015; Walter & Heringlake, 2020).

Unlike cAF and pAF, where there is sufficient mechanistic evidence, the pathophysiological mechanisms in poAF are obscure. Transient perioperative factors are postulated to trigger poAF in cardiac surgery patients. The two major transient factors include the autonomic nervous system and inflammation (Dobrev et al., 2019). Increased sympathetic activation has been suggested by many findings to participate in the development of poAF. For instance, patients who develop poAF are associated with increased pre- and postoperative norepinephrine levels, compared to patients without poAF (Anderson et al., 2017; Kalman et al., 1995). Also, the occurrence of poAF is often preceded by an increased sympathetic tone, reflected by increased sinus rate and ectopic activity (Amar et al., 2003; Dimmer et al., 1998). Also, pharmacological enhancement of the sympathetic tone with agents such as the phosphodiesterase inhibitor milrinone and the β1-agonist dobutamine have been shown to increase the incidence of poAF (Feneck et al., 2001; Fleming et al., 2008). In line with this result, perioperative use of β-blockers, which diminish sympathetic activity, has been demonstrated to reduce incidences of poAF in many clinical studies (Walter & Heringlake, 2020; Workman et al., 2006).

Also, semblance between the time course of AF occurrence within the postoperative period and the secretory levels of pro-inflammatory markers suggests a role of inflammation in the mechanism facilitating AF occurrence (Dobrev et al., 2019; Maesen et al., 2012). An increased preoperative blood level of the interleukins, interleukin-2 and interleukin-6, which are inflammation-mediating cytokines, have been reported in patients who develop poAF (Gaudino et al., 2003; Hak et al., 2009; Pretorius et al., 2007); however, contradictory findings have also been reported (Girerd et al., 2009). Similarly, the complement reactive protein (CRP), which is a standard marker for inflammation, shows a similar trend in concentration changes when compared with incidences of poAF, as peak CRP blood concentrations are observed to overlap peak incidences of poAF (Maesen et al., 2012). Furthermore, elevated white blood cell count in poAF patents is suggested to be an independent predictor for poAF (Lamm et al., 2006). Together, these findings indicate a role of inflammation in the development of AF.

Although, inflammation and sympathetic activation are believed to facilitate the development poAF, the cellular and molecular mechanisms by which these triggers initiate and propagate poAF are unknown. Hence, a more detailed understanding of the causative mechanisms initiating and propagating poAF is essential for the development of novel therapeutic options.

1.7 Hypothesis and objectives

AF in recent times has advanced into an epidemic, progressing on a global scale not only in prevalence but also in its detrimental complications, which includes stroke. Despite this public health problem, management of this aberrant arrhythmia remains insufficient, hence, indicating a clinical need for novel therapeutic approaches. Remodelling of the atria, including changes in cellular electrophysiology and intarcellular Ca^{2+} handling, are backed with mechanistic evidence to contribute to the development of AF. However, insights into how these remodellings contribute to different forms of AF and their associated complications are still fragmentary. Therefore, in this present study, we aim to investigate:

1. the role of abnormal Ca^{2+} handling in the contractile dysfunction associated with cAF (Chapter 3),
2. the participation of Ca^{2+} handling abnormalities in both the pro-arrhythmogenic mechanisms predisposing patients to poAF and the contractile dysfunction associated with poAF (Chapter 4), as well as
3. the remodelling in ECM protein secretion as well as its contribution to the proarrhythmic mechanisms and contractile dysfunction associated with poAF and cAF (Chapter 5).

2 Materials and methods

2.1 Patients

Echocardiographic recordings and right atrial appendages utilised in this study were obtained from patients undergoing open-heart surgery. Atrial samples were obtained from patients with normal sinus rhythm and clinically defined persistent atrial fibrillation (cAF). For poAF classification, the rhythm of recovering patients during the postoperative period of 6 days was monitored with a continuous 3-lead electrocardiogram recorder and subsequently stored on a monitoring system. An experienced clinician conducted a manual analysis of the recorded data for the presence of abnormal rhythms. Regular sinus rhythm patients that had no previous documented episode of AF and no episode of AF both during surgery and postoperative monitoring period were assigned to the control group (Ctrl).

In contrast, sinus rhythm patients with no prior documented history of AF pre-surgery and during surgery, but developed AF episodes lasting more than 30 sec within the monitoring period were assigned to the poAF group. Written informed consent was obtained from all patients included in this study. Experimental protocols were also approved by the ethics committee of the University Medical Centre Göttingen (No. 4/11/18)

2.2 Speckle-tracking echocardiography

Standard 4 apical-chamber transthoracic greyscale images, acquired at 50 Hz over three cardiac cycles prior to cardiac surgery by a trained personnel, were obtained and analysed to assess left atrial function as described previously (Badano et al., 2018) using a speckle-tracking software (TOMTEC ARENA™ REF TTA2 LOT 31.00, TOMTEC, Germany).

Using the QRS onset as the initiation phase of the cardiac cycle, the endocardial border of the left atrium was manually traced from the septal to the lateral-mitral annulus, extrapolating traces across the pulmonary vein (see **Figure 5**). Traces were automatically segmented into six parts, followed by automatic tracking of the longitudinal deformation of each segment by the software. A generated deformation curve was then analysed to derive strain during the three phases of atrial deformation, i.e. reservoir, conduit and contraction phases. The reservoir strain (LASr) corresponds to deformation during atrial filling at the end of ventricular diastole till mitral valve opening while the conduit strain (LAScd) represents the strain during passive ventricular inflow due to diastasis after mitral opening

until the onset of left atrial contraction. Finally, contraction strain (LASct) denotes atrial deformation during ventricular filling due to actual left atrial contraction, which is defined by the sharp downslope in the curve, until the closure of the mitral valve.

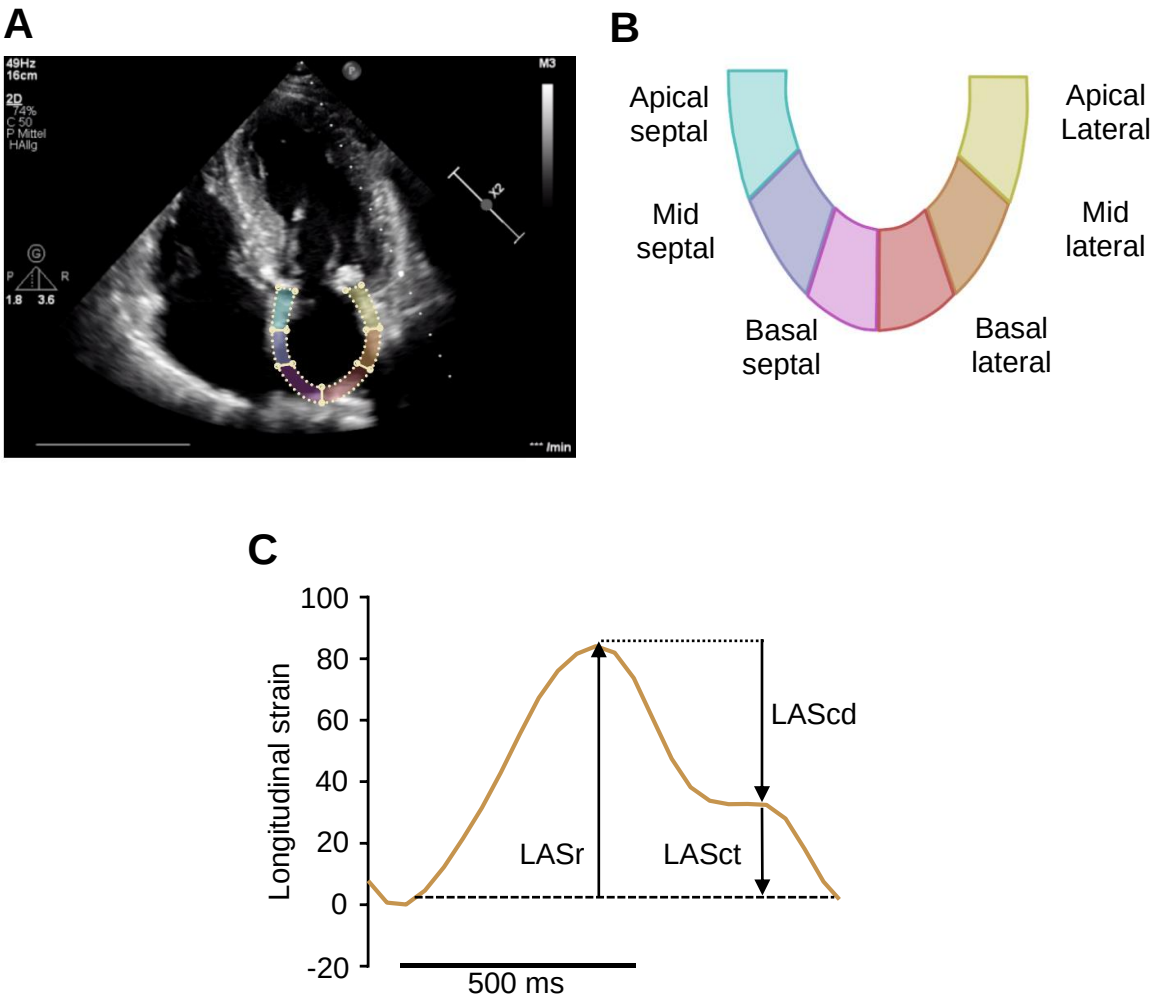

Figure 5. Echocardiographic speckle-tracking strain analysis. A, Representative apical four-chamber echocardiogram of a patient. The multi-coloured area defines the region of interest along the inner contour of the LA wall. **B**, Segment nomenclature of the LA wall. **C**, A typical mean strain curve of all segments indicating the three measurement points required for calculation of the reservoir strain (LASr), conduit strain (LASct) and the contraction strain (LASct). Adapted from Fakuade et al., 2020 (with permission)

2.3 Isolation of human atrial myocytes

2.3.1 Collection and preparation of tissue

Human right atrial appendages were obtained during routine cannulation of the right atrium (for extracorporeal circulation) of patients undergoing open-heart coronary bypass grafting and mitral valve replacement cardiac surgery. Excised tissue was immediately collected in a cardioplegic-based sterile transport solution (30 mM 2,3-butanedione monoxime, 20 mM

glucose, 10 mM KCl, 1.2 mM KH_2PO_4, 5 mM $MgSO_4$, 5 mM MOPS, 100 mM NaCl, 50 mM taurine; pH 7.0) to reduce energy and oxygen demands, thus reducing the production of toxic metabolic products (Voigt et al., 2015). Collected tissue was immediately transported to the laboratory within 10-20 minutes for cardiomyocyte isolation. An adapted protocol from a previously published method (Voigt et al., 2013) was used to isolate human atrial myocytes for patch-clamp experiments.

In brief, obtained atrial tissue was carefully trimmed of fat and weighed. Approximately, 200-700 mg was designated as the appropriate weight for cardiomyocyte isolation. Excess tissue was snap-frozen in liquid nitrogen and stored at -80°C for biochemical analysis. Weighed tissue was minced into small pieces of approximately 1 mm^3 in 4°C Ca^{2+}-free solution (**Table 1**), and subsequently washed three times at 37°C with fresh Ca^{2+}-free solution by stirring and gentle bubbling with 100% O_2 for 3 minutes in a jacketed heat beaker. Washed tissue was then strained with a nylon mesh to remove supernatant and subsequently subjected to two enzymatic digestion steps.

Table 1. Ca^{2+}-free solution

Components	Concentration
Glucose	20 mM
KCl	10 mM
KH_2PO_4	1.2 mM
$MgSO_4$	5 mM
MOPS	5 mM
NaCl	100 mM
Taurine	50 mM

pH adjusted to 7.0 with 1 M NaOH

2.3.2 Enzymatic digestion and storage of atrial myocytes

In the first digestion step, strained tissue pieces were resuspended in the jacketed beaker using a 20 ml Ca^{2+}-free solution (**Table 1**) containing 286 U/ml collagenase type I (Worthington, USA) and 5 U/ml protease XXIV (Sigma-Aldrich) enzymes and stirred gently for 45 minutes, adding 40 µl from a 10 mM $CaCl_2$ on the 10^{th} minute to obtain a final Ca^{2+} concentration of 20 µM. After 45 minutes, the supernatant was discarded by straining tissue with a nylon mesh (200 µm). Strained tissue pieces were returned to the jacketed beaker for the commencement of the second digestion step.

In the second digestion step, tissue pieces were resuspended again and stirred for 5 minutes in 20 ml Ca^{2+}-free solution containing only 286 U/ml collagenase type I (Worthington) with 40 µl of 10 mM $CaCl_2$ (to obtain a final concentration of 20 µm Ca^{2+}) at 37°C. After 5 minutes, samples were observed under the microscope to check for dissociated myocytes. This process was repeated every 3 minutes until striated rod-shaped myocytes were seen. Upon detection of myocytes, stirring was stopped and tissue chunks were collected after discarding the supernatant. Retained tissue chunk was immediately resuspended with 20 ml storage solution (1% w/v albumin, 10 mM glucose, 10 mM β-hydroxybutyric acid, 70 mM L-glutamic acid, 20 mM KCl, 10 mM KH_2PO_4, 10 mM taurine; pH 7.4 adjusted with 1 M KOH) to stop enzyme activity. Gentle mechanical trituration (taking care to avoid the formation of bubbles) for 3 minutes was then conducted using a 20 ml serological pipette to dislodge myocytes from the tissue. The supernatant containing dissociated myocytes was carefully strained into a 50 ml falcon tube using the nylon mesh. The 50 ml falcon tube was centrifuged at 90 *g* for 7 minutes to pellet myocytes after which supernatant was gently removed without disturbing the pellet. The pellet was then resuspended in 1.5 ml storage solution. With an interval of 10 minutes between each addition, 2 x 7.5 µl, and 15 µl of 10 mM $CaCl_2$ was added to resuspended myocytes to have a final concentration of 0.2 mM $CaCl_2$.

2.3.3 Fluo-3 loading of myocyte for patch-clamp experiments

Human atrial myocytes were loaded with the acetoxymethyl ester of the Ca^{2+}-sensitive fluorescence indicator Fluo-3 (ThermoFisher Scientific) as described previously (Voigt et al., 2013). In brief, a 1 mM Fluo-3 AM stock solution was prepared by reconstituting 50 µg of Fluo-3 AM with 44 µl of 20% w/v pluronic acid F-127 (Low UV, ThermoFisher Scientific) in anhydrous DMSO (Hybrid-Max, Sigma-Aldrich), which can be stored at -20°C. In total, 15 µl of the Fluo-3 AM stock solution was then added to 1.5 ml of myocytes suspension (1:100 dilution) and mixed gently using a serological pipette. Myocyte suspension was then incubated at room temperature away from light for 10 minutes, followed by centrifugation at 90 *g* for 7 minutes. The supernatant was carefully removed, while the myocyte pellet was resuspended in the appropriate volume of bath solution, usually 1.5 ml. Myocyte suspension was then allowed to stand for a minimum of 30 minutes to enable complete de-esterification of the Ca^{2+} indicator. Experiments were subsequently conducted for a maximum time of 6 hours after de-esterification. Only rod-shaped myocytes with clear and defined striations, which are established morphological markers that indicate high-quality myocytes, were utilised in experiments.

2.4 Cellular electrophysiology and Ca^{2+} imaging

2.4.1 The whole-cell patch-clamp setup

Ion fluxes across membranes and the corresponding changes in membrane potential of human atrial myocytes were quantified using the whole-cell patch-clamp technique. **Figure 6** shows a schematic of the experimental set up used for whole-cell patch-clamp experiments.

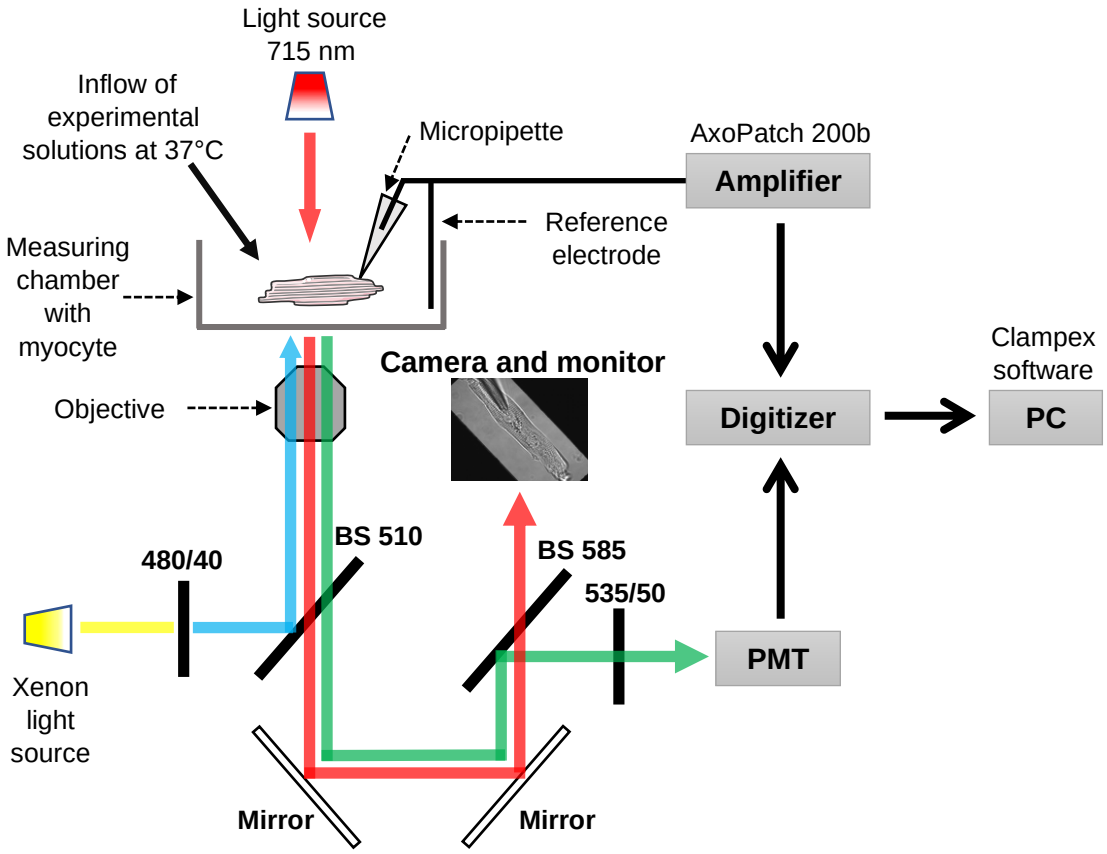

Figure 6. Experimental setup for cellular electrophysiology and Ca^{2+} epifluorescence measurements. Myocytes are dispensed into a measuring chamber, perfused with experimental solutions maintained at 37°C and viewed using a camera/monitor under a transilumination light of 710 nm. Electrophysiological recordings are obtained by establishing an electrical circuit between the recording electrode (micropipette), the reference electrode submerged in the bath and the amplifier. Analogue signals are digitised and viewed/recorded in a PC. For epifluorescence measurement, a xenon light source is beamed through a 480 nm excitation filter which is focused unto a beam splitter (BS, 510) which excites the myocyte in the measuring chamber. Emitted light at 510 nm from the myocyte is directed via two beam splitters (BS, 510 and BS 585) through an emission filter (535/50) unto the photomultiplier (PMT) which amplifies the optical signal. Modified optical signals are digitised and transmitted to the PC for recording/ analysis.

Firstly, a measuring chamber (RC-24E, Warner Instruments, USA) sealed with a glass coverslip was mounted on the head stage of an inverted microscope (Motic AE31). Suspended human atrial myocytes were subsequently dispensed into the diamond-shaped bath of the measuring chamber and allowed to settle at the bottom. Borosilicate

glass micropipettes of 1.5 mm diameter (World Precision Instruments, USA) were pulled and polished using a DMZ-universal electrode puller (Zeitz Instruments, Germany) to obtain a resistance of 2-4 MΩ (in bath solution) for voltage-clamp studies and 5-8 MΩ for current-clamp experiments. A pulled micropipette was subsequently filled with an internal solution (**Table 2**) and connected to a CV 203BU headstage (Axon, Molecular Devices, Sunnyvale, USA) via a pipette holder (1-HL-U, Axon, Molecular Devices, USA) with an extended silver/silver chloride (Ag/AgCl) electrode, ensuring that the electrode is submerged in the internal solution. A second Ag/AgCl electrode (reference electrode) running out of the CV 203BU headstage (Molecular Devices) was inserted into an isolated well on the measuring chamber containing 50 mM KCl, and connected to the bath via an agar bridge. Ag/AgCl electrodes were prepared by the chlorination of silver wires (Ag) (Axon, Molecular Devices) using automated electrolysis (ACl-01, npi electronics, Germany) in a 3 M KCl solution.

Table 2. Pipette solution for patch-clamp electrophysiology

Components	Concentration
DL-Aspartate K^+-Salt	92 mM
EGTA	0.02 mM
Fluo-3	0.1 mM
GTP-Tris	0.1 mM
HEPES	10 mM
KCl	48 mM
Mg-ATP	1 mM
Na_2ATP	4 mM

pH adjusted to 7.2 with 1 M KOH

Micropipette connected to the CV 203BU headstage (Molecular Devices) was then finely lowered into the bath solution using a micromanipulator (Scientifica, UK) and gently navigated towards the surface of an identified myocyte with the visual aid of a camera (MyoCAM-S w CFA300, IonOptix, USA). Upon contact with the myocyte membrane, gentle suction was applied using a glass syringe (Fortuna Optima, Poulten & Graf, Germany), until a high resistance seal in the giga-ohm range (2-6 GΩ) was formed between the tip of the micropipette and the membrane of the myocyte. At this point, the myocyte was perfused with normal bath solution (**Table 3**) via a gravity-driven perfusion system (VC3-8xG, ALA Scientific Instruments, USA) connected to a multi-tube heated inflow tip (MPRE8, Cell MicroControls, USA), at a constant temperature of 37°C. The measuring

chamber volume during constant perfusion was maintained by suction from the aspirator port of the chamber using a vacuum pump suction system (VWK, ALA Scientific Instruments, USA).

The gigaseal was allowed to stabilise for a few seconds after perfusion, followed by rupture of membrane portion in the pipette tip, by steady increasing suction or gentle suction pulses, to expose the intracellular content of the myocyte to the recording electrode. Myocytes were then subjected to either voltage-clamp or current-clamp protocols.

Data acquisition and protocols were performed using the Clampex 10.7 software (Molecular Devices) of the Axopatch 200B amplifier with an inbuilt low pass filter of 2 kHz, and its complimentary Axon Digidata 1440A, analogue to digital converter with a sampling rate of 10 kHz. All analyses of obtained data were conducted using the Clampfit 10.7 software (Molecular Devices).

Table 3. Bath solutions for patch-clamp electrophysiology.

Components	Bath solutions	
	Normal	**4-AP**
$CaCl_2$	2 mM	2 mM
Glucose	10 mM	10 mM
HEPES	10 mM	10 mM
KCl	4 mM	4 mM
$MgCl_2$	1 mM	1 mM
NaCl	140 mM	140 mM
Probenecid	2 mM	2 mM
4-aminopyridine		5 mM
$BaCl_2$		0.1 mM

pH adjusted to 7.35 with 1 M NaOH or 1 M HCl.

2.4.2 Epifluorescence Ca^{2+} measurement

Intracellular Ca^{2+} ($[Ca^{2+}]_i$) changes were simultaneously measured during patch-clamp experiments using the Ca^{2+}-sensitive fluorescent indicator, Fluo-3 (see **Figure 6**). Fluo-3 is single wavelength Ca^{2+} indicator, with maximum absorption and emission at 506 nm and 526 nm respectively, which upon binding to Ca^{2+} produces a 100-fold increase in fluorescence intensity. Human atrial myocytes were loaded before experiments using Fluo-3-AM (ThermoFisher Scientific), as described in **section 2.3.3**.

For $[Ca^{2+}]_i$ measurements, atrial myocytes in view under the microscope were framed in a rectangular area with the aid of a camera (MyoCAM-S w CFA300, IonOptix), to reduce background signal. Isolated myocytes were then excited using a xenon light source (UXL S50A, USHIO, JP) at 460–500 nm. The emitted fluorescence signal was transmitted via a dichroic mirror to the photomultiplier (PMT 400, IonOptix), where the signal was amplified, then digitised (1440A, Axon Digidata, Molecular Devices) and recorded using the Clampex 10.7 software (Molecular Devices).

To analyse $[Ca^{2+}]_i$ changes, emitted fluorescence light was converted to intracellular $[Ca^{2+}]_i$ assuming

$$[Ca^{2+}]_i = k_d \left(\frac{F}{F_{max} - F} \right)$$

where k_d is the dissociation constant of Fluo-3 at 37°C (864 nmol/L), F is Fluo-3 fluorescence, and F_{max} is saturated fluorescence of Fluo-3 by Ca^{2+}, acquired upon impaling of myocytes at the end of experiments (Trafford et al., 1999).

2.4.3 Whole-cell voltage-clamp protocols

After rupture of the membrane with an access resistance of <20 MΩ, myocytes were held at -60 mV while the capacitance and series resistance generated by microelectrode was compensated by 50-60% to enable an accurate measure of ionic currents.

2.4.3.1 Simultaneous measurement of L-type Ca^{2+} current ($I_{Ca,L}$) and Ca^{2+} transient

Ca^{2+} influx from the L-type Ca^{2+} channel ($I_{Ca,L}$) was measured by episodic stimulation of myocytes, as described previously (Voigt et al., 2012). Myocytes were stimulated at 0.5 Hz using a ramp and step protocol. Myocytes were held at -80 mV and gradually increased using a ramp of 20 ms to -40 mV to bypass and prevent the activation of the voltage-gated Na^+ current. An immediate quick step to +10 mV was used to activate the L-type Ca^{2+} channel and held on for 100 ms before returning to -80 mV. Interfering voltage-gated potassium currents were inhibited by perfusing myocytes with bath solution containing 4-aminopyridine and $BaCl_2$ (see **Table 3**), both of which synergistically inhibit K^+ channels. Isoprenaline was added to the bath solutions to investigate its effects on the $I_{Ca,L}$ upon

episodic stimulation at 0.5 Hz. Data obtained were analysed and interpreted using the Clampfit 10.7 software (Molecular Devices).

For $I_{Ca,L}$ and Ca^{2+} transient, 5 sweeps of recorded raw traces during steady-state were averaged for analysis. The peak $I_{Ca,L}$ was determined by positioning vertical cursors at the beginning and the inactivating end of the current (search cursors). A pair of vertical cursors were also positioned at proximity to one another at the inactivating end of the current (reference cursors) to define the baseline. The peak was defined as the maximum inward deflection from the baseline within the search area. The $I_{Ca,L}$ recorded in pA, was normalised to cell capacitance (pF), to be expressed as a function of cell size (pA/pF).

Also, the integral $I_{Ca,L}$, was quantified. Both search cursors and reference cursors were positioned as described above. With reference to the baseline, the area between the search cursors was quantified as a function of the current, i.e. $I_{Ca,L}$ (pA) over time (pA*s = pC). The integral of $I_{Ca,L}$ was also expressed as a function of cell size; thus normalisation to cell capacitance (pF), to give a unit of pC/pF which provides a measure of the total Ca^{2+} entering the cell per beat.

2.4.3.2 Determination of SR Ca^{2+} content

The total amount of Ca^{2+} in the SR available for systolic Ca^{2+} release was determined by the application of a high concentration of caffeine (Voigt et al., 2012). After steady-state episodic stimulation of myocytes at 0.5 Hz as described earlier (see **section 2.4.3.1**), cells were held at -80 mV and perfused with bath solution containing 10 mM caffeine. Caffeine causes an almost complete emptying of the SR by increasing the open probability of the RYR2. The rise in cytosolic Ca^{2+} causes an immediate extrusion of the Ca^{2+} from the cytosol by the NCX. Calculating the Integral of the NCX current (I_{NCX}) similarly to the integral of $I_{Ca,L}$ (see **section 2.4.3.1**), provides a measure for the SR Ca^{2+} content.

2.4.3.3 Estimation of diastolic SR Ca^{2+} leak

SR Ca^{2+} leak from the RyR2 was quantified as described previously (Shannon et al., 2002). Cells were stimulated at 0.5 Hz until steady state, followed by perfusion with a Na^{+}- and Ca^{2+}-free bath solution (5 mM 4-aminopyridine, 0.1 mM $BaCl_2$, 1 mM EGTA, 10 mM glucose, 10 mM HEPES, 4 mM KCl, 140 mM LiCl, 1 mM $MgCl_2$, 2 mM probenecid; pH 7.45 adjusted with 1 M LiOH) for 2 minutes to abolish trans-sarcolemmal Na^{+} and Ca^{2+} flux, i.e. NCX. Myocytes were then perfused with same bath solution including 1 mM tetracaine, to inhibit the RyR2. The difference in diastolic Ca^{2+} before and after tetracaine treatment gave an estimate of the diastolic SR Ca^{2+} leak.

2.4.4 Whole-cell current-clamp protocol

The whole-cell current clamp configuration was used to measure simultaneous APs and the corresponding $[Ca^{2+}]_i$ changes. With a continuous injection of current to hold membrane voltage at approximately -80 mV, APs were induced by the application of increasing 1 ms-current pulses (1-10 nA) to 20% above AP threshold, to depolarise the myocytes. APs were measured across a stepwise increase in stimulation frequency, initially starting from 0.25 Hz to 0.5 Hz, then 1–8 Hz with a constant increment of 1 Hz. Myocytes were perfused during all experimental steps with normal bath solution.

2.4.4.1 AP analysis and quantification of alternans

Simultaneous AP and CaT data acquired using the Clampex 10.7 software (Molecular Devices) were analysed, using a modified custom-written software developed and described previously (Pearman, 2014). Briefly, 32 acquired sweeps of APs and CaTs recordings were selected for each stimulation frequency, ignoring the initial 10 sweeps of every frequency. The selected recordings were superimposed, with the start of the upstroke of each signal chosen as the onset of each recording. The amplitude of individual APs and CaTs at defined time points were extracted for each beat in series. Oscillations between beat amplitudes in series were then quantified using a discrete Fourier transform, generating a magnitude spectrum that enables identification of deviations in measured amplitudes along the beat series. The manifestation of a peak at 0.5 cycles per beat in the generated magnitude spectrum (corresponding to every second AP) indicated the presence of beat-to-beat alternans, with the height of the manifested peak representing the difference in amplitude between average odd and even beats. The presence of true alternans barring the influence of noise was estimated by calculating the *k*-score

$$k\text{-score} = \frac{\sum T - \mu_{noise}}{\sigma_{noise}}$$

Where ΣT is the spectral magnitude at 0.5 cycles/beat. μ_{noise} is the mean spectral magnitude from 0.33 to 0.49 cycles/beat. σ_{noise} is the standard deviation of the spectral magnitude from 0.33 to 0.49 cycles/beat. *k*-score ≥ 3 was deemed to imply the presence of significant alternans.

2.5 Protein biochemistry

2.5.1 Tissue protein isolation

2.5.1.1 Membrane protein isolation and solubilisation

Approximately 20-30 mg of liquid nitrogen frozen right human atrial appendage was washed in a homogenising buffer (50 mM NaCl, 30 mM sucrose, 2 mM Na-EDTA and 20 mM HEPES) containing protease (cOmplete, Mini, EDTA-free protease Inhibitor cocktail, Roche, Switzerland) and phosphatase inhibitors (PhosSTOP, Roche) to remove residual blood. Washed tissue was lysed in fresh, ice-cold homogenising buffer using an electrical homogeniser (MICCRA-D1) followed by a brief period of douncing strokes (20-30 strokes). The homogenisation step was repeated two more times to get rid of excess fat in tissue. The resulting clear homogenate was centrifuged at 4°C and 100,000 *g* for 30 minutes to separate cytosol (in the supernatant) from membranes (in the pellet). The supernatant was discarded, while the pellet was solved in fresh homogenising buffer using the electrical homogeniser. The protein concentration was then determined using the Bradford assay (see **section 2.5.2.1**). The separated membranes were solubilized at 1 mg/ml of total protein in solubilization buffer (1.5% Triton X-100, 0.75% sodium deoxycholate, 0.1% SDS, 50 mM Tris-HCl pH 7.4, 10 mM NaCl, 0.5 mM Na-EDTA and 2.5 mM Na-EGTA) containing protease and phosphatase inhibitors for 30 minutes on ice. The solubilised product was further centrifuged at 55,000 *g* for 30 minutes at 4°C, with the supernatant containing the solubilised proteins collected afterwards in fresh tubes. The protein concentration of solubilised proteins was subsequently determined and followed by trichloroacetic acid (TCA) precipitation of the desired amount of solubilised protein.

2.5.1.2 Sarcomeric protein isolation

Sarcomeric proteins were isolated for phosphorylation studies and immunoblotting, as described previously (Layland et al., 2005), including minor modifications. Briefly, Snap-frozen tissue was thawed on ice and homogenised in 1 ml of relaxing buffer (see **Table 4**) including 1% Triton-X 100. The clear supernatant was centrifuged at 10,000 *g* for 10 minutes after which the supernatant was discarded. The pellet was then resuspended and homogenised three more times in 800 µl of rigor buffer (see **Table 4**) with 1% Triton-X 100 and centrifuged at 10,000 *g* for 10 minutes each time, discarding the supernatant after each centrifugation step. The resulting pellet was resuspended and washed with only rigor buffer to remove Triton-X 100. At this point, the protein concentration of samples was then determined using the DC assay kit (see **section 2.5.2.2**). The homogenised samples were

then pelleted by a 10 minute centrifugation step at 10,000 *g*. The recovered pellet was subjected to two more wash steps with wash buffer (see **Table 4**), centrifuging at 10, 000 *g* after each wash step and then solubilised in sample buffer (see **Table 4**) with an end concentration of 4 µg/µl. All buffers utilised for the isolation and processing of sarcomeric proteins were supplemented with protease (cOmplete™, Mini, EDTA-free protease inhibitor cocktail) and phosphatase inhibitors (PhosSTOP). Finally, 50 µg of total protein from each sample were loaded into each well of a sodium dodecyl sulphate-polyacrylamide gel electrophoresis (SDS-PAGE) gel for electrophoresis.

Table 4. Buffers for isolation of sarcomeric proteins

Components	Concentration			
	Relaxing buffer	**Rigor buffer**	**Wash buffer**	**Sample buffer**
ATP	1 mM			
2,3-Butanedione monoxime	50 mM			
Benzamidine-HCl	1 mM			
Bromophenol blue				0,05% v/v
DTT	1 mM			75 mM
EDTA	10 mM	2 mM		
EGTA	2 mM	2 mM		
Imidazole (pH 7.2)	10 mM	10 mM		
KCl	75 mM	75 mM	60 mM	
Leupeptin	1.25 mg/L	1.25 mg/L	1.25 mg/L	1.25 mg/L
$MgCl_2$	2 mM	2 mM	2 mM	
MOPS (pH 7.0)			20 mM	
NaF	50 mM	50 mM	50 mM	50 mM
NaN_3 (Sodium azide)	1mM	1mM		
Pepstatin	1.25 mg/L	1.25 mg/L	1.25 mg/L	1.25 mg/L
Phosphocreatine	4 mM			
PMSF	0.25 mM	0.25 mM	0.25 mM	0.25 mM
SDS				3% w/v
Sodium orthovanadate	0.25 mM	0.25 mM	0.25 mM	0.25 mM
Thiourea				2 M
Tris HCl (pH 6.8)				50 mM
Urea				8 M

2.5.2 Protein quantification

2.5.2.1 Bradford assay

The concentration of protein extracts was determined using Bradford assay, a colourimetric assay based on the measurement of the shift in absorbance of the Bradford (Coomassie) reagent (Bio-Rad, USA) from 470 nm to 595 nm upon interaction with proteins. To every 5 µl standard protein solutions of bovine serum albumin (BSA) (ranging 0.025 mg/ml – 2 mg/ml) and 5 µl of each sample, 200 µl of the 1:5 diluted Bradford reagent

was added in a 96-well plate and allowed to stand at room temperature for 15 minutes. The optical density at 595 nm (OD_{595}) was measured with a microplate reader (Flexstation 3, Molecular Devices, US; SPECTROstar nano, BMG LABTECH, Germany) and the protein concentration extrapolated from the BSA-generated standard curve.

2.5.2.2 Lowry assay

Sarcomeric proteins were quantified using the Lowry based DC protein assay (Bio-Rad). This assay is a detergent compatible colourimetric assay that measures the absorbance intensity of interactions between proteins and both copper-tartrate solution (Reagent A) and Folin reagent (Reagent B). Briefly, 25 µl of the working reagent A (Reagent A, 1:50 Reagent S) was added to 5 µl of both BSA standard solutions (0.025 mg/ml - 2 mg/ml) and protein samples in a microtiter plate. 200 µl of reagent B was then added to each well and agitated on a plate shaker to ensure proper mixing of reagents. The microtiter plate was kept at room temperature for 15 minutes, followed by the measurement of the absorbance at 650 nm in a microplate reader (Flexstation 3, Molecular Devices). The unknown protein concentration of samples was estimated from generated standard curves.

2.5.3 Trichloroacetic acid (TCA) protein precipitation

Trichloroacetic acid was added to known amounts of solubilised heart membrane proteins (300–500 µg) to a final TCA concentration of 12.5% w/v. Samples were vortexed gently and incubated for 30 minutes on ice. After incubation, samples were centrifuged for 8 minutes at 11,000 *g* with a constant temperature of 4°C. The resulting supernatant was discarded, and the pellet was washed twice by resuspending and mixing with 700 µl cold acetone (-20°C), centrifuging at 11, 000 *g* for 7 minutes after each wash step. After the last wash step, the supernatant was removed, and the pellet was dried for 10 minutes at 37°C to ensure complete evaporation of residual acetone. Dried pellet was resuspended in Laemmli buffer (250 mM Tris-HCl pH 6.8, 10% SDS, 0.50% bromophenol blue and 50% glycerol) (Laemmli, 1970) including 100 mM dithiothreitol (DTT), followed by incubation with gentle agitation at 40°C for 20 minutes to ensure complete dissolution of the pellet. Samples were loaded into wells for SDS-PAGE gel electrophoresis and subsequent immunoblotting.

2.5.4 Gel electrophoresis

Sample proteins were electrically separated based on their molecular weight using SDS-PAGE (Laemmli, 1970). For each sample, 50–70 µg of total protein was incubated at 95°C for 5 minutes in modified Laemmli buffer. Samples were loaded onto a Tris-glycine

discontinuous gel with a 4% stacking component and 7.5% resolving component (7.5% Mini-PROTEAN TGX Precast Protein Gels, Bio-Rad, USA), and electrophoresed at 200 V for 30 minutes in running buffer (25 mM Tris, 192 mM glycine, 0.1% SDS). PageRuler Plus or HI Mark Pre-stained standards were used to determine molecular weights of proteins. The electrophoresed gel was either used for further phosphorylation assays or immunoblotting.

2.5.5 Immunoblotting

After gel electrophoresis, the separated proteins were transferred to nitrocellulose membranes (pore size - 0.2 µM, Bio-Rad, Germany) using a high throughput Trans-Blot Turbo transfer system (Bio-Rad), as described by the manufacturer. Briefly, transfer stacks (comprising 7 filter pads each) and nitrocellulose membranes (both Transfer-Blot Turbo RTA transfer kit, Bio-Rad) were equilibrated in 1X transfer buffer (5X transfer buffer stock, Bio-Rad) containing 20% ethanol. A gel and a nitrocellulose membrane were stacked between the two wetted transfer stacks placed between the anode and cathode of the cassette. The cassette was then inserted into the Turbo base unit, and transfer was conducted for 7 minutes at 2.5 A (Mixed MW protocol). After transfer, nitrocellulose membranes were rinsed briefly with water and stained for total protein by incubation in 5 ml of Revert 700 total protein stain (LI-COR, USA) for 5 minutes with gentle agitation. Stained nitrocellulose membranes were rinsed twice with wash solution comprising 6.7% glacial acetic acid and 30% methanol in H_2O (Revert wash solution, LI-COR) to remove unbound dye and later visualised using a digital imaging system (Odyssey CLx, LI-COR). Nitrocellulose membranes were destained for 5-10 minutes in 0.1 M NaOH and 30% methanol in H_2O (Revert reversal solution, LI-COR) followed by blocking in 0.1% tween in Tris-buffered saline (TBST) containing 5% fat-free milk for 2 hours or in 1X Roti Block blocking reagent (Carl Roth, Germany) for an hour for chemiluminescence detection and infrared detection, respectively. Blocked membranes were washed three times in TBST for 15 minutes each and incubated overnight at 4°C in primary antibody (see **Table 5**) diluted in their corresponding blocking solutions. Nitrocellulose membranes were washed three times in TBST for 15 minutes after incubation in primary antibody, and subsequently incubated for 1 hour at room temperature in horseradish peroxidase (HRP) conjugated secondary antibodies or secondary antibodies labelled with near-infrared dyes (incubation in the dark) (see **Table 6**) in 5% milk in TBST and 1X Roti Block blocking reagent, respectively. Finally, membranes were washed three times with TBST for 15 minutes. For chemiluminescence detection, membranes were incubated in enhanced

chemiluminescent reagent (SuperSignal, West Femto Maximum Sensitivity substrate, ThermoFisher Scientific) for 1 minute, followed by visualisation using the digital imaging scanner (C-Digit Blot Scanner, LI-COR). For fluorescence detection, membranes were visualised using an infrared imaging system (Odyssey CLx, LI-COR). Band intensity was quantified using Image Lab software (Bio-Rad) and corrected using total protein normalisation.

Table 5. Primary antibodies used for immunoblotting studies

Antigen	Species	Source	Cat. No.	Dilution
COL4A2 (Collagen IV)	Rabbit	Abcam	ab6586	1:1000
DCN (Decorin)	Goat	ThermoFisher Sci.	PA5-19151	1:500
GAPDH	Rabbit	Cell Signalling	2118S	1:1000
LGALS3 (Galectin-3)	Rabbit	Abcam	ab31707	1:1000
MFAP-4	Rabbit	Abcam	ab169757	1:1000
NCX1	Mouse	ThermoFisher Sci.	MA3-926	1:500
Phospholamban	Mouse	Abcam	ab 2865	1:500
POSTN (Periostin)	Rabbit	Novus Biologicals	NBP1-30042	1:1000
pSer 16 Phospholamban	Rabbit	Badrilla Ltd	A010-12	1:500
pThr 17 Phospholamban	Rabbit	Badrilla Ltd	A010-13	1:500
RYR2	Mouse	ThermoFisher Sci.	MA3-916	1:250
SAP (Serum Amyloid P)	Rabbit	Abcam	ab45151	1:10000
Ser2808 RYR2	Rabbit	Badrilla Ltd	A010-30	1:250
Ser2814 RYR2	Rabbit	Badrilla Ltd	A010-31	1:250
SERCA2a	Goat	SantaCruz	Sc-8095	1:1000
TGFβ1	Rabbit	Abcam	ab179695	1:1000
VCAN	Rabbit	Merck	AB1033	1:1000
VIM (Vimentin)	Mouse	Abcam	ab8069	1:1000

Table 6. Secondary antibodies used for immunoblotting studies

Antibody	Source	Colour	Cat. No.	Dilution
Goat anti-mouse, H+L chain specific peroxidase conjugate	Merck Millipore	Greyscale	401215-2ML	1:10000
IRDye 680RD Donkey anti-Mouse 1gG (H+L)	LI-COR Biosciences	Red	P/N 926-68072	1:10000
IRDye 800CW Donkey anti-mouse IgG (H+L)	LI-COR Biosciences	Green	P/N 926-32212	1:10000
IRDye 800CW Donkey anti-rabbit IgG (H+L)	LI-COR Biosciences	Green	P/N 926-32213	1:10000
IRDye 800CW Donkey anti-goat IgG (H+L)	LI-COR Biosciences	Green	P/N 926-32214	1:10000
Mouse anti-Rabbit, HRP conjugated	Jackson ImmunoResearch	Greyscale	211032171	1:5000
Rabbit anti-Goat HRP conjugated	Dako	Greyscale	PO449	1:5000
Goat anti-Mouse HRP conjugated	Jackson ImmunoResearch	Greyscale	115035174	1:5000

2.5.6 Protein phosphorylation assay

The phosphorylation status of sarcomeric proteins was quantified using the fluorescent-based gel-staining dyes, ProQ Diamond (Invitrogen, USA) and SYPRO™ Ruby (Invitrogen), which stain phosphoproteins and total proteins, respectively. For phosphoprotein quantification, gels were incubated at room temperature in fixing solution (50% methanol and 10% acetic acid) for 30 minutes with gentle agitation. The fixing step was repeated one more time to ensure complete removal of SDS. Fixed gels were washed three times by gentle agitation in $_{dd}H_2O$ for 10 minutes. After washing, gels were incubated in 60 ml of ProQ Diamond in the dark for 1 hour on an orbital shaker. Gels were immersed in ProQ Diamond destaining solution and incubated with gentle agitation for 30 minutes in the dark. The destaining step was repeated two more times to ensure complete removal of background staining, followed by two washes with $_{dd}H_2O$ for 5 minutes. For detection, images of gels were acquired with the ChemiDoc Imaging System (Bio-Rad, USA) using excitation and emission wavelengths of 555 nm and 580 nm, respectively. After imaging, gels were immediately incubated at room temperature overnight in 60 ml SYPRO Ruby gel stain on an orbital shaker. Gels were washed for 30 minutes in 100 ml wash buffer (10% methanol and 7% acetic acid) while gently shaking. Next, gels were washed with $_{dd}H_2O$ for 5 minutes twice. ChemiDoc imaging system was then used to image and document gels

using 450 nm and 610 nm as excitation and emission parameters. Phosphorylation levels were measured by normalising ProQ™ Diamond phosphoprotein dye signal to SYPRO™ Ruby total protein signal.

2.6 Gene expression analysis

2.6.1 Ribonucleic acid isolation

Total RNA was isolated from human right atrial tissue samples using the TRIzol reagent (#15596018, ThermoFisher Scientific) as described by the manufacturer. In brief, frozen tissue samples were first homogenised in liquid nitrogen using a pestle and mortar. One ml of TRIzol reagent was added to 50 mg each of homogenised tissue samples in nuclease-free tubes followed by gentle mixing using a vortex. Next, 200 µl of Chloroform was subsequently added to the homogenised samples and mixed thoroughly. Samples were briefly incubated for 3 minutes and then centrifuged at 12,000 *g* for 15 minutes at 4°C. The upper aqueous phase of each sample containing RNA was gently removed and mixed with 500 µl isopropanol in new nuclease-free tubes followed by subsequent incubation at 4°C for 10 minutes for RNA precipitation. Samples were then centrifuged at 12,000 *g* for 10 minutes at 4°C. The supernatant was carefully removed, while the resultant RNA pellet was washed by resuspension and gentle vortexing in 1 ml of 75% ethanol, followed by centrifugation at 12,000 *g* for 10 minutes. After centrifugation, the supernatant was discarded while the pellet was air-dried at room temperature. The RNA pellet was resuspended in 20 µl nuclease-free water and quantified using a spectrophotometer (NanoPhotometer, Implen, Germany). One µg of RNA from each sample was incubated in 10 µl DNase treatment buffer (1U DNase I, 10 mM Tris-HCl pH 7.5, 2.5 mM $MgCl_2$ 0.1 mM $CaCl_2$ in DEPC-treated water; ThermoFisher Scientific) at 37°C for 10 minutes to rid RNA samples of contaminating DNA. Isolated RNA samples were then stored at -80°C until subsequent experiments.

2.6.2 Complementary DNA (cDNA) synthesis

Complementary DNA (cDNA) was synthesised from 1 µg DNase-treated RNA using the RevertAid First Strand cDNA synthesis kit (#K1622, ThermoFisher Scientific) as recommended by the manufacturer. Briefly, 1 µg of DNase-treated RNA added to components of the kit to obtain a reaction mix comprising 10 U/µL of reverse transcriptase, 1 U/µl of RNase inhibitor, 1 mM deoxyribonucleotide triphosphate (dNTPs), 5 µM random hexamer primers and 1 µg RNA in a total volume of 20 µl. cDNA synthesis was started with a 5-minute incubation at 25°C, followed by 60 minutes at 42°C and was terminated

by heating to 70°C for 5 minutes. The reverse-transcribed cDNA was then used for real-time polymerase chain reaction (PCR).

2.6.3 Quantitative reverse-transcription polymerase chain reaction (RT-qPCR)

To assess relative levels of gene expression, real-time RT-qPCR was employed. To this end, 25 ng of cDNA were added to a master mix comprising 10 µl SsoAdvanced Universal SYBR Green supermix (1725271, Bio-Rad), forward and reverse primers (see **Table 7**) and nuclease-free water to make a final volume of 20 µl. The RT-qPCR reaction was then performed using a CFX96 Real-Time System (Bio-Rad) at 95°C for 10 minutes, followed by 40 cycles of 95°C for 15 sec and 60°C for 1 minute, with a melt curve analysis performed after 40 cycles to ensure amplicon specificity. For relative quantification of amplicon levels, the ΔΔCq method was employed (Livak & Schmittgen, 2001). Expression of all target genes was first normalised to the respective reference gene. Fold changes were calculated by subtracting average Cq values of test group from that of the Ctrl group to obtain ΔΔCq values.

Table 7. Primer sequences (5' to 3') for RT-qPCR.

Gene	Forward primer	Reverse primer
GAPDH	GGAAGGTGAAGGTCGGAGTCA	GTCATTGATGGCAACAATATCCACT
HPRT1	CCTGGCGTCGTGATTAGTGAT	AGACGTTCAGTCCTGTCCATAAT
ATP2A2	CATCAAGCACACTGATCCCGT	CCACTCCCATAGCTTTCCCAG
PLB	ACCTCACTCGCTCAGCTATAA	CATCACGATGATACAGATCAGCA
SLN	ATGGTCCTGGGATTGACTGAG	GTGCCCTCGGATGGAGAATG
RYR2	GGCAGCCCAAGGGTATCTC	ACACAGCGCCACCTTCATAAT
SLC8A1	GACCTCGGTCCTAGCACCAT	ACACCAGGAGATATGACAGACAA

2.7 Force measurement of skinned right atrial muscle fibres

2.7.1 Skinning of right atrial muscle fibres

Human atrial skinned muscle fibres were processed as described previously (Bening & Leyh, 2016; Morano et al., 1988). In brief, right atrial appendages were obtained during cardiac surgery in ice-cold (4°C) Krebs-Henseleit cardioplegic solution (118.07 mM NaCl, 11.1 mM glucose, 4.7 mM KCl, 25 mM $NaHCO_3$, 1.2 mM KH_2PO_4, 1.2 mM $MgSO_4$,

1.8 mM $CaCl_2$) containing 30 mM 2,3-butanedione monoxime. The collected sample was transported immediately to the laboratory and transferred into a chilled preparation solution (68.08 mM imidazole, 65.01 mM NaN_3, 380.4 mM EGTA, 154.3 mM DTT, 203.3 mM $MgCl_2$ and 605.2 mM 5'-ATP-Na_2) for processing. Muscle bundles were excised from the atrial appendage and incubated with gentle agitation for 24 hours in preparation solution containing 1% Triton X-100 to permeabilise muscle fibre membranes (skinning). Skinned right atrial bundles were afterwards transferred to fresh, chilled preparation solution, followed by dissection under the microscope (Leica S6D, Leica Microsystems, Germany) to produce single right atrial muscle strips of approximately 2.5 mm × 0.3 mm in size. Muscle fibres were subsequently investigated for their calcium-induced force developments.

2.7.2 Isometric force measurement

Force measurements of right atrial muscle fibres were investigated using a gradient muscle investigation system (Scientific Instruments, Heidelberg, Germany), as described previously (Bening & Leyh, 2016). Briefly, right atrial muscle strips were fixed between two forceps in a perfusion chamber and incubated with a relaxation solution (68.08 mM imidazole, 65.01 mM NaN_3, 380.4 mM EGTA, 154.2 mM DTT, 203.3 mM $MgCl_2$, 605.2 mM 5'-ATP-Na_2 and 400 U/ml creatine kinase). A calcium contraction solution was made by adding $CaCl_2$ (147.02 mM) to the relaxation solution, which was subsequently utilised to produce desired free calcium concentrations by dilution with appropriate volumes of relaxation solution. Desired calcium concentrations were calculated using a software (Gradient program, Scientific Instruments) based on the Fabiato and Fabiato equation (Fabiato & Fabiato, 1972) and presented as pCa (-log of free Ca^{2+}). Right atrial muscle strips were exposed to increasing pCa solutions from 6.5–4.5 in 0.5 increments with their corresponding force developments recorded. Calcium-induced force measurements were conducted on three muscle fibres from each patient.

2.8 Proteomics analysis

2.8.1 Tissue processing and conditioning

Right atrial appendages were obtained during cardiac surgery in sterile cardioplegic transport solution (30 mM 2,3-butanedione monoxime, 20 mM glucose, 10 mM KCl, 1.2 mM KH_2PO_4, 5 mM $MgSO_4$, 5 mM MOPS, 100 mM NaCl, 50 mM taurine; pH 7.0) containing 0.1 mM $CaCl_2$, to prevent the occurrence of Ca^{2+} paradox during Ca^{2+} reintroduction (Rebeyka et al., 1990). Tissue was then trimmed of fat and washed three

times using ice-cold sterile transport solution. Approximately 100 mg tissue with all cardiac layers represented was used for further processing. Tissue was minced into small 2-3 mm strips in transport solution, which contains 2,3-butanedione monoxime to prevent contracture, which arises from the cutting injury (Mulieri et al., 1989). Tissue was minced delicately such that all cardiac layers were represented in each strip and washed with phosphate-buffered saline (14040133, Gibco, ThermoFisher Scientific) for 1 minute with gentle agitation. The wash step was repeated five times, and tissue was submerged in phosphate-buffered saline (PBS) for 2 minutes to ensure optimal removal of 2,3-butanedione monoxime and blood remnants. Tissue samples were then transferred into 24-well plates and incubated in serum-free medium (31053-028, Gibco) supplemented with 2 mM glutamine (25030-024, Gibco) and 100 U/ml penicillin/streptomycin (15140-122, Gibco) for 48 hours, whilst humified with 95% O_2 and 5% CO_2. Conditioned media was collected on the 24th (1st collection) and 48th hour (2nd collection) of incubation, replacing collected media with fresh medium after 1st collection. Both conditioned media and processed tissue samples were frozen at -80°C until further analysis. Conditioned media from the 2nd collection was utilised for mass spectrometry (MS), while frozen processed tissue was utilised for ECM protein extraction.

2.8.2 Processing of conditioned media

Schematic illustrating the processing of conditioned media for MS is shown in **Figure 7**. Conditioned media was concentrated using centrifugal filters (3 kDa Amicon Ultra-0.5 centrifugal filters, MilliporeSigma, USA) by centrifuging at 14,000 *g* for 20 minutes, and quantified of its protein concentration using the Bradford assay (see **section 2.5.2.1**). Next, 20 µg of conditioned media proteins were then precipitated by addition of pre-refrigerated (-20°C) 100% acetone (1:6, conditioned media: acetone) followed by incubation at -20°C overnight. Precipitated proteins were then pelleted by centrifugation at 16,000 *g* for 45 minutes at 0°C. The acetone supernatant was removed carefully without disturbing the pellet and discarded, followed by drying on a vacuum concentrator (Savant SPD131DDA SpeedVac, ThermoFisher Scientific, UK). Precipitated proteins were subsequently deglycosylated as previously described (Barallobre-Barreiro et al., 2017). Briefly, dried proteins were resuspended using 20 µl of deglycosylation buffer (50 mM sodium acetate, 50 mM Tris HCl, 25 mM EDTA; pH 6.8) containing a cocktail of enzymes (Glycoprotein Deglycosylation Kit, Merck, Germany) including 0.25 U/ml β-N-acetyl-glucosaminidase (1:200), 0.015 U/ml β-1,4 galactosidase (1:200) and 0.025 U/ml recombinant α-2-3,6,8,9-neuraminidase (1:200) to debranch complex N-linked oligosaccharides and 0.013 U/ml

endo-α-N-acetyl-galactosaminidase (1:200) to rid glycoproteins of O-linked saccharides. In addition, 0.5 U/ml chondroitinase (1:100), 0.1 U/ml heparinase (1:500) and 0.1 U/ml endo-β-galactosidase (1:500) were added to remove large and repetitive glycosaminoglycan residues of proteoglycans. Samples were then incubated initially at 25°C for 2 hours, followed by 36 hours at 37°C with agitation (240 rpm). After incubation, samples were vacuum dried for 45 minutes then resuspended and incubated in 20 µl of labelled $H_2{}^{18}O$ containing PNGaseF (1:100) at 37°C for 48 hours with agitation, to cleave and ^{18}O-label asparagine residues containing N-linked oligosaccharides.

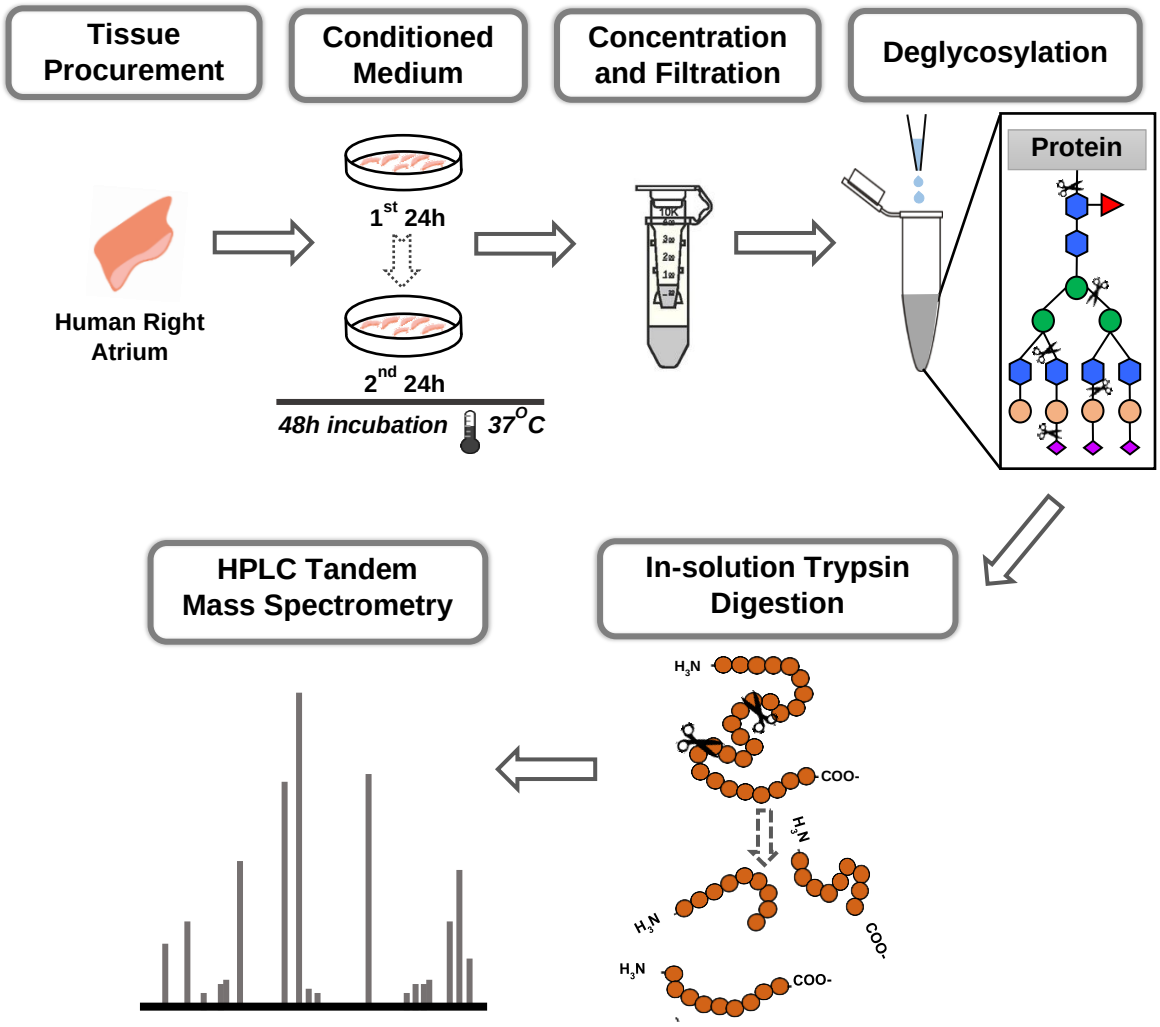

Figure 7. Illustration on the processing of conditioned media for mass spectrometry. Conditioned media was collected on the 24th and 48th hour of human right atrial sample incubation. 48th hour conditioned media were concentrated by ultra-centrifugal filtration using 3 kDa filter units. Protein concentrates were deglycosyated by sequential incubation with deglycosylating enzymes, followed by denaturation, reduction and alkylation of proteins samples. Samples were then digested in solution by trypsin into peptides. Peptide mixture was injected into the columns of the coupled High-performance liquid chromatography mass spectrometer for analysis of peptides.

2.8.3 In-solution trypsin digestion

Deglycosylated samples were denatured, reduced and alkylated prior to digestion as described previously (Barallobre-Barreiro et al., 2017). To denature proteins, a 9 M urea and 3 M thiourea mixture was added to deglycosylated samples in a 2:1 ratio with sample volume (final concentration of 6 M urea and 2 M thiourea). Sample proteins were reduced by aliquoting 100 mM DTT in a ratio of 1:9 to sample volume (final concentration 10 mM DTT) and incubating at 37°C for 1 h. 500 mM iodoacetamide (1:9) was then added to sample volume (final concentration 50 mM) to alkylate protein extracts in the dark for 45 minutes. Alkylated proteins were precipitated and pelleted by incubation with acetone (9:1) at -20°C overnight and centrifugation at 16, 000 *g* as described in the previous

section. Pelleted proteins were vacuum dried and resuspended in 176 µl of 0.1 M triethylammonium bicarbonate (TEAB; pH 8.2). Lyophilised trypsin/LysC (Promega, V5073) was resuspended in 50 mM acetic acid (pH 3) and 0.67 µg of trypsin/LysC were added to the alkylated protein solution to produce a trypsin/LysC: alkylated protein ratio of 1:30 (w/w). The reaction mix was vortexed and briefly centrifuged before incubation at 37°C for 20 hours with agitation. Enzymatic digestion was stopped by acidification of reaction mix using 10% v/v trifluoroacetic acid (TFA, pH 0) in a ratio of 1:9 with sample volume (final concentration 1% TFA), and resulting peptides were submitted for clean up.

Peptide clean-up was done using an automated high-throughput liquid handling platform (AssayMAP Bravo, Agilent Technologies, USA). Peptides were purified using AssayMAP C18 Cartridges (prod. no. 5190-6532, Agilent Technologies) using a methodological sequence described by the manufacturer. In brief, the cartridge resin was primed using 100 µl of 50% acetonitrile (ACN) + 0.1% TFA in H_2O at a flow rate of 300 µl/minute and equilibrated using 50 µl of 1% ACN + 0.1% TFA in H_2O (flow rate 10 µl/minute). Peptide samples were then loaded onto the C18 cartridges using a controlled flow rate (5 µl/minute) to ensure adequate exposure of samples to the resin and subsequently washed with 50 µl of 1% ACN + 0.1% TFA in H_2O (flow rate 10 µl/minute) to remove impurities with a low affinity to the C18 resin. Finally, cleaned peptides were eluted with 30 µl of 70% ACN + 0.1% TFA in H_2O at a flow rate of 5 µl/minute into a 96-well plate. Eluates were then vacuum dried for 45 minutes, followed by resuspension of dried peptides with 2% ACN + 0.05% TFA in H_2O. Peptides were then analysed using liquid chromatography-tandem MS.

2.8.4 Liquid chromatography-tandem mass spectrometry (LC-MS/MS) analysis

Resuspended peptides were separated using a nano-liquid chromatography system (Dionex Ultimate 3000 RSLCnano, ThermoFisher Scientific). Peptides were loaded onto a trap cartridge (prod. no. 160454, ThermoFisher Scientific) for 3 minutes using 0.1% formic acid in H_2O at a flow rate of 25 µl/minute. The sample peptides were subsequently separated using a nano-LC solvent gradient as stated; flow rate 0.25 µl/min; 0-10 minutes, 4-10% B; 10-75 minutes, 10-30% B; 75-80 minutes, 30-40% B; 80-85 minutes, 40-99% B; 85-89.8 minutes, 99% B; 89.8-90 minutes, 99-4% B; 90-120 minutes, 4% B; where A was 0.1% formic acid in H_2O and B was 80% ACN, 0.1% formic acid in H_2O. The nano column (prod. no. ES803A, ThermoFisher Scientific) was connected to an Easy-Spray NG Source (ThermoFisher Scientific) and kept at 45°C. Mass spectra were obtained using an Orbitrap Fusion Lumos Tribrid mass spectrometer (ThermoFisher Scientific) operating in data-

dependent Top Speed mode (cycle time 3 s). Survey full scan spectra were acquired over the mass-to-charge (m/z) range 350–1500 using Orbitrap detection (resolution of 120,000 at 200m/z). Dynamic exclusion duration was 60 s. Data-dependent MS2 scans were performed using Quadrupole isolation, collision-induced dissociation activation and Ion Trap detection.

2.8.5 Database search of LC-MS/MS data and data filtering

Raw data were analysed using Proteome Discoverer (version 2.3.0.523, ThermoFisher Scientific) and Mascot (version 2.6.0, Matrix Science). Raw files were searched against the human database (UniProtKB/Swiss-Prot version of January 2019, 20,425 entries) while the mass tolerance was set at 10 ppm for precursor ions and 0.8 Da for fragment ions. Trypsin was set as the protein-digesting enzyme with up to two missed cleavages being allowed. Carbamidomethylation of cysteine was chosen as a static modification. Oxidation of lysine, methionine and proline, and deamidation of asparagine in the presence of $H_2{}^{18}O$ were chosen as variable modifications. High-confidence identifications were accepted, with high confidence being determined by a q-value threshold of 0.01 as determined by the False Discovery Rate (FDR) approach of Proteome Discoverer's Percolator and Protein FDR Validator nodes. Additionally, identified proteins were filtered for a number of unique peptides greater than one. Peptide abundances were determined based on precursor ion intensity with the total peptide amount utilised for normalisation for every sample. Normalised precursor intensity was used for quantification and comparison.

2.8.6 ECM proteins extraction

Cardiac ECM proteins were isolated from processed right atrial samples obtained post-production of conditioned media (see **section 2.8.1**), using a modified protocol already described previously (Barallobre-Barreiro et al., 2017). All buffers utilised in this protocol were supplemented with a cocktail of protease inhibitors (P8340, Sigma Aldrich, USA) before use, to inhibit an extensive range of protease activity. Briefly, 30 mg each of processed right atrial samples were minced and rinsed gently in 300 µl PBS containing 25 mM EDTA (for metalloproteinases inhibition) to rid tissue of media contaminants. Washed samples were decellularised by incubation in 300 µl of 0.1% SDS buffer (0.1% SDS + 25 mM EDTA) accompanied with gentle agitation at a vortex speed of 600 rpm (to minimise mechanical ECM disruption) at 4°C for 16 hours. After incubation, SDS buffer was removed and stored at -20°C. Decellularized tissues were then rinsed in $_{dd}H_2O$ to remove residual SDS and subsequently incubated in 300 µl of guanidine hydrochloride (GuHCl) buffer (4 M GuHCl, 50 mM sodium acetate, 25 mM EDTA, p.H 5.8) for 48 hours at 4°C.

Incubation was accompanied with moderate agitation using a vortex speed of 700 rpm to ensure mechanical ECM disruption. The GuHCl extracts were then collected and stored at -20°C pending further use. GuHCl extracts were quantified for their proteins using Bicinchoninic (BCA) protein assay (Pierce BCA assay kit, Thermofisher Scientific), as described by the manufacturer, using BSA solutions (0.025 – 2mg/ml) as standards. In total, 30 µg of GuHCl extract proteins were precipitated by the addition of ice-cold 100% ethanol (1:10, extract: ethanol) and subsequent incubation at -20°C for 16 hours. After incubation, protein precipitates were pelleted by centrifugation at 14,000 *g* for 45 minutes at a constant temperature of 0°C. The supernatant was removed, and pellets were dried using the SpeedVac (Savant SPD131DDA SpeedVac, ThermoFisher Scientific). Dried protein pellets were resuspended in 30 µl of deglycosylation buffer containing all enzymes described earlier (see **section 2.8.2**), including PNGaseF (without $H_2{}^{18}O$). Samples were then incubated with gentle agitation for 2 hours at 25°C followed by 48 hours at 37°C to ensure proper deglycosylation of ECM glycoproteins. Deglycosylated protein extracts were subsequently investigated by immunoblotting.

2.8.7 Immunoblotting for ECM proteins

Deglycosylated proteins were precipitated using cold acetone as described above (see **section 2.8.2**), then denatured and reduced by the addition of a sample loading buffer (50 mM Tris, 1% SDS, 20% glycerol, 0.01% bromophenol blue and 0.25% β-mercaptoethanol) and subsequent incubation at 95°C for 5 minutes. Protein components of samples were separated by gel electrophoresis using 4–12% polyacrylamide gradient gels (NuPage, Invitrogen) in 4-morpholinepropanesulfonic acid-SDS running buffer (MOPS-SDS, Nupage, Invitrogen), with a voltage set at 130 V. After electrophoresis, separated proteins were transferred from the polyacrylamide gel unto a nitrocellulose membrane (Amersham Protran 0.45 µm, GE Healthcare Lifesciences, UK) in pre-chilled transfer buffer (25 mM Tris base, 200 mM glycine and 20% methanol) using 350 mA for 2 hours. The membrane was stained for total protein using a Ponceau S solution (Sigma) and scanned afterwards. The membrane was briefly washed with 0.1% Tween in PBS (PBST) to rid the membrane of Ponceau dye and blocked with 5% fat-free milk in PBST for 1 hour on a rocking table. After blocking, the membrane was washed briefly with PBST and incubated with primary antibody (see **Table 5**) in PBST containing 5% bovine serum albumin and 0.01% sodium azide overnight at 4°C on a rocking table. Following incubation, membranes were washed three times with PBST for 15 minutes and incubated for a further 1 hour at room temperature in a HRP-labelled secondary antibody (see **Table 6**) diluted in PBST

containing 5% fat-free milk. Membranes were subjected to 3 more washes with PBST (15 minutes each) and exposed to a chemiluminescence detection reagent (ECL, Amersham, GE Healthcare Life Sciences, UK) for 2 minutes. The membranes were exposed to chemiluminescent X-ray films (Amersham Hyperfilm, GE Healthcare Life Sciences, UK) and developed in an automatic film processor (Optimax 2010, Protec, Germany). Processed films were scanned (Epson perfection V700 Photo scanner, Epson, UK), with the intensities of immunoblots subsequently analysed by densitometry using Image J (NIH, USA), to assess differential protein expression amongst groups.

2.9 Statistical analysis

All statistical analyses were conducted using GraphPad Prism (Version 8.01, GraphPad Software, UK), SPSS (IBM, USA) and Microsoft Excel (Version 1908, Microsoft, USA) software. Distribution of data was tested for normality using the Shapiro-Wilk test. For continuous data, means of normally distributed data were compared using paired or unpaired Student's t-test where appropriate, while non-normal data were compared using Mann-Whitney's U-test and Wilcoxon's matched-pairs signed-ranks test for unpaired and paired data sets, respectively. Comparison between categorical data was assessed using Fisher's exact test. Statistical differences between three or more experimental groups were determined by a one-way analysis of variance (ANOVA), followed by a Dunnett's *post-hoc* analysis for normally distributed data, while the Kruskal Wallis test followed by a Dunn's *post-hoc* test. Kaplan-Meier curves were compared using Gehan-Breslow-Wilcoxon test. For ECM protein abundance, p-values were adjusted using the Benjamini-Hochberg approach, and a false discovery rate (FDR) threshold of 0.05 was used for adjusted p-values to infer statistical significance. Adjusted p-values are only stated in **Supplemental Table 1**. Data are presented as mean±standard error of the mean (SEM), except for clinical data presented as mean±standard deviation (SD) and otherwise stated. P-values <0.05 were considered statistically significant.

3 Ca^{2+} handling and contractile dysfunction in chronic atrial fibrillation (cAF)

Atrial contractile dysfunction is a characteristic feature of cAF that increases the vulnerability of cAF patients to stroke, which is the principal culprit for most AF-associated deaths (Darlington & McCauley, 2020). The atrial hypocontractility in cAF patients persists even after cardioversion from AF to SR for as long as 8 weeks, leading to atrial stasis which predisposes patients to thromboembolic events that contribute to the mortality associated with cAF (Darlington & McCauley, 2020; Denham et al., 2018). Also, the coexistence of AF with heart failure leads to the loss of the "atrial kick" which refers to the specialized atrial contraction required for ventricular filling, further worsening cardiac function (Brandenburg et al., 2019; Zafrir et al., 2018). These deleterious effects of the atrial contractile dysfunction associated with cAF are well-recognised (Goette et al., 2016), yet, the mechanism regulating this phenomenon is still not entirely clear.

Several studies in time past have focused on deciphering the mechanisms responsible for the AF-associated atrial hypocontractility using different animal models (reviewed in Clauss et al., 2019; Schüttler et al., 2020). Electrical remodelling, including the shortening of the APD and reduction of $I_{Ca,L}$, has been implicated in the atrial contractile dysfunction seen in these AF models. Structural alterations, including fibrosis, have also been highlighted by studies in different animal models of AF, to facilitate the impairment of atrial contractility (Clauss et al., 2019; Schüttler et al., 2020). Similarly, studies with cAF patient samples have also revealed electrical remodelling and structural alterations as contributing factors to the atrial contractile dysfunction seen in AF (Denham et al., 2018). However, most experiments in cAF patients were conducted in tissues bundles, which do not reflect in its entirety, cellular responses and changes, given that the reduction in contractility observed in these studies, could be influenced by other underlying factors that also contribute to atrial contractile dysfunction.

Furthermore, Ca^{2+} is the prime mediator of cardiac excitation-contraction coupling, making Ca^{2+}-handling abnormalities likely contributors to diminished atrial contractility seen in cAF (Voigt et al., 2012). However, although cytosolic Ca^{2+}-handling abnormalities are established contributors to AF pathophysiology, there is limited knowledge concerning their role in the impaired atrial contractility seen in atrial fibrillation. Therefore, here we aim to investigate on a cellular level the role of abnormal Ca^{2+} handling in the atrial contractile dysfunction seen in cAF patients.

3.1 Simultaneous $I_{Ca,L}$, CaT and cell shortening in atrial myocytes from cAF patients

To assess the effect of altered Ca^{2+} handling on cellular contractility in cAF patients. $I_{Ca,L}$, its corresponding triggered transient (CaT) and the resulting myocyte contractility were measured concurrently in human atrial myocytes. Both $I_{Ca,L}$ and CaT were measured using voltage-clamp techniques and simultaneous epifluorescence measurement, while the shortening of atrial myocytes was measured with the aid of an optical cell-edge tracking camera system (IonOptix). Patient characteristics in both cAF and Ctrl patients were comparable except for the significant increase observed in the left atrial diameter (LAD) of cAF patients (see **Table 8**).

Table 8. Characteristics of Ctrl and cAF patients used for voltage-clamp experiments

		Ctrl	cAF
General	Patients, n	28	11
	Sex, male/female	24/4	8/3
	Age, y	61.5±12.0	64.4±14.5
	Body mass index, kg/m^2	28.2±3.6	26.6±4.4
Intervention	CAD, n	17	4
	MVD/AVD, n	10	5
	CAD+MVD/AVD, n	0	2
	Intervention time, min	277.4±80.3	308.7±51.4
	ECC time, min	130.6±48.4	128.3±10.7
Anamnesis	Hypertension, n	21	7
	Diabetes, n	7	1
	Hyperlipidemia, n	15	2
	NYHA (I/II/III), n	8/6/9	1/2/2
	Stroke, n	1	2
	TIA, n	3	1
CC	Creatinin, µmol/L	1.00±0.27	1.00±0.17
Echocardiography	LAD, mm	40.5±5.9	52.6±5.8***
	LVEDD, mm	47.7±6.5	45.0±1.4
	IVSd, mm	13.3±3.1	11.7±1.3
	LVPWd, mm	12.5±3.0	11.3±1.2
	LVEF, %	51.2±12.7	50.8±13.4
	Diastolic dysfunction, Grade I/II/III	12/3/1	0/1/1
Medication	Digitalis, n	0	1
	ACE inhibitors, n	12	6
	AT1 blockers, n	10	2
	β-Blockers, n	20	4
	Dihydropyridines, n	6	2
	Diuretics, n	8	6
	Nitrates, n	3	1
	Lipid-lowering drugs, n	22	6

ACE, angiotensin-converting enzyme; AT, angiotensin receptor; CC, clinical chemistry; CAD, coronary artery disease; ECC, extracorporeal circulation; IVSd, interventricular septum thickness at end-diastole; LAD, left atrial diameter; LVEDD, left ventricular end-diastolic diameter; LVEF, left ventricular ejection fraction; LVPWd, left ventricular posterior wall thickness at end-diastole; NYHA, New York Heart Association Functional Classification; MVD/AVD, mitral/aortic valve disease; TIA, transient ischemic attack. Continuous data are expressed as mean±SD. ****P*<0.001.

Cell size was comparable in both cAF and Ctrl, as indicated by their similar mean capacitance values (cAF: 103.64±12.54 pF, n/N=8/5; Ctrl; 96.69±10.80 pF, n/N=17/10; *P*=0.539), as well as the sarcomere lengths between both groups (**Figure 8**). **Figure 9A** shows representative traces of the $I_{Ca,L}$ induced by a voltage-step protocol (0.5 Hz stimulation frequency), the corresponding CaT and cellular shortening measured simultaneously in Fluo-3-loaded right atrial myocytes. Both peak $I_{Ca,L}$ and its integral, which estimates the total amount of Ca^{2+} that enters the cell per beat, were markedly reduced in cAF compared to Ctrl (peak $I_{Ca,L}$,: 2.62±0.75 vs 7.65±0.47 $pApF^{-1}$, *P*<0.001; Integrated $I_{Ca,L}$: 0.05±0.02 vs 0.09±0.01 $pCpF^{-1}$, *P*<0.01, n/N=8/5 cAF vs n/N=17/10 Ctrl; **Figure 9B**). Furthermore, although no differences in the triggered systolic and diastolic Ca^{2+} levels were seen in both cAF and Ctrl groups, a significant reduction in the CaT amplitude was observed in cAF, which is consistent with previous studies (diastolic: 373±77 vs 192±19 nM, *P*<0.05; CaT amplitude: 143±28 vs 373±29 nM, *P*<0.01, n/N=8/5 cAF vs 17/10 Ctrl, **Figure 9C**). The contractile response of atrial myocytes to $I_{Ca,L}$ activation was also lower in cAF as demonstrated by the significant reduction of the fractional shortening of cAF atrial myocytes (cAF: 0.81±0.21%, n/N=8/5; Ctrl: 1.78±0.30%, n/N=17/10; *P*<0.01; **Figure 9D**) despite the similar cell length in cAF compared to Ctrl. These results suggest an important contribution of the L-type Ca^{2+} channel to the impaired contractility seen in cAF.

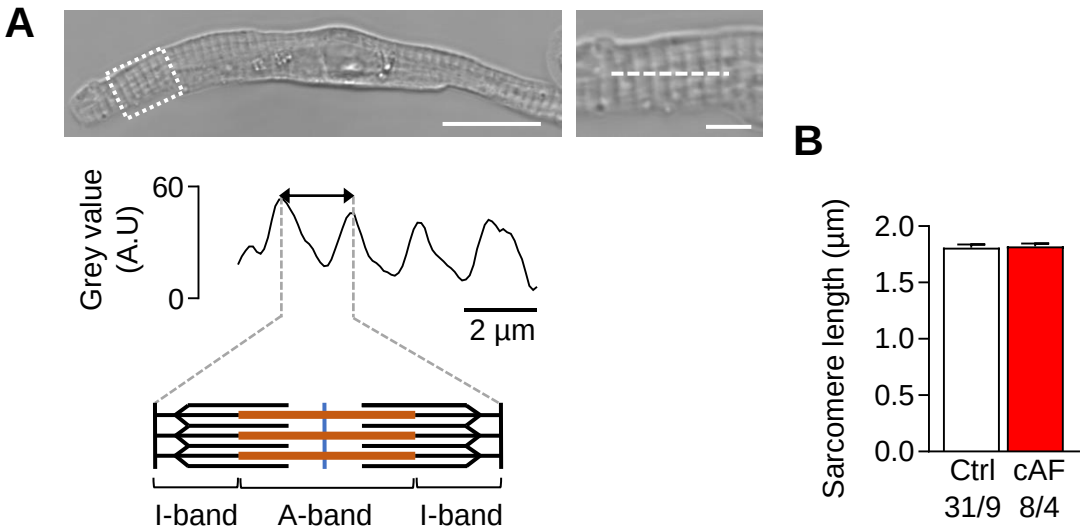

Figure 8. Optical measurement of sarcomere length in human atrial myocytes from Ctrl and cAF patients. A, Representative atrial myocyte (top left) with a marked (dotted box) and magnified (top right) region of interest showing the line trace for generating grey values for sarcomere length measurement. The peak and troughs of the grey value (bottom) represent the I- and A- bands of the sarcomeres, respectively. The distance between the two I-bands on both sides of an A-band is considered a sarcomeric unit, which in multiples allow sarcomere length measurements. **B,** Mean±SEM of sarcomere length measured from images of human atrial myocytes. n/N = number of myocytes/patients. Scale bar of whole myocyte image and magnified region of interest are 10 µm and 5 µm respectively.

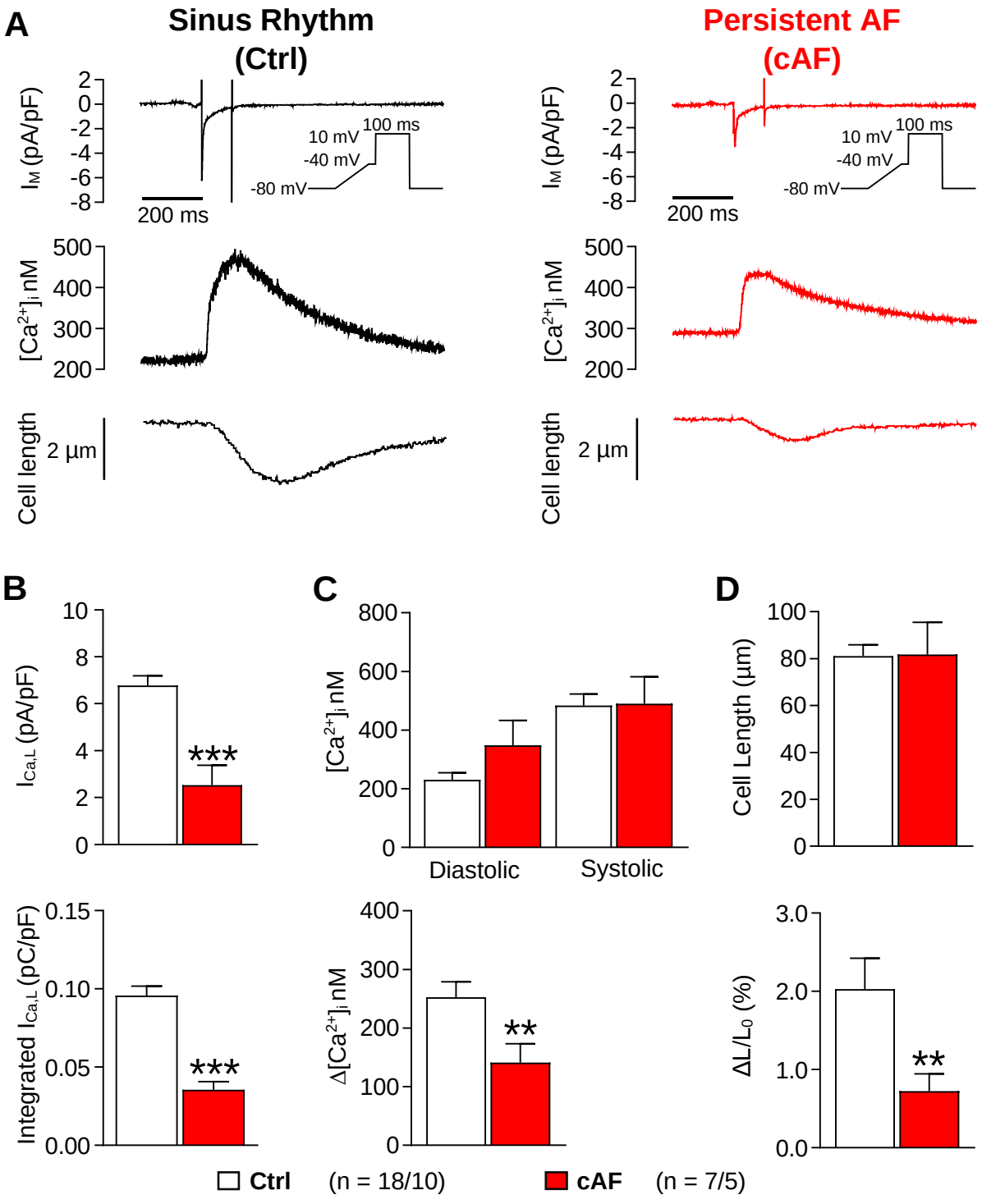

Figure 9. $I_{Ca,L}$-triggered Ca^{2+} transients (CaT) and corresponding cell shortening in atrial myocytes from sinus rhythm (Ctrl) and persistent atrial fibrillation (cAF) patients. A, Representative simultaneous recordings of $I_{Ca,L}$ (upper), CaT (lower) and cell shortening in Ctrl (left) and cAF (right) myocytes. 0.5 Hz Voltage clamp protocol (insert). **B**, Mean±SEM peak $I_{Ca,L}$ (upper) and integrated $I_{Ca,L}$ (lower). **C**, Mean±SEM diastolic and systolic $[Ca^{2+}]_i$ (upper) and resulting CaT-amplitude (lower). **D**, Mean±SEM cell length (upper) and cell fractional shortening (lower). **P*<0.05, ***P*<0.01 ****P*<0.001 vs Ctrl. n/N=number of myocytes/patients). Comparison using Mann Whitney U-test.

3.2 SR Ca^{2+} content and Ca^{2+} buffering of atrial myocytes from cAF patients

$[Ca^{2+}]_i$ levels regulate contractility of cardiac tissue, and alterations such as a decrease in systolic CaT amplitude could disrupt the normal contractile function of the heart. In addition to a decreased $I_{Ca,L}$, a reduced SR Ca^{2+} content could also result in a reduced systolic CaT amplitude, thus impairing atrial contractility. Therefore, to assess the role of the SR in both the decreased CaT amplitude and cell shortening detected in atrial myocytes from cAF patients, SR Ca^{2+} content was investigated. SR Ca^{2+} load was determined by the application of caffeine (10 mM) to induce an almost complete emptying of Ca^{2+} from the SR, after the termination of steady-state stimulation of human atrial myocytes using the $I_{Ca,L}$-activating protocol. No differences were seen in the amplitude of the resulting caffeine-induced Ca^{2+} transient (cCaT) and the corresponding charge accumulation (NCX-mediated inward current) in both Ctrl and cAF patients (**Figure 10B**). This finding absolves the SR Ca^{2+} content of contributing to the smaller Ca^{2+} amplitude and diminished contractility reported in the cAF group of this study.

The cytoplasmic Ca^{2+} buffering properties of the human atrial myocytes were subsequently evaluated, since alterations in Ca^{2+} buffering could greatly affect $[Ca^{2+}]_i$ concentration and kinetics, given as little as approximately 1% of cytoplasmic Ca^{2+} is free with the other 99% bound to cytoplasmic buffers (Fabiato, 1983; Smith & Eisner, 2019). Increased Ca^{2+} buffering has been demonstrated to reduce systolic CaT amplitude (Díaz et al., 2001) and by proxy may affect cardiac contraction and contribute to arrhythmogenesis. Therefore, the cytoplasmic Ca^{2+} buffering properties of myocytes from Ctrl and cAF patients were assessed from the cCaTs and its corresponding NCX-mediated inward current (**Figure 10A**), for their possible role in the alteration in CaT and contractility seen in cAF myocytes. The NCX current was integrated cumulatively over time to provide an index of "total" Ca^{2+} and plotted against the amplitudes of the relaxation phase of the cCaT ("free" Ca^{2+}), to generate buffer curves (**Figure 10C**) (Trafford et al., 1999). Buffer curves were fitted with a hyperbolic function to extrapolate B_{max} and k_d values which represents the maximum buffer capacity and the affinity of intracellular buffers for Ca^{2+}, respectively. The maximum buffer capacity (B_{max}) was significantly reduced in cAF compared to Ctrl, indicating a decrease in the amount of cytoplasmic Ca^{2+} buffers available. However, the affinity of available buffers for Ca^{2+} was higher in cAF, as reflected by the lower extrapolated K_d value seen in cAF myocytes compared to Ctrl (B_{max}: 2.47±0.26 vs 4.68±0.45 $pCpF^{-1}$, P<0.001; K_d: 0.47±0.13 vs 1.34±0.16 µM, P<0.001, n/N=9/6 cAF vs n/N=18/6 Ctrl, (**Figure**

10D). The mean buffer curve generated from the B_{max} and K_d values (**Figure 10E**) was flatter in cAF patients compared to Ctrl, which indicates a reduction in Ca^{2+} buffering in atrial myocytes of cAF patients. This result provides an interesting perspective on the influence of buffering on the altered Ca^{2+} handling observed in this study. The reduced number of buffers recorded in cAF myocytes may signify a reduction in contractile proteins like cTnC, which contributes approximately 50% to the total cytoplasmic Ca^{2+} buffers (Smith & Eisner, 2019). However, the reduction in Ca^{2+} buffering suggests no contribution of buffering to the reduced CaT amplitude.

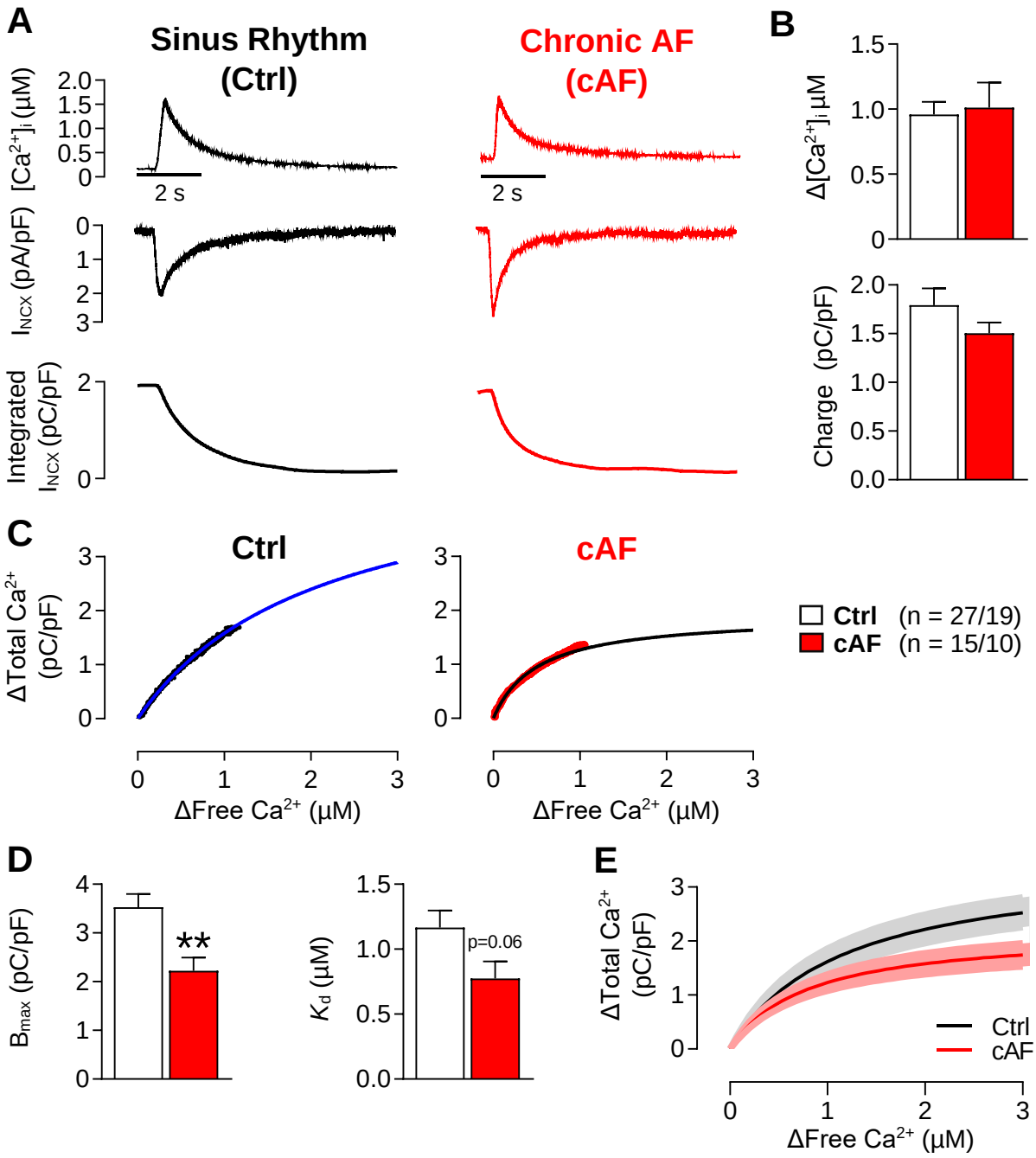

Figure 10. Quantification of SR Ca^{2+} content and Ca^{2+} buffering from caffeine-induced Ca^{2+} transients (cCaT) and generated inward currents (I_{NCX}) in atrial myocytes from sinus rhythm (Ctrl) and chronic atrial fibrillation (cAF) patients. A, Representative cCaT (free $[Ca^{2+}]_i$) (upper) and corresponding I_{NCX} (middle) integrated cumulatively to provide an index of "total" Ca^{2+} (lower) in atrial myocytes of Ctl and cAF patients. **B**, cCaT amplitude (upper) and integrated NCX estimating SR Ca^{2+} load (lower). **C**, Buffer curves depicting the relationship between total Ca^{2+} and free Ca^{2+} fitted with a hyperbolic function (blue and black nonlinear fit). **D**, Extrapolated B_{max} and k_d values. **E**.Mean (bold line) ±SEM (shaded) buffering curves derived from corresponding mean±SEM B_{max} and *K*d values. ***P*<0.01 vs Ctrl. n/N=number of myocytes/patients. Comparison using Mann Whitney's U-test.

3.3 Ca^{2+} sensitivity of skinned atrial muscle fibres of cAF patients

To closely examine the altered Ca^{2+} buffering observed in atrial myocytes from cAF patients, the force regulation of skinned human atrial muscle fibres by Ca^{2+} was investigated. Atrial muscle fibres were permeabilized, mounted between a force transducer and investigated for their force response to varying pCa solutions. A value of pCa 4.5 was used to determine maximum Ca^{2+}-induced force and pCa 7 for complete relaxation of muscle fibres. pCa-force points were fitted with a Hill equation to determine the pCa-force relationship.

The induced force at maximum Ca^{2+} concentration (F_{max}), i.e. pCa 4.5, was significantly reduced in cAF atrial muscle fibres compared to that of Ctrl (0.64±0.06 vs 0.87±0.04 mN, *P*<0.05, n=8 cAF vs n=8 Ctrl, **Figure 11A**). Also, the sensitivity of the contractile machinery to Ca^{2+} increased significantly in cAF, as demonstrated by the leftward shift of the pCa-force relationship in cAF compared to Ctrl, as well as the lower concentration of Ca^{2+} required to achieve 50% of the maximal generated force (pCa_{50}: 5.4±0.02 vs 5.6±0.06, *P*<0.05 n=8 cAF vs n=8 Ctrl, **Figure 11B**) in cAF. This observed increase in sensitivity is congruent with the results of our earlier described buffering experiments.

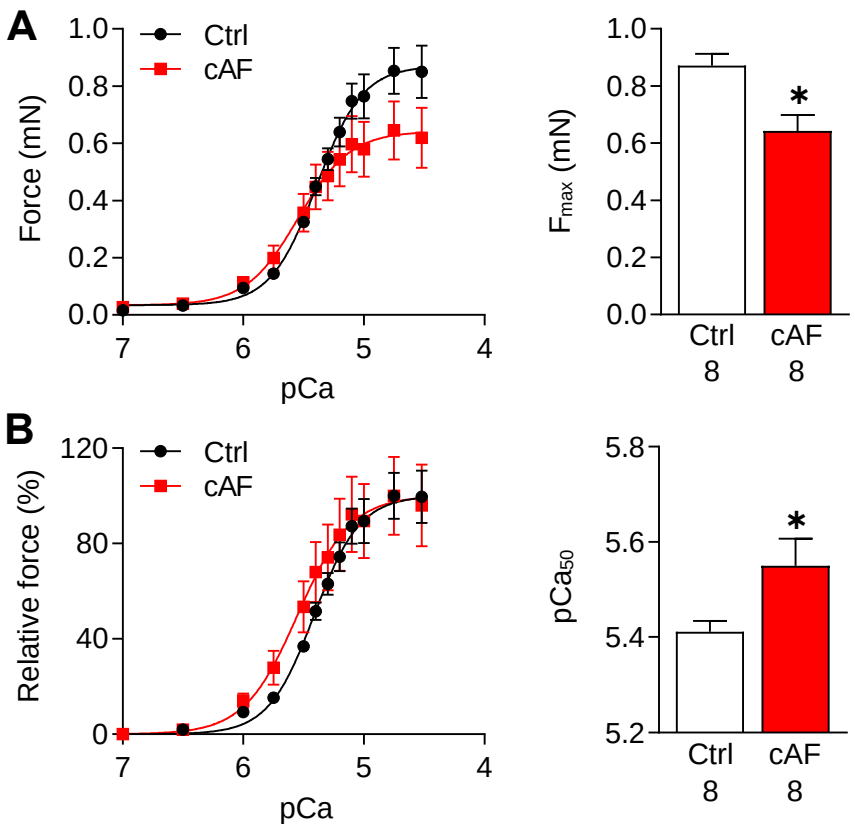

Figure 11. pCa-force relationship of muscle fibres from right atrial tissue of sinus rhythm (Ctrl) and chronic atrial fibrillation (cAF) patients. A, Absolute (top left) and **B**, normalized (bottom left) relative force-pCa relationship of skinned right atrial muscle fibres of Ctl and cAF patients. Bar graphs show mean±SEM of maximum force (F_{max}) and pCa_{50}. N = number of patients. Comparison using Mann Whitney's U-test.

3.4 Expression and phosphorylation of Ca^{2+} handling sarcomeric proteins in cAF patients

To identify molecular determinants of the reduced number of cytosolic Ca^{2+} buffers and their enhanced affinity for Ca^{2+} in cAF, sarcomeric proteins known to buffer Ca^{2+} were investigated majorly. Sarcomeric proteins were isolated from human atrial tissue, as described previously (see **section 2.5.1.2**) and analysed to determine their content and phosphorylation status using SYPRO and ProQ Diamond staining. The protein expression of the Ca^{2+}-binding cTnC was evaluated by immunoblotting. Characteristic of patients utilised in this study were similar (**Table 9**).

Table 9. Characteristics of Ctrl and cAF patients used for protein analysis

	Ctrl	cAF
Patients, n	14	14
Sex, male/female	24/4	12/2
Age, y	66.2±7.6	68.6±9.2
Body mass index, kg/m^2	30.2±5.2	28.6±4.7
Diabetes, n	7	5
LVEF, %	54.2±8.1	51.5±10.7
Digitalis, n	0	1
ACE inhibitors, n	5	3
AT1 blockers, n	3	3
β-Blockers, n	7	11
Lipid-lowering drugs, n	9	5

ACE, angiotensin-converting enzyme; AT, angiotensin receptor; LVEF, left ventricular ejection fraction; LVPWd, left ventricular posterior wall thickness at end-diastole. Continuous data are expressed as mean±SD.

Figure 12A shows representative PRO-Q Diamond- and SYPRO-Ruby-stained 2-D gels. Among all selected proteins for phosphorylation studies, only an inclination towards increased phosphorylation of cardiac troponin T (cTnT) and a significant increase in the phosphorylation of myosin light chain-2 (MLC-2) was observed in cAF groups compared to Ctrl (**Figure 12B**). cTnC on the other hand, was significantly reduced in cAF (**Figure 13**), which may explain the reduced buffer capacity observed in this study.

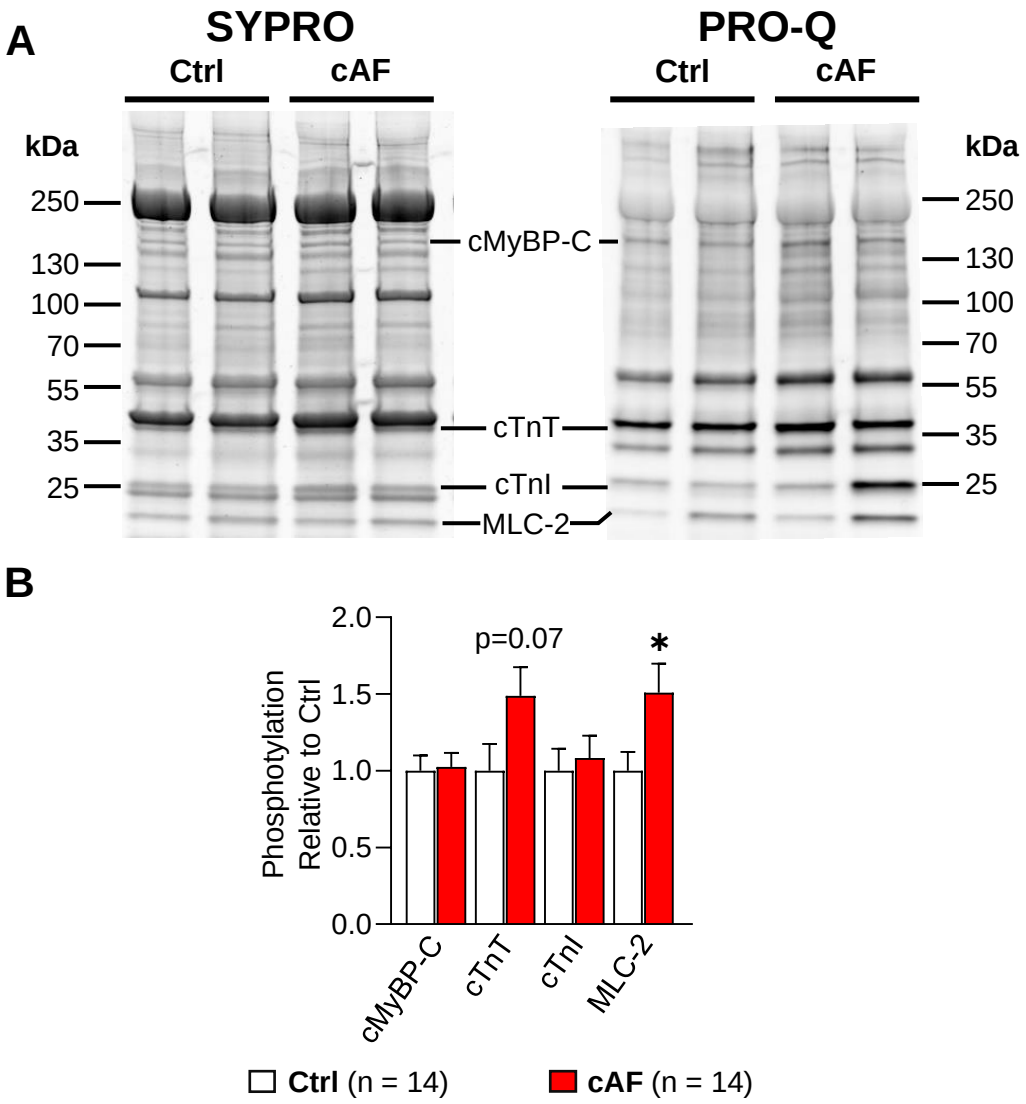

Figure 12. Phosphorylation of key sarcomeric proteins in right atrial tissue from sinus rhythm (Ctrl) and chronic atrial fibrillation (cAF) patients. A, Representative Pro-Q Diamond/SYPRO ruby stained SDS gels. **B**, Mean±SEM phosphorylation levels (right) of sarcomeric proteins in Ctrl and cAF atrial tissue samples. Phosphorylation data normalized against respective SYPRO total protein levels. *p<0.05 vs Ctl. N= number of patients. Comparison using Mann Whitney's U-test.

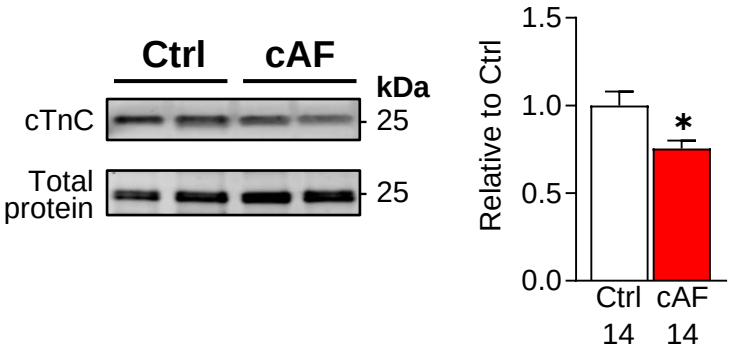

Figure 13. Protein expression of cTnC in right atrial tissue from with sinus rhythm (Ctrl) and chronic atrial fibrillation (cAF) patients.
Representative Western blots (upper left, greyscale) and quantification of cTnC expression (right) in atrial tissue samples. Data normalized against total protein (lower left, lower). *p<0.05 vs Ctl. N= number of patients. Comparison was made using unpaired students t-test.

3.5 Discussion

In this chapter, we illustrate, for the first time, the relationship between $[Ca^{2+}]_i$ and cellular shortening of human atrial myocytes. We demonstrate in addition to the classical remodelling associated with AF, including the reduction of $I_{Ca,L}$ and the reduced CaT amplitude, severe depression of human atrial myocyte contractility. This impaired contractility was corroborated by the observed reduction in maximum force of skinned myofibres from cAF patients. The diminished myocyte contractility was identified to be a consequence of not only the reduced CaT amplitude but the reduced expression of the Ca^{2+} binding cTnC along with prospective hyperphosphorylation of cTnT. In addition, we showed reduced cytosolic Ca^{2+} buffering in human atrial myocytes, attributable to a depleted amount of cytoplasmic Ca^{2+} buffers which could encourage the occurrence of arrhythmogenic Ca^{2+} waves. Altogether, our findings suggest that reduced expression of cTnC is not just a critical causative mechanism for the diminished atrial contractility seen in cAF but a likely contributor to the arrhythmogenic pathophysiology of AF.

3.5.1 $I_{Ca,L}$ is a major contributor to impaired contractility of cAF atrial myocytes

We and others have shown a reduction of $I_{Ca,L}$ in atrial myocytes of cAF patients and other AF animal models, which is known to be a hallmark of electrical remodelling in AF (Greiser et al., 2014; Voigt et al., 2012; Yue et al., 1997). The reduced $I_{Ca,L}$ by virtue of cardiac induced Ca^{2+} release is suggested to be a crucial determinant of the impaired atrial function peculiar to cAF (Denham et al., 2018). Consistent with this hypothesis, for the first time, we relate $I_{Ca,L}$ to cellular shortening in human atrial myocytes of cAF patients. We demonstrate, in addition to the classical reduction of $I_{Ca,L}$ and its triggered CaT amplitude, a severe reduction in fractional shortening of atrial myocytes from cAF patients (**Figure 9**). Owing to the $I_{Ca,L}$ being the primary determinant of the SR Ca^{2+} release and subsequent contractile response (Eisner et al., 2017), our findings demonstrate that the consequential reduction of systolic CaT amplitude, due to the smaller $I_{Ca,L}$, is an important contributor to the diminished contractile response of atrial myocytes obtained from cAF patients in this study. This finding is in agreement with the outcomes of studies in canine, ovine and rabbit models of AF, where the perturbed atrial contractile function in these models was attributed to either the pronounced reduction of the Ca^{2+} transient or the depressed $I_{Ca,L}$ (Greiser et al., 2014; Lenaerts et al., 2009; Sun et al., 1998; Yue et al., 1997). In humans, Schotten and colleagues also attributed the contractile dysfunction of intact atrial myofibres

stimulated using an electrical pulse to a reduction in L-type Ca^{2+} channel activity (Schotten et al., 2001).

Further corroborating the role of the $I_{Ca,L}$ in the atrial hypocontractility seen in cAF, we did not detect differences in SR Ca^{2+} content (**Figure 10**), which, if altered, could influence the systolic Ca^{2+} release. This outcome is compatible with the findings of a previous study (Voigt et al., 2012), as well as other studies where no SR dysfunction was noted in AF (Lenaerts et al., 2009; Schotten et al., 2001). However, a previous study has demonstrated a reduction in the SR Ca^{2+} load in a goat AF model, when measured at higher physiological frequencies (Greiser et al., 2009). It would be of high interest to investigate the SR Ca^{2+} load-frequency relationship in human atrial myocytes of cAF patients. Collectively, our findings highlight the pivotal role of the L-type Ca^{2+} channel in the atrial contractile dysfunction seen in cAF patients.

3.5.2 Reduced protein levels of cTnC and increased phosphorylation of cTnT underlie the impaired contractile response of cAF myocytes

Existing studies have highlighted that altered handling of cytosolic Ca^{2+} and myofilament Ca^{2+} responsiveness aid the decrease in myocyte contractility (J. H. Chung et al., 2016; Vikhorev & Vikhoreva, 2018). Interestingly, our data revealed a more severe reduction in cellular shortening (~70%) compared to the decrease in systolic CaT amplitude (~44%) in cAF atrial myocytes **(Figure 9)**, implying an impaired response of contractile proteins to $[Ca^{2+}]_i$. Furthermore, we detected comparable sarcomere lengths in both groups (**Figure 8**), suggesting that the decreased Ca^{2+} responsiveness of myofilaments is unlikely to be caused by length-dependent Frank Starlings mechanisms (Sequeira & van der Velden, 2015). These discoveries are in accordance with the observations of a canine model of AF where in addition to the reduced CaT amplitude, abnormal function of the contractile apparatus was reported to be responsible for the atrial contractile dysfunction seen in this model (Sun et al., 1998). Also, in consonance with the impaired contractility of atrial myocytes seen in our cAF group, we recorded a decrease in the maximum force of skinned atrial myofibres from cAF patients at similar Ca^{2+} stimulation (**Figure 11**). Corroborating our findings is the reports of Belus et al., where a similar reduction in force of skinned atrial myofibres at maximal Ca^{2+} stimulation was observed in cAF patients (Belus et al., 2010).

However, despite the reduced maximal force, an increase in Ca^{2+} sensitivity for force generation was observed in the skinned myofibres from the cAF group (**Figure 11**). Reduced PKA phosphorylation of the troponin subunit cTnI is known to increase

myofilament Ca^{2+} sensitivity (Vikhorev & Vikhoreva, 2018). Interestingly, phosphorylation of cTnI was comparable between groups in this study, thus excluding its contribution to the myofilament sensitivity exhibited by cAF myofibres (**Figure 12**). However, we detected increased phosphorylation of MLC-2, which is associated with an increase in myofilament sensitivity to Ca^{2+}, although to a lesser extent when compared to cTnI (Belus et al., 2010; Vikhorev & Vikhoreva, 2018). This increase in myofilament Ca^{2+} sensitivity may be a compensatory mechanism to counteract the reduced force seen in atrial fibres of cAF patients. However, an increase in myofilament sensitivity could compromise the relaxation of tissue which could further worsen cardiac contractility (J. H. Chung et al., 2016).

Although altered myofilament sensitivity may influence the relaxation kinetics of the atrial tissue, this does not explain the reduced contractile force generated by myofibres stimulated at similar Ca^{2+} concentrations nor the severe reduction in cellular shortening. Phosphorylation of cTnT has been demonstrated by *in-vitro* studies to reduce myocardial contractility (Streng et al., 2013). Interestingly, in agreement with a previous study (Belus et al., 2010), we observed a propensity towards increased phosphorylation of cTnT in our cAF group (**Figure 12**), which may contribute to the diminished cellular contractility and myofibre force seen in cAF patients. Also, for the first time, we show lower protein expression of Ca^{2+} binding cTnC in cAF patients, which is a major determinant in the strength of contraction (Shettigar et al., 2016). This reduced expression may explain the impaired contractile response of myocytes from cAF patients.

3.5.3 Ca^{2+} buffering is impaired in right atrial myocytes of cAF patients

The intracellular buffering of Ca^{2+}, predominated by cTnC, plays a significant role in the governance of Ca^{2+} signalling. This buffering regulates kinetics and levels of cytosolic Ca^{2+}, and in essence, influences myocyte contraction (Smith & Eisner, 2019). To the extent of our knowledge, we report for the first time the measurement of cytoplasmic Ca^{2+} buffering in isolated atrial myocytes from cAF patients (**Figure 10**). We discovered impaired buffering of cytosolic Ca^{2+}, characterized by a reduction in the total amount of buffers (B_{max}), which is in line with the reduced protein expression of cTnC observed in our cAF patient cohort. We also detected a non-significant increase in affinity of buffers for Ca^{2+}, which in conjunction with the reduced number of buffers, correlates with the findings of our skinned myofibril experiments discussed above. In agreement with our findings, a similar reduction in buffering was noted in atrial myocytes of ovine models of both AF and heart failure (Clarke et al., 2015; Macquaide et al., 2015). However, a rabbit model of AF

exhibited increased buffering, which was ascribed to the phosphorylation of the cTnI (Greiser et al., 2014). A possible reason for the contrasting finding in this AF model stems from the fact that the rapid pacing of the atria was conducted for only five days, which is a better representation for early and paroxysmal episodes of AF, not persistent AF (Denham et al., 2018). The reduced buffering of Ca^{2+} in our study may exist to partially manage the alteration in cytosolic Ca^{2+} caused by the reduced $I_{Ca,L}$ current. However, the reduced Ca^{2+} buffering may facilitate the diffusion of free Ca^{2+} which may activate proximal clusters of RYR2s which go on to promote arrhythmogenic waves, which are established facilitators of AF (Macquaide et al., 2015). Therefore, we propose that modulation of the Ca^{2+} binding of cTnC will not only ameliorate the diminished atrial contractility but may also exert antiarrhythmic effects by improving Ca^{2+} buffering in cAF.

3.5.4 Limitations

In this study, as a consequence of limited availability of human atrial tissue, only right atrial appendages obtained during cardiac surgery were utilised. Thus, observations in this study might not necessarily reflect the changes in other atrial regions. Also, only a small number of cAF myocytes were evaluated of their contractile function, hence prospective studies with a robust sample size is necessary.

Furthermore, the method applied in the measurement of cytosolic Ca^{2+} buffering in this study only takes into account the fast-cytoplasmic calcium buffers i.e. SERCA and cTNC. However, although other buffers contribute to total Ca^{2+} buffering, their contribution is only modest and not of great significance in the time scale of measurement applied in this study (Briston et al., 2014; Smith & Eisner, 2019). Also, although we assessed the role of the troponins in the altered buffering seen in cAF myocytes of this study, SERCA2a could also contribute to the reduced buffering exhibited by cAF myocytes. A previous study have reported unchanged expression and activity of SERCA2a in tissues of cAF patients (Voigt et al., 2012), which supports our conclusion that cTNC seems to play a major part in the altered Ca^{2+} buffering seen in myocytes from cAF patients. Nevertheless, further studies assessing the role of SERCA2a in the impaired buffering observed in cAF patients need to be conducted.

4 Ca^{2+} handling abnormalities in post-operative atrial fibrillation (poAF)

PoAF, a new-onset AF occurring within the immediate postoperative days, is a frequent complication of cardiac surgery affecting as many as 40% of open-heart surgery patients (Dobrev et al., 2019). Although poAF is often transient with episodes occurring within 6 postoperative days, its development is associated with poorer outcomes, including higher risks of stroke and increased mortality (Ahlsson et al., 2010). Despite, the application of several preventive strategies to curb poAF occurrence, including the use of pharmacological agents like amiodarone, β-blockers and sotalol, high incidences persist, owing in part to the inadequate insight into the underlying mechanisms of poAF (Dobrev et al., 2019).

Extensive studies in the last decade have broadened the understanding of the causative mechanisms of general AF (as discussed in chapter 1), but poAF remains poorly understood. Conceptually, poAF is assumed to be initiated by the interaction of perioperative triggers such as adrenergic activation or inflammation, with preexisting pro-arrhythmic substrates (Dobrev et al., 2019). Many studies have identified preoperative structural modifications, including atrial fibrosis and cellular hypertrophy to be linked to poAF (Swartz et al., 2009; G. D. Wang et al., 2009). These structural alterations are believed to be major determinants of the arrhythmogenic substrate that predisposes cardiac surgery patients to poAF (Dobrev et al., 2019). However, unlike pAF and cAF, which are characterised by alterations in cellular electrophysiology such as decreased duration of APs, that encourages the maintenance of AF (Heijman et al., 2014), no evidence of preexisting electrical remodelling has been documented to contribute to the arrhythmogenic substrate that predisposes patients to poAF.

In recent times, Ca^{2+} handling abnormalities have been demonstrated to play a prominent role in the initiation and perpetuation of both pAF and cAF as well as in heart failure patients with increased vulnerability to AF (Molina et al., 2018; Voigt et al., 2012, 2014). However, the participation of such Ca^{2+} handling alterations in the arrhythmogenic substrate that predisposes patients to poAF is unknown. Also, recent studies have reported preoperative impairment of both left and right atrial contractile function in poAF patients, as a predictive alteration for the development of poAF in patients undergoing cardiac surgery (Aksu et al., 2019; Verdejo et al., 2016). Therefore, since Ca^{2+} handling is the critical factor driving contractile function and is demonstrated to contribute to the

contractile abnormality in our cAF patient group (chapter 3), we hypothesise that modifications in the intracellular handling of Ca^{2+} contribute to the atrial contractile dysfunction observed in patients who go on to develop poAF.

In this study, using right atrial myocytes from patients undergoing open-heart surgery, we assessed the potential role of Ca^{2+} handling abnormalities in the contractile dysfunction associated with poAF and in the pro-arrhythmogenic mechanisms predisposing patients to poAF.

4.1 Speckle-tracking analysis of echocardiography recordings of poAF patients

LA function has been reported to be impaired in patients who developed poAF by a series of studies (Pernigo et al., 2017; Verdejo et al., 2016), and by virtue touted as a predictor for poAF development. Therefore, to test this relationship in our patient cohort, the left atrial function in Ctrl and poAF patients was assessed by speckle-tracking echocardiography. Segments of the left atrial wall in electrocardiograms with optimal visualisation of the left atrial and ventricular chambers obtained preoperatively were tracked to quantify the global strain of the left atrium during the reservoir, conduit and contraction phases of the left atrial cardiac cycle.

In total, 42 patients had preoperative echocardiograms that were optimal for speckle-tracking analysis, of which 21 of the eligible patients developed poAF after cardiac surgery. Clinical parameters of patients were similar for both poAF and Ctrl patients except for a significant difference in age (PoAF: 60.9±7.9 years vs Ctrl: 68.8±8.9 years, $P<0.01$, n=21 vs 21, **Table 10**). Patients who went on to develop poAF exhibited significantly reduced global atrial contraction strain (LASct) prior to cardiac surgery compared to Ctrl patients (-10.94±5.69% vs -15.50±6.56%, $P<0.05$, n=21 vs 21, $P<0.05$, **Figure 14D**). The impaired LASct, which is a measure of the strain from the onset of atrial systole until mitral valve closure, indicates a reduced systolic function in patients in the poAF group. Similarly, the reservoir strain (LASr), which pertains to the cardiac cycle phase between ventricular systole and atrial filling was significantly reduced in poAF patients (poAF: 23.75±8.89%, n=21; Ctrl 31.37±8.91%, n=21, $P<0.01$), while the conduit strain (LAScd), which represents the measure of the deformation during passive ventricular filling was unaltered.

Table 10. Characteristics of patients used for speckle-tracking analysis

		Ctrl	poAF
General	Patients, n	21	21
	Day of first poAF episode	-	3.8±2.2
	Sex, male/female	18/3	17/4
	Age, y	60.9±7.9	68.8±8.9**
	Body mass index, kg/m^2	27.4±3.6	26.8±3.4
Intervention	CAD, n	13	12
	MVD/AVD, n	6	3
	CAD+MVD/AVD, n	2	6
	Intervention time, min	254.1±81.5	258.3±86,5
	ECC time, min	129.9±57.6	122.4±72.5
Anamnesis	Hypertension, n	18	19
	Diabetes, n	5	2
	Hyperlipidemia, n	10	12
	NYHA (I/II/III), n	3/7/7	1/6/6
	Stroke, n	2	5
	TIA, n	0	0
CC	Creatinin, µmol/L	1.06±0.47	0.96±0.22
Echocardiography	LAD, mm	39.9±6.5	42.2±6.3
	LVEDD, mm	50.9±8.3	50.6±10.3
	IVSd, mm	13.2±2.7	14.1±2.4
	LVPWd, mm	12.1±2.1	13.5±3.3
	LVEF, %	55.8±7.8	54.2±9.3
	Diastolic dysfunction, Grade I/II	11/4	7/4
Medication	Digitalis, n	0	0
	ACE inhibitors, n	12	11
	AT1 blockers, n	6	4
	β-Blockers, n	13	12
	Dihydropyridines, n	3	7
	Diuretics, n	4	5
	Nitrates, n	0	3
	Lipid-lowering drugs, n	13	17

ACE, angiotensin-converting enzyme; AT, angiotensin receptor; CC, clinical chemistry; CAD, coronary artery disease; ECC, extracorporeal circulation; IVSd, interventricular septum thickness at end-diastole; LAD, left atrial diameter; LVEDD, left ventricular end-diastolic diameter; LVEF, left ventricular ejection fraction; LVPWd, left ventricular posterior wall thickness at end-diastole; NYHA, New York Heart Association Functional Classification; MVD/AVD, mitral/aortic valve disease; TIA, transient ischemic attack. Continuous data are expressed as mean±SD. ***P*<0.01. Replotted from Fakuade et al., 2020 (with permission).

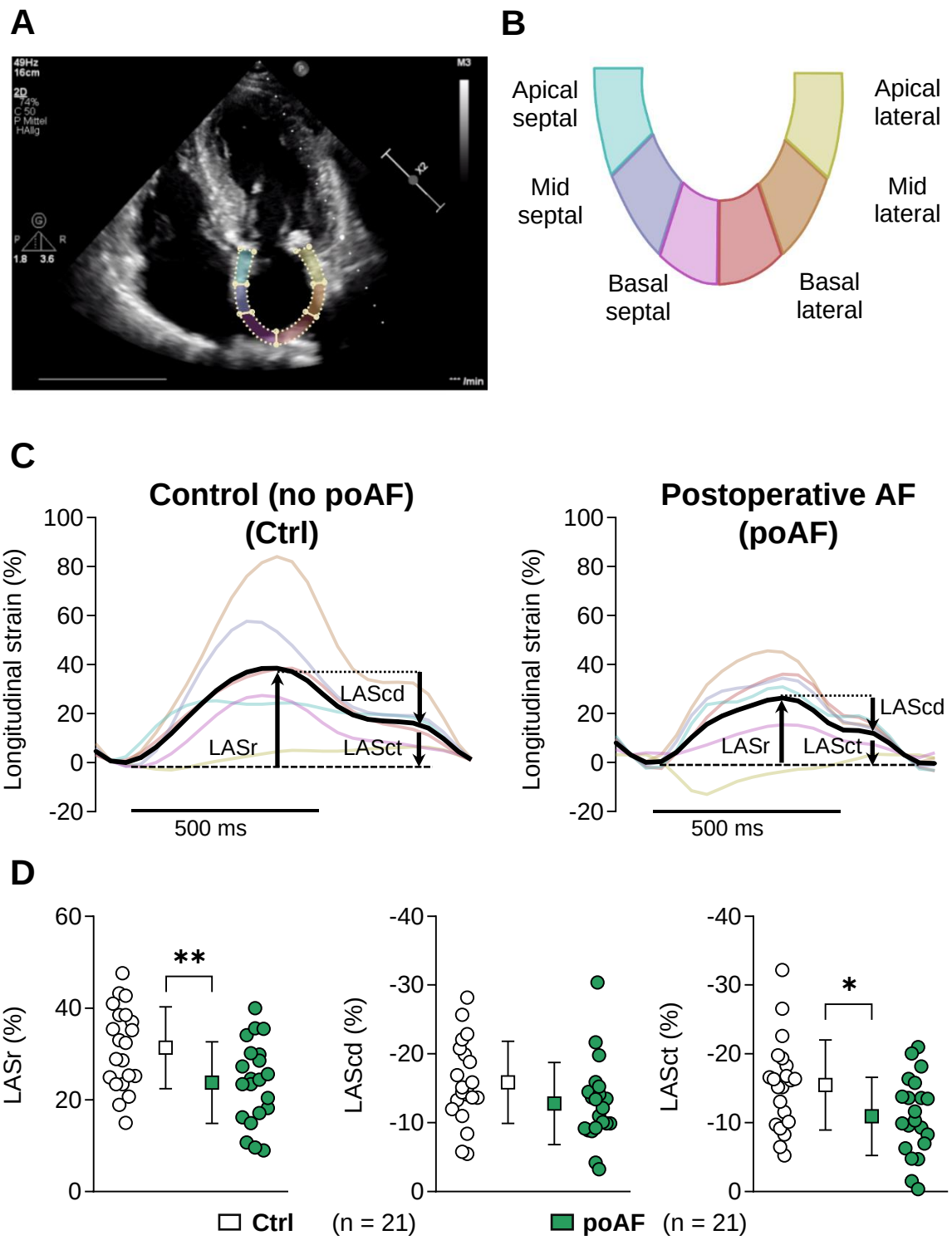

Figure 14. Preoperative speckle-tracking echocardiography to quantify left atrial (LA) strain in patients who do not (Ctrl) and who do develop postoperative atrial fibrillation (poAF). A, Representative apical four-chamber echocardiogram of a poAF patient. The multi-coloured area defines the region of interest along the inner contour of the LA wall. **B,** Segment nomenclature of the LA wall. **C,** Representative strain curves of Ctrl (left) and poAF (right) patients. Coloured lines show strain of the different segments shown in B. Global mean strain, denoted by the black line, is used for the measurement of total left atrial reservoir strain (LASr), left atrial conduit strain (LAScd) and left atrial contraction strain (LASct) as indicated by arrows. **D,** Mean±SD LASr (left), LAScd (middle) and LASct (right). **P*<0.05, ***P*<0.01, vs Ctrl. n=patients. Comparisons using unpaired Student's t-test. Replotted from Fakuade et al., 2020 (with permission).

4.2 Simultaneous $I_{Ca,L}$ and CaT in atrial myocytes from poAF patient

To investigate the role of excitation-contraction coupling in the development of poAF and its contribution to the depressed left atrial contractile function seen in poAF (**Figure 14**), $I_{Ca,L}$ and its corresponding CaT, were measured in human right atrial myocytes, as described previously. All clinical characteristics of patients enrolled in voltage-clamp studies were similar, barring the higher age observed in poAF patients compared to Ctrl (poAF: 60.9±7.9 years vs Ctrl: 68.8±8.9 years, *P*<0.01, n=38 vs 22, **Table 11**)

No difference in membrane capacitance was found between poAF and Ctrl groups (poAF: 90.38±5.92 pF, n/N=35/22; Ctrl; 95.97±5.79 pF, n/N=78/38; *P*=0.558), indicating comparable cell size. Neither the peak nor the integral of $I_{Ca,L}$, were different in poAF when compared to Ctrl (**Figure 15B**). Epifluorescence measurement showed comparable diastolic $[Ca^{2+}]_i$ levels in both groups with a tendency to reduced systolic $[Ca^{2+}]_i$ observed in poAF. The calculated CaT amplitude was significantly reduced in poAF vs Ctrl (149.30±14.20 vs 224.01±16.69 nM, n/N=35/22 poAF vs 78/38 Ctrl, *P*<0.001, **Figure 15C**). The time constant of CaT decay (τ), determined by a single exponential fitting of the decay phase of the CaT, was observed to be significantly higher in poAF when compared with Ctrl, pointing to a slower rate of Ca^{2+} removal from the cytosol during systole in poAF (527.38±45.31 vs 405.44±18.77 ms, n/N=35/22 poAF vs 78/38 Ctrl, *P*<0.05, **Figure 15D**).

Table 11. Characteristics of patients used for voltage-clamp experiments

		Ctrl	poAF
General	Patients, n	38	22
	Day of first poAF episode	-	2.9±2.2
	Sex, male/female	35/3	17/5
	Age, y	63.4±10.3	72.0±10.8**
	Body mass index, kg/m^2	28.3±3.9	27.0±3.5
Intervention	CAD, n	25	18
	MVD/AVD, n	10	3
	CAD+MVD/AVD, n	3	1
	Intervention time, min	278.0±79.5	278.0±85.8
	ECC time, min	124.8±35.8	124.4±46.2
Anamnesis	Hypertension, n	31	18
	Diabetes, n	11	4
	Hyperlipidemia, n	22	8
	NYHA (I/II/III), n	6/14/14	1/12/8
	Stroke, n	3	0
	TIA, n	4	1
CC	Creatinin, µmol/L	1.00±0.28	1.00±0.24
Echocardiography	LAD, mm	41.0±6.3	43.2±5.5
	LVEDD, mm	48.6±7.6	49.7±8.1
	IVSd, mm	13.2±2.8	12.3±2.4
	LVPWd, mm	12.6±2.4	11.5±2.4
	LVEF, %	51.5±10.7	50.6±11.8
	Diastolic dysfunction, Grade I/II	22/8	13/4
Medication	Digitalis, n	0	0
	ACE inhibitors, n	21	9
	AT1 blockers, n	10	6
	β-Blockers, n	26	15
	Dihydropyridines, n	8	7
	Diuretics, n	11	10
	Nitrates, n	5	2
	Lipid-lowering drugs, n	30	15

ACE, angiotensin-converting enzyme; AT, angiotensin receptor; CC, clinical chemistry; CAD, coronary artery disease; ECC, extracorporeal circulation; IVSd, interventricular septum thickness at end-diastole; LAD, left atrial diameter; LVEDD, left ventricular end-diastolic diameter; LVEF, left ventricular ejection fraction; LVPWd, left ventricular posterior wall thickness at end-diastole; NYHA, New York Heart Association Functional Classification; MVD/AVD, mitral/aortic valve disease; TIA, transient ischemic attack. Continuous data are expressed as mean±SD. ***P*<0.01. Adapted from Fakuade et al., 2020 (with permission).

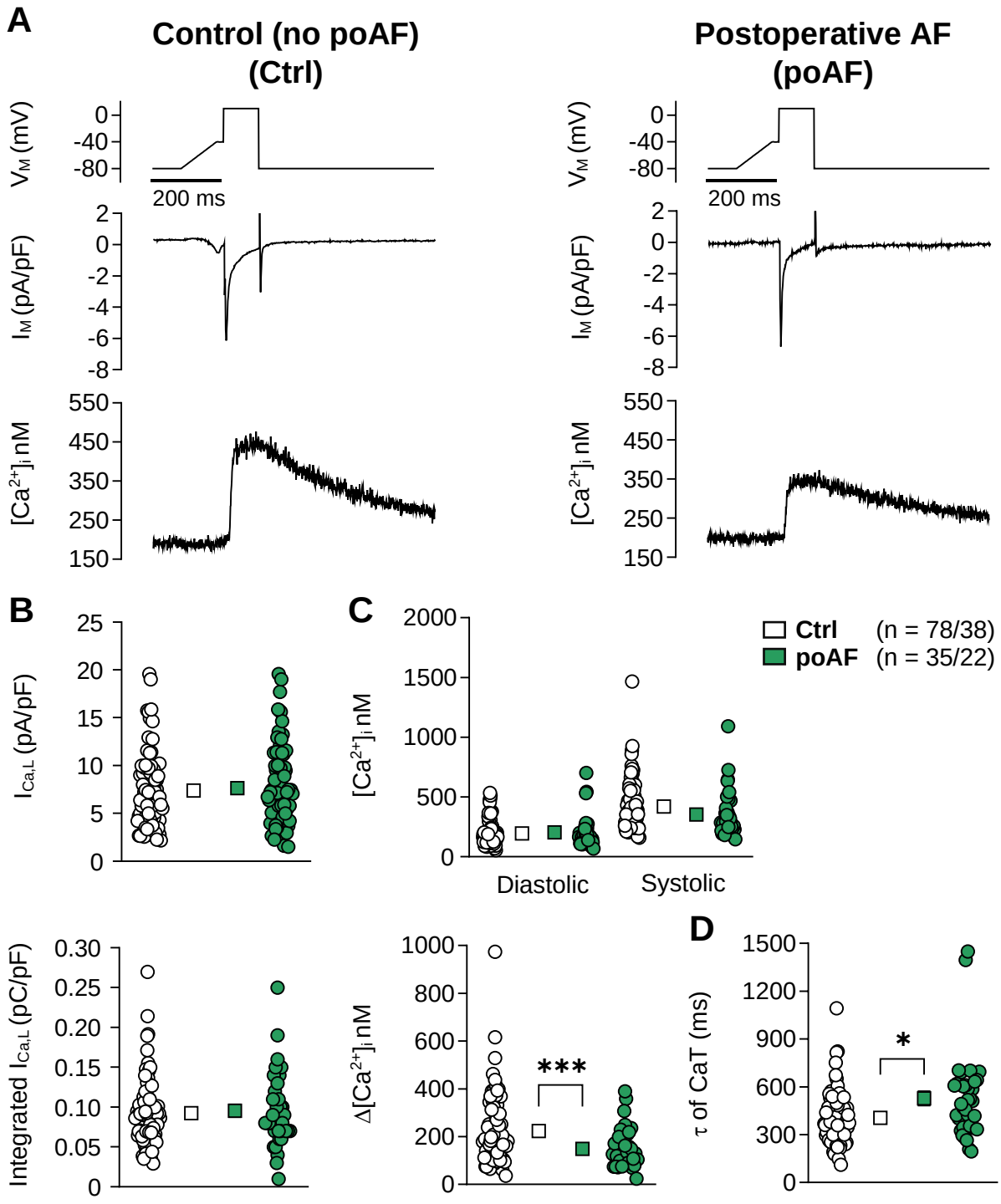

Figure 15. $I_{Ca,L}$-triggered Ca^{2+} transients (CaT) in atrial myocytes from control patients (Ctrl) and patients who developed postoperative atrial fibrillation (poAF). A, Voltage-clamp protocol (0.5 Hz) (upper), representative simultaneous recordings of $I_{Ca,L}$ (middle) and triggered CaT (lower) in Ctrl (left) and poAF (right) myocytes. **B,** Mean±SEM peak $I_{Ca,L}$ (upper) and integrated $I_{Ca,L}$ (lower). **C,** Mean±SEM diastolic and systolic $[Ca^{2+}]_i$ (upper) and resulting CaT-amplitude ($\Delta[Ca^{2+}]_I$, lower). **D,** Mean±SEM time constant of decay (τ) of $I_{Ca,L}$-triggered CaT. **P*<0.05 ****P*<0.001 vs Ctrl. n/N=number of myocytes/patients. Comparison using unpaired t-test with Welch's correction (C bottom, D**)**. Adapted from Fakuade et al., 2020 (with permission).

4.3 SR Ca^{2+} content and Ca^{2+} buffering in atrial myocytes from poAF patients

The CaT amplitude is governed by a number of factors including $I_{Ca,L}$ and the SR Ca^{2+} content. Given that $I_{Ca,L}$ was similar between poAF and Ctrl groups as described above, the role of the SR Ca^{2+} content in the observed reduction in CaT amplitude was investigated. SR Ca^{2+} load was estimated by determining the integral of the I_{NCX} and the amplitude of the CaT induced by the application of caffeine (cCaT), as described above (see **section 2.4.3.2**).

Both the integral of the I_{NCX} and the amplitude of cCaT were significantly smaller in poAF when compared with Ctrl, indicating smaller SR Ca^{2+} content in poAF (amplitude: 0.63±0.06 vs 0.97±0.08 nM, P<0.001; charge: 1.53±0.08 vs 1.80±0.06 pC/pF, P<0.01, n/N=35/22 poAF vs 78/38 Ctrl, **Figure 16B**). The observed reduction in SR load could contribute to the reduced systolic CaT amplitude observed in myocytes from poAF patients. The cCaT decay rate (**Figure 16C**) and the slope of the line relating I_{NCX} to $[Ca^{2+}]_i$ during the decay of cCaT **(Figure 16D-E)**, both which are a measure of NCX function, were comparable between both poAF and Ctrl groups, suggesting similar NCX activity.

In addition to reduced SR Ca^{2+} content, increased Ca^{2+} buffering has also been demonstrated to reduce both amplitude and the rate of decay of systolic Ca^{2+} transients (Díaz et al., 2001). Thus, cytoplasmic Ca^{2+} buffering properties of atrial myocytes from poAF patients were estimated, as described above (**section 3.2**). Both B_{max} and k_d were not different between poAF and Ctrl groups (**Figure 17C**), exempting the participation of buffering in the reduced amplitude and rate of decay of the systolic Ca^{2+} transients observed in poAF.

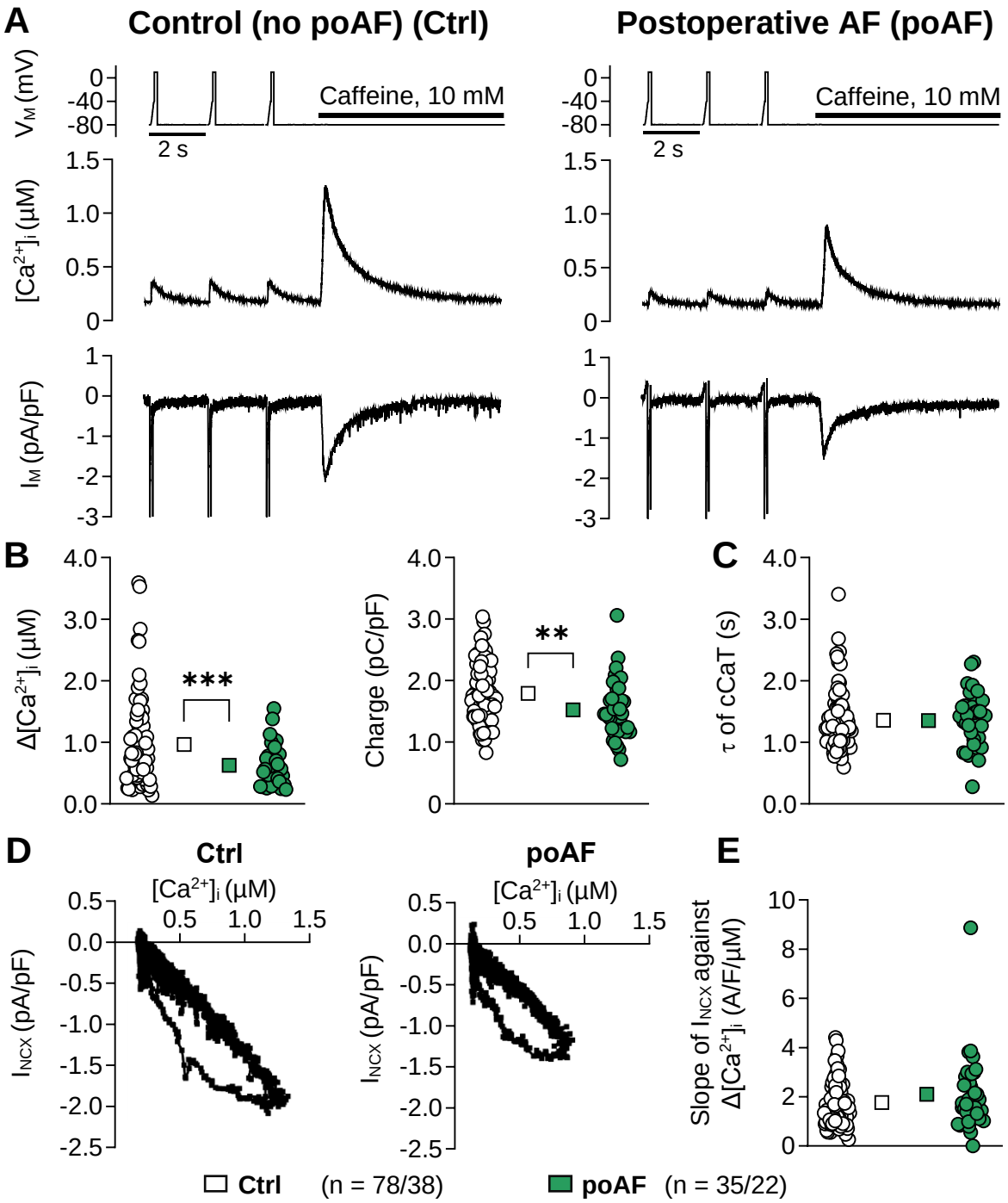

Figure 16. Caffeine-induced Ca^{2+} transients (cCaT) and the corresponding transient inward currents (I_{NCX}) to assess SR Ca^{2+} content in atrial myocytes from control patients (Ctrl) and patients who develop postoperative atrial fibrillation (poAF). A, Voltage-clamp protocol (upper), representative CaT and cCaT (middle) and corresponding membrane currents (I_M, lower). **B,** SR Ca^{2+} load, quantified with cCaT amplitude (left), or integrated membrane current (right). **C,** Time constants of cCaT decay (indicating Ca^{2+} extrusion via NCX). **D,** I_{NCX} as a function of $[Ca^{2+}]_i$. **E,** Ca^{2+}-dependence of I_{NCX}, based on the slope of linear fit to the $I_{NCX}/[Ca^{2+}]_i$ relationship during the decay of the cCaT. ***P*<0.01, ****P*<0.001 vs Ctrl. n/N=number of myocytes/patients. Comparison using unpaired Student's t-test and t-test with Welch's correction (B, left). Adapted from Fakuade et al., 2020 (with permission).

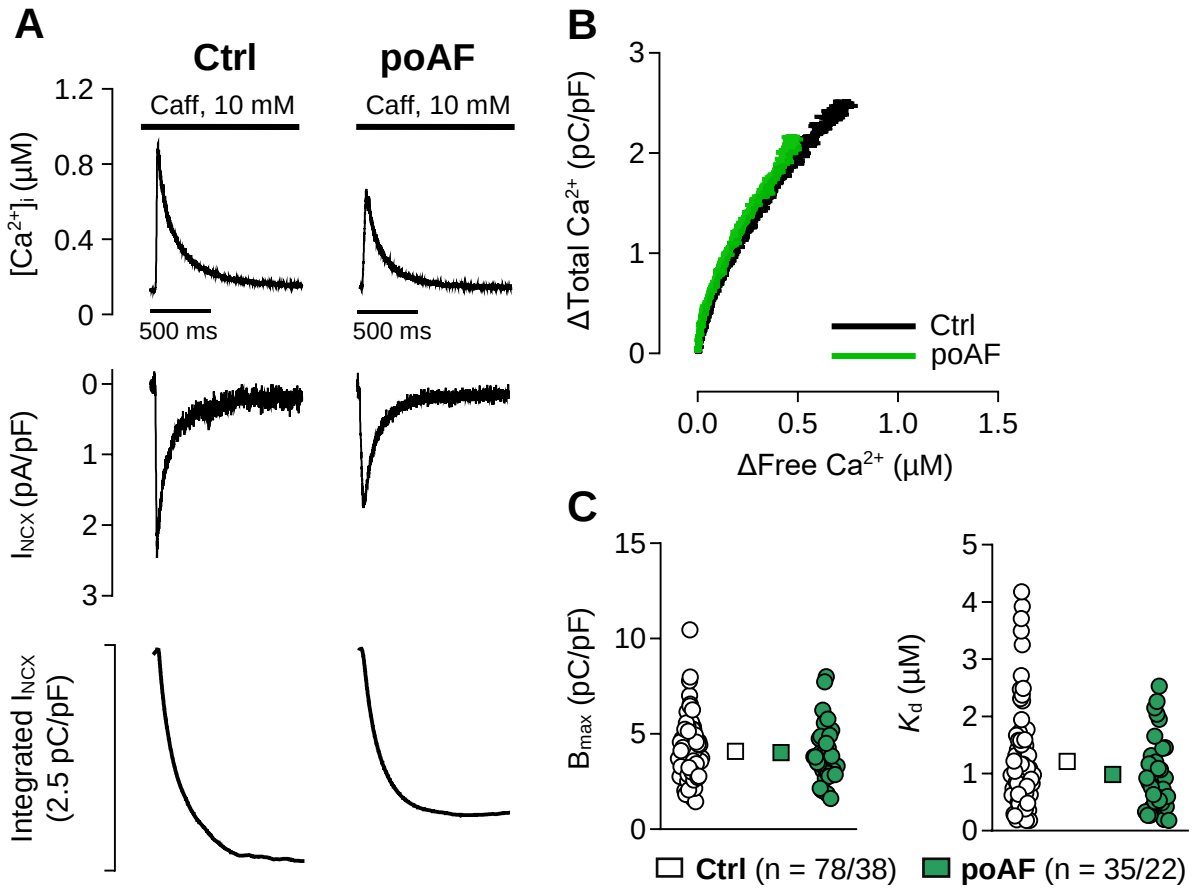

Figure 17. Assessment of intracellular Ca^{2+} buffering in atrial myocytes from patients who do not (Ctrl) and who do develop postoperative atrial fibrillation (poAF). A, Representative simultaneous recordings of caffeine-induced "free" CaT, (top) and corresponding depolarising I_{NCX} (middle), cumulatively integrated to provide an index of "total" calcium (bottom) in atrial myocytes of Ctrl and poAF patients. **B,** Buffer curves depicting the relationship between cellular free and total calcium. **C,** Maximum buffer capacity (B_{max}) and buffer Ca^{2+} affinity (k_d) extrapolated from buffer curves fitted with a hyperbolic function. n/N=number of myocytes/patients. Adapted from Fakuade et al., 2020 (with permission).

4.4 SR Ca^{2+} leak in atrial myocytes from poAF patients

Diastolic SR Ca^{2+} fluxes such as the SR Ca^{2+} leak can considerably influence the SR Ca^{2+} content, consequently resulting in depressed contractility of the heart (Marx et al., 2000; Shannon et al., 2002). Therefore, to exclude a role for increased SR Ca^{2+} leak in the lowering of the SR Ca^{2+} content seen in poAF, total SR Ca^{2+} leak was quantified using the tetracaine method of Shannon et al. (Shannon et al., 2002) (see **section 2.4.3.3**). Atrial myocytes were clamped at -80 mV and perfused with Na^{+} and Ca^{2+} free bath solution to inhibit NCX removal of cytosolic Ca^{2+}. A subsequent application of the RYR2 blocker tetracaine was effected on the myocytes to determine the contribution of SR fluxes to diastolic Ca2+ levels (**Figure 18A**). Diastolic SR leak was not different in poAF and Ctrl

groups (**Figure 18B**) indicating no contribution of SR leak to the depleted SR Ca^{2+} content observed in poAF.

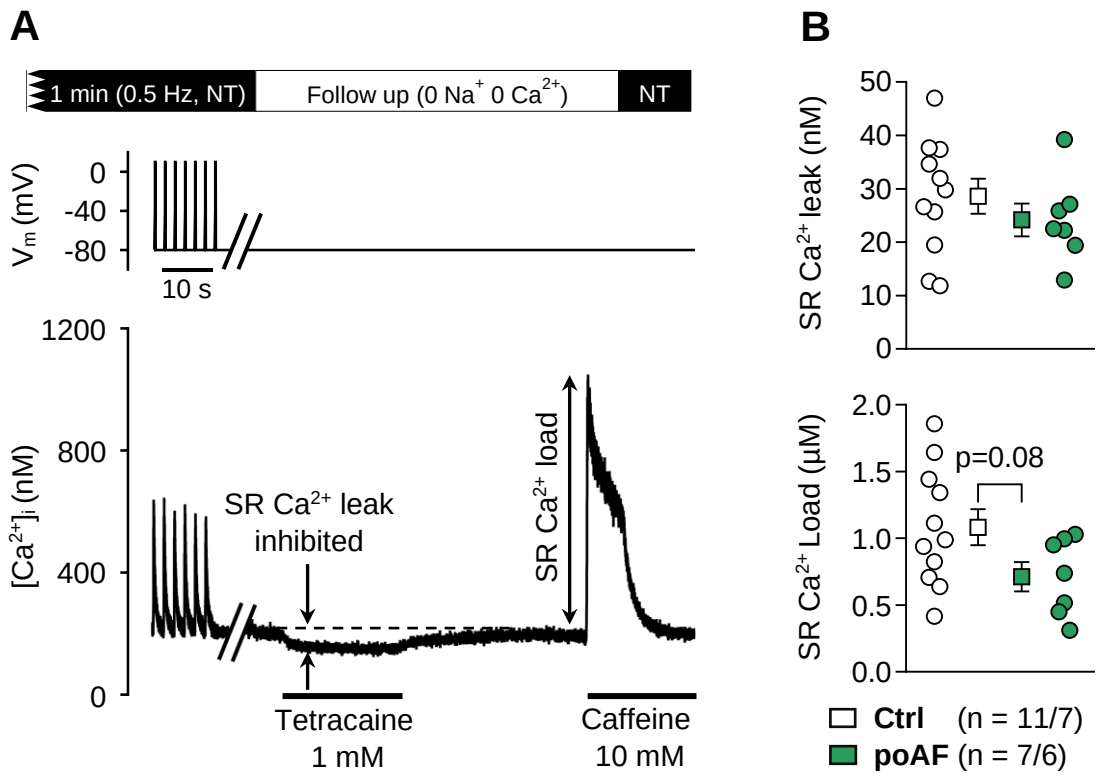

Figure 18. SR Ca^{2+} leak in atrial myocytes from control patients (Ctrl) and those who developed postoperative atrial fibrillation (poAF). A, Voltage-clamp protocol (upper) and $[Ca^{2+}]_i$ (lower) in a representative Ctrl experiment, showing the method for SR Ca^{2+} leak and SR Ca^{2+} content quantification in human atrial myocytes using tetracaine. **B,** Mean±SEM total SR Ca^{2+} leak in Ctrl and poAF patients (upper) and SR Ca^{2+} load quantified using caffeine-triggered Ca^{2+} transient amplitude (lower). Comparison using Mann-Whitney's U test. Adapted from Fakuade et al., 2020 (with permission).

4.5 Cytosolic Ca^{2+} transport mechanisms in atrial myocytes from poAF patients

The uptake of Ca^{2+} into the SR by SERCA and the extrusion of Ca^{2+} into the extracellular space by the sarcolemmal mechanisms were next studied. NCX and plasma membrane Ca^{2+} ATPase (PMCA) are the major pathways for cytosolic removal of Ca^{2+} in myocytes. Alterations in the activity of these mechanisms, SERCA in particular, could affect myocardial excitation-contraction coupling, thus affecting myocardial contractility and performance. A decrease in the uptake of Ca^{2+} by SERCA could contribute to the slower decay rate of the systolic CaT and the diminished SR Ca^{2+} content seen in poAF. Therefore, SERCA function was ascertained from the rate constants, *k* (inverse of τ)

determined from fitting single exponential curves on the decay phase of both systolic and caffeine-induced CaTs, as described previously (Choi & Eisner, 1999; Voigt et al., 2012).

SERCA activity, expressed as the rate constant k_{SERCA}, was calculated by having the rate constant of cCaT decay (k_{Caff}), which represents the extrusion of cytosolic Ca^{2+} predominantly via NCX, since SR uptake via SERCA is negligible in the presence of caffeine, subtracted from the rate constant of the systolic CaT (k_{sys}), which represents the rate of the combined transport of both SERCA and NCX (**Figure 19A**). k_{SERCA} was found to be significantly lower in poAF compared to Ctrl (1.48±0.17 vs 2.08±0.15 s^{-1}, n/N=35/22 poAF vs 78/38 Ctrl, *P*<0.01, **Figure 19B**), with the NCX activity similar in both groups. These results are likely to underlie both the slower decay rate of the systolic CaT and the smaller SR Ca^{2+} load in poAF.

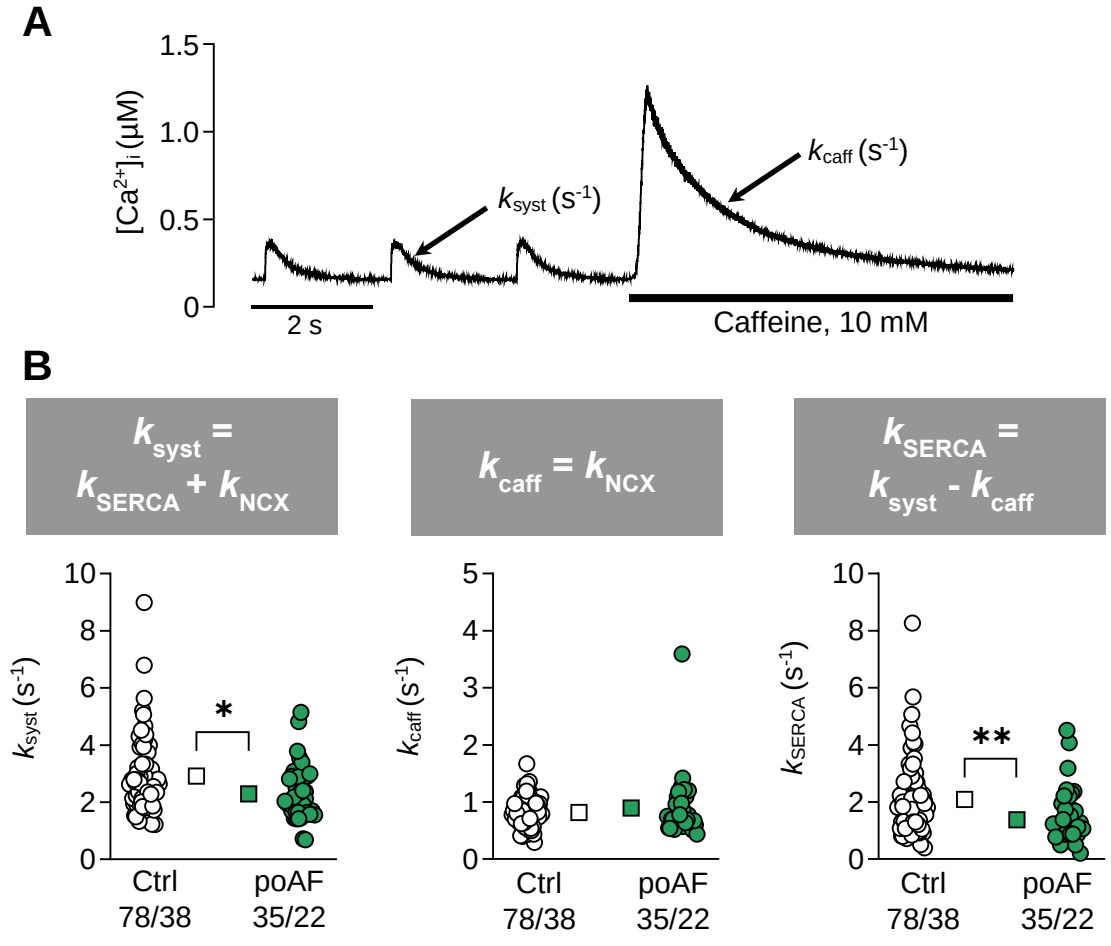

Figure 19. SR Ca^{2+} ATPase (SERCA2a) function in atrial myocytes from patients who do not (Ctrl) and who do develop postoperative atrial fibrillation (poAF). A, Representative caffeine experiment, indicating the decay rate constant of the systolic ($I_{Ca,L}$-triggered) Ca^{2+} transient (k_{syst}) and the decay rate constant of the caffeine-induced Ca^{2+} transient (k_{caff}). **B,** Respective rate constants k_{syst} (left), k_{caff} (middle) and k_{SERCA} (right), calculated as the difference between k_{syst} and k_{caff}) in Ctrl and poAF. **P*<0.05, ***P*<0.01 vs Ctrl. n/N=number of myocytes/patients. Comparison using unpaired Student's t-test. Adapted from Fakuade et al., 2020 (with permission).

However, although NCX predominates the expulsion of Ca^{2+} upon application of caffeine, PMCA also contributes to this removal and has been identified to participate significantly in Ca^{2+} homeostasis (Choi & Eisner, 1999). As such, the activity of PMCA was determined as described previously (Choi & Eisner, 1999; Voigt et al., 2012). Atrial myocytes were stimulated at 0.5 Hz to attain steady-state activity. Caffeine (10 mM) was subsequently applied whilst the bath was perfused with Na^{+}- and Ca^{2+}-free bath solution to abolish NCX removal of cytosolic Ca^{2+} (**Figure 20A**). Under this condition, the time constant (τ) of the cCaT decay provides an estimate of the PMCA activity, which was observed to be unchanged in poAF vs Ctrl (**Figure 20B**). This observation affirms our findings of unaltered NCX activity in poAF groups.

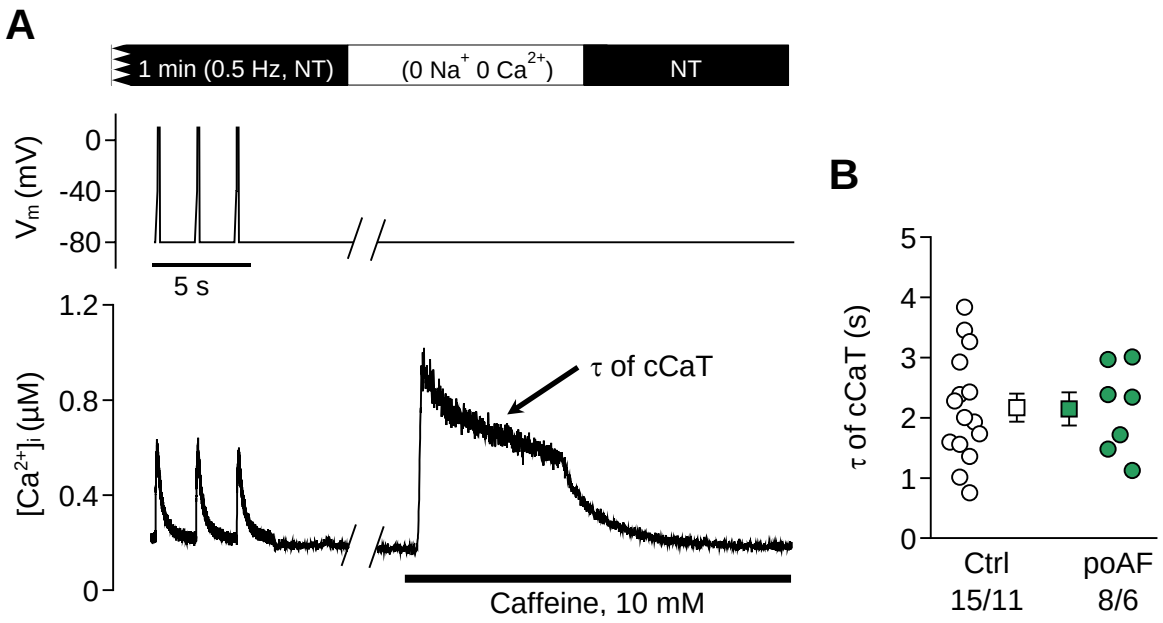

Figure 20. Quantification of plasmalemmal Ca^{2+}-ATPase (PMCA) activity in atrial myocytes from patients who do not (Ctrl) and who do develop postoperative atrial fibrillation (poAF). A, Representative recording demonstrating the protocol applied to determine the extrusion of Ca^{2+} by PMCA. **B,** Mean±SEM time constants (τ) determined by fitting an exponential to the decay phase of caffeine-triggered Ca^{2+} transient (cCaT) in the presence of Na^{+}- and Ca^{2+}-free bath solution. NT=Normal bath solution. n/N=numbers of myocytes/patients. Adapted from Fakuade et al., 2020 (with permission).

4.6 Beta-adrenergic signalling in atrial myocytes from poAF patients

Sympathetic stimulation mediated via activation of β-adrenergic receptors not only enhances ionotropic and chronotropic properties of the heart but also promotes excitability and automaticity of the myocytes therein (Maesen et al., 2012; Workman, 2010). Increased sympathetic activity has been implicated in the pathogenesis of poAF by several reports

(Anderson et al., 2017; Kalman et al., 1995; Maesen et al., 2012) and is known to influence excitation-contraction coupling via PKA-mediated phosphorylation of related proteins (Ginsburg & Bers, 2005). By virtue of this, we investigated the response of atrial myocytes to maximal β-adrenergic stimulation using 1 μM isoprenaline. Atrial myocytes were stimulated to steady-state, as described above (see **section 4.2**), in the presence and absence of isoprenaline to measure changes in $I_{Ca,L}$ and its corresponding triggered transient CaT (**Figure 21A**).

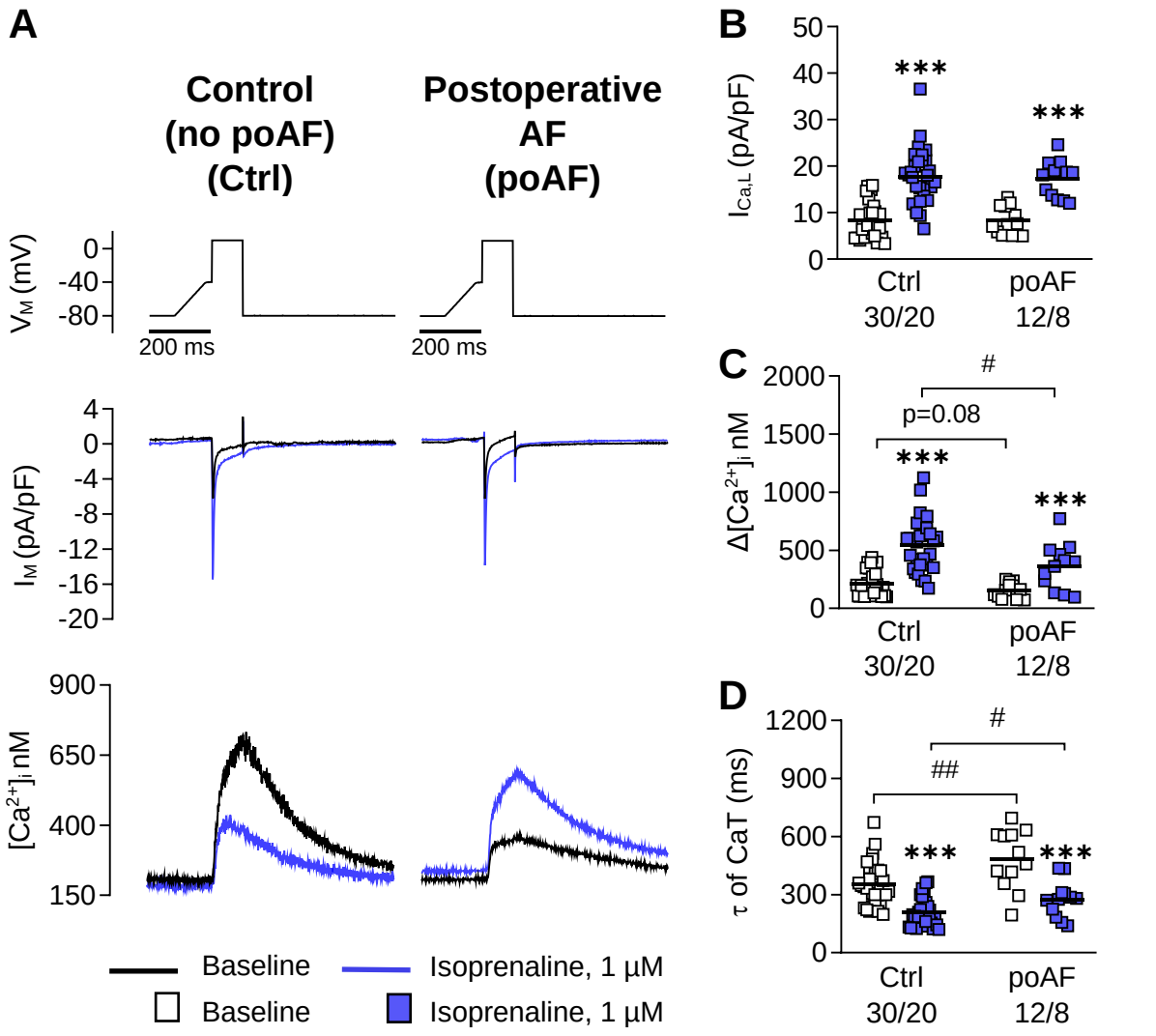

Figure 21. Beta-adrenergic stimulation of atrial myocytes from patients who do not (Ctrl) and who do develop postoperative atrial fibrillation (poAF). A, Voltage-clamp protocol (top), with representative simultaneous recordings of $I_{Ca,L}$ (middle) and triggered CaT (bottom) in Ctrl and poAF myocytes, before and after superfusion with isoprenaline. **B,** Corresponding Peak $I_{Ca,L}$, **C,** triggered CaT amplitude $\Delta[Ca^{2+}]_i$ and **D,** CaT decay time constants (τ). **P<0.01 ***P<0.001, #P<0.05, ##P<0.01 vs corresponding mean baseline values and Ctrl myocytes, respectively. n/N=numbers of myocytes/patients. Comparison using paired and unpaired Student's t-test. Adapted from Fakuade et al., 2020 (with permission).

Upon stimulation by isoprenaline, $I_{Ca,L}$ and the triggered CaT amplitude were significantly increased in both Ctrl and poAF, while a significant reduction in the time constant (τ) of CaT decay was observed, with each parameter having an approximate change of 200%, 150% and 60%, respectively in both Ctrl and poAF (**Figure 21B-D**). $I_{Ca,L}$ peak amplitude was similar between poAF and Ctrl in both the presence and absence of isoprenaline. However, in the absence of isoprenaline an inclination towards a reduced CaT amplitude was observed in poAF compared to Ctrl, while a significant reduction in CaT was recorded with isoprenaline exposure in poAF vs Ctrl (545.9±41.97 vs 360.3±51.38 nM, n/N=12/8 poAF vs 30/20 Ctrl, *P*<0.05, **Figure 21B**). The time constant (τ) of CaT decay was increased in poAF compared to Ctrl, regardless of whether isoprenaline was present (without isoprenaline: 484.1±44.24 vs 358.9.1±21.22 ms, *P*<0.01; with isoprenaline: 275.1±27.21 vs 210.1±13.20 ms, *P*<0.05, n/N=12/8 poAF vs 30/20 Ctrl, **Figure 21C**). This result indicates a persistence of the delayed removal of cytosolic Ca^{2+} observed during systole in poAF, upon isoprenaline stimulation.

Considering the phosphorylation events of Ca^{2+}-handling proteins associated with β-adrenergic stimulation (Ginsburg & Bers, 2005) and the slower cytosolic Ca^{2+} removal seen in poAF with isoprenaline stimulation in this study, the effect of isoprenaline on the Ca^{2+} transport mechanisms was investigated. The rate constants of systolic CaTs and cCaTs of atrial myocytes which enable the estimation of NCX and SERCA activity were determined as previously reported (see **section 4.5**), in the presence of isoprenaline (**Figure 22A**). NCX activity was unaltered by isoprenaline in both poAF and Ctrl as indicated by the unchanged rate constant (k_{caff}). Also, the rate constant k_{SERCA}, was increased in both poAF and Ctrl groups in the presence of isoprenaline compared to their baseline values. However, SERCA rate constant was significantly reduced in poAF regardless of adrenergic stimulation, indicating a diminished SERCA-mediated SR Ca^{2+} uptake (without isoprenaline: 2.942±0.49 vs 5.098±0.61 ms, *P*<0.05; with isoprenaline: 1.315±0.18 vs 2.386±0.35 ms, *P*<0.05, n/N=6/5 poAF vs 12/9 Ctrl, **Figure 22B**).

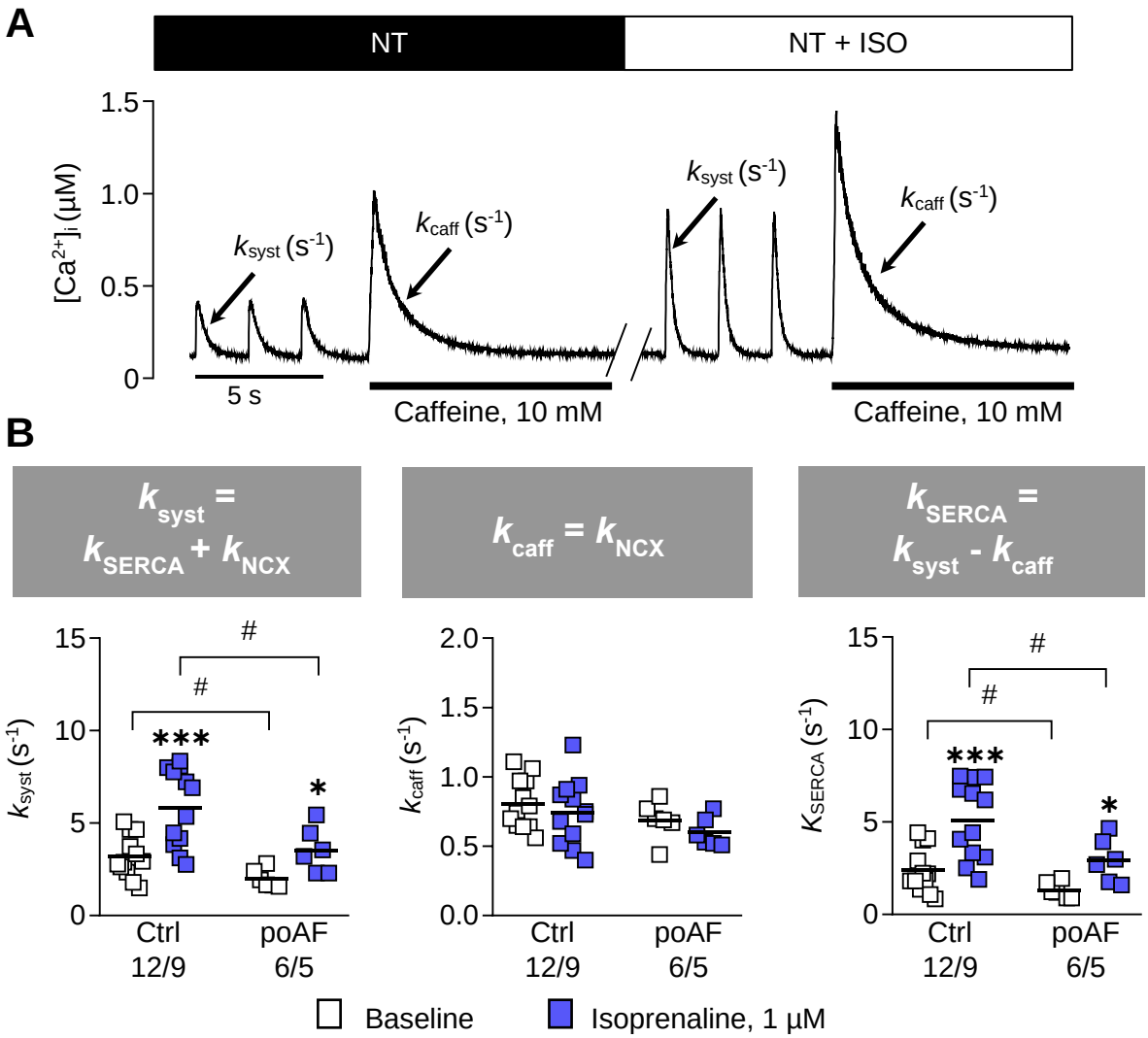

Figure 22. Effect of beta-adrenergic stimulation on NCX and SERCA function in atrial myocytes from patients who do not (Ctrl) and who do develop postoperative atrial fibrillation (poAF). A, Representative caffeine experiment, indicating the decay rate constant of the systolic ($I_{Ca,L}$-triggered) Ca^{2+} transient (k_{syst}) and the decay rate constant of the caffeine-induced Ca^{2+} transient (k_{caff}) in the presence and absence of isoprenaline **B,** Respective rate constants k_{syst} (left), k_{caff} (middle) and k_{SERCA} (right), calculated as the difference between k_{syst} and k_{caff}) in Ctrl and poAF. *P<0.05 ***P<0.001, #P<0.05, vs corresponding mean baseline values and Ctrl myocytes, respectively. n/N=numbers of myocytes/patients. Comparison using Mann-Whitney's U test and Wilcoxon matched-pairs signed rank test for unpaired and paired data respectively.

4.7 Susceptibility to APs and CaT alternans of atrial myocytes from poAF patients

Diminished sequestration of Ca^{2+} into the SR resulting from reduced SERCA activity has been implicated in the development of alternans in ventricular myocytes (Edwards & Blatter, 2014; Rosenbaum et al., 2009). Alternans, which on a cellular level describes beat-to-beat oscillation in the shape of both CaTs and APs at a constant stimulation frequency,

has been identified as a risk factor in the development of cardiac arrhythmia (Kanaporis & Blatter, 2017). Therefore, to determine if this phenomenon is synonymous with atrial myocytes with altered SERCA activity, computational modelling was performed utilising the atrial-specific Courtemanche model (Courtemanche et al., 1998). SR Ca^{2+} uptake compartment parameter was varied to simulate altered sarcoplasmic reticulum Ca^{2+}-ATPase (SERCA) activity in modelled APs and CaTs with different cycle lengths (Clerx et al., 2016). A decrease in SERCA function by 20% or 40% in this model, reduced alternans-stimulation frequency threshold (approximately 3.45 and 3.6 Hz, respectively) in both of AP and of CaT, as shown in **Figure 23B-C**. In comparison, a 20% increase in SERCA activity did not influence the stimulation frequency threshold for alternans.

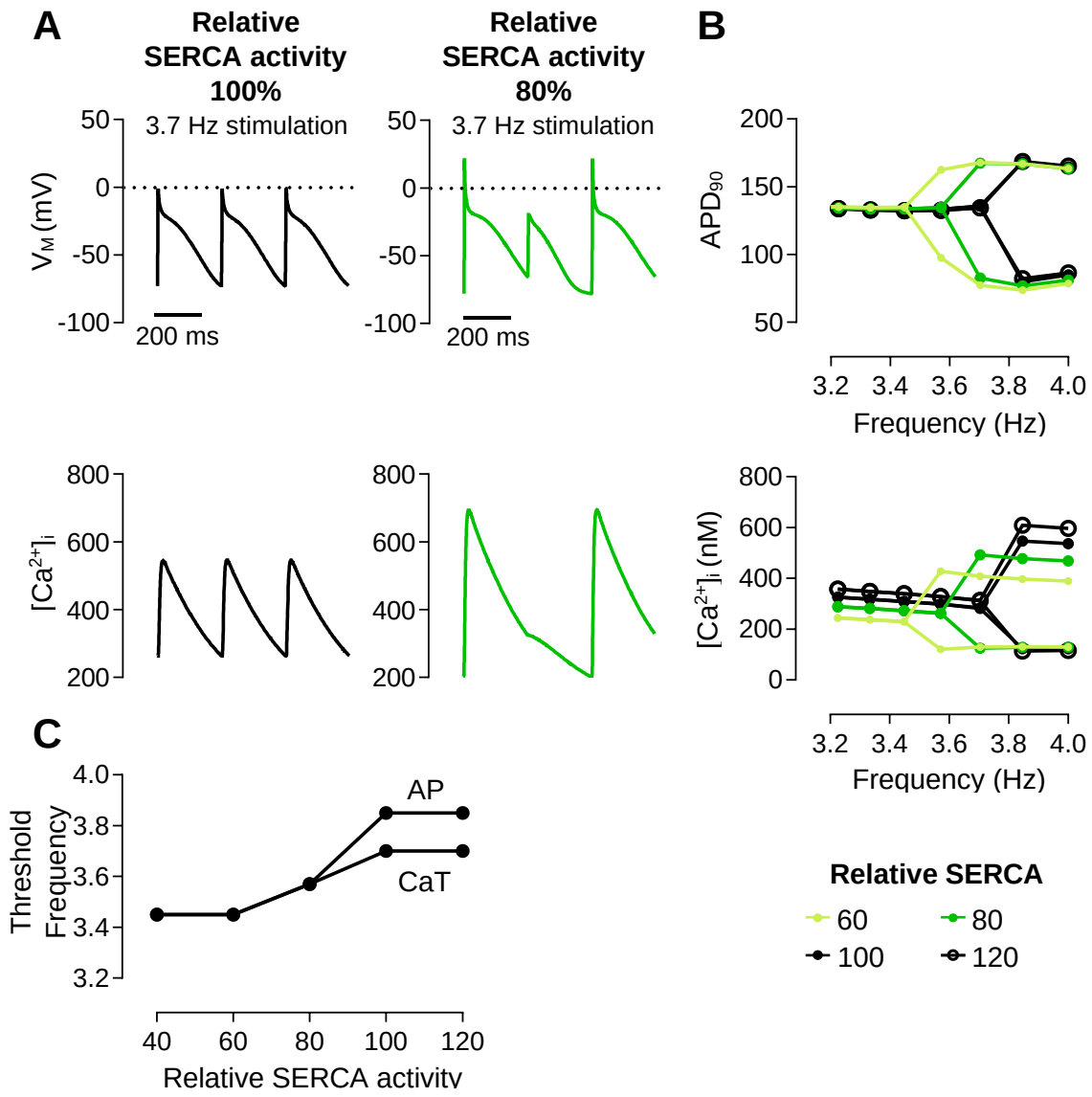

Figure 23. Computational modelling of SERCA-mediated alternans in human atrial myocytes. A, Modelled atrial action potentials (APs, upper) and Ca^{2+} transients (CaTs, lower) evoked at 3.7 Hz (270 ms cycle length) with 100% (left) and 80% SERCA function (right) using the Courtemanche model.[31] **B,** APD_{90} (upper) and CaT amplitude (lower) as a function of pacing frequency at varying SERCA activity levels. Point of divergence indicates threshold for alternans initiation. Resulting bifurcated branches represent the values for odd and even beats respectively. **C,** Threshold for alternans initiation of AP and CaT at varying levels of SERCA activity. Adapted from Fakuade et al., 2020 (with permission).

To further examine our in-silico findings, the effect of stimulation frequency on cardiac electrophysiology and Ca^{2+} handling in human atrial myocytes was investigated further. Fluo-3-loaded right atrial myocytes from Ctrl and poAF groups were paced at frequencies ranging from 0.25 to 8 Hz in current-clamp configuration, to elicit APs and accompanying CaTs (**Figure 24A**). Clinical characteristics of all patients were the same in both Ctrl and poAF groups (**Table 12**).

Table 12. Characteristics of patients used for current-clamp experiments

		Ctrl	poAF
General	Patients, n	16	13
	Day of first poAF episode	-	2.7±2.3
	Sex, male/female	15/1	10/3
	Age, y	63.0±9.4	68.5±11.3
	Body mass index, kg/m^2	27.6±3.5	26.8±5.5
Intervention	CAD, n	14	10
	MVD/AVD, n	2	3
	CAD+MVD/AVD, n	0	0
	Intervention time, min	266.7±73.9	268.1±116.5
	ECC time, min	126.5±48.1	123.2±49.7
Anamnesis	Hypertension, n	13	10
	Diabetes, n	3	1
	Hyperlipidemia, n	7	4
	NYHA (I/II/III), n	5/9/2	2/7/4
	Stroke, n	0	2
	TIA, n	0	1
CC	Creatinin, µmol/L	1.03±0.31	0.97±0.18
Echocardiography	LAD, mm	39.3±5.8	41.7±8.5
	LVEDD, mm	49.5±6.6	46.7±8.7
	IVSd, mm	12.6±3.1	12.9±3.4
	LVPWd, mm	11.5±1.6	11.0±2.0
	LVEF, %	55.3±9.8	52.0±11.9
	Diastolic dysfunction, Grade I/II	10/2	7/2
Medication	Digitalis, n	0	0
	ACE inhibitors, n	8	7
	AT1 blockers, n	6	3
	β-Blockers, n	9	7
	Dihydropyridines, n	3	3
	Diuretics, n	4	3
	Nitrates, n	1	1
	Lipid-lowering drugs, n	12	6

ACE, angiotensin-converting enzyme; AT, angiotensin receptor; CC, clinical chemistry; CAD, coronary artery disease; ECC, extracorporeal circulation; IVSd, interventricular septum thickness at end-diastole; LAD, left atrial diameter; LVEDD, left ventricular end-diastolic diameter; LVEF, left ventricular ejection fraction; LVPWd, left ventricular posterior wall thickness at end-diastole; NYHA, New York Heart Association Functional Classification; MVD/AVD, mitral/aortic valve disease; TIA, transient ischemic attack. Continuous data are expressed as mean±SD. Adapted from Fakuade et al., 2020 (with permission).

Resting membrane potential, mean AP duration at 90% repolarisation (APD_{90}), maximal slope of AP restitution curve, and diastolic $[Ca^{2+}]_i$ were not significantly different in poAF vs Ctrl (**Figure 24**). However, the CaT amplitude, over the examined frequencies, was significantly lower in the poAF group (**Figure 24D**), which is in agreement with the voltage-clamp experiments.

The occurrence of alternans in recorded APs and their corresponding CaTs at each stimulation frequency was subsequently investigated using a discrete Fourier spectrum transform method. **Figure 25A** depicts representative AP- and CaT-alternans observed at 4 Hz stimulation. Over the range of tested frequencies, 54% of Ctrl myocytes and 63% of poAF myocytes developed AP alternans. Also, 17% and 42% of myocytes from Ctrl and poAF patients, respectively, exhibited CaT alternans. Kaplan-Meier analysis over the whole range of frequencies revealed higher susceptibility to AP- and CaT-alternans in poAF patients when compared with Ctrl (**Figure 25B**). Also, the threshold for AP alternans (2.62±0.52 vs 5.15±0.68 Hz; n/N=12/10 poAF vs 13/12 Ctrl) was significantly lower in the poAF group (**Figure 25C**), which aligns with the predictions of the computational modelling demonstrating a reduced SERCA function (**Figure 23**). Also, the threshold for CaT alternans showed a propensity to be lower in poAF when compared with Ctrl (**Figure 25C**).

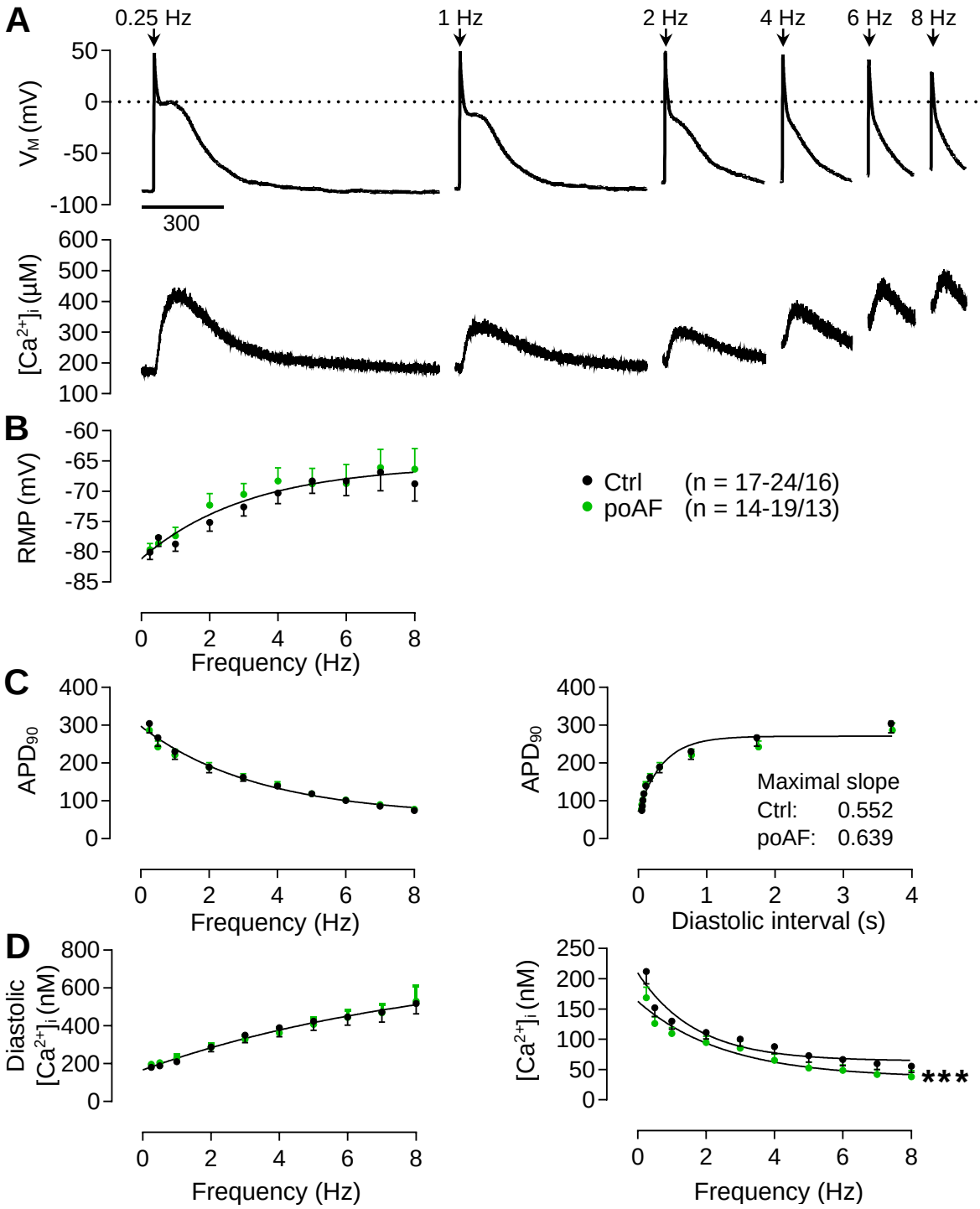

Figure 24. Combined measurements of action potentials (APs) and Ca^{2+} transients (CaTs) in atrial myocytes from patients who do not (Ctrl) and who do develop postoperative atrial fibrillation (poAF). A, Representative traces of simultaneous AP (upper) and CaT (lower) recorded at various frequencies from a patient proceeding to develop poAF. **B,** Mean±SEM of resting membrane potential (RMP) at increasing pacing frequencies. **C,** Mean±SEM of APD_{90} at increasing pacing frequencies (left) and diastolic intervals (right, AP restitution). **D,** Mean±SEM frequency-dependent effects on diastolic calcium (left) and CaT-amplitude (right) in myocytes from Ctrl and poAF-patients. **B-D,** A single decay curve was fitted when no significant difference between groups was detected with an extra sum-of-squares F test. Two curves imply a global significant difference between both groups. ***P<0.001. n-n/N=range of myocytes/patients. Adapted from Fakuade et al., 2020 (with permission).

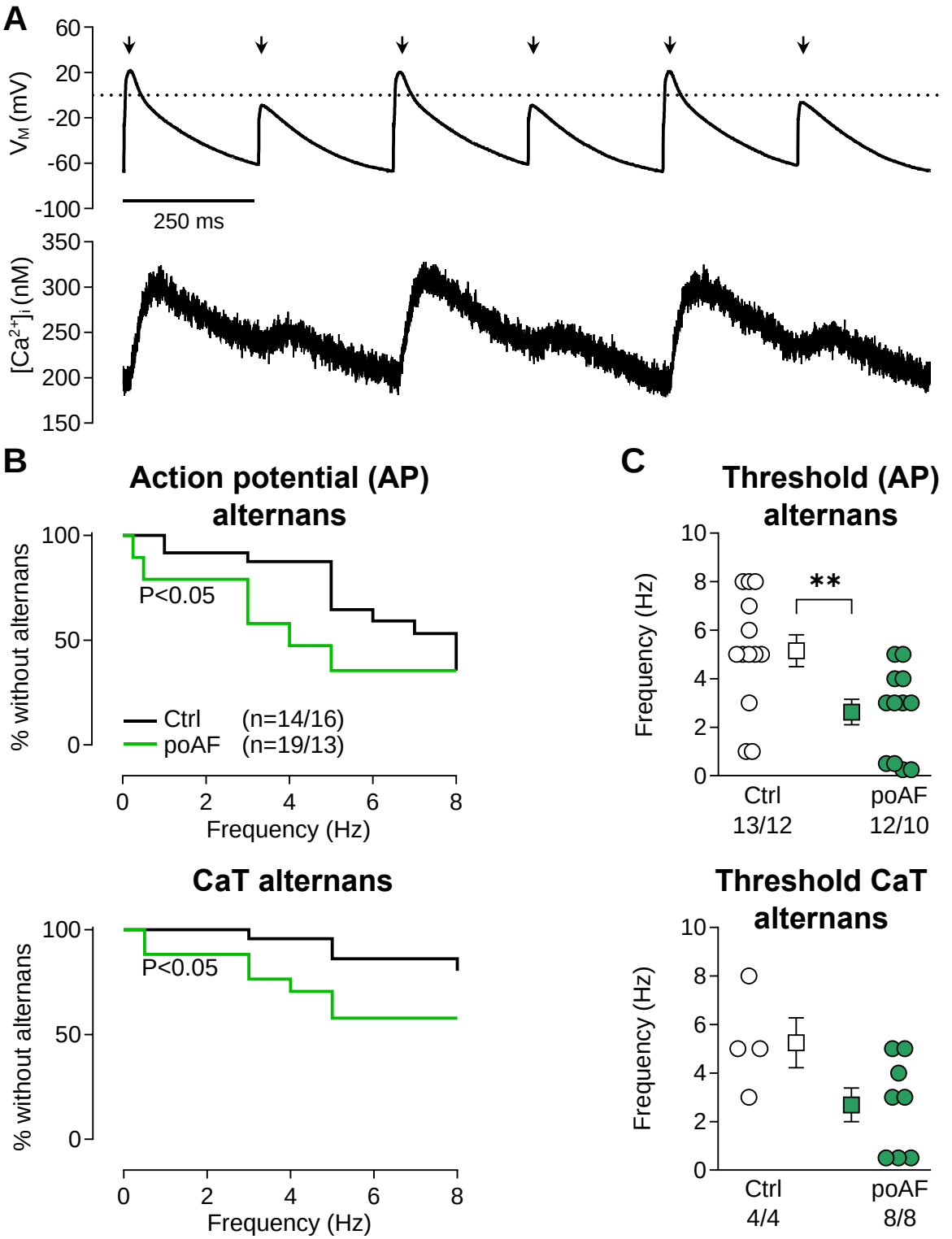

Figure 25. Occurrence of alternans in atrial myocytes with respect to the development of postoperative atrial fibrillation (poAF). A, Representative traces of concordant alternans in AP (amplitude and repolarization alternans; upper) and CaT (amplitude and diastolic alternans; lower) at 4 Hz measured from a patient proceeding to develop poAF. **B,** The first occurrence of frequency-dependent alternans as a Kaplan-Meyer plot in AP (upper panel) and CaT (lower panel). **C,** Alternans threshold frequency. Data are mean±SEM. Kaplan-Meyer curves compared with Gehan-Breslow-Wilcoxon test. ***P*<0.01 vs Ctrl. n/N=number of myocytes/patients. Alternans threshold frequency compared using Mann-Whitney's U test. Adapted from Fakuade et al., 2020 (with permission).

4.8 Gene and protein expression of Ca^{2+} handling proteins in poAF patients

To understand the molecular basis for the observed changes demonstrated by our functional experiments above, the protein and gene expression of major cellular Ca^{2+} handling proteins were evaluated. For immunoblotting studies, protein levels and phosphorylation status of the RYR protein were examined in whole right atrial tissue extract, while the proteins associated with cytosolic Ca^{2+} removal, i.e. SERCA2a, phospholamban (PLB) and NCX1, were quantified in solubilised membranes using Western blot. On the other hand, for gene expression analysis, total RNA was isolated from right human atrial tissue and quantified using RT-qPCR.

Immunoblotting revealed unchanged protein levels of RYR2 and its phosphorylated states (Ser2808- and Ser2814-phosphorylated RyR2) in poAF compared to Ctrl (**Figure 26A**). Similarly, RYR2 mRNA level was unchanged in poAF vs Ctrl (**Figure 28**). These findings agree with the similar diastolic leak observed in Ctrl and poAF groups in our functional studies (**Section 4.4**). In the same vein, both the protein expression/phosphorylation status and gene expression of PLB, which is a SERCA2a regulatory protein, was similar in poAF and Ctrl (**Figure 26B** and **Figure 28**). Likewise, the mRNA level of sarcolipin (SLN), another regulatory protein of SERCA2a, was unchanged (**Figure 28)**.

However, a reduction in the protein content of SERCA2a was observed in the poAF compared to Ctrl (**Figure 26C),** which may explain the reduced SERCA activity identified in our functional experiments above. Interestingly, no difference in gene expression of SERCA2a (*ATP2A2*) was detected in poAF compared to Ctrl groups (**Figure 28**). This discovery suggests the participatory role of posttranslational modifications of SERCA2a in the reduced SERCA-mediated extrusion of Ca^{2+} detected in poAF. Finally, protein and gene expression of NCX1, on the other hand, was unaltered in poAF vs Ctrl (**Figure 27** and **Figure 28**).

Table 13. Characteristics of patients used for immunoblotting and gene analysis

		Ctrl	poAF
General	Patients, n	48	45
	Day of first poAF episode	-	2.8±2.0
	Sex, male/female	42/6	38/7
	Age, y	64.7±8.1	68.3±8.3
	Body mass index, kg/m^2	27.9±3.0	28.0±3.3
Intervention	CAD, n	34	29
	MVD/AVD, n	6	9
	CAD+MVD/AVD, n	8	7
	Intervention time, min	261.5±81.1	287.0±106.0
	ECC time, min	128.0±57.6	139.1±58.7
Anamnesis	Hypertension, n	44	41
	Diabetes, n	11	16
	Hyperlipidemia, n	23	27
	NYHA (I/II/III), n	5/17/10	1/19/14
	Stroke, n	3	4
	TIA, n	1	2
CC	Creatinin, µmol/L	0.98±0.19	1.03±0.29
Echocardiography	LAD, mm	39.3±8.3	41.1±9.6
	LVEDD, mm	47.9±6.6	49.5±7.5
	IVSd, mm	12.8±3.4	12.6±2.9
	LVPWd, mm	11.6±3.4	12.2±3.0
	LVEF, %	53.6±10.0	49.4±11.5
	Diastolic dysfunction, Grade I/II/III	22/9/0	19/2/2
Medication	Digitalis, n	0	0
	ACE inhibitors, n	26	18
	AT1 blockers, n	17	14
	β-Blockers, n	31	31
	Dihydropyridines, n	14	16
	Diuretics, n	15	17
	Nitrates, n	5	5
	Lipid-lowering drugs, n	40	35

For abbreviations, see **Table 12**. Continuous data are expressed as mean±SD. Adapted from Fakuade et al., 2020 (with permission).

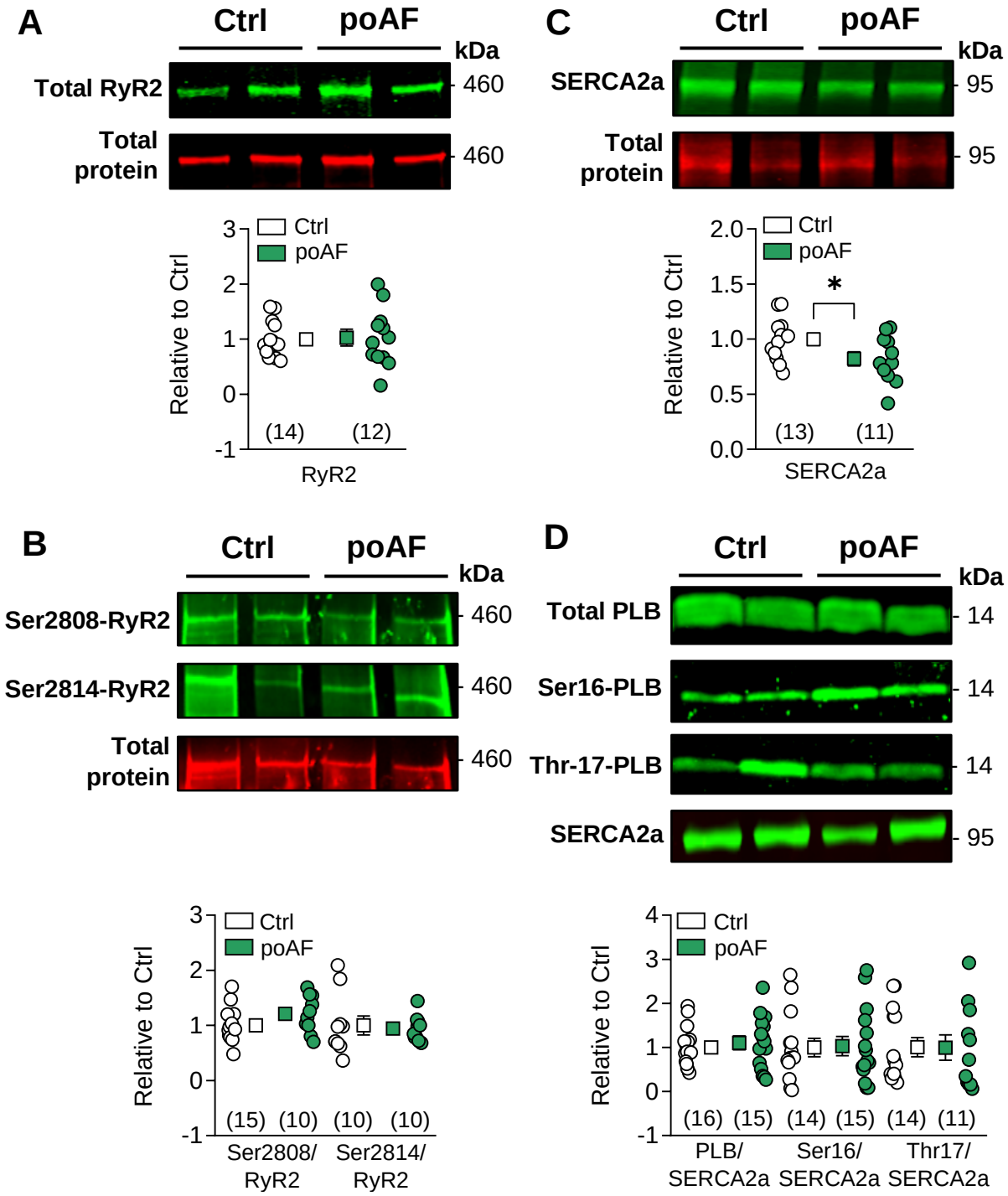

Figure 26. Protein expression and phosphorylation status of RYR2, PLB and SERCA2a in atrial tissue of patients who do not (Ctrl) and who do develop postoperative atrial fibrillation (poAF). A. Representative blots (upper) showing the expression of total RyR2 (green) against total protein in the same gel area (red) and its quantification (lower) normalized to total protein. **B,** Representative blots (upper) showing RyR2 phosphorylation at Ser2808 and Ser2814 (green) against total expression of RyR2 (red) and their quantification normalized against total RyR2. **C,** Representative Western blots (upper) showing the expression of SERCA2a (green) against total protein in the same gel area (red). And its quantification normalized against total protein. **D,** Representative blots (upper) showing the expression of total PLB, PLB phosphorylation at Ser16 and Thr17, respectively, against SERCA2a and their quantification (lower) normalized to SERCA2a. **P*<0.05 vs Ctrl. n=number of tissue samples (C, D). Comparison using unpaired Student's t-test. Adapted from Fakuade et al., 2020 (with permission).

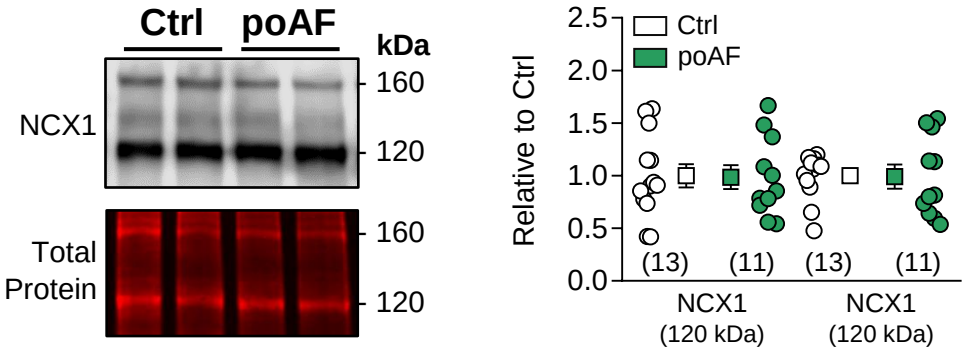

Figure 27. Protein expression of NCX1 in atrial tissue of patients who do not (Ctrl) and who do develop postoperative atrial fibrillation (poAF). Representative Western blots (upper left, greyscale) and quantification of NCX1 expression (right) in atrial tissue samples. Data normalized against total protein (lower left, red) in the same gel area. n= number of tissue samples. Adapted from Fakuade et al., 2020 (with permission).

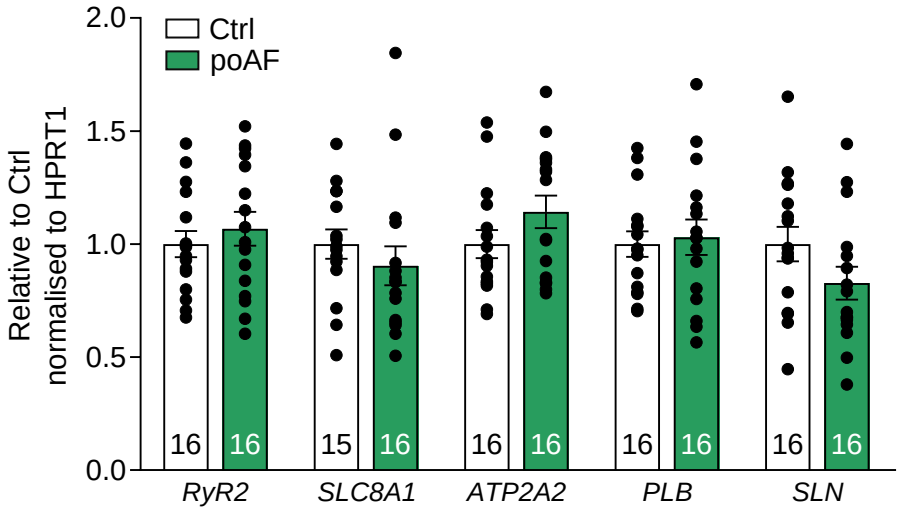

Figure 28. Gene expression of components regulating intracellular Ca^{2+} handling in patients who do not (Ctrl) and who do develop postoperative atrial fibrillation (poAF). Measurements carried out in duplicate, shown as mean±SEM. n=patients. Adapted from Fakuade et al., 2020 (with permission).

4.9 Discussion

In this part of the study, we demonstrate for the first time a detailed analysis of the alterations of $[Ca^{2+}]_i$ handling predisposing patients to the development of poAF (**Figure 29**). We report the absence of electrical remodelling in patients who developed poAF, as demonstrated by similar $I_{Ca,L}$, its integral, as well as the similar APDs observed in poAF patients compared to Ctrl. However, speckle-tracking strain analysis indicated diminished atrial contractile function, which was determined to be attributable to a reduction in the SR Ca^{2+} release of atrial myocytes. The impaired SR Ca^{2+} release was identified to occur because of reduced SR Ca^{2+} content and impaired diastolic SR Ca^{2+} sequestration. Furthermore, *in silico* modelling postulated a higher predisposition of atrial myocytes to AP and CaT alternans when SR Ca^{2+} uptake is impaired. Accordingly, a higher vulnerability and a lower threshold frequency for both CaT and AP alternans were exhibited by right atrial myocytes from poAF patients. Collectively, our findings highlight impaired SR Ca^{2+} uptake as a common underlying mechanism that facilitates both the impaired contractile function as a pre-existing independent risk factor, as well as the arrhythmogenic substrate that predisposes patients to the development of AF.

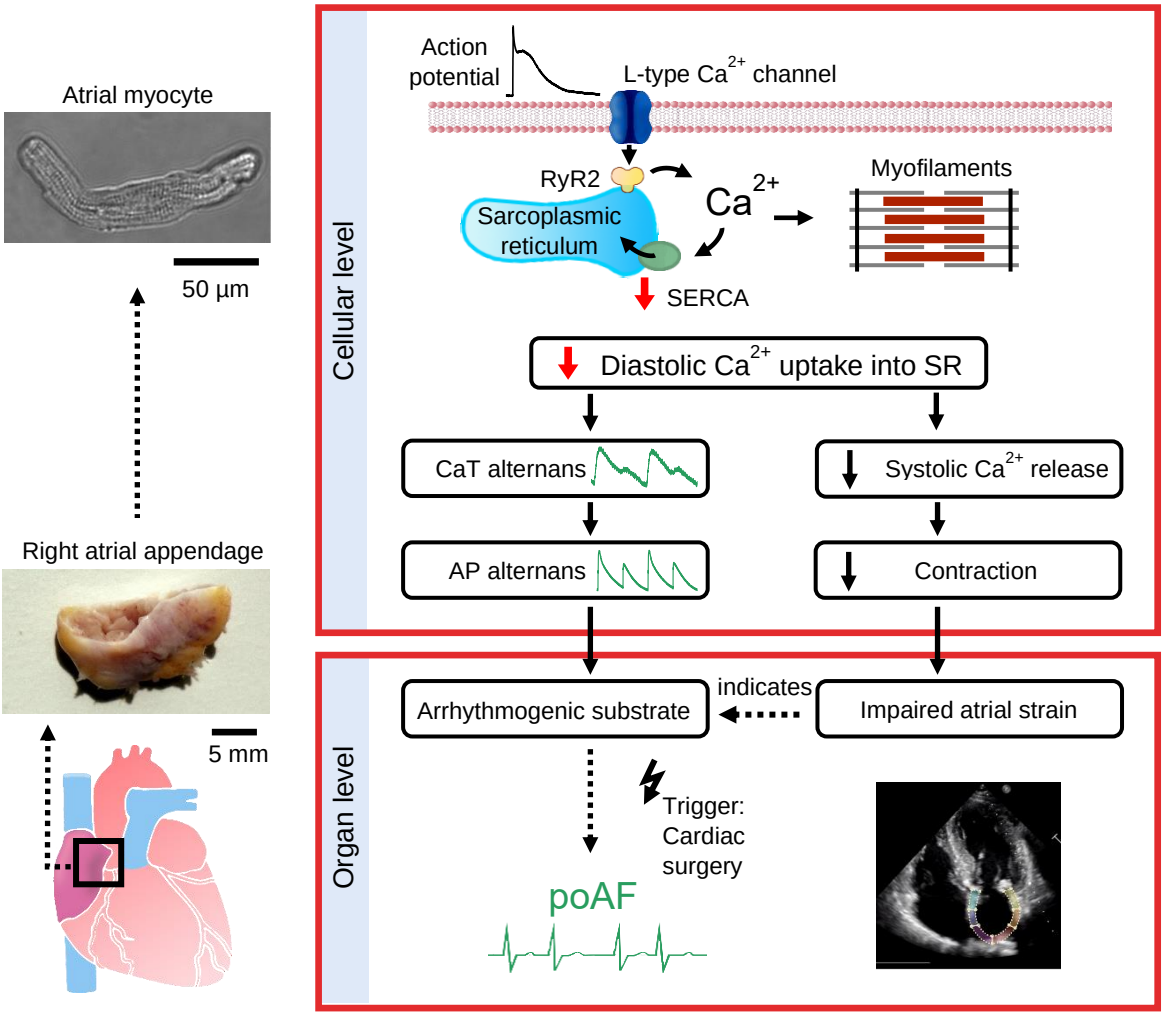

Figure 29. Graphical abstract outlining the pre-existing cellular mechanisms in postoperative atrial fibrillation development. Replotted from Fakuade et al. 2020 (with permission)

4.9.1 poAF atrial myocytes show distinct electrical and Ca^{2+} remodelling compared to cAF and pAF

Electrical remodelling is one of the principal mechanisms that contribute to the development of AF (Nattel & Harada, 2014). Decreased $I_{Ca,L}$, increased I_{K1} and constitutive $I_{K,ACh}$, are well identified electrical remodellings of ion currents associated with cAF (Dobrev et al., 2005; Van Wagoner et al., 1997; Voigt et al., 2012). Remodelling of these ion currents leads to the shortening of the atrial APD, which is a promoter of re-entry, the major mechanism responsible for the maintenance of AF (Voigt et al., 2012). Our data showed no electrical remodelling in poAF. In our study, electrical parameters such as $I_{Ca,L}$ amplitude and its integral (**Figure 15B**) were both unchanged at the time of surgery in atrial myocytes of poAF patients compared to Ctrl. Similarly, both APD and its frequency dependence, as well as the RMP (**Figure 24**) were identified by our current-clamp experiments to be unchanged in poAF compared to Ctrl, signifying similar ion channel

activities. These findings are in accord with observations of previous reports where the I_{Na} and $I_{Ca,L}$, both depolarizing currents, and the repolarizing potassium currents in poAF patients remained unaltered both in activity and expression (Brandt et al., 2000; Dobrev et al., 2002; Workman et al., 2006), thus resulting in comparable APD and RMP. On the other hand, an investigation conducted by Van Wagoner et al., documented an increase in $I_{Ca,L}$ in poAF patients (Van Wagoner et al., 1999). The reason for this reported disparity may result from differing clinical characteristics and experimental strategies.

Furthermore, Ca^{2+} handling remodelling is a typical mechanism implicated in both pAF and cAF (Nattel & Harada, 2014). The most significant profibrillatory contribution of abnormal Ca^{2+} handling associated with pAF and cAF is the promotion of ectopic firing, via Ca^{2+}-mediated delayed afterdepolarizations (DAD) (Dobrev et al., 2019). These DADs are believed to be caused by increased SR Ca^{2+} leak and spontaneous Ca^{2+} release events (Voigt et al., 2012, 2014). However, in this study, no evidence for an increase in SR Ca^{2+} leak was detected in atrial myocytes from poAF patients at the time of surgery (**Figure 18**). This observation conforms with our data demonstrating unchanged protein expression and phosphorylation for RYR2, including unchanged mRNA levels (**Figure 26** and **Figure 28**). A corroborating finding was reported by Lezoulac'h et al., where unaltered RYR2 mRNA levels were observed in poAF (Lezoualc'h et al., 2007). Collectively, our data indicate that the occurrence of cellular Ca^{2+}-dependent DADs does not seem to facilitate pre-existing arrhythmogenic substrates in patients that develop poAF.

4.9.2 Atrial myocytes from poAF patients are more susceptible to AP and CaT alternans

The occurrence of alternans on a cellular level can amount to spatially discordant electrical alterations in excitation (irregular distribution of prolonged and reduced APDs) as well as electrical heterogeneity (different regions with different repolarisation properties) within atrial tissues. These alterations increase the probability for the induction of re-entry, which promotes the maintenance of AF (Florea & Blatter, 2012; Narayan et al., 2002). There is an exhibition of higher magnitudes of monophasic AP alternans by both cAF and pAF patients, at lower stimulation frequencies (Lalani et al., 2013). Our data reveal that right atrial myocytes obtained from poAF patients during cardiac surgery exhibit a higher susceptibility to AP alternans at the time of surgery when paced at increasing frequencies (**Figure 25**). To the best of our knowledge, this is the first study demonstrating the occurrence of alternans in human atrial myocytes.

The well-accepted mechanism for AP alternans postulates that its emergence is based on the corresponding shortening of APs in response to preceding diastolic interval (Weiss et al., 2011). Plotting of our APD_{90} measurements of human atrial myocytes against the preceding diastolic interval showed no difference in the resulting AP restitution curve (**Figure 24C**). Furthermore, the maximum slope of the AP restitution curves was less than 1 (**Figure 24C**), which, according to the "restitution hypothesis" needs to be greater than 1 for cellular alternans to occur (Fox et al., 2002). Our findings indicate that changes in sarcolemmal ion-channel fluxes are not responsible for the cellular alternans seen in our study.

Recent studies postulate that $[Ca^{2+}]_i$ alternans serves as the primary driver for AP alternation. In other words, beat-to-beat alterations in cytosolic CaT can initiate and sustain alterations of AP shapes due to a perturbed interaction between $[Ca^{2+}]_i$ and its transport mechanisms, such as $I_{Ca,L}$ channels and NCX1 (W. Wang et al., 2018). Alternans driven by $[Ca^{2+}]_I$ can be enhanced by disturbances of Ca^{2+} handling that augment SR Ca^{2+} release, such as increased SR Ca^{2+} leak (Weiss et al., 2011). In this present study, neither expression and phosphorylation of RYR2 nor diastolic SR Ca^{2+} leak were altered in atrial myocytes of poAF patients compared to Ctrl myocytes (**Figure 18** and **Figure 26**). Our findings absolve SR Ca^{2+} leak of contributing to the increased susceptibility to alternans observed in poAF.

4.9.3 Reduced SERCA activity underlies the vulnerability of poAF atrial myocytes to alternans

Disruption in Ca^{2+} handling processes that reduce Ca^{2+} sequestration from the cytosol can also initiate $[Ca^{2+}]_i$-driven alternans (Weiss et al., 2011). In concordance, our *in-silico* data indicated that a slower uptake of Ca^{2+} in the SR, encourages the occurrence of alternans in atrial myocytes (**Figure 23**). Therefore, the slower Ca^{2+} uptake in our *in-vitro* findings (**Figure 19**), appears to underpin the higher susceptibility of atrial myocytes from poAF patients to alternans.

In agreement with previous reports (Dobrev et al., 2019), expression and phosphorylation of the SERCA-regulatory protein, PLB, was not altered in poAF patients, suggesting that the detected reduction in expression of the SERCA2a protein in our membrane preparations, is a major contributor to reduced SR Ca^{2+} uptake in poAF patients (**Figure 26**). This claim is buttressed further by our observation of unaltered buffering of cytosolic Ca^{2+} in atrial myocytes of poAF patients (**Figure 17**), of which if increased, could delay SR Ca^{2+} reuptake (Díaz et al., 2001). Furthermore, the activity of SERCA2a, which is

augmented upon β-adrenergic stimulation, due to PKA-mediated phosphorylation of PLB, was diminished in right atrial myocytes of poAF patients compared to Ctrl, irrespective of the presence of isoprenaline (**Figure 22)**. This finding further validates the contribution of decreased SERCA2a expression in the slower SR Ca^{2+} uptake observed in poAF.

Also, besides the primary inhibitory regulator of SERCA2a, i.e. PLB, SLN also acts to inhibit SERCA2a-mediated sequestration of Ca^{2+} into the SR in the atria. Although no significant difference in the gene expression of SLN was detected in this present study, we observed a strong propensity towards reduced SLN mRNA levels in poAF patients (**Figure 28**), which may reflect an adaptive mechanism to mitigate the effects of reduced SERCA2a expression (Zaman et al., 2016). The mechanisms responsible for reduced expression of SERCA2a in poAF patients remain unknown and may constitute several factors, which could be environmental or genetic in origin. The unchanged SERCA2a mRNA levels in poAF patients of this study (**Figure 28**) infer a possible role of posttranslational mechanisms in the aforementioned reduced protein levels of SERCA2a. Small ubiquitin-like modifiers (SUMO) interact post-translationally with SERCA2a to regulate its stability and expression levels (Mendler et al., 2016). A recent study reported the SUMOylation of SERCA2a as a participating mechanism responsible for the reduced SERCA2a expression seen in heart failure (Kho et al., 2011). Thus, possible participation of this mechanism in the impaired atrial SERCA2a expression in patients developing poAF needs to be investigated in future studies.

4.9.4 Reduced SERCA activity contributes to the impaired contractility in poAF

Many studies have reported atrial contractile dysfunction to be associated with poAF patients, with the consistency of this observation, ensuring its inclusion in the possible predictors of patients at risk of developing poAF (Aksu et al., 2019; Verdejo et al., 2016), which is in agreement with our atrial strain findings (**Figure 5**). The reduced SERCA2a activity observed in our study may contribute to the preoperative atrial hypocontractility seen in patients who developed poAF, and by reason, provide an interlink between atrial contractile dysfunction and atrial arrhythmogenesis. This atrial mechanical dysfunction is identified by consensus as an integral determinant of atrial cardiomyopathy, which represents atrial phenotypes that may facilitate clinical relevant manifestations such as thromboembolic stroke that are independent of AF (Guichard & Nattel, 2017). The prognosis of early stroke after cardiac surgery as well as a long term risk of stroke is known to be associated with the development poAF (Dobrev et al., 2019). However, the role of

SERCA2a-mediated atrial contractile dysfunction (atrial cardiomyopathy) in the predisposition of patients to stroke, independent of AF, remains unknown.

4.9.5 Limitations

In this study, as a result of limited availability of human atrial tissue, we used only right atrial appendages obtained during cardiac surgery. Therefore, experimental changes observed in this study, may not represent other regions of the atria. Similarly, speckle-tracking echocardiographic analysis was limited to the left atrium, due to poor sonographic conditions of the right atrium. However, a recent report documented altered right atrial strain parameters in patients who developed poAF, indicating that the diminished contractile function is a global occurrence in both atria of poAF patients, thereby suggesting that the observed alterations identified in our study are most likely similar to other atrial regions (Aksu et al., 2019). Regardless, strain measurements of both left and right atria in patients that develop poAF need to be investigated.

Secondly, we only focused on arrhythmogenic mechanisms in isolated atrial myocytes that could facilitate the development of poAF in this study. However, poAF is multifactorial and as such, additional factors such as genetics, the surgery type and inflammation that could influence the predisposition of patients to the development of poAF need to be investigated (Dobrev et al., 2019). For instance, pre-existing fibrosis is reported to be a key facilitator for the induction of re-entry in patients that develop poAF (Swartz et al., 2009). Interestingly, neither left atrial diameter nor LAScd were significantly different (**Table 10-13** and **Figure 14**), implying substantial structural alterations were not different between the two groups.

Lastly, we primarily investigated the Ca^{2+}-handling anomalies contributing to the pre-existing cellular substrate predisposing patients to the development of poAF. However, the autonomic nervous system and inflammatory mechanisms, which are activated during cardiac surgery, are major players in triggering of poAF in patients after surgery (Dobrev et al., 2019). A recent report has shown in both ventricular and atrial myocytes that β-adrenergic stimulation and pro-inflammatory cytokines including TNF-α and IL-1β increase the occurrence of spontaneous Ca^{2+} release events (Y. F. Hu et al., 2015), and by inference, facilitate the induction of poAF (Dobrev et al., 2019). The impact of inflammatory mediators on cytosolic Ca^{2+} handling in patients with and without the development of poAF needs to be addressed in future studies.

5 Extracellular matrix (ECM) remodelling in atrial fibrillation (AF)

Cardiac fibrosis is a deleterious process characterized by an imbalance between secretion and degradation of ECM proteins within the heart, thereby leading to an accumulation of ECM proteins in the interstitial space (Pellman et al., 2010). It is the hallmark of structural remodelling in most cardiovascular diseases, including AF, where it substantially increases the risk of AF patients to stroke and sudden death (Barallobre-Barreiro, Lynch, et al., 2016; Darlington & McCauley, 2020). The development and progression of fibrosis in the atria stabilize reentrant mechanisms, which leads to the perpetuation of AF (Dzeshka et al., 2015). Also, the accumulation of ECM proteins in AF increases the stiffness of the atria, thereby contributing to the contractile dysfunction associated with AF, which is an independent risk factor for stroke (Bisbal et al., 2020; Darlington & McCauley, 2020). Although tremendous progress has been made over the years in understanding the mechanisms propagating the development of atrial fibrosis, the impact of atrial fibrosis in the initiation and maintenance of AF and its complications has not still been explored in detail.

Previous studies have documented the presence of fibrosis in the atria of both poAF and cAF patients (reviewed in Dobrev et al., 2019; Dzeshka et al., 2015). However, the characterization of the ECM proteins has been sparsely investigated due to limitations attached to available analytical tools (Barallobre-Barreiro, Lynch, et al., 2016). Also, most studies investigating atrial fibrosis in AF have focused mainly on the structural ECM components, especially the collagens, paying little attention to other non-structural proteins which are responsible for the dynamic adaptation of the ECM in the heart (Frangogiannis, 2019). Also, recent evidence on ECM protein interactions and cardiomyocytes have demonstrated that in addition to their structural functions, they also transduce essential signals modulating cardiac myocyte function (Frangogiannis, 2019). Therefore, it is pertinent to characterize the ECM remodelling in both poAF and cAF patients.

With the advent of proteomics, which enables concurrent quantification of multiple proteins without the restrictions of antibody-based detection methods, exceptional insights into the pathological remodelling of the ECM have recently been unveiled. Barallobre-Barreiro and colleagues from the Mayr group in our collaborating partner institute, Kings College London, have recently employed proteomic studies to characterize the ECM proteins deposited in cardiac tissues, including those of AF patients, providing new insights into the

ECM remodelling in cardiac conditions (Barallobre-Barreiro et al., 2012; Barallobre-Barreiro, Gupta, et al., 2016; Barallobre-Barreiro, Lynch, et al., 2016). However, an in-depth analysis of the remodelling in ECM secretion in poAF and cAF has not been studied.

Therefore, using proteomics, we investigated the secretory remodelling of ECM proteins of human atrial tissues from poAF and cAF patients, to understand their role in the arrhythmogenic mechanisms and contractile dysfunction observed in these patients.

5.1 Evaluation of conditioned media quality for mass spectrometry (MS)

The quality of generated conditioned media is a significant challenge in the characterisation of the secretome from tissue samples by means of MS (Alvarez-Llamas et al., 2007). Tissue secretome is often contaminated by serum proteins and intracellular proteins, which is attributed to the respective diffusion of serum proteins trapped in tissues and the discharge of intracellular proteins from cells damaged during necessary mincing of tissue into the culture medium (Alvarez-Llamas et al., 2007; Hocking et al., 2010). Such contaminants could dramatically influence the detection and profiling of secreted proteins, particularly for low abundance proteins which are usually masked by those with high abundance (Hynes, 2014). Therefore, to determine the optimal strategy for generation of tissue-derived conditioned media suitable for analysis using MS, conditioned media were obtained, as described above, and investigated for contaminant proteins using immunoblotting. Conditioned media collected every 24th hour over a 48-hour tissue culturing time (1st and 2nd collection) were enzymatically deglycosylated (see **section 2.8.2**) and investigated for the protein contents of selected ECM proteins, intracellular proteins and serum proteins using Western blot. Prior to deglycosylation, the 2nd collection of conditioned media was concentrated by ultracentrifugation to ensure similar protein amounts were used for immunoblotting studies.

All secreted ECM proteins were abundant in the 2nd collection of conditioned media compared to the 1st in all three patient atrial samples (**Figure 30**). However, for the intracellular proteins, GAPDH was less abundant in the 2nd collection of conditioned media compared to the 1st; however, VIM was the same. Similarly, the serum protein serum amyloid-P was little to non-existent in the 2nd 24th-hour conditioned media compared to the 1st. These findings demonstrate a higher presence of contaminant proteins in the conditioned media collected 1st within the 48-hour culture period and as such, suggest that the 2nd collection of conditioned media is better suited for proteomic analysis of the ECM.

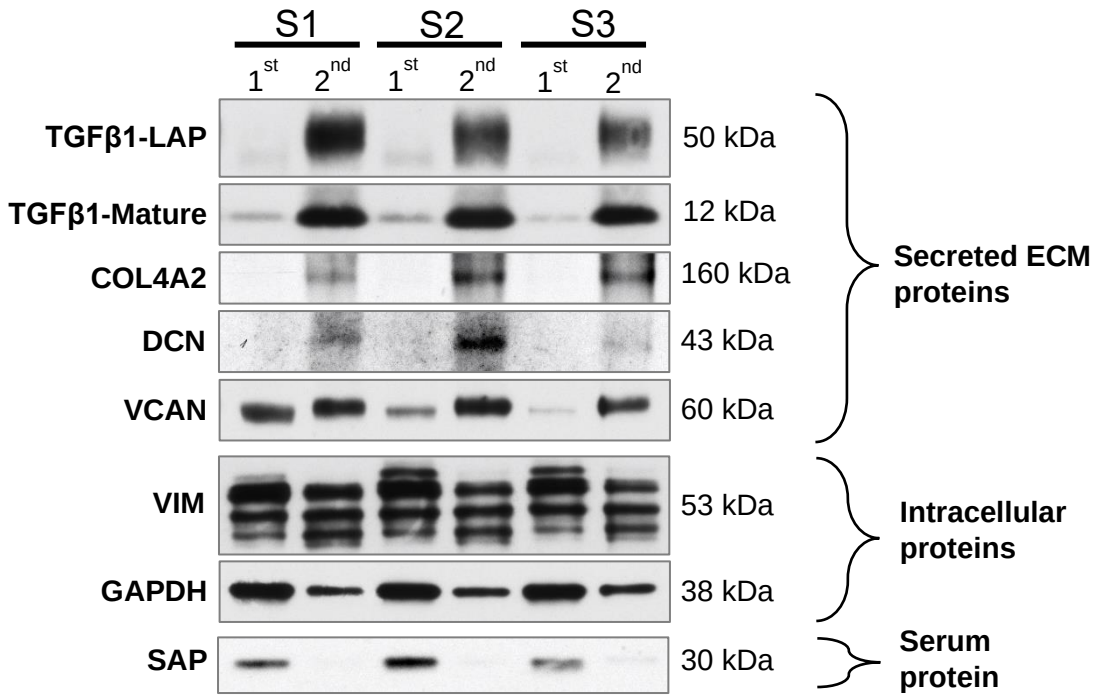

Figure 30. Evaluation of conditioned media quality by immunoblotting. Immunoblots comparing conditioned media obtained on the 1st and 2nd 24th hour of human atrial tissue incubation in serum free media over a 48 hour period. Protein levels of Transforming growth factor beta 1 (TGFβ1), collagen type IV alpha 2 chain (COL4A2), decorin (DCN), versican (VCAN), vimentin (VIM), glyceraldehyde 3-phosphate dehydrogenase (GAPDH) and serum amyloid P component (SAP) were assessed. S*n*=Sample identification number. n=3 patients. LAP=Latency associated peptide

5.2 Proteomic analysis of ECM proteins in atrial tissue secretome from poAF and cAF patients

Accumulation of excessive amounts of ECM proteins in cardiac tissue is a common occurrence in the pathogenesis of most cardiac diseases (Frangogiannis, 2019). Identified as a cardinal event in the development of atrial fibrosis, ECM protein accumulation may lead to diminished contraction and subsequent cardiac dysfunction (Dzeshka et al., 2015; Frangogiannis, 2019). Therefore, to ascertain the possible role of the ECM in the observed impaired atrial contractility reported in both poAF and cAF patients, the profile of ECM proteins in human atrial tissue was investigated using a secretomic approach. Conditioned media obtained after 48 hours of atrial tissue incubation from Ctrl, poAF and cAF patients, were deglycosylated and processed as described previously for protein analysis using LC-MS/MS (see **section 2.8.4** and **Figure 7**). Identified ECM proteins were allocated into divisions and sub-categories using the Matrisome project annotator (Naba et al., 2017).

Table 14. Characteristics of patients used for proteomic analysis.

		Ctrl	poAF	cAF
General	Patients, n	10	6	9
	Sex, male/female	10/0	6/0	7/1
	Age, y	62.1±11.4	72.3±5.6	69.8±8.7
	Body mass index, kg/m^2	29.0±5.7	29.8±2.4	28.8±3.83
Intervention	CAD, n	9	6	6
	MVD/AVD, n	0	0	1
	CAD+MVD/AVD, n	1	1	0
	Intervention time, min	238.8±40.3	275.0±74.1	303.8±76.3
	ECC time, min	106.4±27.0	131.8±34.3	157.3±57.4
Anamnesis	Hypertension, n	10	6	6
	Diabetes, n	2	2	1
	Hyperlipidemia, n	5	4	3
	NYHA (I/II/III), n	1/2/5	0/2/2	1/1/4
	Stroke, n	1	1	1
	TIA, n	0	0	0
CC	Creatinin, µmol/L	0.99±0.17	1.19±0.62	1.23±0.66
Echocardiography	LAD, mm	39.1±3.8	45.0±7.2	43.5±3.1
	LVEDD, mm	47.7±5.8	53.8±12.1	54.5±11.1
	IVSd, mm	11.4±2.0	13.2±2.4	14.2±2.1
	LVPWd, mm	11.6±1.4	10.3±1.2	12.2±1.7
	LVEF, %	57.2±15.8	48.3±8.1	46.8±10.7
	Diastolic dysfunction, Grade I/II/III	5/2/0	3/2/0	1/4/0
Medication	Digitalis, n	0	0	1
	ACE inhibitors, n	6	4	2
	AT1 blockers, n	3	2	2
	β-Blockers, n	7	3	6
	Dihydropyridines, n	4	3	3
	Diuretics, n	4	2	4
	Nitrates, n	1	0	1
	Lipid-lowering drugs, n	9	6	3

ACE, angiotensin-converting enzyme; AT, angiotensin receptor; CC, clinical chemistry; CAD, coronary artery disease; ECC, extracorporeal circulation; IVSd, interventricular septum thickness at end-diastole; LAD, left atrial diameter; LVEDD, left ventricular end-diastolic diameter; LVEF, left ventricular ejection fraction; LVPWd, left ventricular posterior wall thickness at end-diastole; NYHA, New York Heart Association Functional Classification; MVD/AVD, mitral/aortic valve disease; TIA, transient ischemic attack. Continuous data are expressed as mean±SD.

An overall total of 212 ECM proteins were identified, with the ECM glycoproteins category having the highest percentage (29%) with 61 proteins, while the least were the proteoglycans (6%) having only 12 proteins (**Figure 31)**. For clarity, differentially regulated proteins are subsequently described based on their categorical classifications.

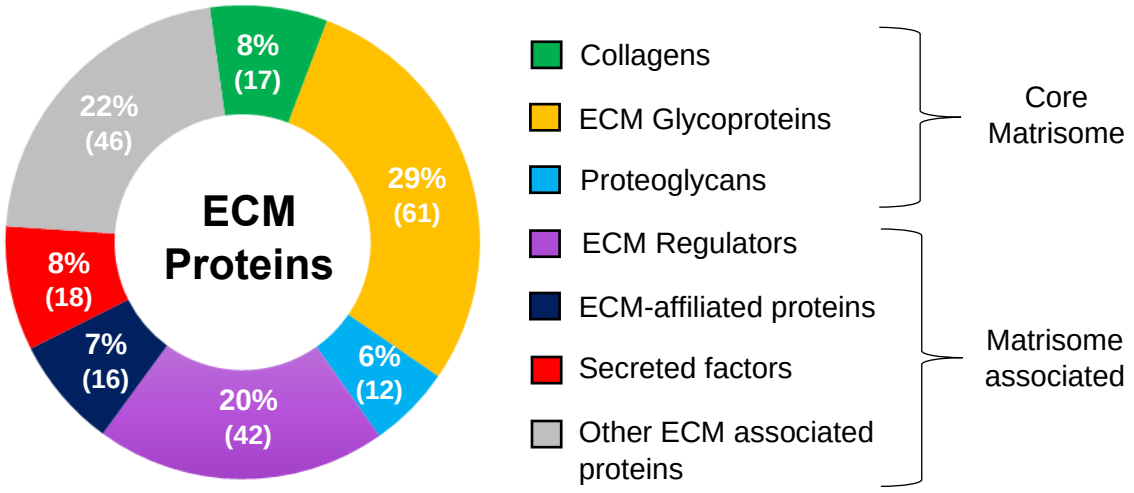

Figure 31. Profile of extracellular matrix (ECM) proteins identified in human atrial tissue secretome. A, Pie chart showing the distribution of categorised ECM proteins identified in conditioned media of human atrial tissue by mass spectrometry. Proteins were categorised as described by the matrisome project annotator (Naba et al., 2017), except for the category "other ECM associated protein". Numbers in brackets represent number of proteins identified in each class. n = 25 patient samples.

5.3 Differential regulation of ECM proteins in poAF patients

Upon quantification of ECM proteins, only 12 proteins were differentially abundant in the poAF group, with all the altered proteins upregulated in poAF compared to Ctrl (**Figure 32**). Among the collagens, only collagen I was upregulated in poAF, with its pro-α2(I) chain component (COL1A2: Log2 FC 1.32; *P*<0.05) being significantly upregulated, while a strong propensity towards upregulation observed in its pro-α1(I) chain component (COL1A1: Log2 FC 1.26; *P*=0.08, **Supplemental Table 1**). Also, the glycoproteins vitronectin (VTN: Log2 FC 1.79; P<0.05) and connective tissue growth factor (CTGF: Log2 FC 0.92; P<0.01) were significantly more abundant in poAF compared to Ctrl, while protein levels of all proteoglycans were unchanged in poAF. Also, 7 matrisome-associated proteins were significantly abundant in poAF. Of these, three of the ECM regulatory proteins were upregulated in poAF patients, including the microfibril-associated glycoprotein 4 (MFAP4: Log2 FC 0.72; P<0.05). A similar pattern was demonstrated by

annexin A5 (ANXA5: Log2 FC 0.96; *P*<0.05) and cadherin-1 (CDH1: Log2 FC 1.22; *P*<0.01), both Ca^{2+}-binding ECM-associated proteins, where their protein levels were increased significantly in poAF patients. Altogether, these findings suggest that the profile of the ECM in patients who developed poAF after cardiac surgery seems to be altered, which may be profound in later phases, as seen in tissues from patients with cAF.

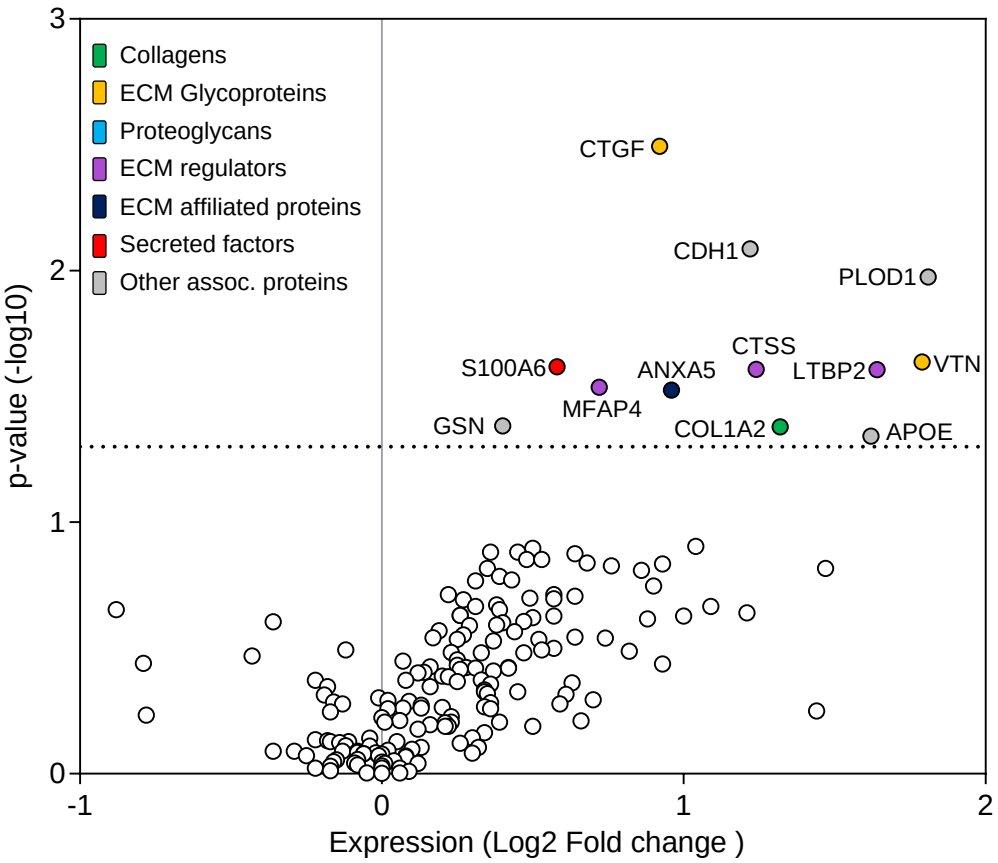

Figure 32. Proteomic analysis of the extracellular matrix (ECM) in the right atrial secretome from patients who developed postoperative atrial fibrillation (poAF). Volcano plots showing the difference in the expression of ECM proteins in the right atrial tissue secretome of poAF patients compared to Ctrl (control). Coloured data points represent significantly altered protein expressions in poAF vs Ctrl. Dotted lines denote threshold of significance (*P*<0.05). n = 10 patients for Ctrl and 6 patients for poAF. Comparison was made using Kruskal Wallis test followed by a Dunns post-hoc test. List of abbreviations can be found in supplement table.

5.4 Differential regulation of ECM proteins in cAF patients

In cAF patients, 85 out of the 212 ECM proteins identified were differentially abundant compared to Ctrl (**Figure 33**). Of these differentially regulated proteins, only 5 proteins were downregulated, with the other proteins having an increased abundance in cAF compared to Ctrl. Structural and basement proteins such as the collagens, including

collagen alpha-2(IV) chain (COL4A2: Log2 FC 1.12; *P*<0.01), were markedly elevated in cAF (**Figure 33** and **Figure 34**). Similarly, glycoproteins, like periostin (POSTN: Log2 FC 1.74; *P*<0.01), fibronectin 1 (FN1: Log2 FC 1.98; *P*<0.01) and MFAP4 (Log2 FC 0.89; *P*<0.01) were highly abundant in cAF patients when compared to Ctrl, except for laminin subunit beta-2 (LAMB2: Log FC -0.38; *P*<0.05), which was downregulated in cAF (**Figure 33** and **Figure 34**). This trend was also consistent in the proteoglycan family of proteins, where 33% of identified proteins, including biglycan (BCN: Log2 FC 1.05; *P*<0.001), versican (VCN: Log2 FC 1.36; *P*<0.01), perlecan (HSPG2: Log2 0.33; *P*<0.05), hyaluronan and proteoglycan link protein-1 (HAPLN1: Log2 2.92; *P*<0.03) showed a significant increase in protein abundance in cAF (**Figure 33** and **Figure 34**).

ECM-associated proteins (i.e. proteins with non-structural roles, but associated with the core ECM) also displayed a similar abundance pattern with that of the core proteins. Increased abundance of the regulatory protein cathepsin Z (CTSZ: Log2 FC 0.73; *P*<0.01) was observed in cAF patients; likewise, the categorised ECM affiliated proteins, galectin-1 (LGALS1: Log2 FC 0.93; *P*<0.001) and glypican (GPC1: Log2 FC 1.67; *P*<0.001). Notably, downregulation of galectin-3 binding protein (LGALS3BP: Log2 FC -0.84; *P*<0.001), categorised as an ECM-associated protein, was recorded in cAF, while CDH1 (Log2 FC 1.42; *P*<0.01) and protein disulphide isomerase (P4AB: Log2 FC 1.06; *P*<0.001) were both markedly increased in cAF compared to Ctrl (**Figure 33** and **Figure 34**).

Thus far, these findings demonstrate a dramatic upregulation of several ECM proteins indicating significant remodelling of ECM secretion in cAF compared to Ctrl, which appears exacerbated in comparison with poAF, where a similar trend but minimal ECM remodelling was observed. Notably, all differentially expressed ECM proteins in poAF were also altered in cAF, barring ANXA5, CTSS and VTN, which were unchanged in cAF (**Figure 34)**.

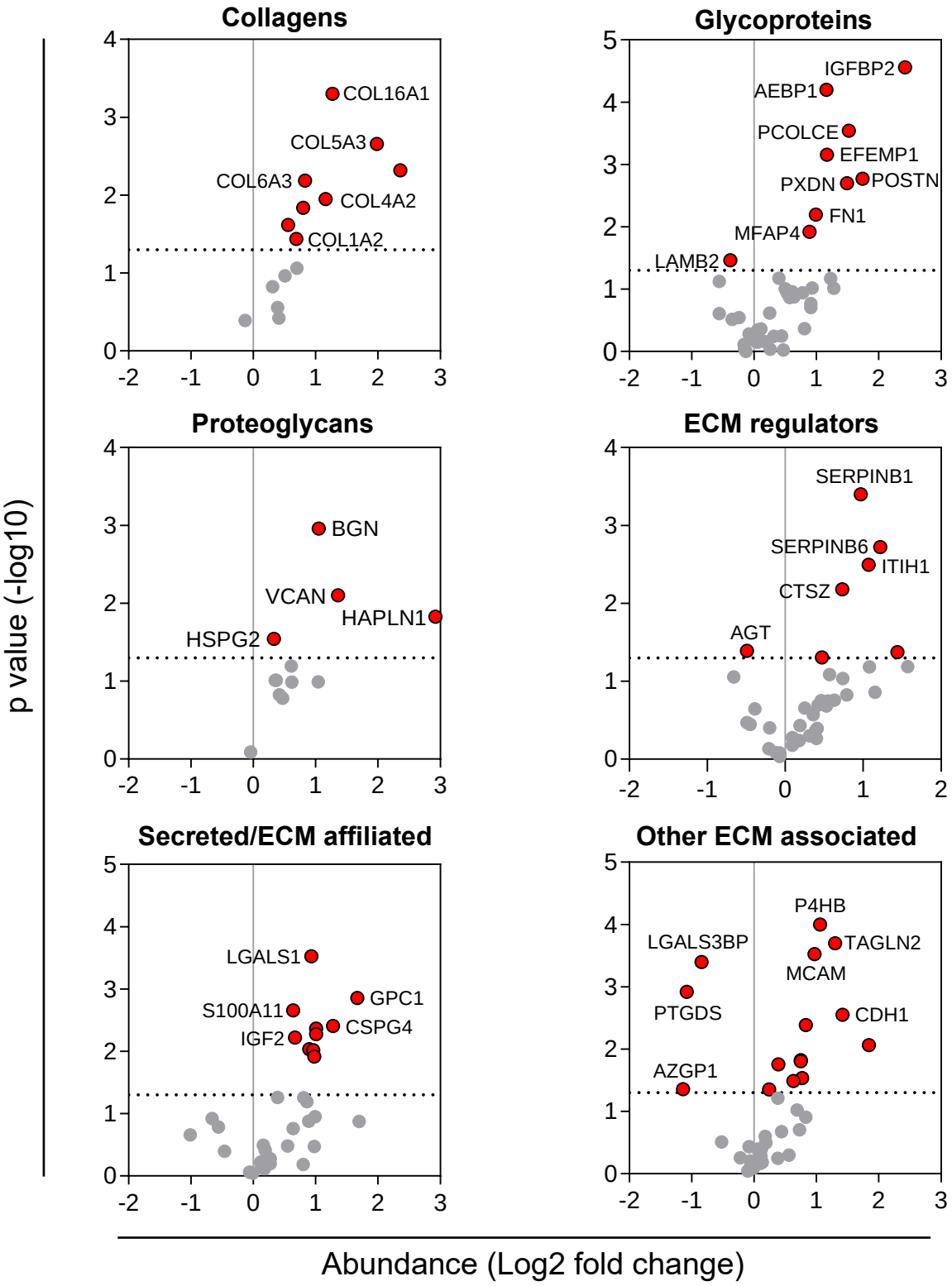

Figure 33. Proteomic analysis of the extracellular matrix (ECM) in the right atrial secretome from patients with chronic atrial fibrillation (cAF). Volcano plots showing the difference in expression of ECM proteins in the right atrial tissue secretome of cAF patients compared to Ctrl (control). Red data points represent significantly altered protein expressions in cAF vs Ctrl. Dotted lines signifies threshold of significance (P<0.05). n = 10 patients for Ctrl and 9 patients for cAF. Comparison was made using Kruskal Wallis test followed by a Dunns post-hoc test. List of abbreviations can be found in supplement table.

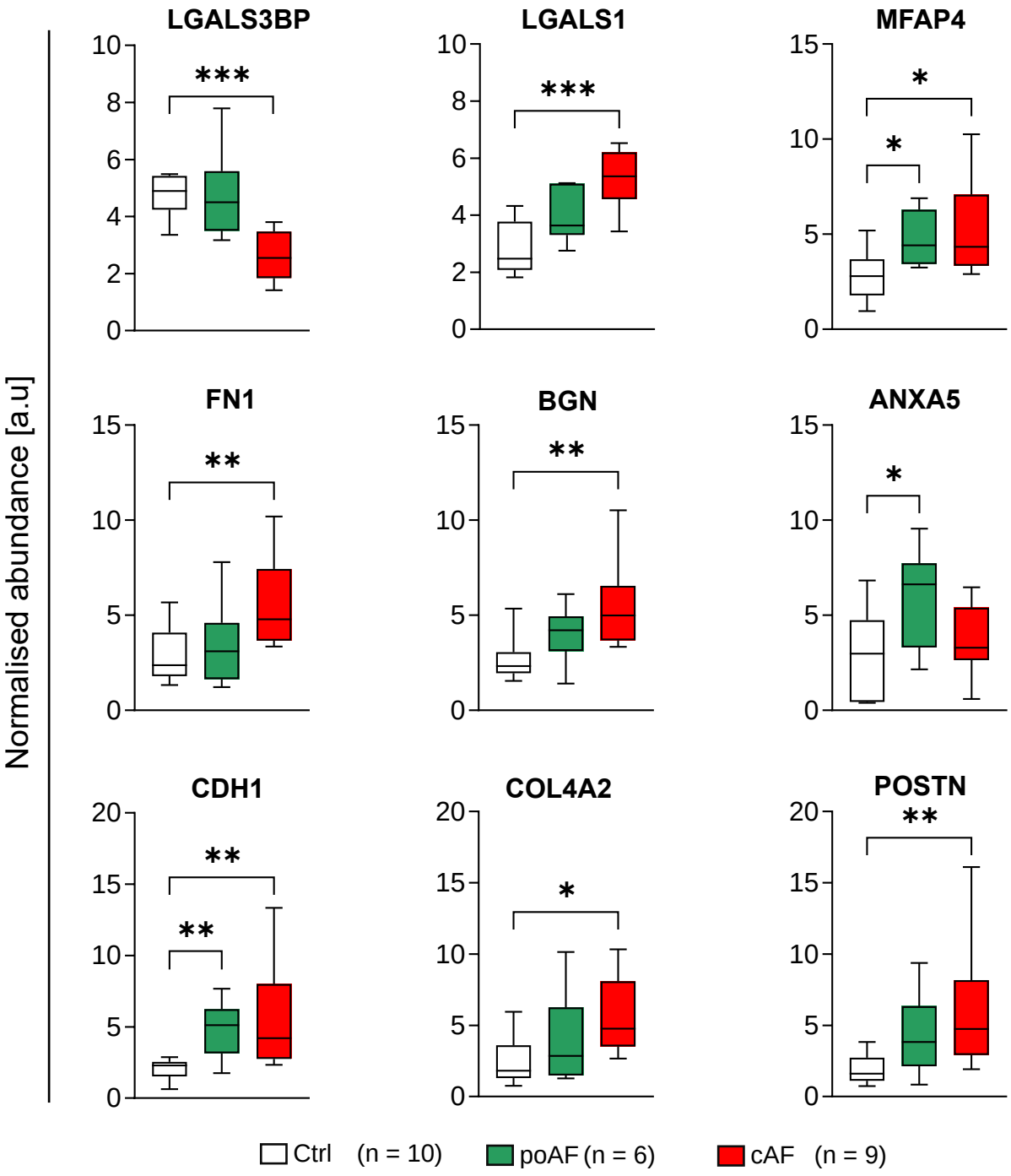

Figure 34. Differential abundance of selected ECM proteins in postoperative atrial fibrillation (poAF) and chronic atrial fibrillation (cAF). Box and whisker plots showing differences in abundance of ECM proteins in poAF and cAF compared to Ctrl. Box represents upper and lower quartiles while error bars represent maximum and minimum observed abundance. *P<0.05, **P<0.01 vs Ctrl. Comparison was made using Kruskal Wallis test followed by a Dunns post-hoc test. List of abbreviations can be found in supplement table.

5.5 Accumulation of ECM proteins in processed atrial tissue of poAF and cAF patients

In order to substantiate the findings of the above described proteomic data, the ECM protein deposition in processed human right atrial tissue was examined. ECM proteins extracted from frozen atrial tissues obtained post-production of conditioned media using a stepwise protocol, as described previously (**Section 2.8.6**), were deglycosylated and investigated for their expression using Western blot.

In general, a similar pattern of differential regulation of the selected ECM proteins was observed in the immunoblots (**Figure 35 and Figure 36**) when compared to the proteomic data described above. The expression of the ECM glycoprotein, periostin showed a non-significant trend for increased expression in poAF compared to Ctrl, which was complementary to the abundance pattern seen in our proteomic data. On the other hand, periostin was profoundly increased in cAF compared to Ctrl, corroborating the similar increase detected by our proteomic analysis. Interestingly, both VCAN and COL4A2 (**Supplemental Table 1** and **Figure 34**), which had similar protein abundance in poAF vs Ctrl in our proteomic data, displayed a tendency towards an increased protein expression levels for VCAN and COL4A2 respectively, in immunoblots comparing poAF to Ctrl. However, this was not the case in cAF, as the protein expressions of VCAN and COL4A2 increased significantly when compared to Ctrl, which is in line with our proteomics data.

Transforming growth factor-beta 1 (TGFβ1), regarded as one of the most potent mediators of fibrogenesis (Frangogiannis, 2020; Roberts et al., 1986), is produced as part of a proprotein comprising in addition to itself, the regulatory latency-associated peptide (TGFβ1-LAP). Both parts are linked together noncovalently when secreted as a large latent complex (LLC) with latent TGFβ binding protein (LTBPs) in the ECM, to ensure inactivation of the growth factor subunit (Annes et al., 2004; Robertson & Rifkin, 2016). Proteolytic cleavage of the LAP subunit activates TGFβ1, which interacts with its receptors, subsequently evoking downstream signalling events (Frangogiannis, 2020).

Protein expression of the active subunit TGFβ1 leaned towards an increase in poAF, while a significant increment was observed in cAF. Also, the regulatory subunit TGFβ1-LAP was not differentially expressed in poAF, but a disposition towards an increased protein expression of TGFβ1-LAP was observed in cAF when compared to Ctrl. TGFβ1-LAP and TGFβ1 were not identified in our proteomics data, which may stem from their preferred localisation and storage in the ECM when secreted (Robertson & Rifkin, 2016).

Besides, no significant change in protein expression of the glycoprotein MFAP4 was detected by immunoblotting in both poAF and Ctrl. These findings differ with our proteomic data, where protein abundance levels of MFAP4 were significantly higher in poAF and cAF when compared to Ctrl. In contrast, both decorin (DCN) and galectin-3 (LGALS3) showed no change in protein expression, which aligns with our proteomic findings (**Supplemental Table 1**).

Taken together, these experimental findings in no small extent agree with our proteomic results, thereby validating the differential changes in ECM proteins detected in the secretome of human right atrial tissues.

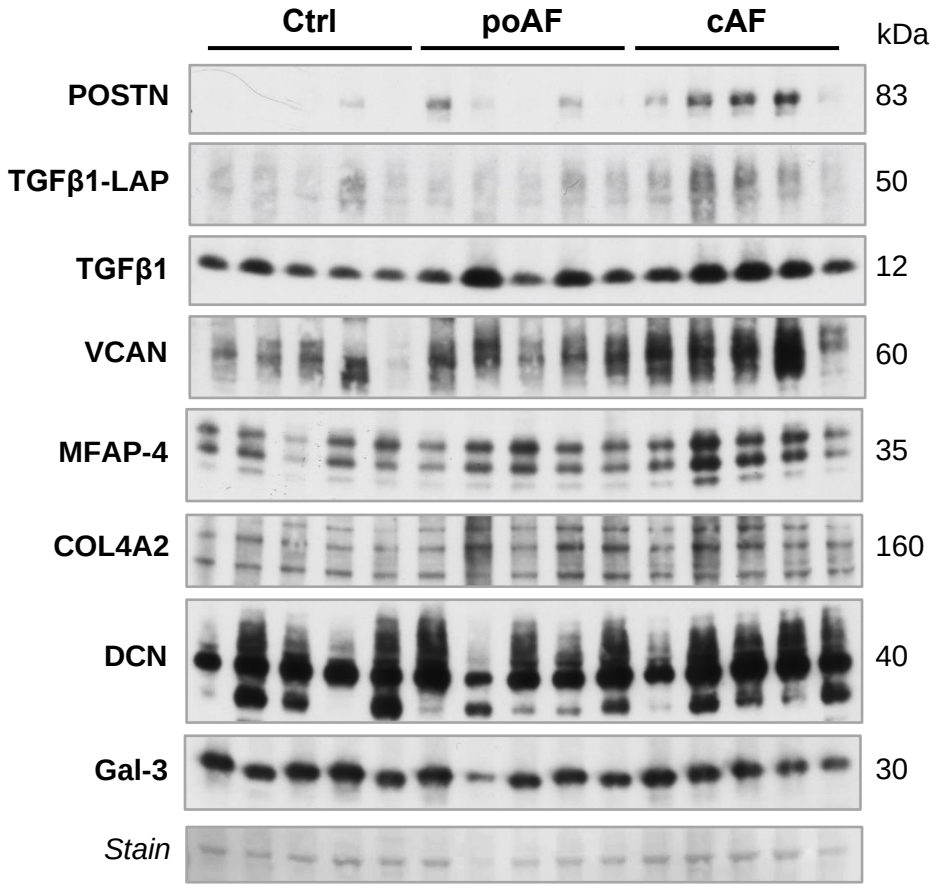

Figure 35. Immunoblots of extracted ECM proteins from processed right atrial tissue of postoperative atrial fibrillation (poAF) and chronic atrial fibrillation (cAF) patients. GuHCl extracts of processed tissue obtained after incubation with serum-free medium for 48 hours, were deglycosylated and investigated for periostin (POSTN), transforming growth factor-beta 1 (TGFβ1), versican (VCAN) microfibrillar associated protein-4 (MFAP-4), collagen type IV alpha 2 chain (COL4A2), decorin (DCN) and Galectin-3 (GAL-3) using Western blotting (n=5 patients each from Ctrl, poAF and cAF). Ponceau stain shown below immunoblots. Ctrl=Control

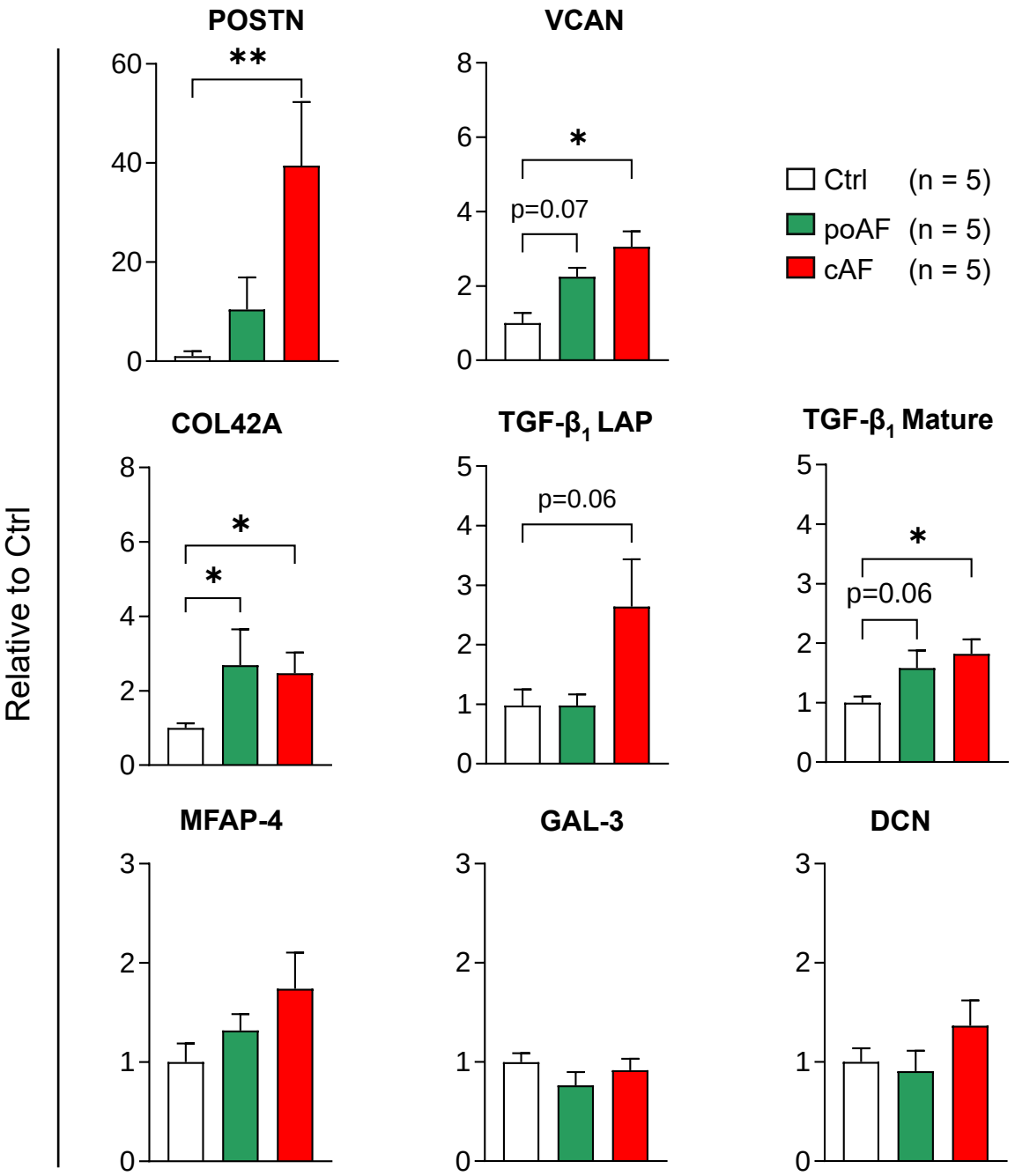

Figure 36. Quantification of immunoblots of extracted ECM proteins from processed right atrial tissue of postoperative atrial fibrillation (poAF) and chronic atrial fibrillation (cAF) patients. Bar graps represent Mean±SEM of analysed optical densities of selected ECM protein immunoblots. *P<0.05, **P<0.01 vs Ctrl (control). Comparison was made using Kruskal Wallis test followed by a Dunns post-hoc test. N=number of patients.

5.6 Discussion

Here, to the best of our knowledge, we present the first characterization of the human atrial tissue secretome using proteomics. This study describes the distinct ECM profile of poAF and cAF patients compared to Ctrl patients. We identified a total of 212 ECM proteins in all patient groups. Only 12 of the ECM proteins were differentially regulated in the secretome of poAF patients with all the identified proteins upregulated compared to Ctrl. Conversely, a high number of 85 identified ECM proteins, including 9 of those detected in the secretome of poAF patients, were differentially regulated in cAF. Of these, only 5 ECM proteins were downregulated with the others all upregulated. Immunoblotting studies validated trends observed in proteomic analysis, with selected ECM proteins showing similar expression patterns with their proteomic counterpart. Altogether, our findings show minimal remodelling of the secretory mechanism of ECM proteins in poAF, that is exacerbated in cAF patients, which may contribute to the pathophysiology and atrial mechanical dysfunction associated with AF. Also, we provide novel insights to biomarkers and regulatory proteins that may participate in the ECM remodelling associated with poAF and cAF.

5.6.1 Secretome profile of ECM proteins in poAF and cAF

Atrial fibrosis, typified by ECM accumulation, has been identified as a common feature of AF (Dzeshka et al., 2015). Investigation of ECM remodelling has conventionally been done using antibody-based approaches, which are restricted by challenges including a limited number of analysable proteins within a period and reduced epitope specificity of antibodies due to the characteristic PTMs associated with ECM proteins (Barallobre-Barreiro, Lynch, et al., 2016). Also, ECM remodelling studies using *in-vitro* experiments have mainly focused on analysing the secretome of fibroblasts using proteomic approaches. However, in addition to fibroblasts, atrial tissue comprises of myocytes and other non-myocyte cells such as, endothelial and perivascular cells that modulate ECM protein production and secretion (Dzeshka et al., 2015; Pellman et al., 2016). Therefore, atrial tissue secretome, unlike the fibroblast cell secretome, offers more information inclined towards the *in-vivo* physiological situation. However, it is essential to note that the atrial tissue secretome is a reflection of active secretion of cardiac cells within the culture period, which provide insight on the active remodelling occurring in the tissue, but does not necessarily indicate the accumulation of ECM protein in the tissue. This study provides the first investigation of human atrial tissue secretome.

In this study, we detected ECM remodelling, though minimal, in the secretome of the right atrium of poAF patients, with 6% of the identified ECM proteins upregulated (see **Figure 32**). Reports of several studies have shown no difference in fibrosis of the right atrium of poAF patients (Cosgrave et al., 2006; Garcia et al., 2012; Swartz et al., 2012). However, a considerable number of reports have shown significant ECM protein accumulation in the right atrium of patients who developed AF after cardiac surgery (Goette et al., 2002; J. Y. Li et al., 2008; Tinica et al., 2015). Differing clinical characteristics of patients participating in these studies and experimental approaches may account for the observed discrepancies in findings. The extent to which these changes in ECM protein secretions contribute to the remodelling of the ECM in the atria of poAF patients needs to be further investigated. On the other hand, our data demonstrated marked ECM protein upregulation in cAF (**Figure 33**), which is coherent with many published findings (Pellman et al., 2016).

Activation of pro-fibrotic signalling factors like TGFβ1, which is usually stored as an inactive complex (LCL) in the ECM, promote ECM protein secretion and cardiac fibrogenesis (Reese-Petersen et al., 2020). We detected by immunoblotting a non-significant and a significant upregulation of TGFβ1 in processed atrial tissues of both poAF and cAF patients, respectively, when compared to Ctrl in our study (**Figure 35** and **Figure 36**). The activation of TGFβ1 in the ECM of atrial tissue could trigger an increase in the secretion of ECM proteins, which could contribute to the differential changes in the secreted ECM proteins seen in the conditioned media of poAF and cAF, respectively, when compared to Ctrl.

The release and activation of TGFβ1 from complexes (LCL) can be triggered by several processes, including mechanisms mediated by cell surface integrins (Robertson et al., 2015). The LTBPs, which regulates TGFβ1 by forming the large latent complexes (LLCs), assist integrin-mediated activation of TGFβ1 (Robertson & Rifkin, 2016). In line with this, we observed abundant levels of LTBPs (LTBP-1 and LTBP-4) in the secretome of cAF patients but not poAF in this study (**Supplemental Table 1**). This finding may suggest a higher predisposition of cAF tissues to integrin-mediated activation of TGFβ1 (Annes et al., 2004; Robertson et al., 2015), which may contribute to the contrasting profiles of ECM secretion in cAF and poAF conditioned media when compared to Ctrl patients.

Also, secretion of CTGF, which can be induced by TGFβ1 (Chen et al., 2000), has been demonstrated to increase the production of structural proteins like fibronectin and collagen (Adam et al., 2011). Along the same line, exposure of fibroblasts *in-vitro* to recombinant CTGF enhanced the secretion of collagen in a recent study (Ko et al., 2011). Based on

these observations, the upregulation of CTGF, in both poAF and cAF in our study, may contribute to both the minimal and marked increase in the secretion of ECM proteins observed in poAF and cAF patients, respectively.

5.6.2 ECM contribution to arrhythmogenesis and atrial contractile dysfunction

Several reports with different experimental models have suggested that atrial fibrosis, characterized by ECM deposition, contributes to the arrhythmogenic substrate that promotes the development of AF (D. Li et al., 1999; Verheule, Sat, et al., 2004). Such substantial ECM protein accumulation in the interstitial space, majorly the collagens I, III and VI, interferes with the electrical communication between atrial myocytes by forming an insulating barrier between cells. This ECM alteration consequently impairs atrial conduction which leads to re-entry that initiates and maintains AF (Nattel, 2017).

Although many ECM proteins accumulate in the ECM during atrial fibrosis, early studies have mainly focused on the main structural protein, i.e. collagens (Frangogiannis, 2019), due to the limitations associated with using antibody-based techniques like Western blots and immunohistochemistry (Barallobre-Barreiro, Lynch, et al., 2016). Therefore, to ensure comprehensive cross-referencing of our findings with existing literature, this section would be addressed along the line of the collagens.

In this present study, of all the identified interstitial ECM collagens, we only detected an increased secretion of collagen I in atrial tissue from poAF patients. This increase in secretion could lead to the accumulation of the collagen in atrial tissue of poAF patients. However, a study by Swartz et al. showed no change in expression of collagen I in the right atrium in poAF patients (Swartz et al., 2012). On the other hand, in our cAF patient cohort, except for collagen III, all major interstitial collagens (I and VI) were upregulated in the atrial tissue secretome. Collagen I and collagen III have been shown to be increased and unchanged, respectively, by immunohistochemical stainings in right atrial tissues of persistent AF patients (Xu et al., 2004). In another study, collagen I and III were both increased in cAF patients. However, the increased level of collagen III was attributed to the presence of underlying mitral valve disease, as patients with lone AF (no cardiovascular diseases, pulmonary disease, hypertension or diabetes mellitus) in the same study showed normal levels of collagen III (Boldt et al., 2004). Interestingly, only one out of all cAF patients in this study had underlying mitral valve disease (**Table 14**), which may explain the unchanged protein secretion levels of collagen III in atrial tissue secretome. Therefore, our findings suggest an increased accumulation of collagens I and

VI in right atrial tissue of cAF patients, which may contribute to the arrhythmogenic substrate that maintains AF in cAF patients.

Furthermore, not only an increased deposition of collagen is responsible for the impaired mechanical function and stiffness attributed to fibrosis, but the cross-linking of the deposited collagen. Cross-linking, which describes the covalent linking of collagen fibres to one another, increases stiffness and promotes resistance of collagen fibres to proteolytic degradation (Polyakova et al., 2008; Reese-Petersen et al., 2020). In this present study, we demonstrate that fibronectin 1, which is crucial in mediating the assembly and cross-linking of different ECM proteins, including the collagens (Valiente-Alandi et al., 2018), is highly abundant in the secretome of cAF patients, but unchanged in poAF when compared to Ctrl patents. Also, recent studies using mice knockout models reported that the glycoprotein periostin and the proteoglycan biglycan increase collagen cross-linking, stabilization and deposition (Oka et al., 2007; Westermann et al., 2008). Interestingly, although unchanged in our poAF cohort, both periostin and biglycan were upregulated in the atrial tissue secretome of cAF patients. In addition, we detected an increased accumulation of periostin in tissues from cAF patients. The increased secretion of fibronectin 1, biglycan and periostin in our cAF patients perhaps may encourage the cross-linking and assembly of collagens in cAF patients, thereby increassing the resistance of collagens to proteolytic degradation. However, further studies investigating the cross-linking of collagens in poAF and cAF patients are necessary.

In addition to the interstitial ECM remodelling, basement membrane ECM proteins, which provide the interface between atrial myocytes and the interstitial ECM, contribute to the global fibrosis of the atria (Chute et al., 2019). Basement membrane expansion in a mouse knockout model of annexin 7, exhibited severe disruption in electrical conductivity, increasing susceptibility of the knockout mouse to AF (Schrickel et al., 2007). In line with this finding, an earlier report also associated the disorganization of the basement membrane to poor electrical conductivity in ventricular tissues (Van Rijen et al., 2004). We detected unchanged secretion levels of the main structural components of the basement proteins, which include the type IV collagen (COL4A1 and COL4A2), and the proteoglycan perlecan (HSPG2) in poAF patients. However, the secretion of these basement proteins increased significantly in cAF patients. Interestingly, our immunoblotting data revealed increased protein accumulation of the type IV collagen subunit (COL4A2) in the right atrial tissue of both poAF and cAF patients, thus suggesting existing remodelling of the ECM in atrial tissues of these patients. Therefore, the increased secretion of these ECM proteins

into the basement membrane could further aggravate the disconnect between cells by worsening the expansion of the intercellular space, which impairs cell-to-cell communication and electrical conductivity, subsequently leading to arrhythmia.

Collectively, our findings communicate minimal remodelling in the secretion of ECM proteins in poAF patients, which perhaps may indicate the early stage in the development of atrial fibrosis, and as such may not contribute to the structural arrhythmogenic substrate that predisposes patients to poAF. At the same time, the secretory profile of ECM proteins in cAF patients suggests the accumulation of ECM proteins and evidence that favours increased cross-linking of ECM proteins in cAF, and as such may favour heterogeneous electrical conduction in the atria which promote the initiation and maintenance of AF.

Lastly, in addition to the remodelling of the electrical pathway in the atrium, increased fibrosis can impair atrial contractile function (Travers et al., 2016). The excess secretion and deposition of ECM proteins, which we observed minimally in our poAF cohort and maximally in our cAF patients, could distort the architecture of the atria and increase stiffness which could lead to atrial contractile dysfunction (Travers et al., 2016). Also, the imbalance in protein abundance between collagen I and III in the secretome of both poAF and cAF patients in this study could further increase the stiffness of the ECM, by reducing the elasticity of the ECM matrix, which is partly maintained by collagen III (Kong et al., 2014). However, the extent to which these changes may contribute to the impaired contractility seen in poAF and cAF patients needs to be further investigated.

5.6.3 Other ECM proteins

Apart from the proteins that actively contribute to the intricate structural network of the ECM, some other proteins only regulate and interact with the ECM. In our study, we showed increased protein levels of ECM-associated proteins identified by our proteomic analysis in the secretome of both poAF and cAF patients, which may provide new insight in mechanisms of atrial ECM remodelling observed in AF as well as new biomarkers for AF.

The carbohydrate-binding protein galectin-1 (LGALS1) is a member of the family of galectins, which has been shown by recent studies to reduce the voltage-gated L-type Ca^{2+} current in smooth muscles by causing a reduction in expression of this channel (Z. Hu et al., 2018; J. Wang et al., 2011). It would be of good research interest to identify the role of LGALS1, which is upregulated in our cAF patient cohort, in the reduced $I_{Ca,L}$ observed in atrial myocytes of cAF patients. Similarly, the growth factor insulin-like growth

factor 2, IGF2, is increased in our cAF patient cohort. Little is known about its role in the heart; however, a study showed that IGF2 overexpression caused abnormalities in the architecture of the heart, including cardiomegaly (Zaina et al., 2003). The increased levels of the insulin-like growth factor-binding protein 2 (IGFBP2) in our cAF patients might be a compensatory mechanism to manage the upregulation of IGF2 (Allard & Duan, 2018). More investigation on the role of IGF2 in cAF needs to be considered. Another interesting ECM protein is the adipocyte enhancer-binding protein 1 (AEBP1), which is upregulated in the cAF group of our study. A porcine model of ischemia/reperfusion injury reported increased AEBP1 expression in the left ventricle, implicating the protein in contributing to the ECM remodelling identified in this model (Barallobre-Barreiro et al., 2012). The specific function of this protein in cAF is yet to be identified and would need further investigation.

5.6.4 Limitations

A peculiar limitation to most secretomic approaches is the non-physiological state of the serum-free medium utilised to generate conditioned media. Although this minimises contamination of the culture medium by serum proteins, it could lead to death and apoptosis of some cells (Méndez & Villanueva, 2015). Our data should be interpreted with caution and backed by an extensive study of the viability of the tissue at different time points during the generation of conditioned media.

Secondly, we only utilised right atrial appendages from patients undergoing cardiac surgery due to tissue availability, and as such, our findings do not represent other regions of the atria. Further studies investigating both left and right atrium in poAF and cAF patients would be necessary.

Thirdly, a significant problem with secretome approaches is the contamination by plasma proteins from serum slowly diffusing out from tissues and intracellular proteins from damaged cells. We adopted a washing protocol and utilised the 2nd 24-hours conditioned medium to minimise contamination from plasma proteins and intracellular proteins. However, more sophisticated approaches have been established, where proteins are labelled with isotopes to allow quantitative distinction between secreted proteins or contaminant proteins. Further investigation with approaches like stable isotope dynamic labelling of secretomes (SILDS) or stable isotope labelling with an amino acid in cell culture (SILAC) would provide more detailed insight on the profile on the secretomes (Hammond et al., 2018; Shin et al., 2019).

6 Summary and conclusion

This thesis was aimed primarily towards understanding the role of altered Ca^{2+} handling and ECM remodelling in the development of AF and its associated contractile dysfunction. In pursuance of this aim, the work described in this thesis has confirmed and provided new mechanistic insight on the involvement of abnormal Ca^{2+} handling in the pathophysiology of poAF and cAF. Also, this work has provided a new perspective on the distinct ECM remodelling in poAF and cAF patients.

In chapter 3, a focused analysis of the role of altered Ca^{2+} handling in the atrial contractile dysfunction seen in cAF patients was reported and discussed. Indeed, abnormal intracellular handling of Ca^{2+} participates in the atrial hypocontractility observed in cAF patients. Reduction in $I_{Ca,L}$ was identified to contribute majorly to the diminished fractional shortening of atrial myocytes from cAF patients, by triggering a smaller Ca^{2+} release from the SR. However, the contractile response of atrial myocytes from cAF patients to systolic rise in Ca^{2+} was impaired compared to Ctrl myocytes, as reflected by the degree of reduction in fractional shortening (~70%) compared to CaT (~44%). The perturbed contractile response was also observed in atrial muscle fibres from cAF patients, with cAF muscle fibres generating less force at similar Ca^{2+} concentrations compared to those of Ctrl myofibres. Accompanying the diminished force was an increase in myofilament Ca^{2+} sensitivity of myofibres from cAF patients, which may be a compensatory response to the depressed contractile force. Our data suggest that the increased phosphorylation of MLC-2 account for the increased myofilament Ca^{2+} sensitivity seen in cAF. On the other hand, the increased phosphorylation of cTnT and the reduced expression of cTnC are the principal culprits for the reduced contractile force and shortening observed in cAF myofibres and myocytes, respectively. Additionally, intracellular buffering of Ca^{2+} is impaired in cAF myocytes, as reflected by the reduced number of cytoplasmic Ca^{2+} buffers (decreased B_{max}), which we suggest is a consequence of the reduced cTnC which accounts for approximately 50% of cytosolic Ca^{2+} buffering. Altogether, our findings indict abnormal Ca^{2+} handling, championed by the reduction in cTnC expression, as not only a contributor to the atrial contractile dysfunction peculiar to cAF but also a possible player in AF arrhythmogenesis.

To improve cardiac contraction, genetic and pharmacological approaches have been used and, in particular, strategies to augment the binding affinity of cTnC to Ca^{2+} have been investigated (Pollesello et al., 2016). Recently, expression of exogenous cTnC, engineered to exhibit increased sensitivity for Ca^{2+} in a mouse model, enhanced both

cardiac contractility on an organ level and myocyte shortening on a cellular level (Shettigar et al., 2016). Also, *in-vitro* studies have applied this concept and demonstrated improved sensitivity and force generations of myofilaments (Feest et al., 2014; B. Liu et al., 2012). Additionally, lead cTnC Ca^{2+}-sensitizing substances, including levosimendan, omecamtiv and pimobendane, have been shown to improve cardiac contractility and, as a result, touted as promising therapeutics in the treatment of heart failure (Pollesello et al., 2016). However, levosimendan possesses ancillary PDE inhibitory effect, which could lead to arrhythmia (Maack et al., 2019). Nevertheless, the application of these Ca^{2+}-sensitizing concepts in future AF studies would be welcomed in enabling proper deciphering of their potential in the management of the atrial contractile dysfunction associated with cAF.

With mechanistic evidence demonstrating that abnormal Ca^{2+} handling facilitates the initiation and perpetuation of pAF and cAF (Voigt et al., 2012, 2014), we conducted a comprehensive investigation of Ca^{2+} handling alterations in poAF patients, and its proarrhythmic role in poAF development (chapter 4). Distinctive from cAF and pAF, electrical remodelling was non-existent in atrial myocytes from poAF patients, as demonstrated by unchanged AP morphology and unaltered $I_{Ca,L}$ in poAF myocytes compared Ctrl. Also, the characteristic arrhythmogenic Ca^{2+}-handling abnormality associated with cAF, including SR Ca^{2+} leak which causes DADs, was absent in poAF, with this finding supported by unchanged mRNA and protein expression levels of RYR2 observed in poAF when compared to Ctrl.

Our data for the first time demonstrate modifications in Ca^{2+} handling in poAF that promote the development of poAF. Right atrial myocytes from poAF patients at increasing frequencies exhibited increased vulnerability to AP alternans, which is known to promote re-entry. Changes in sarcolemmal fluxes of ion channels, a recognized mechanism driving cellular AP alternans, was not responsible for the increased susceptibility of poAF myocytes to AP alternans. Instead, the cellular AP alternans in poAF was identified to be driven by the alternation of CaT in myocytes of poAF patients. Our findings suggest reduced sequestration of Ca^{2+} into the SR as the underlying factor increasing the susceptibility of poAF myocytes to AP alternans. Phosphorylation of PLB, the SERCA2a regulator and Ca^{2+} buffering, which are known mechanisms that could delay SR Ca^{2+} reuptake, were shown not to contribute to the decreased sequestration of Ca^{2+} into the SR. However, our data indicate that the reduced protein expression of SERCA2a accounts for the impaired reuptake of Ca^{2+} into the SR in atrial myocytes of poAF patients. With reduced SERCA2a protein expression responsible for the diminished SR Ca^{2+} content in poAF

myocytes, we postulate that the reduced SERCA2a expression contributes to the diminished atrial contractility in poAF patients highlighted by our strain analysis. Taken together, our findings highlight the impaired reuptake of Ca^{2+}, due to reduced SERCA2a protein levels as the underlying mechanism facilitating the arrhythmogenic substrate that predisposes patients to poAF and its associated contractile dysfunction.

With a reduced SERCA2a function identified as the focal mechanism responsible for the contractile dysfunction and the arrhythmogenic substrate predisposing patients to poAF in this study, strategies aimed at improving SERCA2a function may represent a promising preventive approach towards the development of poAF and its associated detrimental outcomes. Many strategies have been employed to augment SERCA2a expression in ventricular tissues of patients with heart failure. Of note is pharmacological activation of SERCA2a with istaroxime (Gheorghiade et al., 2008; Shah et al., 2009) and the adeno-associated viral-mediated expression of SERCA2a (Zsebo et al., 2014), which enhanced systolic function of patients in phase-2 trials. The adoption of these strategies could provide an appropriate guide for future studies on the prevention of poAF development after surgery as well as the improvement of atrial contractile function in patients with atrial cardiomyopathy.

On account of the common existence of contractile dysfunction in the atria of both cAF (chapter 3) and poAF (chapter 4) patients, we investigated the role of ECM remodelling as a possible contributor to the arrhythmogenesis of AF and its associated contractile dysfunction. ECM accumulation due to fibrosis is known to cause stiffness and diminished contractility of the atria. We for the first time analysed the secretome of right atrial tissue from poAF and cAF patients using proteomics. ECM remodelling was demonstrated to be minimal and marked in the right atrial secretome of poAF and cAF patients, respectively. Our data suggest increased TGFβ1 and CTGF protein levels in tissues and secretomes of the right atrium, respectively, contribute to the increased ECM secretion observed in poAF and cAF. Of note, collagen I was upregulated in secretomes obtained from both poAF and cAF patients, with an additional collagen IV upregulated only in cAF. The ECM proteins fibronectin 1, biglycan and periostin which have been shown to participate in the assembly of collagens for cross-linking, were upregulated in the atrial secretome of cAF patients. Increased secretions of these proteins are postulated to encourage collagen cross-linking, and subsequent resistance to degradation. Basement membrane ECM protein secretion was also remodelled, with HSPG2 and type IV collagen (COL4A1 and COL4A2) upregulated in cAF but not poAF patients. However, our immunoblotting data revealed

increased accumulation of COL4A2 protein in both poAF and cAF right atrial tissue, indicating existing remodelling of the basement membrane in both poAF and cAF patients. Hence, the increased secretion of the basement membrane proteins could worsen cell-cell communication in atrial myocytes, which could facilitate AF maintenance by causing heterogeneous conduction in these tissues. Collectively, our observations indicate remodelling in the secretion of ECM proteins in poAF and cAF patients, which could promote the deleterious accumulation of ECM proteins in tissues that contribute to impaired contractility and conduction blocks favouring AF arrhythmogenesis.

In recent years, the focus has been directed towards identifying new therapeutic approaches in managing cardiac fibrosis, owing to the maintained high mortality in heart failure patients (T. Liu et al., 2017). Serelaxin, a drug that targets collagen production has been shown to effectively suppress fibrosis progression and improve myocardial deformity in animal models of heart failure (Lapinskas et al., 2020; Samuel et al., 2014). The diuretic torasemide has also been reported to decrease collagen cross-linking by reducing lysyl oxidase expression in mice and human patients (Adam et al., 2015; López et al., 2009). Investigating the effect of these molecules in the ECM remodelling resulting from AF would provide valuable information on its contribution to atrial contractile dysfunction associated with AF. Also, with the recent focus on non-invasive biomarkers of AF in recent times (Reese-Petersen et al., 2020), further investigation of the ECM proteins in the atrial secretome could provide novel biomarkers which could serve as predictive and prognostic tools for both poAF and cAF occurrence in risk patients.

In conclusion, the work presented in this thesis provides novel mechanistic insights, indicating active participation of abnormal Ca^{2+} handling in the development of cAF and poAF and their associated atrial contractile dysfunction. In addition, we submit a detailed analysis of the remodelling in ECM protein production, which provides a repository of ECM proteins for further studies on their roles in the pathophysiology of AF. Overall, our data will help in the organisation of new treatment strategies to effectively manage both cAF and poAF, as well as provide long-term protection from complications like stroke, which is associated with the contractile dysfunction peculiar to both cAF and poAF.

7 References

Adam, O., Theobald, K., Lavall, D., Grube, M., Kroemer, H. K., Ameling, S., Schäfers, H. J., Böhm, M., & Laufs, U. (2011). Increased lysyl oxidase expression and collagen cross-linking during atrial fibrillation. *Journal of Molecular and Cellular Cardiology*, *50*(4), 678–685.

Adam, O., Zimmer, C., Hanke, N., Hartmann, R. W., Klemmer, B., Böhm, M., & Laufs, U. (2015). Inhibition of aldosterone synthase (CYP11B2) by torasemide prevents atrial fibrosis and atrial fibrillation in mice. *Journal of Molecular and Cellular Cardiology*, *85*, 140–150.

Ahlsson, A., Fengsrud, E., Bodin, L., & Englund, A. (2010). Postoperative atrial fibrillation in patients undergoing aortocoronary bypass surgery carries an eightfold risk of future atrial fibrillation and a doubled cardiovascular mortality. *European Journal of Cardio-Thoracic Surgery*, *37*(6), 1353–1359.

Aksu, U., Kalkan, K., Gulcu, O., Aksakal, E., Öztürk, M., & Topcu, S. (2019). The role of the right atrium in development of postoperative atrial fibrillation: A speckle tracking echocardiography study. *Journal of Clinical Ultrasound*, *47*(8), 470–476.

Allard, J. B., & Duan, C. (2018). IGF-binding proteins: Why do they exist and why are there so many? *Frontiers in Endocrinology*, *9*, 117.

Allessie, M. A., Bonke, F. I. M., & Schopman, F. J. G. (1973). Circus Movement in Rabbit Atrial Muscle as a Mechanism of Tachycardia. *Circulation Research*, *33*(1), 54–62.

Almassi, G. H., Wagner, T. H., Carr, B., Hattler, B., Collins, J. F., Quin, J. A., Ebrahimi, R., Grover, F. L., Bishawi, M., & Shroyer, A. L. W. (2015). Postoperative atrial fibrillation impacts on costs and one-year clinical outcomes: The veterans affairs randomized on/off bypass trial. *Annals of Thoracic Surgery*, *99*(1), 109–114.

Alvarez-Llamas, G., Szalowska, E., de Vries, M. P., Weening, D., Landman, K., Hoek, A., Wolffenbuttel, B. H. R., Roelofsen, H., & Vonk, R. J. (2007). Characterization of the human visceral adipose tissue secretome. *Molecular and Cellular Proteomics*, *6*(4), 589–600.

Amar, D., Zhang, H., Miodownik, S., & Kadish, A. H. (2003). Competing autonomic mechanisms precede the onset of postoperative atrial fibrillation. *Journal of the American College of Cardiology*, *42*(7), 1262–1268.

Anderson, E. J., Efird, J. T., Kiser, A. C., Crane, P. B., O'Neal, W. T., Ferguson, T. B., Alwair, H., Carter, K., Williams, J. M., Gehi, A. K., & Kypson, A. P. (2017). Plasma Catecholamine Levels on the Morning of Surgery Predict Post-Operative Atrial Fibrillation. *JACC: Clinical Electrophysiology*, *3*(12), 1456–1465.

Anné, W., Willems, R., Roskams, T., Sergeant, P., Herijgers, P., Holemans, P., Ector, H., & Heidbüchel, H. (2005). Matrix metalloproteinases and atrial remodeling in patients with mitral valve disease and atrial fibrillation. *Cardiovascular Research*, *67*(4), 655–666.

Annes, J. P., Chen, Y., Munger, J. S., & Rifkin, D. B. (2004). Integrin αvβ6-mediated activation of latent TGF-β requires the latent TGF-β binding protein-1. *Journal of*

Cell Biology, *165*(5), 723–734.

Antzelevitch, C., & Burashnikov, A. (2011). Overview of Basic Mechanisms of Cardiac Arrhythmia. *Cardiac Electrophysiology Clinics*, *3*(1), 23–45.

Ausma, J., Van der Velden, H. M. W., Lenders, M. H., Van Ankeren, E. P., Jongsma, H. J., Ramaekers, F. C. S., Borgers, M., & Allessie, M. A. (2003). Reverse structural and gap-junctional remodeling after prolonged atrial fibrillation in the goat. *Circulation*, *107*(15), 2051–2058.

Badano, L. P., Kolias, T. J., Muraru, D., Abraham, T. P., Aurigemma, G., Edvardsen, T., D'Hooge, J., Donal, E., Fraser, A. G., Marwick, T., Mertens, L., Popescu, B. A., Sengupta, P. P., Lancellotti, P., Thomas, J. D., Voigt, J.-U., Industry representatives, & Reviewers: This document was reviewed by members of the 2016–2018 EACVI Scientific Documents Committee. (2018). Standardization of left atrial, right ventricular, and right atrial deformation imaging using two-dimensional speckle tracking echocardiography: a consensus document of the EACVI/ASE/Industry Task Force to standardize deformation imaging. *European Heart Journal Cardiovascular Imaging*, *19*(6), 591–600.

Barallobre-Barreiro, J., Baig, F., Fava, M., Yin, X., & Mayr, M. (2017). Glycoproteomics of the extracellular matrix: A method for intact glycopeptide analysis using mass spectrometry. *Journal of Visualized Experiments*, *2017*(122).

Barallobre-Barreiro, J., Didangelos, A., Schoendube, F. A., Drozdov, I., Yin, X., Fernández-Caggiano, M., Willeit, P., Puntmann, V. O., Aldama-López, G., Shah, A. M., Doménech, N., & Mayr, M. (2012). Proteomics analysis of cardiac extracellular matrix remodeling in a porcine model of ischemia/reperfusion injury. *Circulation*, *125*(6), 789–802.

Barallobre-Barreiro, J., Gupta, S. K., Zoccarato, A., Kitazume-Taneike, R., Fava, M., Yin, X., Werner, T., Hirt, M. N., Zampetaki, A., Viviano, A., Chong, M., Bern, M., Kourliouros, A., Domenech, N., Willeit, P., Shah, A. M., Jahangiri, M., Schaefer, L., Fischer, J. W., … Mayr, M. (2016). Glycoproteomics Reveals Decorin Peptides with Anti-Myostatin Activity in Human Atrial Fibrillation. *Circulation*, *134*(11), 817–832.

Barallobre-Barreiro, J., Lynch, M., Yin, X., & Mayr, M. (2016). Systems biology-opportunities and challenges: the application of proteomics to study the cardiovascular extracellular matrix. *Cardiovascular Research*, *112*(3), 626–636.

Barana, A., Matamoros, M., Dolz-Gaitón, P., Pérez-Hernández, M., Amorós, I., Núñez, M., Sacristán, S., Pedraz, Á., Pinto, Á., Fernández-Avilés, F., Tamargo, J., Delpón, E., & Caballero, R. (2014). Chronic atrial fibrillation increases MicroRNA-21 in human atrial myocytes decreasing L-type calcium current. *Circulation: Arrhythmia and Electrophysiology*, *7*(5), 861–868.

Bartos, D. C., Grandi, E., & Ripplinger, C. M. (2015). Ion channels in the heart. *Comprehensive Physiology*, *5*(3), 1423–1464.

Belus, A., Piroddi, N., Ferrantini, C., Tesi, C., Cazorla, O., Toniolo, L., Drost, M., Mearini, G., Carrier, L., Rossi, A., Mugelli, A., Cerbai, E., Van Der Velden, J., & Poggesi, C. (2010). Effects of chronic atrial fibrillation on active and passive force generation in human atrial myofibrils. *Circulation Research*, *107*(1), 144–152.

Bening, C., & Leyh, R. (2016). Right atrial contractile dynamics are impaired in patients with postcapillary pulmonary hypertension. *Experimental and Therapeutic Medicine*, *12*(2), 792–798.

Berlin, J. R., Bassani, J. W., & Bers, D. M. (1994). Intrinsic cytosolic calcium buffering properties of single rat cardiac myocytes. *Biophysical Journal*, *67*(4), 1775–1787.

Bers, D. M. (2002). Cardiac excitation-contraction coupling. *Nature*, *415*(6868), 198–205.

Bhave, P. D., Goldman, L. E., Vittinghoff, E., Maselli, J., & Auerbach, A. (2012). Incidence, predictors, and outcomes associated with postoperative atrial fibrillation after major noncardiac surgery. *American Heart Journal*, *164*(6), 918–924.

Bisbal, F., Baranchuk, A., Braunwald, E., Bayés de Luna, A., & Bayés-Genís, A. (2020). Atrial Failure as a Clinical Entity: JACC Review Topic of the Week. *Journal of the American College of Cardiology*, *75*(2), 222–232.

Boldt, A., Wetzel, U., Lauschke, J., Weigl, J., Gummert, J., Hindricks, G., Kottkamp, H., & Dhein, S. (2004). Fibrosis in left atrial tissue of patients with atrial fibrillation with and without underlying mitral valve disease. *Heart*, *90*(4), 400–405.

Bosch, R. F., Zeng, X., Grammer, J. B., Popovic, K., Mewis, C., & Kühlkamp, V. (1999). Ionic mechanisms of electrical remodeling in human atrial fibrillation. *Cardiovascular Research*, *44*(1), 121–131.

Brandenburg, S., Pawlowitz, J., Eikenbusch, B., Peper, J., Kohl, T., Mitronova, G. Y., Sossalla, S., Hasenfuss, G., Wehrens, X. H. T., Kohl, P., Rog-Zielinska, E. A., & Lehnart, S. E. (2019). Junctophilin-2 expression rescues atrial dysfunction through polyadic junctional membrane complex biogenesis. *JCI Insight*, *4*(12).

Brandt, M. C., Priebe, L., Böhle, T., Südkamp, M., & Beuckelmann, D. J. (2000). The ultrarapid and the transient outward K+ current in human atrial fibrillation. Their possible role in postoperative atrial fibrillation. *Journal of Molecular and Cellular Cardiology*, *32*(10), 1885–1896.

Briston, S. J., Dibb, K. M., Solaro, R. J., Eisner, D. A., & Trafford, A. W. (2014). Balanced changes in Ca buffering by SERCA and troponin contribute to Ca handling during β-adrenergic stimulation in cardiac myocytes. *Cardiovascular Research*, *104*(2), 347–354.

Brundel, B. J. J. M., Ausma, J., Van Gelder, I. C., Van Der Want, J. J. L., Van Gilst, W. H., Crijns, H. J. G. M., & Henning, R. H. (2002). Activation of proteolysis by calpains and structural changes in human paroxysmal and persistent atrial fibrillation. *Cardiovascular Research*, *54*(2), 380–389.

Brundel, B. J. J. M., Van Gelder, I. C., Henning, R. H., Tieleman, R. G., Tuinenburg, A. E., Wietses, M., Grandjean, J. G., Van Gilst, W. H., & Crijns, H. J. G. M. (2001). Ion channel remodeling is related to intraoperative atrial effective refractory periods in patients with paroxysmal and persistent atrial fibrillation. *Circulation*, *103*(5), 684–690.

Brundel, B. J. J. M., Van Gelder, I. C., Henning, R. H., Tuinenburg, A. E., Deelman, L. E., Tieleman, R. G., Grandjean, J. G., Van Gilst, W. H., & Crijns, H. J. G. M. (1999).

Gene expression of proteins influencing the calcium homeostasis in patients with persistent and paroxysmal atrial fibrillation. *Cardiovascular Research*, *42*(2), 443–454.

Brundel, B. J. J. M., Van Gelder, I. C., Henning, R. H., Tuinenburg, A. E., Wietses, M., Grandjean, J. G., Wilde, A. A. M., Van Gilst, W. H., & Crijns, H. J. G. M. (2001). Alterations in potassium channel gene expression in atria of patients with persistent and paroxysmal atrial fibrillation: Differential regulation of protein and mRNA levels for K+ channels. *Journal of the American College of Cardiology*, *37*(3), 926–932.

Chelu, M. G., Sarma, S., Sood, S., Wang, S., Van Oort, R. J., Skapura, D. G., Li, N., Santonastasi, M., Müller, F. U., Schmitz, W., Schotten, U., Anderson, M. E., Valderrábano, M., Dobrev, D., & Wehrens, X. H. T. (2009). Calmodulin kinase II-mediated sarcoplasmic reticulum Ca2+ leak promotes atrial fibrillation in mice. *Journal of Clinical Investigation*, *119*(7), 1940–1951.

Chen, M. M., Lam, A., Abraham, J. A., Schreiner, G. F., & Joly, A. H. (2000). CTGF expression is induced by TGF-β in cardiac fibroblasts and cardiac myocytes: A potential role in heart fibrosis. *Journal of Molecular and Cellular Cardiology*, *32*(10), 1805–1819.

Choi, H. S., & Eisner, D. A. (1999). The role of sarcolemmal Ca 2+ -ATPase in the regulation of resting calcium concentration in rat ventricular myocytes. *The Journal of Physiology*, *515*(1), 109–118.

Christ, T., Boknik, P., Wöhrl, S., Wettwer, E., Graf, E. M., Bosch, R. F., Knaut, M., Schmitz, W., Ravens, U., & Dobrev, D. (2004). L-type Ca2+ current downregulation in chronic human atrial fibrillation is associated with increased activity of protein phosphatases. *Circulation*, *110*(17), 2651–2657.

Chugh, S. S., Havmoeller, R., Narayanan, K., Singh, D., Rienstra, M., Benjamin, E. J., Gillum, R. F., Kim, Y. H., McAnulty, J. H., Zheng, Z. J., Forouzanfar, M. H., Naghavi, M., Mensah, G. A., Ezzati, M., & Murray, C. J. L. (2014). Worldwide epidemiology of atrial fibrillation: A global burden of disease 2010 study. *Circulation*, *129*(8), 837–847.

Chung, J. H., Biesiadecki, B. J., Ziolo, M. T., Davis, J. P., & Janssen, P. M. L. (2016). Myofilament calcium sensitivity: Role in regulation of in vivo cardiac contraction and relaxation. *Frontiers in Physiology*, *7*(DEC), 562.

Chung, M. K., Eckhardt, L. L., Chen, L. Y., Ahmed, H. M., Gopinathannair, R., Joglar, J. A., Noseworthy, P. A., Pack, Q. R., Sanders, P., & Trulock, K. M. (2020). Lifestyle and Risk Factor Modification for Reduction of Atrial Fibrillation: A Scientific Statement from the American Heart Association. *Circulation*, *141*, E750–E772.

Chute, M., Aujla, P., Jana, S., & Kassiri, Z. (2019). The Non-Fibrillar Side of Fibrosis: Contribution of the Basement Membrane, Proteoglycans, and Glycoproteins to Myocardial Fibrosis. *Journal of Cardiovascular Development and Disease*, *6*(4), 35.

Clarke, J. D., Caldwell, J. L., Horn, M. A., Bode, E. F., Richards, M. A., Hall, M. C. S., Graham, H. K., Briston, S. J., Greensmith, D. J., Eisner, D. A., Dibb, K. M., &

Trafford, A. W. (2015). Perturbed atrial calcium handling in an ovine model of heart failure: Potential roles for reductions in the L-type calcium current. *Journal of Molecular and Cellular Cardiology*, *79*, 169–179.

Clauss, S., Bleyer, C., Schüttler, D., Tomsits, P., Renner, S., Klymiuk, N., Wakili, R., Massberg, S., Wolf, E., & Kääb, S. (2019). Animal models of arrhythmia: classic electrophysiology to genetically modified large animals. *Nature Reviews Cardiology*, *16*(8), 457–475.

Clerx, M., Collins, P., de Lange, E., & Volders, P. G. A. (2016). Myokit: A simple interface to cardiac cellular electrophysiology. *Progress in Biophysics and Molecular Biology*, *120*(1–3), 100–114.

Cosgrave, J., Foley, J. B., Flavin, R., O'Briain, D. S., Fitzpatrick, E., Bennett, K., Young, V., Tolan, M., & McGovern, E. (2006). Preoperative atrial histological changes are not associated with postoperative atrial fibrillation. *Cardiovascular Pathology*, *15*(4), 213–217.

Courtemanche, M., Ramirez, R. J., & Nattel, S. (1998). Ionic mechanisms underlying human atrial action potential properties: Insights from a mathematical model. *American Journal of Physiology - Heart and Circulatory Physiology*, *275*(1), H301–H321.

Cunha, S. R., Hund, T. J., Hashemi, S., Voigt, N., Li, N., Wright, P., Koval, O., Li, J., Gudmundsson, H., Gumina, R. J., Karck, M., Schott, J. J., Probst, V., Le Marec, H., Anderson, M. E., Dobrev, D., Wehrens, X. H. T., & Mohler, P. J. (2011). Defects in ankyrin-based membrane protein targeting pathways underlie atrial fibrillation. *Circulation*, *124*(11), 1212–1222.

Darlington, A., & McCauley, M. D. (2020). Atrial Cardiomyopathy: An Unexplored Limb of Virchow's Triad for AF Stroke Prophylaxis. *Frontiers in Cardiovascular Medicine*, *7*, 11.

Denham, N. C., Pearman, C. M., Caldwell, J. L., Madders, G. W. P., Eisner, D. A., Trafford, A. W., & Dibb, K. M. (2018). Calcium in the pathophysiology of atrial fibrillation and heart failure. *Frontiers in Physiology*, *9*(OCT), 1380.

Díaz, M. E., Trafford, A. W., & Eisner, D. A. (2001). The role of intracellular Ca buffers in determining the shape of the systolic Ca transient in cardiac ventricular myocytes. *Pflugers Archiv European Journal of Physiology*, *442*(1), 96–100.

Dimmer, C., Tavernier, R., Gjorgov, N., Van Nooten, G., Clement, D. L., & Jordaens, L. (1998). Variations of autonomic tone preceding onset of atrial fibrillation after coronary artery bypass grafting. *American Journal of Cardiology*, *82*(1), 22–25.

Dobrev, D., Aguilar, M., Heijman, J., Guichard, J. B., & Nattel, S. (2019). Postoperative atrial fibrillation: mechanisms, manifestations and management. *Nature Reviews Cardiology*, *16*(7), 417–436.

Dobrev, D., Friedrich, A., Voigt, N., Jost, N., Wettwer, E., Christ, T., Knaut, M., & Ravens, U. (2005). The G protein-gated potassium current IK,ACh is constitutively active in patients with chronic atrial fibrillation. *Circulation*, *112*(24), 3697–3706.

Dobrev, D., Graf, E., Wettwer, E., Himmel, H. M., Hála, O., Doerfel, C., Christ, T., Schüler, S., & Ravens, U. (2001). Molecular basis of downregulation of G-protein

-coupled inward rectifying k+ current (ik,ach) in chronic human atrial fibrillation decrease in GIRK4 mrna correlates with reduced IK,ACh and muscarinic receptor-mediated shortening of action potentials. *Circulation*, *104*(21), 2551–2557.

Dobrev, D., Wettwer, E., Kortner, A., Knaut, M., Schüler, S., & Ravens, U. (2002). Human inward rectifier potassium channels in chronic and postoperative atrial fibrillation. *Cardiovascular Research*, *54*(2), 397–404.

Dzeshka, M. S., Lip, G. Y. H., Snezhitskiy, V., & Shantsila, E. (2015). Cardiac Fibrosis in Patients With Atrial Fibrillation: Mechanisms and Clinical Implications. *Journal of the American College of Cardiology*, *66*(8), 943–959.

Edwards, J. N., & Blatter, L. A. (2014). Cardiac alternans and intracellular calcium cycling. *Clinical and Experimental Pharmacology and Physiology*, *41*(7), 524–532.

Eisner, D. A., Caldwell, J. L., Kistamás, K., & Trafford, A. W. (2017). Calcium and Excitation-Contraction Coupling in the Heart. *Circulation Research*, *121*(2), 181–195.

Elayi, C. S., Di Biase, L., Bai, R., Burkhardt, J. D., Mohanty, P., Santangeli, P., Sanchez, J., Hongo, R., Gallinghouse, G. J., Horton, R., Bailey, S., Beheiry, S., & Natale, A. (2013). Administration of isoproterenol and adenosine to guide supplemental ablation after Pulmonary Vein Antrum Isolation. *Journal of Cardiovascular Electrophysiology*, *24*(11), 1199–1206.

Enriquez, A., Liang, J. J., Santangeli, P., Marchlinski, F. E., & Riley, M. P. (2017). Focal atrial fibrillation from the superior vena cava. *Journal of Atrial Fibrillation*, *9*(6), 1593.

Everett IV, T. H., Wilson, E. E., Verheule, S., Guerra, J. M., Foreman, S., & Olgin, J. E. (2006). Structural atrial remodeling alters the substrate and spatiotemporal organization of atrial fibrillation: A comparison in canine models of structural and electrical atrial remodeling. *American Journal of Physiology - Heart and Circulatory Physiology*, *291*(6).

Fabiato, A. (1983). Calcium-induced release of calcium from the cardiac sarcoplasmic reticulum. *American Journal of Physiology*, *245*(1), C1–C14.

Fabiato, A., & Fabiato, F. (1972). Excitation-contraction coupling of isolated cardiac fibers with disrupted or closed sarcolemmas. Calcium-dependent cyclic and tonic contractions. *Circulation Research*, *31*(3), 293–307.

Fakuade, F. E., Steckmeister, V., Seibertz, F., Gronwald, J., Kestel, S., Menzel, J., Pronto, J. R. D., Taha, K., Haghighi, F., Kensah, G., Pearman, C. M., Wiedmann, F., Teske, A. J., Schmidt, C., Dibb, K. M., El-Essawi, A., Danner, B. C., Baraki, H., Schwappach, B., … Voigt, N. (2020). Altered Atrial Cytosolic Calcium Handling Contributes to the Development of Postoperative Atrial Fibrillation. *Cardiovascular Research*, In press.

Feest, E. R., Steven Korte, F., Tu, A. yue, Dai, J., Razumova, M. V., Murry, C. E., & Regnier, M. (2014). Thin filament incorporation of an engineered cardiac troponin C variant (L48Q) enhances contractility in intact cardiomyocytes from healthy and infarcted hearts. *Journal of Molecular and Cellular Cardiology*, *72*, 219–227.

Feneck, R. O., Sherry, K. M., Withington, P. S., & Oduro-Dominah, A. (2001).

Comparison of the hemodynamic effects of milrinone with dobutamine in patients after cardiac surgery. *Journal of Cardiothoracic and Vascular Anesthesia*, *15*(3), 306–315.

Fleming, G. A., Murray, K. T., Yu, C., Byrne, J. G., Greelish, J. P., Petracek, M. R., Hoff, S. J., Ball, S. K., Brown, N. J., & Pretorius, M. (2008). Milrinone use is associated with postoperative atrial fibrillation after cardiac surgery. *Circulation*, *118*(16), 1619–1625.

Florea, S. M., & Blatter, L. A. (2012). Regulation of cardiac alternans by β-adrenergic signaling pathways. *American Journal of Physiology. Heart and Circulatory Physiology*, *303*(8), H1047–H1056.

Fox, J. J., McHarg, J. L., & Gilmour, R. F. (2002). Ionic mechanism of electrical alternans. *American Journal of Physiology - Heart and Circulatory Physiology*, *282*(2 51-2), 516–530.

Frangogiannis, N. G. (2019). The extracellular matrix in ischemic and nonischemic heart failure. *Circulation Research*, *125*(1), 117–146.

Frangogiannis, N. G. (2020). Transforming growth factor–β in tissue fibrosis. *Journal of Experimental Medicine*, *217*(3).

Franz, M. R., Karasik, P. L., Li, C., Moubarak, J., & Chavez, M. (1997). Electrical remodeling of the human atrium: Similar effects in patients with chronic atrial fibrillation and atrial flutter. *Journal of the American College of Cardiology*, *30*(7), 1785–1792.

Gaborit, N., Steenman, M., Lamirault, G., Le Meur, N., Le Bouter, S., Lande, G., Léger, J., Charpentier, F., Christ, T., Dobrev, D., Escande, D., Nattel, S., & Demolombe, S. (2005). Human atrial ion channel and transporter subunit gene-expression remodeling associated with valvular heart disease and atrial fibrillation. *Circulation*, *112*(4), 471–481.

Garcia, L., Verdejo, H. E., Kuzmicic, J., Zalaquett, R., Gonzalez, S., Lavandero, S., & Corbalan, R. (2012). Impaired cardiac autophagy in patients developing postoperative atrial fibrillation. *Journal of Thoracic and Cardiovascular Surgery*, *143*(2), 451-459.e1.

Garner, M., Routledge, T., King, J. E., Pilling, J. E., Veres, L., Harrison-Phipps, K., Bille, A., & Harling, L. (2017). New-onset atrial fibrillation after anatomic lung resection: Predictive factors, treatment and follow-up in a UK thoracic centre. *Interactive Cardiovascular and Thoracic Surgery*, *24*(2), 260–264.

Gaudino, M., Andreotti, F., Zamparelli, R., Di Castelnuovo, A., Nasso, G., Burzotta, F., Iacoviello, L., Donati, M. B., Schiavello, R., Maseri, A., & Possati, G. (2003). The -174G/C interleukin-6 polymorphism influences postoperative interleukin-6 levels and postoperative atrial fibrillation. Is atrial fibrillation an inflammatory complication? *Circulation*, *108*(10 SUPPL.).

Gheorghiade, M., Blair, J. E. A., Filippatos, G. S., Macarie, C., Ruzyllo, W., Korewicki, J., Bubenek-Turconi, S. I., Ceracchi, M., Bianchetti, M., Carminati, P., Kremastinos, D., Valentini, G., & Sabbah, H. N. (2008). Hemodynamic, Echocardiographic, and Neurohormonal Effects of Istaroxime, a Novel Intravenous Inotropic and Lusitropic Agent. A Randomized Controlled Trial in

Patients Hospitalized With Heart Failure. *Journal of the American College of Cardiology*, *51*(23), 2276–2285.

Ginsburg, K. S., & Bers, D. M. (2005). Isoproterenol does not enhance Ca-dependent Na/Ca exchange current in intact rabbit ventricular myocytes. *Journal of Molecular and Cellular Cardiology*, *39*(6), 972–981.

Girerd, N., Pibarot, P., Fournier, D., Daleau, P., Voisine, P., O'Hara, G., Després, J. P., & Mathieu, P. (2009). Middle-aged men with increased waist circumference and elevated C-reactive protein level are at higher risk for postoperative atrial fibrillation following coronary artery bypass grafting surgery. *European Heart Journal*, *30*(10), 1270–1278.

Goette, A., Juenemann, G., Peters, B., Klein, H. U., Roessner, A., Huth, C., & Röcken, C. (2002). Determinants and consequences of atrial fibrosis in patients undergoing open heart surgery. *Cardiovascular Research*, *54*(2), 390–396.

Goette, A., Kalman, J. M., Aguinaga, L., Akar, J., Cabrera, J. A., Chen, S. A., Chugh, S. S., Corradi, D., D'Avila, A., Dobrev, D., Fenelon, G., Gonzalez, M., Hatem, S. N., Helm, R., Hindricks, G., Ho, S. Y., Hoit, B., Jalife, J., Kim, Y. H., … Nattel, S. (2016). EHRA/HRS/APHRS/SOLAECE expert consensus on Atrial cardiomyopathies: Definition, characterisation, and clinical implication. *Journal of Arrhythmia*, *32*(4), 247–278.

Gramley, F., Lorenzen, J., Knackstedt, C., Rana, O. R., Saygili, E., Frechen, D., Stanzel, S., Pezzella, F., Koellensperger, E., Weiss, C., Münzel, T., & Schauerte, P. (2009). Age-related atrial fibrosis. *Age*, *31*(1), 27–38.

Grammer, J. B., Bosch, R. F., Kühlkamp, V., & Seipel, L. (2000). Molecular remodeling of Kv4.3 Potassium channels in human atrial fibrillation. *Journal of Cardiovascular Electrophysiology*, *11*(6), 626–633.

Grant, A. O. (2009). Cardiac ion channels. *Circulation: Arrhythmia and Electrophysiology*, *2*(2), 185–194.

Greiser, M., Kerfant, B. G., Williams, G. S. B., Voigt, N., Harks, E., Dibb, K. M., Giese, A., Meszaros, J., Verheule, S., Ravens, U., Allessie, M. A., Gammie, J. S., Van Der Velden, J., Lederer, W. J., Dobrev, D., & Schotten, U. (2014). Tachycardia-induced silencing of subcellular Ca2+ signaling in atrial myocytes. *Journal of Clinical Investigation*, *124*(11), 4759–4772.

Greiser, M., Neuberger, H. R., Harks, E., El-Armouche, A., Boknik, P., de Haan, S., Verheyen, F., Verheule, S., Schmitz, W., Ravens, U., Nattel, S., Allessie, M. A., Dobrev, D., & Schotten, U. (2009). Distinct contractile and molecular differences between two goat models of atrial dysfunction: AV block-induced atrial dilatation and atrial fibrillation. *Journal of Molecular and Cellular Cardiology*, *46*(3), 385–394.

Guichard, J. B., & Nattel, S. (2017). Atrial Cardiomyopathy: A Useful Notion in Cardiac Disease Management or a Passing Fad? *Journal of the American College of Cardiology*, *70*(6), 756–765.

Haïssaguerre, M., Jaïs, P., Shah, D. C., Takahashi, A., Hocini, M., Quiniou, G., Garrigue, S., Le Mouroux, A., Le Métayer, P., & Clémenty, J. (1998). Spontaneous Initiation of Atrial Fibrillation by Ectopic Beats Originating in the Pulmonary Veins.

New England Journal of Medicine, *339*(10), 659–666.

Hak, Ł., Myśliwska, J., Wi, J., Szyndler, K., Siebert, J., & Rogowski, J. (2009). Interleukin-2 as a predictor of early postoperative atrial fibrillation after cardiopulmonary bypass graft (CABG). *Journal of Interferon and Cytokine Research*, *29*(6), 327–332.

Hammond, D. E., Kumar, J. D., Raymond, L., Simpson, D. M., Beynon, R. J., Dockray, G. J., & Varro, A. (2018). Stable isotope dynamic labeling of secretomes (SIDLs) identifies authentic secretory proteins released by cancer and stromal cells. *Molecular and Cellular Proteomics*, *17*(9), 1837–1849.

Heijman, J., Voigt, N., Nattel, S., & Dobrev, D. (2014). Cellular and molecular electrophysiology of atrial fibrillation initiation, maintenance, and progression. *Circulation Research*, *114*(9), 1483–1499.

Hesselkilde, E. Z., Carstensen, H., Flethøj, M., Fenner, M., Kruse, D. D., Sattler, S. M., Tfelt-Hansen, J., Pehrson, S., Braunstein, T. H., Carlson, J., Platonov, P. G., Jespersen, T., & Buhl, R. (2019). Longitudinal study of electrical, functional and structural remodelling in an equine model of atrial fibrillation. *BMC Cardiovascular Disorders*, *19*(1), 228.

Hocking, S. L., Wu, L. E., Guilhaus, M., Chisholm, D. J., & James, D. E. (2010). Intrinsic depot-specific differences in the secretome of adipose tissue, preadipocytes, and adipose tissue-derived microvascular endothelial cells. *Diabetes*, *59*(12), 3008–3016.

Hove-Madsen, L., Llach, A., Bayes-Genís, A., Roura, S., Font, E. R., Arís, A., & Cinca, J. (2004). Atrial fibrillation is associated with increased spontaneous calcium release from the sarcoplasmic reticulum in human atrial myocytes. *Circulation*, *110*(11), 1358–1363.

Hu, Y. F., Chen, Y. J., Lin, Y. J., & Chen, S. A. (2015). Inflammation and the pathogenesis of atrial fibrillation. *Nature Reviews Cardiology*, *12*(4), 230–243.

Hu, Z., Li, G., Wang, J. W., Chong, S. Y., Yu, D., Wang, X., Soon, J. L., Liang, M. C., Wong, Y. P., Huang, N., Colecraft, H. M., Liao, P., & Soong, T. W. (2018). Regulation of blood pressure by targeting CaV1.2-galectin-1 protein interaction. *Circulation*, *138*(14), 1431–1445.

Hynes, R. O. (2014). Stretching the boundaries of extracellular matrix research. *Nature Reviews Molecular Cell Biology*, *15*(12), 761–763.

January, C. T., Riddle, J. M., & Salata, J. J. (1988). A model for early afterdepolarizations: induction with the Ca2+ channel agonist Bay K 8644. *Circulation Research*, *62*(3), 563–571.

January, C. T., Wann, L. S., Alpert, J. S., Calkins, H., Cigarroa, J. E., Cleveland, J. C., Conti, J. B., Ellinor, P. T., Ezekowitz, M. D., Field, M. E., Murray, K. T., Sacco, R. L., Stevenson, W. G., Tchou, P. J., Tracy, C. M., & Yancy, C. W. (2014). 2014 AHA/ACC/HRS guideline for the management of patients with atrial fibrillation: A report of the American college of Cardiology/American heart association task force on practice guidelines and the heart rhythm society. *Journal of the American College of Cardiology*, *64*(21), e1–e76.

Kalman, J. M., Munawar, M., Howes, L. G., Louis, W. J., Buxton, B. F., Gutteridge, G., & Tonkin, A. M. (1995). Atrial fibrillation after coronary artery bypass grafting is associated with sympathetic activation. *The Annals of Thoracic Surgery*, *60*(6), 1709–1715.

Kanaporis, G., & Blatter, L. A. (2017). Membrane potential determines calcium alternans through modulation of SR Ca2 + load and L-type Ca2 + current. *Journal of Molecular and Cellular Cardiology*, *105*, 49–58.

Kato, T., Iwasaki, Y. K., & Nattel, S. (2012). Connexins and atrial fibrillation: Filling in the gaps. *Circulation*, *125*(2), 203–206.

Kho, C., Lee, A., Jeong, D., Oh, J. G., Chaanine, A. H., Kizana, E., Park, W. J., & Hajjar, R. J. (2011). SUMO1-dependent modulation of SERCA2a in heart failure. *Nature*, *477*(7366), 601–606.

Kim, M. H., Johnston, S. S., Chu, B. C., Dalal, M. R., & Schulman, K. L. (2011). Estimation of total incremental health care costs in patients with atrial fibrillation in the united states. *Circulation: Cardiovascular Quality and Outcomes*, *4*(3), 313–320.

Kirchhof, P., Benussi, S., Kotecha, D., Ahlsson, A., Atar, D., Casadei, B., Castella, M., Diener, H. C., Heidbuchel, H., Hendriks, J., Hindricks, G., Manolis, A. S., Oldgren, J., Popescu, B. A., Schotten, U., Van Putte, B., Vardas, P., Agewall, S., Camm, J., … Duncan, E. (2016). 2016 ESC Guidelines for the management of atrial fibrillation developed in collaboration with EACTS. *European Heart Journal*, *37*(38), 2893–2962.

Kneller, J., Zou, R., Vigmond, E. J., Wang, Z., Leon, L. J., & Nattel, S. (2002). Cholinergic atrial fibrillation in a computer model of a two-dimensional sheet of canine atrial cells with realistic ionic properties. *Circulation Research*, *90*(9), e73–e87.

Ko, W. C., Hong, C. Y., Hou, S. M., Lin, C. H., Ong, E. T., Lee, C. F., Tsai, C. T., & Lai, L. P. (2011). Elevated expression of connective tissue growth factor in human atrial fibrillation and angiotensin II-treated cardiomyocytes. *Circulation Journal*, *75*(7), 1592–1600.

Kong, P., Christia, P., & Frangogiannis, N. G. (2014). The pathogenesis of cardiac fibrosis. *Cellular and Molecular Life Sciences*, *71*(4), 549–574.

Kostin, S., Klein, G., Szalay, Z., Hein, S., Bauer, E. P., & Schaper, J. (2002). Structural correlate of atrial fibrillation in human patients. *Cardiovascular Research*, *54*(2), 361–379.

Krul, S. P. J., Berger, W. R., Smit, N. W., Van Amersfoorth, S. C. M., Driessen, A. H. G., Van Boven, W. J., Fiolet, J. W. T., Van Ginneken, A. C. G., Van Der Wal, A. C., De Bakker, J. M. T., Coronel, R., & De Groot, J. R. (2015). Atrial fibrosis and conduction slowing in the left atrial appendage of patients undergoing thoracoscopic surgical pulmonary vein isolation for atrial fibrillation. *Circulation: Arrhythmia and Electrophysiology*, *8*(2), 288–295.

Laemmli, U. K. (1970). Cleavage of structural proteins during the assembly of the head of bacteriophage T4. *Nature*, *227*(5259), 680–685.

Lalani, G. G., Schricker, A. A., Clopton, P., Krummen, D. E., & Narayan, S. M. (2013). Frequency analysis of atrial action potential alternans: A sensitive clinical index of individual propensity to atrial fibrillation. *Circulation: Arrhythmia and Electrophysiology*, *6*(5), 859–867.

Lamm, G., Auer, J., Weber, T., Berent, R., Ng, C., & Eber, B. (2006). Postoperative white blood cell count predicts atrial fibrillation after cardiac surgery. *Journal of Cardiothoracic and Vascular Anesthesia*, *20*(1), 51–56.

Lane, D. A., Boos, C. J., & Lip, G. Y. H. (2015). Atrial fibrillation (chronic). *BMJ Clinical Evidence*, *2015*, 0217.

Lapar, D. J., Speir, A. M., Crosby, I. K., Fonner, E., Brown, M., Rich, J. B., Quader, M., Kern, J. A., Kron, I. L., & Ailawadi, G. (2014). Postoperative atrial fibrillation significantly increases mortality, hospital readmission, and hospital costs. *Annals of Thoracic Surgery*, *98*(2), 527–533.

Lapinskas, T., Kelle, S., Grune, J., Foryst-Ludwig, A., Meyborg, H., Jeuthe, S., Wellnhofer, E., Elsanhoury, A., Pieske, B., Gebker, R., Kintscher, U., & Stawowy, P. (2020). Serelaxin Improves Regional Myocardial Function in Experimental Heart Failure: An In Vivo Cardiac Magnetic Resonance Study. *Journal of the American Heart Association*, *9*(3), e013702.

Layland, J., Cave, A. C., Warren, C., Grieve, D. J., Sparks, E., Kentish, J. C., Solaro, R. J., & Shah, A. M. (2005). Protection against endotoxemia-induced contractile dysfunction in mice with cardiac-specific expression of slow skeletal troponin I. *FASEB Journal*, *19*(9), 1137–1139.

Lenaerts, I., Bito, V., Heinzel, F. R., Driesen, R. B., Holemans, P., D'hooge, J., Heidbüchel, H., Sipido, K. R., & Willems, R. (2009). Ultrastructural and functional remodeling of the coupling between Ca2+ influx and sarcoplasmic reticulum Ca2+ release in right atrial myocytes from experimental persistent atrial fibrillation. *Circulation Research*, *105*(9), 876–885.

Lezoualc'h, F., Steplewski, K., Sartiani, L., Mugelli, A., Fischmeister, R., & Bril, A. (2007). Quantitative mRNA analysis of serotonin 5-HT4 receptor isoforms, calcium handling proteins and ion channels in human atrial fibrillation. *Biochemical and Biophysical Research Communications*, *357*(1), 218–224.

Li, D., Fareh, S., Leung, T. K., & Nattel, S. (1999). Promotion of Atrial Fibrillation by Heart Failure in Dogs. *Circulation*, *100*(1), 87–95.

Li, J. Y., Lai, Y. J., Yeh, H. I., Chen, C. L., Sun, S., Wu, S. J., & Lin, F. Y. (2008). Atrial gap junctions, NF-κB and fibrosis in patients undergoing coronary artery bypass surgery: The relationship with postoperative atrial fibrillation. *Cardiology*, *112*(2), 81–88.

Lip, G. Y. H., Brechin, C. M., & Lane, D. A. (2012). The global burden of atrial fibrillation and stroke: A systematic review of the epidemiology of atrial fibrillation in regions outside North America and Europe. *Chest*, *142*(6), 1489–1498.

Lip, G. Y. H., Fauchier, L., Freedman, S. B., Van Gelder, I., Natale, A., Gianni, C., Nattel, S., Potpara, T., Rienstra, M., Tse, H. F., & Lane, D. A. (2016). Atrial fibrillation. *Nature Reviews Disease Primers*, *2*(1), 1–26.

Liu, B., Lee, R. S., Biesiadecki, B. J., Tikunova, S. B., & Davis, J. P. (2012). Engineered troponin C constructs correct disease-related cardiac myofilament calcium sensitivity. *Journal of Biological Chemistry*, *287*(24), 20027–20036.

Liu, T., Song, D., Dong, J., Zhu, P., Liu, J., Liu, W., Ma, X., Zhao, L., & Ling, S. (2017). Current understanding of the pathophysiology of myocardial fibrosis and its quantitative assessment in heart failure. *Frontiers in Physiology*, *8*, 238.

Livak, K. J., & Schmittgen, T. D. (2001). Analysis of relative gene expression data using real-time quantitative PCR and the 2-ΔΔCT method. *Methods*, *25*(4), 402–408.

López, B., Querejeta, R., González, A., Beaumont, J., Larman, M., & Díez, J. (2009). Impact of treatment on myocardial lysyl oxidase expression and collagen Cross-linking in patients with heart failure. *Hypertension*, *53*(2), 236–242.

Lu, Y., Zhang, Y., Wang, N., Pan, Z., Gao, X., Zhang, F., Zhang, Y., Shan, H., Luo, X., Bai, Y., Sun, L., Song, W., Xu, C., Wang, Z., & Yang, B. (2010). MicroRNA-328 contributes to adverse electrical remodeling in atrial fibrillation. *Circulation*, *122*(23), 2378–2387.

Maack, C., Eschenhagen, T., Hamdani, N., Heinze, F. R., Lyon, A. R., Manstein, D. J., Metzger, J., Papp, Z., Tocchetti, C. G., Yilmaz, M. B., Anker, S. D., Balligand, J. L., Bauersachs, J., Brutsaert, D., Carrier, L., Chlopicki, S., Cleland, J. G., De Boer, R. A., Dietl, A., … Mebazaa, A. (2019). Treatments targeting inotropy. *European Heart Journal*, *40*(44), 3626-3640D.

Macquaide, N., Tuan, H.-T. M., Hotta, J.-I., Sempels, W., Lenaerts, I., Holemans, P., Hofkens, J., Jafri, M. S., Willems, R., & Sipido, K. R. (2015). Ryanodine receptor cluster fragmentation and redistribution in persistent atrial fibrillation enhance calcium release. *Cardiovascular Research*, *108*(3), 387–398.

Maesen, B., Nijs, J., Maessen, J., Allessie, M., & Schotten, U. (2012). Post-operative atrial fibrillation: A maze of mechanisms. *EP Europace*, *14*(2), 159–174.

Makary, S., Voigt, N., Maguy, A., Wakili, R., Nishida, K., Harada, M., Dobrev, D., & Nattel, S. (2011). Differential protein kinase c isoform regulation and increased constitutive activity of acetylcholine-regulated potassium channels in atrial remodeling. *Circulation Research*, *109*(9), 1031–1043.

Marx, S. O., Reiken, S., Hisamatsu, Y., Jayaraman, T., Burkhoff, D., Rosemblit, N., & Marks, A. R. (2000). PKA phosphorylation dissociates FKBP12.6 from the calcium release channel (ryanodine receptor): Defective regulation in failing hearts. *Cell*, *101*(4), 365–376.

Mayer, A. G. (1906). *Rhythmical pulsation in Scyphomedusae.* Carnegie Institution of Washington,. https://www.biodiversitylibrary.org/item/115383

McBride, D., Mattenklotz, A. M., Willich, S. N., & Brüggenjürgen, B. (2009). The costs of care in atrial fibrillation and the effect of treatment modalities in Germany. *Value in Health*, *12*(2), 293–301.

Melby, S. J., George, J. F., Picone, D. J., Wallace, J. P., Davies, J. E., George, D. J., & Kirklin, J. K. (2015). A time-related parametric risk factor analysis for postoperative atrial fibrillation after heart surgery. *Journal of Thoracic and Cardiovascular Surgery*, *149*(3), 886–892.

Méndez, O., & Villanueva, J. (2015). Challenges and opportunities for cell line secretomes in cancer proteomics. *PROTEOMICS - Clinical Applications*, *9*(3–4), 348–357.

Mendler, L., Braun, T., & Müller, S. (2016). The Ubiquitin-Like SUMO System and Heart Function: From Development to Disease. *Circulation Research*, *118*(1), 132–144.

Mines, G. R. (1914). On circulating excitations in heart muscle and their possible relation to tachycardia and fibrillation. *Trans R Soc Can*, *8*, 43–52.

Molina, C. E., Abu-Taha, I. H., Wang, Q., Roselló-Díez, E., Kamler, M., Nattel, S., Ravens, U., Wehrens, X. H. T., Hove-Madsen, L., Heijman, J., & Dobrev, D. (2018). Profibrotic, electrical, and calcium-handling remodeling of the atria in heart failure patients with and without atrial fibrillation. *Frontiers in Physiology*, *9*, 1383.

Morano, I., Arndt, H., Gartner, C., & Ruegg, J. C. (1988). Skinned fibers of human atrium and ventricle: Myosin isoenzymes and contractility. *Circulation Research*, *62*(3), 632–639.

Mou, L., Norby, F. L., Chen, L. Y., O'Neal, W. T., Lewis, T. T., Loehr, L. R., Soliman, E. Z., & Alonso, A. (2018). Lifetime Risk of Atrial Fibrillation by Race and Socioeconomic Status: ARIC Study (Atherosclerosis Risk in Communities). *Circulation: Arrhythmia and Electrophysiology*, *11*(7), e006350.

Mulieri, L. A., Hasenfuss, G., Ittleman, F., Blanchard, E. M., & Alpert, N. R. (1989). Protection of human left ventricular myocardium from cutting injury with 2,3-butanedione monoxime. *Circulation Research*, *65*(5), 1441–1444.

Naba, A., Pearce, O. M. T., Del Rosario, A., Ma, D., Ding, H., Rajeeve, V., Cutillas, P. R., Balkwill, F. R., & Hynes, R. O. (2017). Characterization of the Extracellular Matrix of Normal and Diseased Tissues Using Proteomics. *Journal of Proteome Research*, *16*(8), 3083–3091.

Narayan, S. M., Bode, F., Karasik, P. L., & Franz, M. R. (2002). Alternans of atrial action potentials during atrial flutter as a precursor to atrial fibrillation. *Circulation*, *106*(15), 1968–1973.

Nattel, S. (2017). Molecular and Cellular Mechanisms of Atrial Fibrosis in Atrial Fibrillation. *JACC: Clinical Electrophysiology*, *3*(5), 425–435.

Nattel, S., & Harada, M. (2014). Atrial remodeling and atrial fibrillation: Recent advances and translational perspectives. *Journal of the American College of Cardiology*, *63*(22), 2335–2345.

Nattel, S., Heijman, J., Zhou, L., & Dobrev, D. (2020). Molecular Basis of Atrial Fibrillation Pathophysiology and Therapy: A Translational Perspective. *Circulation Research*, 51–72.

Neef, S., Dybkova, N., Sossalla, S., Ort, K. R., Fluschnik, N., Neumann, K., Seipelt, R., Schöndube, F. A., Hasenfuss, G., & Maier, L. S. (2010). CaMKII-Dependent diastolic SR Ca2+ leak and elevated diastolic Ca2+ levels in right atrial myocardium of patients with atrial fibrillation. *Circulation Research*, *106*(6), 1134–1144.

Ohtani, K., Yutani, C., Nagata, S., Koretsune, Y., Hori, M., & Kamada, T. (1995). High

prevalence of atrial fibrosis in patients with dilated cardiomyopathy. *Journal of the American College of Cardiology*, *25*(5), 1162–1169.

Oka, T., Xu, J., Kaiser, R. A., Melendez, J., Hambleton, M., Sargent, M. A., Lorts, A., Brunskill, E. W., Dorn, G. W., Conway, S. J., Aronow, B. J., Robbins, J., & Molkentin, J. D. (2007). Genetic manipulation of periostin expression reveals a role in cardiac hypertrophy and ventricular remodeling. *Circulation Research*, *101*(3), 313–321.

Pearman, C. M. (2014). An excel-based implementation of the spectral method of action potential alternans analysis. *Physiological Reports*, *2*(12), e12194.

Pellman, J., Lyon, R. C., & Sheikh, F. (2010). Extracellular matrix remodeling in atrial fibrosis: Mechanisms and implications in atrial fibrillation. *Journal of Molecular and Cellular Cardiology*, *48*(3), 461–467.

Pellman, J., Zhang, J., & Sheikh, F. (2016). Myocyte-fibroblast communication in cardiac fibrosis and arrhythmias: Mechanisms and model systems. *Journal of Molecular and Cellular Cardiology*, *94*, 22–31.

Pernigo, M., Benfari, G., Geremia, G., Noni, M., Borio, G., Mazzali, G., Zamboni, M., Onorati, F., Faggian, G., Vassanelli, C., & Rossi, A. (2017). Atrial Function as an Independent Predictor of Postoperative Atrial Fibrillation in Patients Undergoing Aortic Valve Surgery for Severe Aortic Stenosis. *Journal of the American Society of Echocardiography*, *30*(10), 956-965.e1.

Pollesello, P., Papp, Z., & Papp, J. G. (2016). Calcium sensitizers: What have we learned over the last 25 years? *International Journal of Cardiology*, *203*, 543–548.

Polyakova, V., Miyagawa, S., Szalay, Z., Risteli, J., & Kostin, S. (2008). Atrial extracellular matrix remodelling in patients with atrial fibrillation. *Journal of Cellular and Molecular Medicine*, *12*(1), 189–208.

Pretorius, M., Donahue, B. S., Yu, C., Greelish, J. P., Roden, D. M., & Brown, N. J. (2007). Plasminogen Activator Inhibitor-1 as a Predictor of Postoperative Atrial Fibrillation After Cardiopulmonary Bypass. *Circulation*, *116*(11_suppl), I-1-I–7.

Rebeyka, I. M., Axford-Gatley, R. A., Bush, B. G., del Nido, P. J., Mickle, D. A. G., Romaschin, A. D., & Wilson, G. J. (1990). Calcium paradox in an in vivo model of multidose cardioplegia and moderate hypothermia. *The Journal of Thoracic and Cardiovascular Surgery*, *99*(3), 475–483.

Reese-Petersen, A. L., Olesen, M. S., Karsdal, M. A., Svendsen, J. H., & Genovese, F. (2020). Atrial fibrillation and cardiac fibrosis: A review on the potential of extracellular matrix proteins as biomarkers. *Matrix Biology*, *91–92*(9), 188–203.

Riber, L. P., Larsen, T. B., & Christensen, T. D. (2014). Postoperative atrial fibrillation prophylaxis after lung surgery: Systematic review and meta-analysis. *Annals of Thoracic Surgery*, *98*(6), 1989–1997.

Roberts, A. B., Sporn, M. B., Assoian, R. K., Smith, J. M., Roche, N. S., Wakefield, L. M., Heine, U. I., Liotta, L. A., Falanga, V., & Kehrl, J. H. (1986). Transforming growth factor type β: Rapid induction of fibrosis and angiogenesis in vivo and stimulation of collagen formation in vitro. *Proceedings of the National Academy of Sciences of the United States of America*, *83*(12), 4167–4171.

Robertson, I. B., Horiguchi, M., Zilberberg, L., Dabovic, B., Hadjiolova, K., & Rifkin, D. B. (2015). Latent TGF-β-binding proteins. *Matrix Biology*, *47*, 44–53.

Robertson, I. B., & Rifkin, D. B. (2016). Regulation of the bioavailability of TGF-β and TGF-β-related proteins. *Cold Spring Harbor Perspectives in Biology*, *8*(6), a021907.

Rosenbaum, D. S., Cutler, M. J., Wan, X., Laurita, K. R., & Hajjar, R. J. (2009). Targeted SERCA2a gene expression identifies molecular mechanism and therapeutic target for arrhythmogenic cardiac alternans. *Circulation: Arrhythmia and Electrophysiology*, *2*(6), 686–694.

Rucker-Martin, C., Milliez, P., Tan, S., Decrouy, X., Recouvreur, M., Vranckx, R., Delcayre, C., Renaud, J. F., Dunia, I., Segretain, D., & Hatem, S. N. (2006). Chronic hemodynamic overload of the atria is an important factor for gap junction remodeling in human and rat hearts. *Cardiovascular Research*, *72*(1), 69–79.

Samuel, C. S., Bodaragama, H., Chew, J. Y., Widdop, R. E., Royce, S. G., & Hewitson, T. D. (2014). Serelaxin is a more efficacious antifibrotic than enalapril in an experimental model of heart disease. *Hypertension*, *64*(2), 315–322.

Schmidt, C., Wiedmann, F., Voigt, N., Zhou, X. B., Heijman, J., Lang, S., Albert, V., Kallenberger, S., Ruhparwar, A., Szabó, G., Kallenbach, K., Karck, M., Borggrefe, M., Biliczki, P., Ehrlich, J. R., Baczkó, I., Lugenbiel, P., Schweizer, P. A., Donner, B. C., … Thomas, D. (2015). Upregulation of K2P 3.1 K + Current Causes Action Potential Shortening in Patients with Chronic Atrial Fibrillation. *Circulation*, *132*(2), 82–92.

Schotten, U., Ausma, J., Stellbrink, C., Sabatschus, I., Vogel, M., Frechen, D., Schoendube, F., Hanrath, P., & Allessie, M. A. (2001). Cellular Mechanisms of Depressed Atrial Contractility in Patients With Chronic Atrial Fibrillation. *Circulation*, *103*(5), 691–698.

Schotten, U., Verheule, S., Kirchhof, P., & Goette, A. (2011). Pathophysiological mechanisms of atrial fibrillation: A translational appraisal. *Physiological Reviews*, *91*(1), 265–325.

Schrickel, J. W., Brixius, K., Herr, C., Clemen, C. S., Sasse, P., Reetz, K., Grohé, C., Meyer, R., Tiemann, K., Schröder, R., Bloch, W., Nickenig, G., Fleischmann, B. K., Noegel, A. A., Schwinger, R. H. G., & Lewalter, T. (2007). Enhanced heterogeneity of myocardial conduction and severe cardiac electrical instability in annexin A7-deficient mice. *Cardiovascular Research*, *76*(2), 257–268.

Schüttler, D., Bapat, A., Kääb, S., Lee, K., Tomsits, P., Clauss, S., & Hucker, W. J. (2020). Animal Models of Atrial Fibrillation. *Circulation Research*, *127*, 91–110.

Sequeira, V., & van der Velden, J. (2015). Historical perspective on heart function: the Frank–Starling Law. *Biophysical Reviews*, *7*(4), 421–447.

Severs, N. J., Bruce, A. F., Dupont, E., & Rothery, S. (2008). Remodelling of gap junctions and connexin expression in diseased myocardium. *Cardiovascular Research*, *80*(1), 9–19.

Shah, S. J., Blair, J. E. A., Filippatos, G. S., MacArie, C., Ruzyllo, W., Korewicki, J., Bubenek-Turconi, S. I., Ceracchi, M., Bianchetti, M., Carminati, P., Kremastinos,

D., Grzybowski, J., Valentini, G., Sabbah, H. N., & Gheorghiade, M. (2009). Effects of istaroxime on diastolic stiffness in acute heart failure syndromes: Results from the Hemodynamic, Echocardiographic, and Neurohormonal Effects of Istaroxime, a Novel Intravenous Inotropic and Lusitropic Agent: A Randomized Controlled Trial in P. *American Heart Journal*, *157*(6), 1035–1041.

Shannon, T. R., Ginsburg, K. S., & Bers, D. M. (2002). Quantitative assessment of the SR Ca2+ leak-load relationship. *Circulation Research*, *91*(7), 594–600.

Shettigar, V., Zhang, B., Little, S. C., Salhi, H. E., Hansen, B. J., Li, N., Zhang, J., Roof, S. R., Ho, H. T., Brunello, L., Lerch, J. K., Weisleder, N., Fedorov, V. V., Accornero, F., Rafael-Fortney, J. A., Gyorke, S., Janssen, P. M. L., Biesiadecki, B. J., Ziolo, M. T., & Davis, J. P. (2016). Rationally engineered Troponin C modulates in vivo cardiac function and performance in health and disease. *Nature Communications*, *7*(1), 1–13.

Shin, J., Rhim, J., Kwon, Y., Choi, S. Y., Shin, S., Ha, C. W., & Lee, C. (2019). Comparative analysis of differentially secreted proteins in serum-free and serum-containing media by using BONCAT and pulsed SILAC. *Scientific Reports*, *9*(1), 3096.

Smith, G. L., & Eisner, D. A. (2019). Calcium Buffering in the Heart in Health and Disease. *Circulation*, *139*(20), 2358–2371.

Streng, A. S., de Boer, D., van der Velden, J., van Dieijen-Visser, M. P., & Wodzig, W. K. W. H. (2013). Posttranslational modifications of cardiac troponin T: An overview. *Journal of Molecular and Cellular Cardiology*, *63*, 47–56.

Sun, H., Gaspo, R., Leblanc, N., & Nattel, S. (1998). Cellular Mechanisms of Atrial Contractile Dysfunction Caused by Sustained Atrial Tachycardia. *Circulation*, *98*(7), 719–727.

Swartz, M. F., Fink, G. W., Lutz, C. J., Taffet, S. M., Berenfeld, O., Vikstrom, K. L., Kasprowicz, K., Bhatta, L., Puskas, F., Kalifa, J., & Jalife, J. (2009). Left versus right atrial difference in dominant frequency, K+ channel transcripts, and fibrosis in patients developing atrial fibrillation after cardiac surgery. *Heart Rhythm*, *6*(10), 1415–1422.

Swartz, M. F., Fink, G. W., Sarwar, M. F., Hicks, G. L., Yu, Y., Hu, R., Lutz, C. J., Taffet, S. M., & Jalife, J. (2012). Elevated pre-operative serum peptides for collagen i and III synthesis result in post-surgical atrial fibrillation. *Journal of the American College of Cardiology*, *60*(18), 1799–1806.

Tinica, G., Mocanu, V., Zugun-Eloae, F., & Butcovan, D. (2015). Clinical and histological predictive risk factors of atrial fibrillation in patients undergoing open-heart surgery. *Experimental and Therapeutic Medicine*, *10*(6), 2299–2304.

Trafford, A. W., Díaz, M. E., & Eisner, D. A. (1999). A novel, rapid and reversible method to measure Ca buffering and time- course of total sarcoplasmic reticulum Ca content in cardiac ventricular myocytes. *Pflugers Archiv European Journal of Physiology*, *437*(3), 501–503.

Travers, J. G., Kamal, F. A., Robbins, J., Yutzey, K. E., & Blaxall, B. C. (2016). Cardiac Fibrosis: The fibroblast awakens. *Circulation Research*, *118*(6), 1021–1040.

Tse, G. (2016). Mechanisms of cardiac arrhythmias. *Journal of Arrhythmia*, *32*(2), 75–81.

Valiente-Alandi, I., Potter, S. J., Salvador, A. M., Schafer, A. E., Schips, T., Carrillo-Salinas, F., Gibson, A. M., Nieman, M. L., Perkins, C., Sargent, M. A., Huo, J., Lorenz, J. N., DeFalco, T., Molkentin, J. D., Alcaide, P., & Blaxall, B. C. (2018). Inhibiting Fibronectin Attenuates Fibrosis and Improves Cardiac Function in a Model of Heart Failure. *Circulation*, *138*(12), 1236–1252.

Van Der Velden, H. M. W., Ausma, J., Rook, M. B., Hellemons, A. J. C. G. M., Van Veen, T. A. A. B., Allessie, M. A., & Jongsma, H. J. (2000). Gap junctional remodeling in relation to stabilization of atrial fibrillation in the goat. *Cardiovascular Research*, *46*(3), 476–486.

Van Der Velden, H. M. W., Van Kempen, M. J. A., Wijffels, M. C. E. F., Van Zijverden, M., Groenewegen, W. A., Allessie, M. A., & Jongsma, H. J. (1998). Altered pattern of connexin40 distribution in persistent atrial fibrillation in the goat. *Journal of Cardiovascular Electrophysiology*, *9*(6), 596–607.

Van Rijen, H. V. M., Eckardt, D., Degen, J., Theis, M., Ott, T., Willecke, K., Jongsma, H. J., Opthof, T., & De Bakker, J. M. T. (2004). Slow Conduction and Enhanced Anisotropy Increase the Propensity for Ventricular Tachyarrhythmias in Adult Mice with Induced Deletion of Connexin43. *Circulation*, *109*(8), 1048–1055.

Van Wagoner, D. R., Pond, A. L., Lamorgese, M., Rossie, S. S., McCarthy, P. M., & Nerbonne, J. M. (1999). Atrial L-type Ca2+ currents and human atrial fibrillation. *Circulation Research*, *85*(5), 428–436.

Van Wagoner, D. R., Pond, A. L., McCarthy, P. M., Trimmer, J. S., & Nerbonne, J. M. (1997). Outward K+ current densities and Kv1.5 expression are reduced in chronic human atrial fibrillation. *Circulation Research*, *80*(6), 772–781.

Verdejo, H. E., Becerra, E., Zalaquet, R., Del Campo, A., Garcia, L., Troncoso, R., Chiong, M., Marin, A., Castro, P. F., Lavandero, S., Gabrielli, L., & Corbalán, R. (2016). Atrial Function Assessed by Speckle Tracking Echocardiography Is a Good Predictor of Postoperative Atrial Fibrillation in Elderly Patients. *Echocardiography*, *33*(2), 242–248.

Verheule, S., Sat, T., Everett IV, T., Engle, S. K., Otten, D., Rubart-Von Der Lohe, M., Nakajima, H. O., Nakajima, H., Field, L. J., & Olgin, J. E. (2004). Increased vulnerability to atrial fibrillation in transgenic mice with selective atrial fibrosis caused by overexpression of TGF-β1. *Circulation Research*, *94*(11), 1458–1465.

Verheule, S., Wilson, E., Banthia, S., Everett IV, T. H., Shanbhag, S., Sih, H. J., & Olgin, J. E. (2004). Direction-dependent conduction abnormalities in a canine model of atrial fibrillation due to chronic atrial dilatation. *American Journal of Physiology - Heart and Circulatory Physiology*, *287*(2 56-2), H634–H644.

Vest, J. A., Wehrens, X. H. T., Reiken, S. R., Lehnart, S. E., Dobrev, D., Chandra, P., Danilo, P., Ravens, U., Rosen, M. R., & Marks, A. R. (2005). Defective cardiac ryanodine receptor regulation during atrial fibrillation. *Circulation*, *111*(16), 2025–2032.

Vikhorev, P. G., & Vikhoreva, N. N. (2018). Cardiomyopathies and related changes in contractility of human heart muscle. *International Journal of Molecular Sciences*,

19(8), 2234.

Voigt, N., Friedrich, A., Bock, M., Wettwer, E., Christ, T., Knaut, M., Strasser, R. H., Ravens, U., & Dobrev, D. (2007). Differential phosphorylation-dependent regulation of constitutively active and muscarinic receptor-activated IK,ACh channels in patients with chronic atrial fibrillation. *Cardiovascular Research*, *74*(3), 426–437.

Voigt, N., Heijman, J., Wang, Q., Chiang, D. Y., Li, N., Karck, M., Wehrens, X. H. T., Nattel, S., & Dobrev, D. (2014). Cellular and molecular mechanisms of atrial arrhythmogenesis in patients with paroxysmal atrial fibrillation. *Circulation*, *129*(2), 145–156.

Voigt, N., Li, N., Wang, Q., Wang, W., Trafford, A. W., Abu-Taha, I., Sun, Q., Wieland, T., Ravens, U., Nattel, S., Wehrens, X. H. T., & Dobrev, D. (2012). Enhanced sarcoplasmic reticulum Ca 2+ Leak and increased Na +-Ca 2+ exchanger function underlie delayed afterdepolarizations in patients with chronic atrial fibrillation. *Circulation*, *125*(17), 2059–2070.

Voigt, N., Pearman, C. M., Dobrev, D., & Dibb, K. M. (2015). Methods for isolating atrial cells from large mammals and humans. *Journal of Molecular and Cellular Cardiology*, *86*, 187–198.

Voigt, N., Trausch, A., Knaut, M., Matschke, K., Varró, A., Van Wagoner, D. R., Nattel, S., Ravens, U., & Dobrev, D. (2010). Left-to-right atrial inward rectifier potassium current gradients in patients with paroxysmal versus chronic atrial fibrillation. *Circulation: Arrhythmia and Electrophysiology*, *3*(5), 472–480.

Voigt, N., Zhou, X. B., & Dobrev, D. (2013). Isolation of human atrial myocytes for simultaneous measurements of Ca2+ transients and membrane currents. *Journal of Visualized Experiments*, *77*, e50235.

Wakili, R., Voigt, N., Kääb, S., Dobrev, D., & Nattel, S. (2011). Recent advances in the molecular pathophysiology of atrial fibrillation. *Journal of Clinical Investigation*, *121*(8), 2955–2968.

Waks, J. W., & Josephson, M. E. (2014). Mechanisms of Atrial Fibrillation – Reentry, Rotors and Reality. *Arrhythmia & Electrophysiology Review*, *3*(2), 90.

Walter, E., & Heringlake, M. (2020). Cost-Effectiveness Analysis of Landiolol, an Ultrashort-Acting Beta-Blocker, for Prevention of Postoperative Atrial Fibrillation for the Germany Health Care System. *Journal of Cardiothoracic and Vascular Anesthesia*, *34*(4), 888–897.

Wang, G. D., Shen, L. H., Wang, L., Li, H. W., Zhang, Y. C., & Chen, H. (2009). Relationship between integrated backscatter and atrial fibrosis in patients with and without atrial fibrillation who are undergoing coronary bypass surgery. *Clinical Cardiology*, *32*(9), E56–E60.

Wang, J., Thio, S. S. C., Yang, S. S. H., Yu, D., Yu, C. Y., Wong, Y. P., Liao, P., Li, S., & Soong, T. W. (2011). Splice variant specific modulation of CaV1.2 calcium channel by galectin-1 regulates arterial constriction. *Circulation Research*, *109*(11), 1250–1258.

Wang, T. J., Larson, M. G., Levy, D., Vasan, R. S., Leip, E. P., Wolf, P. A., D'Agostino,

R. B., Murabito, J. M., Kannel, W. B., & Benjamin, E. J. (2003). Temporal relations of atrial fibrillation and congestive heart failure and their joint influence on mortality: The Framingham heart study. *Circulation*, *107*(23), 2920–2925.

Wang, W., Zhang, S., Ni, H., Garratt, C. J., Boyett, M. R., Hancox, J. C., & Zhang, H. (2018). Mechanistic insight into spontaneous transition from cellular alternans to arrhythmia. A simulation study. *PLOS Computational Biology*, *14*(11), e1006594.

Weiss, J. N., Garfinkel, A., Karagueuzian, H. S., Chen, P. S., & Qu, Z. (2010). Early afterdepolarizations and cardiac arrhythmias. *Heart Rhythm*, *7*(12), 1891–1899.

Weiss, J. N., Nivala, M., Garfinkel, A., & Qu, Z. (2011). Alternans and arrhythmias : From cell to heart. *Circulation Research*, *108*(1), 98–112.

Westermann, D., Mersmann, J., Melchior, A., Freudenberger, T., Petrik, C., Schaefer, L., Lüllmann-Rauch, R., Lettau, O., Jacoby, C., Schrader, J., Brand-Herrmann, S.-M., Young, M. F., Schultheiss, H. P., Levkau, B., Baba, H. A., Unger, T., Zacharowski, K., Tschöpe, C., & Fischer, J. W. (2008). Biglycan is required for adaptive remodeling after myocardial infarction. *Circulation*, *117*(10), 1269–1276.

Wettwer, E., Hála, O., Christ, T., Heubach, J. F., Dobrev, D., Knaut, M., Varró, A., & Ravens, U. (2004). Role of IKur in controlling action potential shape and contractility in the human atrium: Influence of chronic atrial fibrillation. *Circulation*, *110*(16), 2299–2306.

Wijffels, M. C. E. F., Kirchhof, C. J. H. J., Dorland, R., & Allessie, M. A. (1995). Atrial fibrillation begets atrial fibrillation: A study in awake chronically instrumented goats. *Circulation*, *92*(7), 1954–1968.

Workman, A. J. (2010). Cardiac adrenergic control and atrial fibrillation. *Naunyn-Schmiedeberg's Archives of Pharmacology*, *381*(3), 235–249.

Workman, A. J., Pau, D., Redpath, C. J., Marshall, G. E., Russell, J. A., Kane, K. A., Norrie, J., & Rankin, A. C. (2006). Post-operative atrial fibrillation is influenced by beta-blocker therapy but not by pre-operative atrial cellular electrophysiology. *Journal of Cardiovascular Electrophysiology*, *17*(11), 1230–1238.

Xu, J., Cui, G., Esmailian, F., Plunkett, M., Marelli, D., Ardehali, A., Odim, J., Laks, H., & Sen, L. (2004). Atrial Extracellular Matrix Remodeling and the Maintenance of Atrial Fibrillation. *Circulation*, *109*(3), 363–368.

Yue, L., Feng, J., Gaspo, R., Li, G.-R., Wang, Z., & Nattel, S. (1997). Ionic Remodeling Underlying Action Potential Changes in a Canine Model of Atrial Fibrillation. *Circulation Research*, *81*(4), 512–525.

Zafrir, B., Lund, L. H., Laroche, C., Ruschitzka, F., Crespo-Leiro, M. G., Coats, A. J. S., Anker, S. D., Filippatos, G., Seferovic, P. M., Maggioni, A. P., De, M., Martin, M., Polonski, L., Silva-Cardoso, J., & Amir, O. (2018). Prognostic implications of atrial fibrillation in heart failure with reduced, mid-range, and preserved ejection fraction: a report from 14 964 patients in the European Society of Cardiology Heart Failure Long-Term Registry. *European Heart Journal*, *39*(48), 4277–4284.

Zaina, S., Pettersson, L., Thomsen, A. B., Chai, C.-M., Qi, Z., Thyberg, J., & Nilsson, J. (2003). Shortened Life Span, Bradycardia, and Hypotension in Mice with Targeted Expression of an *Igf2* Transgene in Smooth Muscle Cells.

Endocrinology, *144*(6), 2695–2703.

Zaman, J. A. B., Harling, L., Ashrafian, H., Darzi, A., Gooderham, N., Athanasiou, T., & Peters, N. S. (2016). Post-operative atrial fibrillation is associated with a pre-existing structural and electrical substrate in human right atrial myocardium. *International Journal of Cardiology*, *220*, 580–588.

Zeng, J., & Rudy, Y. (1995). Early afterdepolarizations in cardiac myocytes: mechanism and rate dependence. *Biophysical Journal*, *68*(3), 949–964.

Zhang, H., Garratt, C. J., Zhu, J., & Holden, A. V. (2005). Role of up-regulation of IK1 in action potential shortening associated with atrial fibrillation in humans. *Cardiovascular Research*, *66*(3), 493–502.

Zsebo, K., Yaroshinsky, A., Rudy, J. J., Wagner, K., Greenberg, B., Jessup, M., & Hajjar, R. J. (2014). Long-term effects of AAV1/SERCA2a gene transfer in patients with severe heart failure: analysis of recurrent cardiovascular events and mortality. *Circulation Research*, *114*(1), 101–108.

Supplement

Supplemental Table 1: Protein analysis of ECM proteins in the right atrial secretome of poAF and cAF patients.

Supplemental Table 2: Identified ECM and ECM associated proteins in human right atrial secretome.

Supplemental Table 1. Protein analysis of ECM and ECM associated proteins in the right atrial tissue secretome of poAF and cAF patients. Conditioned media of right atrial appendages were deglycosylated and analysed using mass spectrometry. ECM Proteins were categorised as described by the matrisome project annotator (Naba et al., 2017), except for the category "other ECM associated protein". Mean±SEM show normalised abundances of ECM proteins. Comparison was made using Kruskal Wallis test followed by Dunn's post-hoc test. P values were adjusted using the Benjamini Hochberg approach. n = Ctrl 10; poAF 6; cAF 9 patient samples.

			CTRL	POAF				CAF			
Category	**Protein Description**	**Gene Symbol**	**Mean±SEM**	**Mean±SEM**	**log2 FC**	**P Value**	**Adj P Value**	**Mean±SEM**	**log2 FC**	**P Value**	**Adj P Value**
Collagens	Collagen alpha-1(XVI) chain	COL16A1	2.9±0.26	4.1±0.66	0.50	0.240	0.65	7±1.03	1.27	**0.001**	0.01
Collagens	Collagen alpha-3(V) chain	COL5A3	0.32±0.11	0.88±0.38	1.47	0.153	0.59	1.26±0.16	1.98	**0.002**	0.02
Collagens	Collagen alpha-1(XII) chain	COL12A1	0.17±0.02	0.31±0.11	0.88	0.243	0.65	0.85±0.24	2.36	**0.005**	0.02
Collagens	Collagen alpha-3(VI) chain	COL6A3	105.93±13.91	146.38±35.5	0.47	0.330	0.70	188.41±24.06	0.83	**0.007**	0.03
Collagens	Collagen alpha-1(IV) chain	COL4A1	4.42±0.76	8.43±3.88	0.93	0.366	0.73	11.52±2.36	1.38	**0.007**	0.03
Collagens	Collagen alpha-2(IV) chain	COL4A2	6.86±1.43	10.65±3.74	0.63	0.435	0.75	15.3±2.41	1.16	**0.011**	0.04
Collagens	Collagen alpha-1(I) chain	COL1A1	36.43±6.86	87.17±27.05	1.26	0.075	0.61	63.59±8.13	0.80	**0.015**	0.05
Collagens	Collagen alpha-1(XVIII) chain	COL18A1	43.56±4.67	63.8±10.22	0.55	0.069	0.61	64.04±6.66	0.56	**0.024**	0.07
Collagens	Collagen alpha-2(I) chain	COL1A2	20.35±3.73	50.69±19.8	1.32	**0.042**	0.81	32.87±4.55	0.69	**0.037**	0.10
Collagens	Collagen alpha-1(V) chain	COL5A1	0.81±0.2	1.03±0.34	0.34	0.687	0.89	1.64±0.41	1.02	**0.049**	0.12
Collagens	Collagen alpha-2(VI) chain	COL6A2	3.55±0.75	4.55±1.39	0.36	0.440	0.75	5.62±0.84	0.66	**0.049**	0.13
Collagens	Collagen alpha-1(VI) chain	COL6A1	5.62±0.84	6.69±1.67	0.25	0.371	0.74	9.16±1.88	0.70	0.087	0.19
Collagens	Collagen alpha-1(XIV) chain	COL14A1	107.68±16.89	133.61±23.33	0.31	0.380	0.73	153.17±20.66	0.51	0.109	0.21
Collagens	Collagen alpha-1(XV) chain	COL15A1	63.2±7.02	73.93±15.96	0.23	0.623	0.85	78.27±8.34	0.31	0.150	0.26
Collagens	Collagen alpha-1(III) chain	COL3A1	298.44±67.73	450.21±155.34	0.59	0.528	0.80	390.25±77.86	0.39	0.277	0.41
Collagens	Collagen alpha-6(VI) chain	COL6A6	0.32±0.1	0.49±0.2	0.61	0.483	0.78	0.43±0.06	0.41	0.378	0.52
Collagens	Collagen alpha-1(XXVIII) chain	COL28A1	2.09±0.2	2.09±0.3	0.00	0.837	0.94	1.9±0.23	-0.13	0.406	0.53
ECM Glycoproteins	Insulin-like growth factor-binding protein 2	IGFBP2	4.54±0.6	8.25±1.29	0.86	0.155	0.58	24.24±5.06	2.42	**0.000**	0.01
ECM Glycoproteins	Adipocyte enhancer-binding protein 1	AEBP1	16.48±1.47	19.93±1.73	0.27	0.281	0.68	36.82±5	1.16	**0.000**	0.01
ECM Glycoproteins	Tenascin-X	TNXB	247.6±19.6	445.37±116.02	0.85	0.116	0.60	762.3±128.7	1.62	**0.000**	0.01
ECM Glycoproteins	Latent-transforming growth factor beta-binding protein 2	LTBP2	15.33±3.04	47.81±13.34	1.64	**0.025**	0.75	77.61±14.19	2.34	**0.000**	0.01
ECM Glycoproteins	Tenascin	TNC	3.04±2.42	3.66±2.21	0.27	0.204	0.64	28.28±11.97	3.22	**0.000**	0.01
ECM Glycoproteins	Procollagen C-endopeptidase enhancer 1	PCOLCE	7.19±1.13	10.68±2.07	0.57	0.194	0.65	20.59±3.57	1.52	**0.000**	0.01
ECM Glycoproteins	EGF-containing fibulin-like extracellular matrix protein 1	EFEMP1	33.07±5.04	43.15±5.95	0.38	0.256	0.65	74.49±9.93	1.17	**0.001**	0.01
ECM Glycoproteins	Cartilage oligomeric matrix protein	COMP	9.82±6.24	20.13±8.3	1.04	0.125	0.59	45.15±9.98	2.20	**0.001**	0.01
ECM Glycoproteins	Thrombospondin-4	THBS4	0.97±0.29	1.58±0.64	0.70	0.508	0.80	6.34±2.44	2.71	**0.001**	0.01
ECM Glycoproteins	Transforming growth factor-beta-induced protein ig-h3	TGFBI	101.54±14.18	194.48±57.27	0.94	0.068	0.63	260.12±44.88	1.36	**0.001**	0.01
ECM Glycoproteins	Fibulin-5	FBLN5	12.81±2.4	20.58±6	0.68	0.145	0.59	24.17±2.03	0.92	**0.002**	0.01
ECM Glycoproteins	Dermatopontin	DPT	1.69±0.18	2.5±0.7	0.57	0.317	0.71	3.77±0.63	1.16	**0.001**	0.01
ECM Glycoproteins	Periostin	POSTN	14.23±2.43	32.95±9.1	1.21	0.066	0.66	47.39±11.3	1.74	**0.002**	0.01

			CTRL	POAF				CAF			
Category	**Protein Description**	**Gene Symbol**	**Mean±SEM**	**Mean±SEM**	**log2 FC**	**P Value**	**Adj P Value**	**Mean±SEM**	**log2 FC**	**P Value**	**Adj P Value**
ECM Glycoproteins	Latent-transforming growth factor beta-binding protein 4	LTBP4	12.89±1.34	20.12±5.75	0.64	0.197	0.65	30.25±3.87	1.23	**0.002**	0.01
ECM Glycoproteins	Peroxidasin homolog	PXDN	3.06±0.6	2.63±0.46	-0.22	0.732	0.93	8.55±1.26	1.49	**0.002**	0.01
ECM Glycoproteins	EGF-containing fibulin-like extracellular matrix protein 2	EFEMP2	2.43±0.36	4.03±0.84	0.73	0.078	0.61	4.52±0.44	0.90	**0.003**	0.02
ECM Glycoproteins	Osteopontin	SPP1	0.45±0.08	0.8±0.07	0.81	0.079	0.58	2.25±0.74	2.30	**0.004**	0.02
ECM Glycoproteins	Laminin subunit beta-1	LAMB1	27.72±2.23	39.14±5.62	0.50	0.087	0.54	44.34±4.65	0.68	**0.005**	0.02
ECM Glycoproteins	Spondin-1	SPON1	20.41±2.34	29.22±5.84	0.52	0.292	0.68	39.24±4.92	0.94	**0.007**	0.03
ECM Glycoproteins	Fibronectin	FN1	175.29±27.5	210.54±58.15	0.26	0.755	0.93	347.26±46.78	0.99	**0.006**	0.03
ECM Glycoproteins	Fibroleukin	FGL2	5.43±1.1	6.98±1.47	0.36	0.551	0.80	14.62±3.62	1.43	**0.012**	0.04
ECM Glycoproteins	Nidogen-1	NID1	15.33±2.28	18.22±3.27	0.25	0.293	0.67	23.75±2.49	0.63	**0.013**	0.04
ECM Glycoproteins	Microfibril-associated glycoprotein 4	MFAP4	1.54±0.21	2.54±0.32	0.72	**0.029**	0.77	2.85±0.47	0.89	**0.012**	0.04
ECM Glycoproteins	Latent-transforming growth factor beta-binding protein 1	LTBP1	11.14±1.55	15.17±2.89	0.45	0.131	0.59	21.38±4.45	0.94	**0.013**	0.04
ECM Glycoproteins	Agrin	AGRN	13.9±1.57	19.98±2.55	0.52	0.087	0.56	21.66±2.53	0.64	**0.016**	0.05
ECM Glycoproteins	Connective tissue growth factor	CTGF	1.35±0.38	2.55±0.64	0.92	**0.003**	0.68	1.71±0.25	0.34	**0.023**	0.07
ECM Glycoproteins	Laminin subunit beta-2	LAMB2	90.43±8.11	92.79±12.52	0.04	0.888	0.96	69.57±4.86	-0.38	**0.035**	0.10
ECM Glycoproteins	von Willebrand factor	VWF	27.77±3.58	35.16±9.64	0.34	0.464	0.77	44.74±5.14	0.69	**0.038**	0.10
ECM Glycoproteins	Vitronectin	VTN	17.51±2.37	60.58±30.41	1.79	**0.023**	1.22	41.04±9.14	1.23	0.067	0.15
ECM Glycoproteins	Laminin subunit alpha-5	LAMA5	6.46±0.44	7.26±1.05	0.17	0.289	0.69	8.52±0.91	0.40	0.067	0.15
ECM Glycoproteins	Hemicentin-2	HMCN2	2.2±0.24	2.09±0.23	-0.08	0.879	0.96	1.5±0.25	-0.56	0.075	0.17
ECM Glycoproteins	Thrombospondin-1	THBS1	75.15±16.17	90.18±21.93	0.26	0.385	0.72	105.96±21.05	0.50	0.099	0.20
ECM Glycoproteins	Insulin-like growth factor-binding protein 7	IGFBP7	39.77±4.63	75.72±28.91	0.93	0.147	0.59	75.77±16.46	0.93	0.096	0.20
ECM Glycoproteins	Insulin-like growth factor-binding protein 5	IGFBP5	2.26±0.29	2.01±0.26	-0.17	0.569	0.81	5.5±1.28	1.28	0.097	0.20
ECM Glycoproteins	EMILIN-1	EMILIN1	26.24±3.43	41.53±16.69	0.66	0.617	0.85	40.11±6.29	0.61	0.110	0.21
ECM Glycoproteins	EMILIN-2	EMILIN2	0.93±0.24	1.86±0.88	1.00	0.236	0.66	1.59±0.4	0.78	0.115	0.22
ECM Glycoproteins	SPARC-like protein 1	SPARCL1	12.11±1.65	12.07±1.92	0.00	0.930	0.97	17.48±2.48	0.53	0.115	0.22
ECM Glycoproteins	SPARC	SPARC	8.89±1.45	13.89±3.57	0.64	0.287	0.69	13.9±2.14	0.64	0.133	0.24
ECM Glycoproteins	Target of Nesh-SH3	ABI3BP	111.56±16.03	130.87±22.77	0.23	0.330	0.71	165.74±29.69	0.57	0.137	0.24
ECM Glycoproteins	Tumor necrosis factor-inducible gene 6 protein	TNFAIP6	2.81±0.81	7.64±3.9	1.44	0.563	0.81	5.27±1.36	0.91	0.170	0.29
ECM Glycoproteins	Thrombospondin-2	THBS2	13.69±3.37	14.72±3.29	0.10	0.799	0.95	25.78±7.34	0.91	0.198	0.32
ECM Glycoproteins	Tubulointerstitial nephritis antigen-like	TINAGL1	0.53±0.04	0.56±0.11	0.09	0.979	0.99	0.63±0.06	0.25	0.242	0.37
ECM Glycoproteins	Leucine-rich alpha-2-glycoprotein	LRG1	0.75±0.18	0.58±0.1	-0.36	0.814	0.95	0.51±0.13	-0.56	0.247	0.37
ECM Glycoproteins	Papilin	PAPLN	2.42±0.26	2.39±0.39	-0.02	0.826	0.95	2.05±0.22	-0.24	0.285	0.42
ECM Glycoproteins	Multimerin-2	MMRN2	1.15±0.16	0.9±0.22	-0.36	0.249	0.65	0.9±0.13	-0.35	0.305	0.45
ECM Glycoproteins	Fibulin-1	FBLN1	144.12±19.98	179.25±23.82	0.31	0.171	0.60	156.06±16.74	0.11	0.434	0.56
ECM Glycoproteins	Insulin-like growth factor-binding protein 4	IGFBP4	9.31±2.52	11.88±3.15	0.35	0.480	0.78	16.27±5.35	0.81	0.432	0.56
ECM Glycoproteins	Matrilin-2	MATN2	33.19±5.01	38.63±5.48	0.22	0.194	0.66	34.68±2.67	0.06	0.452	0.57
ECM Glycoproteins	Laminin subunit alpha-4	LAMA4	33±1.98	32.19±3.14	-0.04	0.722	0.92	31.27±1.88	-0.08	0.524	0.65
ECM Glycoproteins	Insulin-like growth factor-binding protein 3	IGFBP3	48.41±6.63	42.8±7.23	-0.18	0.739	0.93	65.53±16.76	0.44	0.563	0.67

			CTRL	POAF				CAF			
Category	**Protein Description**	**Gene Symbol**	**Mean±SEM**	**Mean±SEM**	**log2 FC**	**P Value**	**Adj P Value**	**Mean±SEM**	**log2 FC**	**P Value**	**Adj P Value**
ECM Glycoproteins	Adiponectin	ADIPOQ	8.69±1.34	9.21±1.81	0.08	0.857	0.94	10.88±2.33	0.32	0.573	0.68
ECM Glycoproteins	Nidogen-2	NID2	10.17±0.89	11.4±1.49	0.16	0.451	0.76	10.91±1.1	0.10	0.674	0.76
ECM Glycoproteins	Laminin subunit gamma-1	LAMC1	75.57±6.9	87.3±13.02	0.21	0.648	0.85	78.51±6.02	0.06	0.691	0.76
ECM Glycoproteins	Fibrillin-1	FBN1	12.85±1.94	18.19±5.36	0.50	0.648	0.85	14.44±2.26	0.17	0.691	0.77
ECM Glycoproteins	Fibulin-2	FBLN2	202.12±26.62	235.6±44.52	0.22	0.648	0.86	206.82±21.47	0.03	0.691	0.77
ECM Glycoproteins	Laminin subunit alpha-2	LAMA2	76.78±6.22	83.84±12.76	0.13	0.786	0.94	79.83±6.82	0.06	0.710	0.78
ECM Glycoproteins	Fibrinogen beta chain	FGB	123.5±18.4	114.5±29.55	-0.11	0.746	0.93	110.48±14.91	-0.16	0.771	0.83
ECM Glycoproteins	Fibrinogen alpha chain	FGA	135.27±19.33	127.62±29.46	-0.08	0.823	0.95	121.68±16.83	-0.15	0.905	0.92
ECM Glycoproteins	Extracellular matrix protein 1	ECM1	42.43±8.72	44.99±10.15	0.08	0.850	0.94	50.93±15.66	0.26	0.916	0.93
ECM Glycoproteins	Insulin-like growth factor-binding protein 6	IGFBP6	0.22±0.05	0.27±0.1	0.32	0.785	0.95	0.3±0.1	0.47	0.951	0.96
ECM Glycoproteins	Fibrinogen gamma chain	FGG	133.61±20.85	130.34±32.19	-0.04	0.776	0.94	121.75±15.54	-0.13	0.993	0.99
ECM Regulators	Leukocyte elastase inhibitor	SERPINB1	6.74±0.71	8.81±0.94	0.39	0.117	0.59	13.23±1.75	0.97	**0.000**	0.01
ECM Regulators	Serpin H1	SERPINH1	1.41±0.49	1.73±0.38	0.29	0.258	0.65	3.45±0.64	1.29	**0.002**	0.01
ECM Regulators	Serpin B6	SERPINB6	31.84±2.9	37.98±4.55	0.25	0.430	0.75	74.24±10.82	1.22	**0.002**	0.01
ECM Regulators	Inter-alpha-trypsin inhibitor heavy chain H1	ITIH1	32.5±6.32	54.92±21.35	0.76	0.149	0.58	68.11±11.11	1.07	**0.003**	0.02
ECM Regulators	Cystatin-B	CSTB	11.88±1.08	13.74±1.83	0.21	0.626	0.84	24.09±3.25	1.02	**0.005**	0.02
ECM Regulators	Cathepsin Z	CTSZ	1.5±0.08	1.46±0.14	-0.05	0.993	1.00	2.5±0.32	0.73	**0.007**	0.03
ECM Regulators	Angiotensinogen	AGT	4.06±0.34	3.74±0.52	-0.12	0.775	0.94	2.89±0.39	-0.49	**0.041**	0.11
ECM Regulators	Inter-alpha-trypsin inhibitor heavy chain H3	ITIH3	1.44±0.4	2.53±0.58	0.82	0.326	0.70	3.91±1.22	1.44	**0.042**	0.11
ECM Regulators	Cathepsin D	CTSD	36.52±3.1	34.96±4.06	-0.06	0.833	0.94	50.68±6.05	0.47	**0.049**	0.12
ECM Regulators	Plasminogen	PLG	12.9±1.82	11.5±1.77	-0.17	0.746	0.94	8.53±1.15	-0.60	0.053	0.13
ECM Regulators	Pigment epithelium-derived factor	SERPINF1	9.11±1.41	12.43±3.01	0.45	0.472	0.78	19.28±4.24	1.08	0.065	0.15
ECM Regulators	72 kDa type IV collagenase	MMP2	7.08±1.3	19.83±7.45	1.48	0.079	0.60	21.02±9	1.57	0.065	0.15
ECM Regulators	A disintegrin and metalloproteinase with thrombospondin motifs 1	ADAMTS1	0.36±0.09	0.3±0.08	-0.29	0.814	0.94	0.54±0.08	0.57	0.082	0.18
ECM Regulators	Alpha-1-antitrypsin	SERPINA1	160.73±23.5	143.02±20.17	-0.17	0.934	0.97	102.01±16.48	-0.66	0.088	0.19
ECM Regulators	Cathepsin L1	CTSL	5±0.64	5.73±1.05	0.20	0.410	0.74	8.37±1.5	0.74	0.093	0.20
ECM Regulators	Glia-derived nexin	SERPINE2	8.64±2.23	19.97±8.43	1.21	0.230	0.67	19.15±5.91	1.15	0.138	0.24
ECM Regulators	Inter-alpha-trypsin inhibitor heavy chain H2	ITIH2	8.76±2.22	11.47±3.81	0.39	0.623	0.85	15.1±2.89	0.79	0.150	0.26
ECM Regulators	Cathepsin S	CTSS	0.61±0.06	1.43±0.42	1.24	**0.025**	0.87	0.94±0.19	0.63	0.175	0.29
ECM Regulators	Protein-lysine 6-oxidase	LOX	0.66±0.07	0.92±0.19	0.47	0.248	0.66	0.97±0.18	0.55	0.179	0.29
ECM Regulators	Coagulation factor IX	F9	2.83±0.35	2.67±0.29	-0.08	0.923	0.97	3.9±0.61	0.46	0.178	0.29
ECM Regulators	Antithrombin-III	SERPINC1	83.31±8.83	112.33±14.83	0.43	0.170	0.61	111.19±17.97	0.42	0.203	0.32
ECM Regulators	A disintegrin and metalloproteinase with thrombospondin motifs 4	ADAMTS4	0.4±0.08	0.35±0.02	-0.19	0.486	0.78	0.57±0.2	0.53	0.207	0.33
ECM Regulators	CD109 antigen	CD109	5.52±0.46	4.88±0.82	-0.18	0.451	0.76	6.54±0.51	0.25	0.222	0.34
ECM Regulators	Prothrombin	F2	15.87±2.24	13.58±2.64	-0.22	0.425	0.74	12.13±2.16	-0.39	0.227	0.35
ECM Regulators	Interstitial collagenase	MMP1	97.14±19.91	125.54±24.69	0.37	0.297	0.68	125.07±23.6	0.36	0.268	0.40
ECM Regulators	Coagulation factor XII	F12	0.85±0.18	0.51±0.22	-0.75	0.073	0.62	0.61±0.17	-0.49	0.340	0.48

			CTRL	POAF				CAF			
Category	**Protein Description**	**Gene Symbol**	**Mean±SEM**	**Mean±SEM**	**log2 FC**	**P Value**	**Adj P Value**	**Mean±SEM**	**log2 FC**	**P Value**	**Adj P Value**
ECM Regulators	Kininogen-1	KNG1	8.18±1.59	7.3±1.04	-0.16	0.895	0.96	5.98±1.04	-0.45	0.358	0.50
ECM Regulators	Coagulation factor XIII A chain	F13A1	28.34±3.43	25.74±5.08	-0.14	0.752	0.93	32.3±3.87	0.19	0.371	0.51
ECM Regulators	Metalloproteinase inhibitor 2	TIMP2	0.65±0.2	0.82±0.29	0.34	0.541	0.81	0.86±0.19	0.41	0.405	0.53
ECM Regulators	Protein AMBP	AMBP	20.86±2.12	35.49±6.58	0.77	0.058	0.69	18.11±2.53	-0.20	0.398	0.54
ECM Regulators	Matrix metalloproteinase-9	MMP9	0.57±0.17	1.22±0.32	1.10	0.053	0.75	0.75±0.18	0.39	0.428	0.56
ECM Regulators	Heparin cofactor 2	SERPIND1	2.36±0.34	2.17±0.67	-0.13	0.813	0.95	2.93±0.6	0.31	0.503	0.63
ECM Regulators	Histidine-rich glycoprotein	HRG	22.09±4.07	19.63±4.27	-0.17	0.972	0.99	23.59±3.39	0.09	0.528	0.65
ECM Regulators	Alpha-2-macroglobulin	A2M	81.24±10.27	81.93±10.34	0.01	0.623	0.84	87.35±12.46	0.10	0.537	0.65
ECM Regulators	Metalloproteinase inhibitor 1	TIMP1	308.45±41.89	390.02±99.38	0.34	0.472	0.78	408.27±89.98	0.40	0.541	0.66
ECM Regulators	Cathepsin B	CTSB	15.6±1.76	20.49±3.27	0.39	0.164	0.60	17.68±2.37	0.18	0.575	0.68
ECM Regulators	Plasma serine protease inhibitor	SERPINA5	0.15±0.03	0.2±0.04	0.40	0.251	0.65	0.16±0.03	0.09	0.665	0.75
ECM Regulators	Alpha-1-antichymotrypsin	SERPINA3	10.67±2.28	10.04±2.08	-0.09	0.906	0.96	9.22±1.88	-0.21	0.738	0.80
ECM Regulators	Plasminogen activator inhibitor 1	SERPINE1	107±14.43	96.62±20.39	-0.15	0.882	0.96	98.41±13.54	-0.12	0.828	0.87
ECM Regulators	Plasma protease C1 inhibitor	SERPING1	19.96±2.48	20.14±3.48	0.01	0.909	0.96	18.99±3.14	-0.07	0.835	0.88
ECM Regulators	Cystatin-C	CST3	16.2±1.73	20.96±4.07	0.37	0.390	0.73	15.46±2.29	-0.07	0.880	0.91
ECM Regulators	Inter-alpha-trypsin inhibitor heavy chain H4	ITIH4	6.78±0.79	6.86±0.87	0.02	0.806	0.95	6.45±0.84	-0.07	0.919	0.93
ECM-affiliated Proteins	Galectin-1	LGALS1	94.8±9.99	133.87±13.12	0.50	0.127	0.58	181.24±11.65	0.93	**0.000**	0.01
ECM-affiliated Proteins	Glypican-1	GPC1	2.36±0.17	4.4±1.35	0.90	0.180	0.62	7.48±1.38	1.67	**0.001**	0.01
ECM-affiliated Proteins	Chondroitin sulfate proteoglycan 4	CSPG4	0.41±0.05	0.52±0.12	0.36	0.522	0.80	0.99±0.14	1.28	**0.004**	0.02
ECM-affiliated Proteins	Complement C1q subcomponent subunit A	C1QA	8.12±1.27	8.55±1.37	0.08	0.425	0.75	16.35±3.01	1.01	**0.004**	0.02
ECM-affiliated Proteins	Complement C1q subcomponent subunit C	C1QC	14.64±2	14.87±2.08	0.02	0.511	0.80	28.52±5.56	0.96	**0.010**	0.04
ECM-affiliated Proteins	Complement C1q subcomponent subunit B	C1QB	8.01±1.12	8.11±1.3	0.02	0.551	0.79	15.76±3.23	0.98	**0.012**	0.04
ECM-affiliated Proteins	Annexin A1	ANXA1	6.64±1.67	7.23±2.22	0.12	0.664	0.86	12.03±2.59	0.86	0.064	0.15
ECM-affiliated Proteins	Hemopexin	HPX	53.9±9.89	51.65±9.17	-0.06	0.833	0.94	34.02±7.22	-0.66	0.120	0.22
ECM-affiliated Proteins	Glypican-4	GPC4	0.24±0.07	0.14±0.02	-0.78	0.584	0.83	0.45±0.13	0.89	0.133	0.24
ECM-affiliated Proteins	Tetranectin	CLEC3B	5.06±0.59	5.07±0.64	0.00	0.951	0.97	7.88±1.32	0.64	0.174	0.29
ECM-affiliated Proteins	Annexin A2	ANXA2	32.42±4.32	51.13±10.25	0.66	0.091	0.55	37±3.34	0.19	0.386	0.52
ECM-affiliated Proteins	Intelectin-1	ITLN1	31.65±7.44	41.55±6.16	0.39	0.108	0.60	22.98±3.81	-0.46	0.403	0.53
ECM-affiliated Proteins	Annexin A5	ANXA5	1.69±0.39	3.27±0.59	0.96	**0.030**	0.70	2.04±0.34	0.27	0.527	0.65
ECM-affiliated Proteins	Annexin A4	ANXA4	0.14±0.02	0.22±0.05	0.64	0.133	0.58	0.15±0.01	0.12	0.632	0.73
ECM-affiliated Proteins	Annexin A6	ANXA6	1.88±0.37	3.46±0.95	0.88	0.116	0.62	2.14±0.38	0.18	0.762	0.82
ECM-affiliated Proteins	Galectin-3	LGALS3	102.35±4.75	116.74±14.17	0.19	0.270	0.67	101.54±4.89	-0.01	0.899	0.93
Other ECM associated	Heat shock 70 kDa protein 4	HSPA4	5.78±0.71	6.39±0.65	0.14	0.395	0.73	11.92±0.91	1.04	**0.000**	0.00

			CTRL	POAF				CAF			
Category	**Protein Description**	**Gene Symbol**	**Mean±SEM**	**Mean±SEM**	**log2 FC**	**P Value**	**Adj P Value**	**Mean±SEM**	**log2 FC**	**P Value**	**Adj P Value**
Other ECM associated	Protein disulfide-isomerase	P4HB	98.1±11.14	133.02±8.29	0.44	0.065	0.72	204.95±22.42	1.06	**0.000**	0.01
Other ECM associated	Galectin-3-binding protein	LGALS3BP	19.44±0.91	19.36±2.72	-0.01	0.500	0.80	10.9±1.21	-0.84	**0.000**	0.01
Other ECM associated	Vinculin	VCL	351.49±12.74	423.52±22.47	0.27	0.056	0.75	507.35±34.62	0.53	**0.001**	0.01
Other ECM associated	Cell surface glycoprotein MUC18	MCAM	2.11±0.2	2.52±0.36	0.25	0.352	0.73	4.14±0.42	0.97	**0.000**	0.01
Other ECM associated	Transgelin-2	TAGLN2	7.53±1.07	10.22±1.33	0.44	0.273	0.67	18.57±1.97	1.30	**0.000**	0.01
Other ECM associated	Heat shock cognate 71 kDa protein	HSPA8	63.24±6.6	66.39±2.54	0.07	0.357	0.73	98.03±8.25	0.63	**0.001**	0.01
Other ECM associated	Heat shock protein HSP 90-beta	HSP90AB1	23.26±1.54	25.52±2.62	0.13	0.534	0.80	44.28±6.96	0.93	**0.001**	0.01
Other ECM associated	Prostaglandin-H2 D-isomerase	PTGDS	26.6±2.62	25.22±2.21	-0.08	0.813	0.96	12.59±1.69	-1.08	**0.001**	0.01
Other ECM associated	Cadherin-1	CDH1	1.5±0.16	3.49±0.59	1.22	**0.008**	0.87	4.01±0.9	1.42	**0.003**	0.02
Other ECM associated	Procollagen-lysine,2-oxoglutarate 5-dioxygenase 1	PLOD1	0.59±0.23	2.07±0.46	1.81	**0.011**	0.75	3.33±0.95	2.50	**0.004**	0.02
Other ECM associated	Xaa-Pro dipeptidase	PEPD	0.99±0.12	1.14±0.1	0.20	0.545	0.81	1.76±0.2	0.83	**0.004**	0.02
Other ECM associated	Heat shock protein HSP 90-alpha	HSP90AA1	90.47±6.82	94.4±12.44	0.06	0.951	0.98	171.71±27.17	0.92	**0.006**	0.03
Other ECM associated	Apolipoprotein E	APOE	7.17±1.25	22.03±8.34	1.62	**0.046**	0.80	28.54±6.53	1.99	**0.007**	0.03
Other ECM associated	Heat shock-related 70 kDa protein 2	HSPA2	8.75±1.75	11.73±1.64	0.42	0.378	0.73	16.07±1.32	0.88	**0.007**	0.03
Other ECM associated	Secretogranin-1	CHGB	0.6±0.12	0.8±0.21	0.42	0.381	0.72	2.14±0.95	1.84	**0.009**	0.03
Other ECM associated	Peroxiredoxin-6	PRDX6	147.04±13.52	172.01±26.11	0.23	0.593	0.83	246.7±37.8	0.75	**0.015**	0.05
Other ECM associated	Peroxiredoxin-2	PRDX2	196.22±12.53	204.47±15.47	0.06	0.993	1.00	328.99±44.73	0.75	**0.016**	0.05
Other ECM associated	Gelsolin	GSN	170.52±7.33	224.36±26.91	0.40	**0.041**	0.88	222.86±17.92	0.39	**0.018**	0.05
Other ECM associated	Cysteine-rich protein 2	CRIP2	9.84±2.68	8.46±1.5	-0.22	0.951	0.98	16.73±2.68	0.77	**0.029**	0.08
Other ECM associated	CD5 antigen-like	CD5L	6.59±1.45	6.85±1.17	0.05	0.746	0.92	10.23±1.55	0.63	**0.032**	0.09
Other ECM associated	Zinc-alpha-2-glycoprotein	AZGP1	2.07±0.46	2.52±0.47	0.28	0.378	0.73	0.94±0.28	-1.14	**0.044**	0.11
Other ECM associated	Calpain-1 catalytic subunit	CAPN1	9.13±0.43	10.68±0.88	0.23	0.110	0.60	10.78±0.55	0.24	**0.045**	0.12
Other ECM associated	Calpastatin	CAST	16.46±1.86	16.31±1.98	-0.01	0.847	0.95	21.38±1.69	0.38	0.062	0.15
Other ECM associated	Apolipoprotein D	APOD	3.03±0.34	4.25±0.7	0.49	0.200	0.65	4.88±0.91	0.69	0.095	0.20
Other ECM associated	Pentraxin-related protein PTX3	PTX3	7.46±2.88	9.16±4.3	0.30	0.719	0.92	13.25±3.43	0.83	0.124	0.23
Other ECM associated	Intercellular adhesion molecule 1	ICAM1	0.55±0.13	1.17±0.42	1.09	0.216	0.66	0.9±0.17	0.73	0.197	0.32
Other ECM associated	Sulfhydryl oxidase 1	QSOX1	5.27±0.39	6.76±0.98	0.36	0.131	0.58	7.13±1.31	0.44	0.211	0.33
Other ECM associated	Peroxiredoxin-1	PRDX1	557.72±41.23	624.64±64.47	0.16	0.376	0.74	633.61±71.84	0.18	0.253	0.38
Other ECM associated	Chymase	CMA1	2.58±0.55	3.36±0.6	0.38	0.213	0.66	1.8±0.28	-0.52	0.310	0.45
Other ECM associated	CD59 glycoprotein	CD59	27.16±1.97	27.09±3.94	0.00	0.899	0.96	30.97±2.6	0.19	0.318	0.46
Other ECM associated	Heat shock protein beta-1	HSPB1	136.16±5.62	149.17±12.61	0.13	0.548	0.81	128.4±14.62	-0.08	0.367	0.51

			CTRL	POAF				CAF			
Category	**Protein Description**	**Gene Symbol**	**Mean±SEM**	**Mean±SEM**	**log2 FC**	**P Value**	**Adj P Value**	**Mean±SEM**	**log2 FC**	**P Value**	**Adj P Value**
Other ECM associated	Granulins	GRN	4.65±0.62	4.65±0.84	0.00	0.599	0.84	4.83±0.43	0.06	0.402	0.54
Other ECM associated	Dystroglycan	DAG1	18.96±1.69	21.17±2.95	0.16	0.639	0.85	20.55±1.38	0.12	0.401	0.54
Other ECM associated	Heat shock protein beta-6	HSPB6	7.76±0.38	9.62±1.21	0.31	0.216	0.65	8.18±1.32	0.08	0.446	0.57
Other ECM associated	Apolipoprotein B-100	APOB	1.93±0.39	1.05±0.22	-0.88	0.223	0.66	2.85±0.7	0.56	0.505	0.63
Other ECM associated	Heat shock 70 kDa protein 1B	HSPA1B	52.82±2.12	57.26±3.01	0.12	0.397	0.73	57.06±4.11	0.11	0.523	0.65
Other ECM associated	Apolipoprotein A-I	APOA1	104.09±26.39	87.76±14.42	-0.25	0.847	0.94	89.14±12.76	-0.22	0.552	0.66
Other ECM associated	Apolipoprotein A-IV	APOA4	3.26±0.61	4.71±1.28	0.53	0.322	0.70	4.23±0.93	0.38	0.568	0.68
Other ECM associated	Basal cell adhesion molecule	BCAM	39.55±1.91	39.58±3.18	0.00	0.997	1.00	37.9±2.54	-0.06	0.624	0.73
Other ECM associated	Clusterin	CLU	31.61±3.05	40.39±4.86	0.35	0.153	0.58	34.65±3.89	0.13	0.654	0.75
Other ECM associated	CD44 antigen	CD44	1.4±0.16	1.53±0.39	0.12	0.909	0.96	1.5±0.17	0.10	0.679	0.76
Other ECM associated	Cadherin-13	CDH13	34.97±5.34	31.88±7.66	-0.13	0.528	0.80	33.56±6.16	-0.06	0.790	0.85
Other ECM associated	Cadherin-2	CDH2	7.63±0.97	7.97±0.56	0.06	0.614	0.85	7.57±1.01	-0.01	0.812	0.86
Other ECM associated	Beta-2-glycoprotein 1	APOH	69.46±8.92	87.52±16.45	0.33	0.330	0.69	65.84±8.89	-0.08	0.877	0.91
Other ECM associated	Apolipoprotein A-II	APOA2	33.15±5.56	34.92±5.5	0.07	0.548	0.80	30.92±3.22	-0.10	0.901	0.92
Proteoglycans	Biglycan	BGN	16.43±2.15	25.02±3.87	0.61	0.085	0.56	34±4.61	1.05	**0.001**	0.01
Proteoglycans	Versican core protein	VCAN	167.87±30.4	279.56±87.91	0.74	0.289	0.68	432.06±98.97	1.36	**0.008**	0.03
Proteoglycans	Hyaluronan and proteoglycan link protein 1	HAPLN1	2.41±0.49	12.24±8.46	2.35	0.305	0.69	18.23±7.65	2.92	**0.015**	0.05
Proteoglycans	Basement membrane-specific heparan sulfate proteoglycan core protein	HSPG2	551.02±42.49	703.97±88.03	0.35	0.057	0.71	692.75±45.99	0.33	**0.029**	0.08
Proteoglycans	Testican-1	SPOCK1	0.76±0.11	1.06±0.22	0.48	0.141	0.60	1.15±0.2	0.61	0.064	0.15
Proteoglycans	Mimecan	OGN	148.32±16.84	178.18±22.22	0.26	0.235	0.66	188.49±17.72	0.35	0.098	0.20
Proteoglycans	Lumican	LUM	754.11±75.54	901.09±117.89	0.26	0.235	0.67	976.21±97.36	0.37	0.098	0.20
Proteoglycans	Fibromodulin	FMOD	6.39±1.05	10.25±2.62	0.68	0.121	0.58	9.81±1.59	0.62	0.103	0.20
Proteoglycans	Endothelial cell-specific molecule 1	ESM1	0.55±0.09	0.68±0.27	0.30	0.828	0.94	1.14±0.34	1.04	0.102	0.20
Proteoglycans	Prolargin	PRELP	10.66±1.37	15.37±2.88	0.53	0.141	0.58	14.21±1.93	0.42	0.149	0.26
Proteoglycans	Decorin	DCN	35.88±3.8	47.13±6.27	0.39	0.223	0.67	49.79±7.64	0.47	0.166	0.28
Proteoglycans	Proteoglycan 4	PRG4	3.51±0.67	6.8±1.71	0.95	0.103	0.59	3.42±0.68	-0.04	0.813	0.86
Secreted Factors	Protein S100-A11	S100A11	8.08±0.79	10.64±0.8	0.40	0.051	0.83	12.63±0.92	0.64	**0.002**	0.01
Secreted Factors	Insulin-like growth factor II	IGF2	0.91±0.13	1.15±0.26	0.33	0.423	0.75	1.84±0.29	1.01	**0.005**	0.02
Secreted Factors	Protein S100-A6	S100A6	26.18±2.41	39.24±4.01	0.58	**0.024**	1.02	41.64±3.85	0.67	**0.006**	0.03
Secreted Factors	Bone morphogenetic protein 10	BMP10	22.97±3.92	35.99±7.03	0.65	0.094	0.55	42.89±3.61	0.90	**0.009**	0.03
Secreted Factors	Follistatin-related protein 1	FSTL1	7.48±0.85	11.35±2.42	0.60	0.120	0.59	13.13±2.78	0.81	0.056	0.13
Secreted Factors	Protein S100-A4	S100A4	8.01±0.84	10.77±0.97	0.43	0.053	0.80	10.48±1.08	0.39	0.055	0.13
Secreted Factors	C-X-C motif chemokine 2	CXCL2	8.37±2.58	32.24±14.13	1.95	0.068	0.66	16.58±3.5	0.99	0.112	0.21
Secreted Factors	C-X-C motif chemokine 3	CXCL3	2.7±0.67	20.94±10.16	2.95	0.084	0.57	8.8±3.01	1.70	0.134	0.24

			CTRL	POAF				CAF			
Category	**Protein Description**	**Gene Symbol**	**Mean±SEM**	**Mean±SEM**	**log2 FC**	**P Value**	**Adj P Value**	**Mean±SEM**	**log2 FC**	**P Value**	**Adj P Value**
Secreted Factors	Protein S100-A9	S100A9	12.94±2.18	11.94±4.25	-0.12	0.322	0.71	8.79±1.49	-0.56	0.164	0.28
Secreted Factors	Transforming growth factor beta-1 proprotein	TGFB1	0.57±0.17	0.33±0.08	-0.79	0.364	0.73	0.28±0.02	-1.01	0.221	0.34
Secreted Factors	Protein S100-A10	S100A10	14.07±1.63	14.97±3.43	0.09	0.516	0.80	15.7±1.05	0.16	0.321	0.46
Secreted Factors	Inhibin beta A chain	INHBA	15.98±2.65	23.75±6.22	0.57	0.202	0.65	23.32±5.74	0.55	0.330	0.47
Secreted Factors	C-X-C motif chemokine 5	CXCL5	6.38±1.64	18.06±6.31	1.50	0.065	0.69	12.56±4.16	0.98	0.338	0.48
Secreted Factors	Protein S100-A1	S100A1	125.29±7.83	112.34±12.93	-0.16	0.519	0.80	136.39±15.75	0.12	0.600	0.70
Secreted Factors	Follistatin	FST	0.38±0.07	0.28±0.05	-0.43	0.340	0.71	0.45±0.17	0.27	0.634	0.73
Secreted Factors	Hornerin	HRNR	0.26±0.06	0.3±0.07	0.22	0.412	0.74	0.44±0.23	0.80	0.653	0.75
Secreted Factors	Platelet basic protein	PPBP	2.63±0.36	3.89±0.85	0.57	0.236	0.65	2.9±0.4	0.14	0.730	0.80
Secreted Factors	Protein S100-A13	S100A13	37.09±4.08	45.14±4.17	0.28	0.081	0.57	35.63±2.57	-0.06	0.864	0.90

Supplemental Table 2. Identified ECM and ECM associated proteins in human right atrial secretome.

Identified Proteins	UniProt name	Uniprot Acc number	MW [kDa]	Total spectra	Unique spectra	Unique Peptides	Max Coverage [%]
72 kDa type IV collagenase	MMP2-HUMAN	P08253	73.8	163	17	17	37
A disintegrin and metalloproteinase with thrombospondin motifs 1	ADAMTS1-HUMAN	Q9UHI8	105.3	15	3	3	8
A disintegrin and metalloproteinase with thrombospondin motifs 4	ADAMTS4-HUMAN	O75173	90.1	11	2	2	5
Adipocyte enhancer-binding protein 1	AEBP1-HUMAN	Q8IUX7	130.8	166	18	17	22
Adiponectin	ADIPOQ-HUMAN	Q15848	26.4	86	4	4	30
Agrin	AGRN-HUMAN	O00468	217.2	340	32	32	26
Alpha-1-antichymotrypsin	SERPINA3-HUMAN	P01011	47.6	89	8	8	26
Alpha-1-antitrypsin	SERPINA1-HUMAN	P01009	46.7	534	22	22	63
Alpha-2-macroglobulin	A2M-HUMAN	P01023	163.2	697	41	41	40
Angiotensinogen	AGT-HUMAN	P01019	53.1	90	4	4	12
Annexin A1	ANXA1-HUMAN	P04083	38.7	66	8	8	34
Annexin A2	ANXA2-HUMAN	P07355	38.6	286	21	21	57
Annexin A4	ANXA4-HUMAN	P09525	35.9	2	2	2	10
Annexin A5	ANXA5-HUMAN	P08758	35.9	36	3	3	11
Annexin A6	ANXA6-HUMAN	P08133	75.8	50	8	8	18
Antithrombin-III	SERPINC1-HUMAN	P01008	52.6	567	20	20	58
Apolipoprotein A-I	APOA1-HUMAN	P02647	30.8	362	17	17	55
Apolipoprotein A-II	APOA2-HUMAN	P02652	11.2	42	4	4	63
Apolipoprotein A-IV	APOA4-HUMAN	P06727	45.4	35	8	8	21
Apolipoprotein B-100	APOB-HUMAN	P04114	515.3	60	13	13	5
Apolipoprotein D	APOD-HUMAN	P05090	21.3	54	5	5	28
Apolipoprotein E	APOE-HUMAN	P02649	36.1	144	13	13	48
Basal cell adhesion molecule	BCAM-HUMAN	P50895	67.4	323	21	21	46
Basement membrane-specific heparan sulfate proteoglycan core protein	HSPG2-HUMAN	P98160	468.5	3432	147	147	60
Beta-2-glycoprotein 1	APOH-HUMAN	P02749	38.3	358	14	14	57
Biglycan	BGN-HUMAN	P21810	41.6	155	10	10	41
Bone morphogenetic protein 10	BMP10-HUMAN	O95393	48	193	14	14	42
Cadherin-1	CDH1-HUMAN	P12830	97.4	6	3	3	3
Cadherin-13	CDH13-HUMAN	P55290	78.2	202	14	14	33
Cadherin-2	CDH2-HUMAN	P19022	99.7	106	10	10	23
Calpain-1 catalytic subunit	CAPN1-HUMAN	P07384	81.8	130	13	13	28
Calpastatin	CAST-HUMAN	P20810	76.5	196	20	20	47
Cartilage oligomeric matrix protein	COMP-HUMAN	P49747	82.8	247	21	19	59
Cathepsin B	CTSB-HUMAN	P07858	37.8	77	8	8	37
Cathepsin D	CTSD-HUMAN	P07339	44.5	318	14	14	54
Cathepsin L1	CTSL-HUMAN	P07711	37.5	66	7	7	26
Cathepsin S	CTSS-HUMAN	P25774	37.5	7	2	2	8
Cathepsin Z	CTSZ-HUMAN	Q9UBR2	33.8	38	3	3	15
CD109 antigen	CD109-HUMAN	Q6YHK3	161.6	144	13	13	13
CD44 antigen	CD44-HUMAN	P16070	81.5	7	2	2	3
CD5 antigen-like	CD5L-HUMAN	O43866	38.1	11	3	3	15
CD59 glycoprotein	CD59-HUMAN	P13987	14.2	91	4	4	25
Cell surface glycoprotein MUC18	MCAM-HUMAN	P43121	71.6	81	9	9	21
Chondroitin sulfate proteoglycan 4	CSPG4-HUMAN	Q6UVK1	250.4	36	7	7	5
Chymase	CMA1-HUMAN	P23946	27.3	45	6	6	38
Clusterin	CLU-HUMAN	P10909	52.5	193	11	11	28
Coagulation factor IX	F9-HUMAN	P00740	51.7	38	3	3	9
Coagulation factor XII	F12-HUMAN	P00748	67.7	21	2	2	6
Coagulation factor XIII A chain	F13A1-HUMAN	P00488	83.2	246	13	13	26
Collagen alpha-1(I) chain	COL1A1-HUMAN	P02452	138.9	794	50	50	59
Collagen alpha-1(III) chain	COL3A1-HUMAN	P02461	138.5	2069	65	64	63
Collagen alpha-1(IV) chain	COL4A1-HUMAN	P02462	160.5	82	7	7	8
Collagen alpha-1(V) chain	COL5A1-HUMAN	P20908	183.4	5	4	4	4
Collagen alpha-1(VI) chain	COL6A1-HUMAN	P12109	108.5	120	14	14	27
Collagen alpha-1(XII) chain	COL12A1-HUMAN	Q99715	332.9	11	5	5	3
Collagen alpha-1(XIV) chain	COL14A1-HUMAN	Q05707	193.4	926	54	54	48
Collagen alpha-1(XV) chain	COL15A1-HUMAN	P39059	141.6	304	14	14	14

Identified Proteins	UniProt name	Uniprot Acc number	MW [kDa]	Total spectra	Unique spectra	Unique Peptides	Max Coverage [%]
Collagen alpha-1(XVI) chain	COL16A1-HUMAN	Q07092	157.7	24	5	5	8
Collagen alpha-1(XVIII) chain	COL18A1-HUMAN	P39060	178.1	422	17	17	17
Collagen alpha-1(XXVIII) chain	COL28A1-HUMAN	Q2UY09	116.6	40	3	3	5
Collagen alpha-2(I) chain	COL1A2-HUMAN	P08123	129.2	451	35	35	47
Collagen alpha-2(IV) chain	COL4A2-HUMAN	P08572	167.4	123	13	13	14
Collagen alpha-2(VI) chain	COL6A2-HUMAN	P12110	108.5	58	7	7	12
Collagen alpha-3(V) chain	COL5A3-HUMAN	P25940	172	30	5	5	5
Collagen alpha-3(VI) chain	COL6A3-HUMAN	P12111	343.5	1067	67	67	29
Collagen alpha-6(VI) chain	COL6A6-HUMAN	A6NMZ7	247	9	2	2	1
Complement C1q subcomponent subunit A	C1QA-HUMAN	P02745	26	61	6	6	40
Complement C1q subcomponent subunit B	C1QB-HUMAN	P02746	26.7	87	5	5	29
Complement C1q subcomponent subunit C	C1QC-HUMAN	P02747	25.8	97	6	6	36
Connective tissue growth factor	CTGF-HUMAN	P29279	38.1	24	5	5	22
C-X-C motif chemokine 2	CXCL2-HUMAN	P19875	11.4	87	5	3	43
C-X-C motif chemokine 3	CXCL3-HUMAN	P19876	11.3	102	4	2	39
C-X-C motif chemokine 5	CXCL5-HUMAN	P42830	12	73	4	4	37
Cystatin-B	CSTB-HUMAN	P04080	11.1	58	3	3	46
Cystatin-C	CST3-HUMAN	P01034	15.8	99	5	5	45
Cysteine-rich protein 2	CRIP2-HUMAN	P52943	22.5	75	3	3	32
Decorin	DCN-HUMAN	P07585	39.7	221	9	9	41
Dermatopontin	DPT-HUMAN	Q07507	24	21	4	4	30
Dystroglycan	DAG1-HUMAN	Q14118	97.4	167	8	8	15
EGF-containing fibulin-like extracellular matrix protein 1	EFEMP1-HUMAN	Q12805	54.6	347	18	18	52
EGF-containing fibulin-like extracellular matrix protein 2	EFEMP2-HUMAN	O95967	49.4	61	7	7	23
EMILIN-1	EMILIN1-HUMAN	Q9Y6C2	106.6	292	19	19	25
EMILIN-2	EMILIN2-HUMAN	Q9BXX0	115.6	26	8	8	10
Endothelial cell-specific molecule 1	ESM1-HUMAN	Q9NQ30	20.1	4	2	2	13
Extracellular matrix protein 1	ECM1-HUMAN	Q16610	60.6	73	8	8	27
Fibrillin-1	FBN1-HUMAN	P35555	312	266	24	24	13
Fibrinogen alpha chain	FGA-HUMAN	P02671	94.9	334	18	18	26
Fibrinogen beta chain	FGB-HUMAN	P02675	55.9	687	25	25	63
Fibrinogen gamma chain	FGG-HUMAN	P02679	51.5	534	20	20	57
Fibroleukin	FGL2-HUMAN	Q14314	50.2	92	11	11	34
Fibromodulin	FMOD-HUMAN	Q06828	43.2	101	8	8	33
Fibronectin	FN1-HUMAN	P02751	262.5	1502	68	68	47
Fibulin-1	FBLN1-HUMAN	P23142	77.2	667	27	27	50
Fibulin-2	FBLN2-HUMAN	P98095	126.5	1207	46	46	59
Fibulin-5	FBLN5-HUMAN	Q9UBX5	50.1	203	11	11	36
Follistatin	FST-HUMAN	P19883	38	11	3	3	21
Follistatin-related protein 1	FSTL1-HUMAN	Q12841	35	79	8	8	30
Galectin-1	LGALS1-HUMAN	P09382	14.7	281	8	8	73
Galectin-3	LGALS3-HUMAN	P17931	26.1	269	7	7	32
Galectin-3-binding protein	LGALS3BP-HUMAN	Q08380	65.3	202	12	12	32
Gelsolin	GSN-HUMAN	P06396	85.6	680	27	27	46
Glia-derived nexin	SERPINE2-HUMAN	P07093	44	81	12	12	37
Glypican-1	GPC1-HUMAN	P35052	61.6	76	9	9	26
Glypican-4	GPC4-HUMAN	O75487	62.4	23	2	2	6
Granulins	GRN-HUMAN	P28799	63.5	125	6	6	20
Heat shock 70 kDa protein 1B	HSPA1B-HUMAN	P0DMV9	70	409	22	17	49
Heat shock 70 kDa protein 4	HSPA4-HUMAN	P34932	94.3	123	20	19	39
Heat shock cognate 71 kDa protein	HSPA8-HUMAN	P11142	70.9	459	24	18	54
Heat shock protein beta-1	HSPB1-HUMAN	P04792	22.8	480	11	11	57
Heat shock protein beta-6	HSPB6-HUMAN	O14558	17.1	17	5	5	46
Heat shock protein HSP 90-alpha	HSP90AA1-HUMAN	P07900	84.6	512	33	22	44
Heat shock protein HSP 90-beta	HSP90AB1-HUMAN	P08238	83.2	470	29	16	42
Heat shock-related 70 kDa protein 2	HSPA2-HUMAN	P54652	70	265	13	7	29
Hemicentin-2	HMCN2-HUMAN	Q8NDA2	541.6	2	2	2	1
Hemopexin	HPX-HUMAN	P02790	51.6	256	13	13	44
Heparin cofactor 2	SERPIND1-HUMAN	P05546	57	24	5	5	12

Identified Proteins	UniProt name	Uniprot Acc number	MW [kDa]	Total spectra	Unique spectra	Unique Peptides	Max Coverage [%]
Histidine-rich glycoprotein	HRG-HUMAN	P04196	59.5	190	12	12	31
Hornerin	HRNR-HUMAN	Q86YZ3	282.2	11	3	3	5
Hyaluronan and proteoglycan link protein 1	HAPLN1-HUMAN	P10915	40.1	67	10	9	36
Inhibin beta A chain	INHBA-HUMAN	P08476	47.4	179	13	13	35
Insulin-like growth factor II	IGF2-HUMAN	P01344	20.1	24	2	2	14
Insulin-like growth factor-binding protein 2	IGFBP2-HUMAN	P18065	34.8	145	11	11	53
Insulin-like growth factor-binding protein 3	IGFBP3-HUMAN	P17936	31.7	228	12	12	53
Insulin-like growth factor-binding protein 4	IGFBP4-HUMAN	P22692	27.9	71	8	8	40
Insulin-like growth factor-binding protein 5	IGFBP5-HUMAN	P24593	30.6	61	6	6	30
Insulin-like growth factor-binding protein 6	IGFBP6-HUMAN	P24592	25.3	2	2	2	17
Insulin-like growth factor-binding protein 7	IGFBP7-HUMAN	Q16270	29.1	318	12	12	51
Intelectin-1	ITLN1-HUMAN	Q8WWA0	34.9	169	10	7	51
Inter-alpha-trypsin inhibitor heavy chain H1	ITIH1-HUMAN	P19827	101.3	295	21	21	34
Inter-alpha-trypsin inhibitor heavy chain H2	ITIH2-HUMAN	P19823	106.4	99	11	11	17
Inter-alpha-trypsin inhibitor heavy chain H3	ITIH3-HUMAN	Q06033	99.8	19	5	5	8
Inter-alpha-trypsin inhibitor heavy chain H4	ITIH4-HUMAN	Q14624	103.3	153	12	12	21
Intercellular adhesion molecule 1	ICAM1-HUMAN	P05362	57.8	18	4	4	10
Interstitial collagenase	MMP1-HUMAN	P03956	54	424	17	17	45
Kininogen-1	KNG1-HUMAN	P01042	71.9	123	11	11	23
Laminin subunit alpha-2	LAMA2-HUMAN	P24043	343.7	990	66	66	34
Laminin subunit alpha-4	LAMA4-HUMAN	Q16363	202.4	210	22	22	18
Laminin subunit alpha-5	LAMA5-HUMAN	O15230	399.5	180	21	21	8
Laminin subunit beta-1	LAMB1-HUMAN	P07942	197.9	369	33	33	30
Laminin subunit beta-2	LAMB2-HUMAN	P55268	195.9	770	50	50	41
Laminin subunit gamma-1	LAMC1-HUMAN	P11047	177.5	901	50	50	46
Latent-transforming growth factor beta-binding protein 1	LTBP1-HUMAN	Q14766	186.7	224	19	19	18
Latent-transforming growth factor beta-binding protein 2	LTBP2-HUMAN	Q14767	194.9	356	26	26	24
Latent-transforming growth factor beta-binding protein 4	LTBP4-HUMAN	Q8N2S1	173.3	343	28	28	32
Leucine-rich alpha-2-glycoprotein	LRG1-HUMAN	P02750	38.2	3	2	2	9
Leukocyte elastase inhibitor	SERPINB1-HUMAN	P30740	42.7	91	9	9	35
Lumican	LUM-HUMAN	P51884	38.4	924	20	20	65
Matrilin-2	MATN2-HUMAN	O00339	106.8	333	16	16	25
Matrix metalloproteinase-9	MMP9-HUMAN	P14780	78.4	14	4	4	10
Metalloproteinase inhibitor 1	TIMP1-HUMAN	P01033	23.2	369	10	10	67
Metalloproteinase inhibitor 2	TIMP2-HUMAN	P16035	24.4	16	3	3	28
Microfibril-associated glycoprotein 4	MFAP4-HUMAN	P55083	28.6	11	2	2	8
Mimecan	OGN-HUMAN	P20774	33.9	414	13	13	47
Multimerin-2	MMRN2-HUMAN	Q9H8L6	104.3	18	5	5	9
Nidogen-1	NID1-HUMAN	P14543	136.3	224	23	22	35
Nidogen-2	NID2-HUMAN	Q14112	151.2	135	16	15	17
Osteopontin	SPP1-HUMAN	P10451	35.4	13	2	2	10
Papilin	PAPLN-HUMAN	O95428	137.6	64	8	8	14
Pentraxin-related protein PTX3	PTX3-HUMAN	P26022	41.9	123	10	10	38
Periostin	POSTN-HUMAN	Q15063	93.3	253	25	25	39
Peroxidasin homolog	PXDN-HUMAN	Q92626	165.2	104	15	15	16
Peroxiredoxin-1	PRDX1-HUMAN	Q06830	22.1	573	16	13	72
Peroxiredoxin-2	PRDX2-HUMAN	P32119	21.9	320	14	13	67
Peroxiredoxin-6	PRDX6-HUMAN	P30041	25	499	18	18	70
Pigment epithelium-derived factor	SERPINF1-HUMAN	P36955	46.3	57	8	8	24
Plasma protease C1 inhibitor	SERPING1-HUMAN	P05155	55.1	179	12	12	32
Plasma serine protease inhibitor	SERPINA5-HUMAN	P05154	45.6	8	2	2	6
Plasminogen	PLG-HUMAN	P00747	45	489	19	19	58
Plasminogen activator inhibitor 1	SERPINE1-HUMAN	P05121	90.5	216	18	18	37
Platelet basic protein	PPBP-HUMAN	P02775	13.9	11	2	2	15
Procollagen C-endopeptidase enhancer 1	PCOLCE-HUMAN	Q15113	47.9	152	11	11	35
Procollagen-lysine,2-oxoglutarate 5-dioxygenase 1	PLOD1-HUMAN	Q02809	83.5	32	8	8	17
Prolargin	PRELP-HUMAN	P51888	43.8	113	8	8	27
Prostaglandin-H2 D-isomerase	PTGDS-HUMAN	P41222	21	105	4	4	31
Protein AMBP	AMBP-HUMAN	P02760	39	225	14	14	45

Identified Proteins	UniProt name	Uniprot Acc number	MW [kDa]	Total spectra	Unique spectra	Unique Peptides	Max Coverage [%]
Protein disulfide-isomerase	P4HB-HUMAN	P07237	57.1	767	31	31	66
Protein S100-A1	S100A1-HUMAN	P23297	10.5	227	7	7	52
Protein S100-A10	S100A10-HUMAN	P60903	11.2	85	5	5	60
Protein S100-A11	S100A11-HUMAN	P31949	11.7	69	4	4	44
Protein S100-A13	S100A13-HUMAN	Q99584	11.5	84	4	4	33
Protein S100-A4	S100A4-HUMAN	P26447	11.7	26	3	3	29
Protein S100-A6	S100A6-HUMAN	P06703	10.2	49	4	4	36
Protein S100-A9	S100A9-HUMAN	P06702	13.2	67	4	4	44
Protein-lysine 6-oxidase	LOX-HUMAN	P28300	46.9	24	2	2	9
Proteoglycan 4	PRG4-HUMAN	Q92954	151	64	12	12	20
Prothrombin	F2-HUMAN	P00734	70	211	14	14	37
Secretogranin-1	CHGB-HUMAN	P05060	78.2	26	10	10	22
Serpin B6	SERPINB6-HUMAN	P35237	42.6	332	16	16	59
Serpin H1	SERPINH1-HUMAN	P50454	46.4	17	6	6	21
SPARC	SPARC-HUMAN	P09486	34.6	122	6	6	33
SPARC-like protein 1	SPARCL1-HUMAN	Q14515	75.2	253	17	17	45
Spondin-1	SPON1-HUMAN	Q9HCB6	90.9	252	15	15	32
Sulfhydryl oxidase 1	QSOX1-HUMAN	O00391	82.5	53	10	10	17
Target of Nesh-SH3	ABI3BP-HUMAN	Q7Z7G0	118.6	666	34	34	52
Tenascin	TNC-HUMAN	P24821	240.7	146	36	36	29
Tenascin-X	TNXB-HUMAN	P22105	458.1	2363	146	146	51
Testican-1	SPOCK1-HUMAN	Q08629	49.1	48	5	5	19
Tetranectin	CLEC3B-HUMAN	P05452	22.5	70	4	4	29
Thrombospondin-1	THBS1-HUMAN	P07996	129.3	595	38	36	41
Thrombospondin-2	THBS2-HUMAN	P35442	129.9	229	20	18	26
Thrombospondin-4	THBS4-HUMAN	P35443	105.8	72	14	11	22
Transforming growth factor beta-1 proprotein	TGFB1-HUMAN	P01137	44.3	7	2	2	8
Transforming growth factor-beta-induced protein ig-h3	TGFBI-HUMAN	Q15582	74.6	689	32	32	60
Transgelin-2	TAGLN2-HUMAN	P37802	22.4	182	9	9	62
Tubulointerstitial nephritis antigen-like	TINAGL1-HUMAN	Q9GZM7	52.4	8	2	2	6
Tumor necrosis factor-inducible gene 6 protein	TNFAIP6-HUMAN	P98066	31.2	31	6	6	30
Versican core protein	VCAN-HUMAN	P13611	372.6	804	59	59	25
Vinculin	VCL-HUMAN	P18206	123.7	1380	56	56	57
Vitronectin	VTN-HUMAN	P04004	54.3	168	14	14	36
von Willebrand factor	VWF-HUMAN	P04275	309.1	582	51	51	29
Xaa-Pro dipeptidase	PEPD-HUMAN	P12955	54.5	22	2	2	5
Zinc-alpha-2-glycoprotein	AZGP1-HUMAN	P25311	34.2	23	4	4	18